frontiers | Research Topics

Development of circadian clock functions, volume II

Edited by
Daisuke Ono, Takahiro J. Nakamura, Jeff Jones, Jihwan Myung and Rae Silver

Published in
Frontiers in Neuroscience

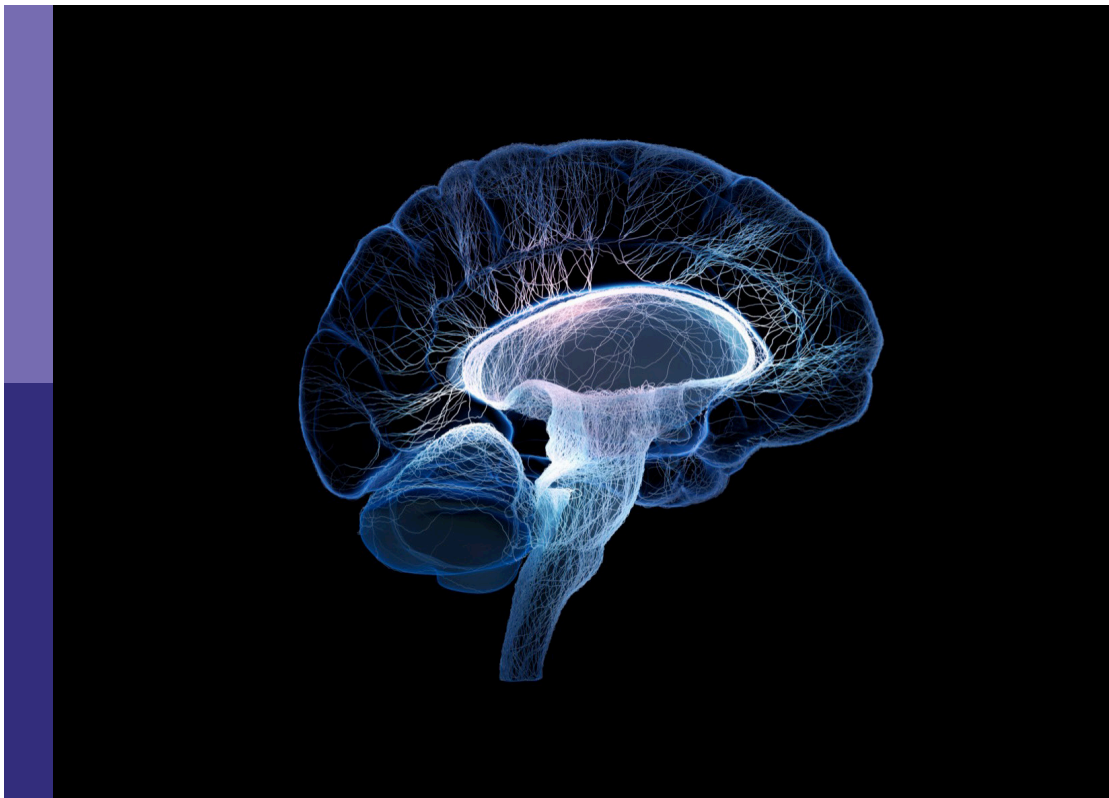

ISSN 1664-8714
ISBN 978-2-8325-5228-5
DOI 10.3389/978-2-8325-5228-5

About Frontiers

Frontiers is more than just an open access publisher of scholarly articles: it is a pioneering approach to the world of academia, radically improving the way scholarly research is managed. The grand vision of Frontiers is a world where all people have an equal opportunity to seek, share and generate knowledge. Frontiers provides immediate and permanent online open access to all its publications, but this alone is not enough to realize our grand goals.

Frontiers journal series

The Frontiers journal series is a multi-tier and interdisciplinary set of open-access, online journals, promising a paradigm shift from the current review, selection and dissemination processes in academic publishing. All Frontiers journals are driven by researchers for researchers; therefore, they constitute a service to the scholarly community. At the same time, the *Frontiers journal series* operates on a revolutionary invention, the tiered publishing system, initially addressing specific communities of scholars, and gradually climbing up to broader public understanding, thus serving the interests of the lay society, too.

Dedication to quality

Each Frontiers article is a landmark of the highest quality, thanks to genuinely collaborative interactions between authors and review editors, who include some of the world's best academicians. Research must be certified by peers before entering a stream of knowledge that may eventually reach the public - and shape society; therefore, Frontiers only applies the most rigorous and unbiased reviews. Frontiers revolutionizes research publishing by freely delivering the most outstanding research, evaluated with no bias from both the academic and social point of view. By applying the most advanced information technologies, Frontiers is catapulting scholarly publishing into a new generation.

What are Frontiers Research Topics?

Frontiers Research Topics are very popular trademarks of the *Frontiers journals series*: they are collections of at least ten articles, all centered on a particular subject. With their unique mix of varied contributions from Original Research to Review Articles, Frontiers Research Topics unify the most influential researchers, the latest key findings and historical advances in a hot research area.

Find out more on how to host your own Frontiers Research Topic or contribute to one as an author by contacting the Frontiers editorial office: frontiersin.org/about/contact

Development of circadian clock functions, volume II

Topic editors

Daisuke Ono — Nagoya University, Japan
Takahiro J. Nakamura — Meiji University, Japan
Jeff Jones — Washington University in St. Louis, United States
Jihwan Myung — Taipei Medical University, Taiwan
Rae Silver — Columbia University, United States

Citation

Ono, D., Nakamura, T. J., Jones, J., Myung, J., Silver, R., eds. (2024). *Development of circadian clock functions, volume II*. Lausanne: Frontiers Media SA.
doi: 10.3389/978-2-8325-5228-5

Table of contents

frontiers | Frontiers in Neuroscience

TYPE Editorial
PUBLISHED 16 July 2024
DOI 10.3389/fnins.2024.1453328

OPEN ACCESS

EDITED AND REVIEWED BY
Radhika Basheer,
United States Department of Veterans Affairs, United States

*CORRESPONDENCE
Jihwan Myung
✉ jihwan@tmu.edu.tw

RECEIVED 22 June 2024
ACCEPTED 01 July 2024
PUBLISHED 16 July 2024

CITATION
Myung J, Silver R, Jones JR, Nakamura TJ and Ono D (2024) Editorial: Development of circadian clock functions, volume II. *Front. Neurosci.* 18:1453328. doi: 10.3389/fnins.2024.1453328

Editorial: Development of circadian clock functions, volume II

Jihwan Myung[1]*, Rae Silver[2,3], Jeff R. Jones[4], Takahiro J. Nakamura[5] and Daisuke Ono[6,7]

[1]Graduate Institute of Mind, Brain, and Consciousness, Taipei Medical University, Taipei, Taiwan, [2]Department of Psychology, Columbia University, New York, NY, United States, [3]Department of Neuroscience and Behavior, Barnard College of Columbia University, New York, NY, United States, [4]Department of Biology, Texas A&M University, College Station, TX, United States, [5]Laboratory of Animal Physiology, School of Agriculture, Meiji University, Kawasaki, Japan, [6]Stress Recognition and Response, Research Institute of Environmental Medicine, Nagoya University, Nagoya, Japan, [7]Department of Neural Regulation, Nagoya University Graduate School of Medicine, Nagoya, Japan

KEYWORDS

circadian clock, development, aging, entrainment, synchronization, suprachiasmatic nucleus (SCN)

Editorial on the Research Topic
Development of circadian clock functions, volume II

In multicellular organisms like ourselves, there exists not only a single circadian clock but rather a network of clocks throughout the body that operate in coordination. The central pacemaker of this system is the suprachiasmatic nucleus (SCN). The SCN is itself synchronized to the environment by local external light-dark cycles and it then communicates this information to the rest of the body. However, this is not a steady state relationship: As our bodies undergo changes throughout their developmental trajectory, there are corresponding adjustments in circadian organization. These adjustments necessitate consideration not only of external synchronizing cues, but also internal circadian cues that entrain and organize clocks throughout the body.

Because the proper maintenance of circadian rhythms is important in early life, addressing the developing circadian clock is critical in the neonatal intensive care unit (NICU). This is particularly pertinent for preterm infants prior to gestational week 30, who have not yet opened their eyes, making photic entrainment unreliable (Arimitsu et al.). Consequently, there is a need to consider alternative methods of entrainment, such as internal entraining signals: It is not known however, which signaling molecules mediate the internal synchronization of circadian clocks. Glucocorticoids are one potential candidate that can be especially relevant during fetal development, as their receptor response can be gated by time (Lehmann et al.). Another potential candidate are Opn4 (melanopsin) aptamers, or melapts. Given that the SCN receives light input directly from melanopsin-expressing intrinsically photosensitive retinal ganglion cells (ipRGCs), melapts can potentially intervene in light-stimulated phase shifts of circadian clocks (Nakazawa et al.). These candidate signaling molecules could have therapeutic implications for circadian entrainment in artificial environments such as the NICU.

The development of circadian clock systems appears to undergo stages of unification (from absence to presence of synchronization) and specification (organized phases through maturation) (Myung et al., 2021). Carmona-Alcocer et al. work tracing the trajectories of nascent SCN neuronal development through the patterns of neuropeptide expression reveals the delayed specification of arginine vasopressin (AVP) and vasoactive intestinal peptide (VIP) neurons. Surprisingly, this time course of specification exhibits some sexual dimorphism. In addition, the synchronization among clock neurons follows a developmental trend that deteriorates with old age. This loss of synchronization may be due to changes in the neurotransmitter GABA, one of the primary interneuronal signaling molecules in the SCN, during aging. Olde Engberink et al. find that GABA, canonically an "inhibitory" neurotransmitter, becomes less inhibitory and progressively more excitatory with age, which effectively affects the coupling strength among neurons within the SCN clock network. In aged mice, this results in changes to the spectral power of circadian rhythmicity and a longer period in the SCN oscillation. The mechanism behind this has a simple theoretical explanation: synchronization is driven by the frequencies of component oscillators, not their periods. If their period distribution of individual oscillators within the SCN is symmetric, the frequency distribution becomes skewed, making the synchronized frequency differ from the mean frequency (Myung et al.).

The molecular clock itself—the transcriptional-translational feedback loop intrinsic to single cells—also changes during development. Indeed, the core clock component *Cryptochrome* (*Cry*) has previously been found to have developmental criticality (Ono et al., 2013). The *Cry1* isoform specifically influences circadian period in behavior across development, summarized as: "when *Cry1* expression was higher for longer [in early development], the free-running period [of locomotor activity] was longer" (Schirmer et al.).

Finally, the development of the circadian clock has effects on physiology in both model organisms and importantly, in humans. A human's intrinsic circadian period is reflected in their chronotype (morningness-eveningness). In a two-sample Mendelian randomization analysis, Yang et al. find a causal relationship between a morning chronotype in humans and the structural features of the cerebral cortex. Intriguingly, in mice, electroencephalography (EEG) recordings of cortex reflect these structural changes and show age-dependent circadian changes with circadian power weakened with age (Masuda et al.). Developing circadian clocks also have significant relevance to neurovascular function (Mitchell and Gillette).

In conclusion, circadian clocks are present in all developing systems and they appear with different strengths and specifications, enabling coordination of multiple subsystems in the brain and the body. The precise mechanisms that determine how such coordination is achieved through various interactions will continue to provoke ongoing investigation.

Author contributions

JM: Writing – original draft, Writing – review & editing. RS: Writing – review & editing. JJ: Writing – review & editing. TN: Writing – review & editing. DO: Writing – review & editing.

Funding

The author(s) declare financial support was received for the research, authorship, and/or publication of this article. This work was financially supported by the Higher Education Sprout Project by the Ministry of Education (MOE) in Taiwan, and the National Science and Technology Council (NSTC), Taiwan (112-2314-B-038-063) (to JM), National Science Foundation (1749500) and National Institute of Health (1R01NS102962) (to RS), National Institute of Health (R35GM151020) (to JJ), and JSPS KAKENHI (19K06360, 24K10029) (to TN), (18H02477, 20KK0177, 21H00422, 21H00307, 21H02526) (to DO).

Conflict of interest

The authors declare that the research was conducted in the absence of any commercial or financial relationships that could be construed as a potential conflict of interest.

The author(s) declared that they were an editorial board member of Frontiers, at the time of submission. This had no impact on the peer review process and the final decision.

Publisher's note

References

Myung, J., Nakamura, T. J., Jones, J. R., Silver, R., and Ono, D. (2021). Development of circadian clock functions. *Front. Neurosci.* 15:735007. doi: 10.3389/fnins.2021.735007

Ono, D., Honma, S., and Honma, K. I. (2013). Cryptochromes are critical for the development of coherent circadian rhythms in the mouse suprachiasmatic nucleus. *Nat. Commun.* 4:1666. doi: 10.1038/ncomms2670

frontiers | Frontiers in Neuroscience

TYPE Mini Review
PUBLISHED 25 April 2023
DOI 10.3389/fnins.2023.1165230

OPEN ACCESS

EDITED BY
Takahiro J. Nakamura,
Meiji University, Japan

REVIEWED BY
Russell D. Romeo,
Columbia University, United States
Yifan Yao,
Columbia University, United States

*CORRESPONDENCE
Mariana Astiz
✉ mariana.astiz@achucarro.org

†These authors have contributed equally to this work

RECEIVED 13 February 2023
ACCEPTED 06 April 2023
PUBLISHED 25 April 2023

CITATION
Lehmann M, Haury K, Oster H and Astiz M (2023) Circadian glucocorticoids throughout development.
Front. Neurosci. 17:1165230.
doi: 10.3389/fnins.2023.1165230

Circadian glucocorticoids throughout development

Marianne Lehmann[1†], Katharina Haury[2†], Henrik Oster[1] and Mariana Astiz[1,2,3*]

[1]Institute of Neurobiology, University of Lübeck, Lübeck, Germany, [2]Achucarro Basque Center for Neuroscience, Science Park of the UPV/EHU, Leioa, Spain, [3]IKERBASQUE, Basque Foundation for Science, Bilbao, Spain

Glucocorticoids (GCs) are essential drivers of mammalian tissue growth and maturation during one of the most critical developmental windows, the perinatal period. The developing circadian clock is shaped by maternal GCs. GC deficits, excess, or exposure at the wrong time of day leads to persisting effects later in life. During adulthood, GCs are one of the main hormonal outputs of the circadian system, peaking at the beginning of the active phase (i.e., the morning in humans and the evening in nocturnal rodents) and contributing to the coordination of complex functions such as energy metabolism and behavior, across the day. Our article discusses the current knowledge on the development of the circadian system with a focus on the role of GC rhythm. We explore the bidirectional interaction between GCs and clocks at the molecular and systemic levels, discuss the evidence of GC influence on the master clock in the suprachiasmatic nuclei (SCN) of the hypothalamus during development and in the adult system.

KEYWORDS

circadian system, hypothalamic-pituitary-adrenal axis, development, perinatal programming, glucocorticoids, glucocorticoid receptor, molecular clock

1. Circadian clock development and organization at systemic, circuit, and molecular level in the adult

Circadian rhythms are controlled by a clock system that conveys ~24 h rhythmicity to almost every physiological function in a living organism. When (and how) does the clock system really start ticking, and more specifically, which cells and mechanisms are involved, are long-standing questions in the field of chronophysiology. In adult mammals, circadian timekeeping is organized hierarchically with a central clock synchronizing subordinated clocks in all tissues to ensure that complex functions such as activity (Moore and Eichler, 1972), sleep (Collins et al., 2020), food intake (Nagai et al., 1978; Koch et al., 2020), and stress responses (Oster et al., 2006; Son et al., 2008) are efficiently adapted to a rhythmic environment.

The master pacemaker of the circadian system is located in the hypothalamic suprachiasmatic nucleus (SCN) (Lehman et al., 1987; Romero et al., 1993; Silver et al., 1996). Environmental factors that set the time (or entrain) internal clocks are called *zeitgebers* (from the German term for "time givers"). The main *zeitgeber* for the SCN is ambient light which reaches the retina and, in turn, the SCN through the retino-hypothalamic tract (RHT) (Ibuka et al., 1977; Hannibal et al., 2000).

The SCN has been traditionally described as a nucleus of around 20,000 neurons localized on each side of the third ventricle. It is topologically divided into "ventral core" and "dorsal shell" (Hastings et al., 2018). Neurons in the core receive direct photic input from the retina and transmit this signal to the surrounding shell. The neurons in the SCN shell, that in absence of

light show autonomous activity with an endogenous period of ~24 h, are then entrained and translate their synchrony by efferent connections to subordinated clocks in multiple brain regions including, importantly, clocks within the medial hypothalamus, where key cell groups organize hormone release and set the tone of the autonomic nervous system (Dibner et al., 2010; Kalsbeek et al., 2011). Interestingly, this neuron-centered view changed recently when astrocyte clocks were found to be partially necessary and completely sufficient to restore neuronal circadian function in the SCN (Brancaccio et al., 2019). Rather than being "mere support cells" for the SCN neuronal circuit, they play an essential role as time-keepers of the adult master clock (Barca-Mayo et al., 2017; Brancaccio et al., 2017, 2019; Tso et al., 2017).

Glucocorticoids (GC) are examples of rhythmic hormonal outputs tightly regulated by the SCN and well-known mediators of circadian entrainment in the peripheral tissues (Pevet and Challet, 2011; Pezük et al., 2012). The circadian regulation of GC release is a result of close interaction between the SCN and clocks along the hypothalamus-pituitary–adrenal (HPA) axis (Oster et al., 2006; Son et al., 2008). Efferences from the SCN influence the release of corticotropin-releasing hormone (CRH) by the paraventricular nucleus of the hypothalamus (PVN), both inhibitory and stimulatory inputs from the SCN, depending on fluctuating arginine vasopressin (AVP) levels, are responsible of generating the complete daily profile of GCs (Kalsbeek et al., 1992, 1996; Buijs et al., 1993). The PVN controls the rhythmic secretion of adrenocorticotropic hormone (ACTH) from the pituitary and, consequently, GC production by the adrenal gland. Via autonomic pathways the SCN-PVN synchronize adrenal clocks regulating the time-of-day-dependent sensitivity of the adrenal to ACTH stimulation (Oster et al., 2006; Son et al., 2008). As a result, GCs are peaking at the beginning of the active phase to coordinate complex functions when high energy demands are expected (Balsalobre et al., 2000). For instance, GCs promote glucose and lipid mobilization through gluconeogenesis in the liver and the release of free fatty acids from adipocytes. GC rhythms are key regulators of mood and cognition, demonstrated by the improvement of learning skills during GC peak (Liston et al., 2013) and the impairment of memory retrieval when circadian GC rise is blocked pharmacologically (Rimmele et al., 2010).

Compared to the knowledge we have on the adult circadian system, little is known about its assembly and function during development. The view of the fetal hypothalamic clock as a "dependent" oscillator entrained by maternal rhythmic signals has been questioned by our own findings and by others (Landgraf et al., 2015; Astiz et al., 2020; Lužná et al., 2020; Greiner et al., 2022). In mice, the SCN circuit develops, matures, and connects to afferent and efferent pathways around birth (Munekawa et al., 2000; Sekaran et al., 2005; Kabrita and Davis, 2008). However, some early rhythmic genes of the molecular clock machinery, such as *RevErbα*, are already expressed in the hypothalamus earlier (Čečmanová et al., 2019; Astiz et al., 2020; Carmona-Alcocer et al., 2020). Since both, astrocytes and neurons, display strong circadian rhythmicity, it seems possible that the two could promote the gain of autonomous function of the developing SCN and participate in organizing the coupling between the SCN and the HPA axis, essential for the adaptation to the environment after birth (Astiz and Oster, 2018). Extensive evidence suggests that during this critical developmental window, the fetal/neonatal SCN and HPA axis are susceptible to GCs. An excess, a deficit or even the exposure at the wrong time of day can have persisting effects later on (Moisiadis and Matthews, 2014a; Busada and Cidlowski, 2017; Astiz et al., 2020).

2. Molecular interaction between Glucocorticoid receptors and the clock machinery

The strong coupling between the clock and the stress system is nourished by a solid bidirectional interaction at the molecular level. GCs activate, in target cells, intracellular GC receptors (GR) and mineralocorticoid receptors (MR). The primary ligands of GR are cortisol and other GCs (i.e., corticosterone, the main GC in rodents), while the primary ligand of MR is aldosterone in the periphery and corticosterone in the central nervous system (CNS) (Fuller et al., 2012). While GR is widely distributed within the body and especially abundant in the brain and the pituitary, MR is prominently present in peripheral tissues and in the brain, the expression is high in the magnocellular neurons and pre-sympathetic neurons of the hypothalamic paraventricular nuclei (PVN) as well as in the hippocampus and cerebral cortex (Oyamada et al., 2008; Fuller et al., 2019). Since MR has a 10-fold higher affinity for GCs than GR, it becomes active even at nadir GC levels (Kolber et al., 2008; Daskalakis et al., 2022). In contrast, GR is only activated at higher GC concentrations, such as those reached during the circadian peak or after stress-induced HPA axis activation (Kolber et al., 2008). The presence of both GR and MR in the neurons of the SCN of adult mice and humans remains a controversial (Rosenfeld et al., 1988; Olejníková et al., 2018). The genes encoding for GR and MR are not expressed in adult SCN neurons in rodents and humans.[1]

GR acts as a ligand-activated transcription factor. In the inactive/unbound state, GR locates in the cytosol bound to the N-terminal and middle region of a chaperone complex containing Heat shock protein 90 (HSP90) (Antunica-Noguerol et al., 2016; Fries et al., 2017; Mazaira and Galigniana, 2019). HSP90 does not form part of the active receptor complex, but is important for correct GR protein folding and stability (Biebl and Buchner, 2019). The HSP90 complex is also formed by co-chaperones important for GR stabilization and feedback, such as FK506-binding protein 5 (FKBP5) (Binder, 2009; Biebl and Buchner, 2019). *Fkbp5* is transcriptionally induced by GC-GR and, in turn, regulates GR sensitivity through an intracellular negative feedback loop, essentially keeping inactive GR in the cytosol (Pratt and Toft, 1997; Nicolaides et al., 2000; Binder, 2009; Klengel et al., 2013; Criado-Marrero et al., 2018). Upon ligand binding, GR monomers dimerize (either with other GR monomer or with MR) and translocate to the nucleus where the dimer binds the DNA at GC response elements (GREs), regulatory regions of target genes (George et al., 2017; Oakley et al., 2021). Through binding of GREs, the transcription of GR target genes is modulated positively or negatively (Reddy et al., 2009; Surjit et al., 2011). Besides this canonical signaling cascade, GR and MR activation have shown

1 https://portal.brain-map.org/

rapid non-genomic changes, mediated by membrane-anchored GR/MR that might mediate the coordination of rapid adaptive responses to stress (Groeneweg et al., 2012).

The clock gene machinery is present in almost every cell of the body and reciprocal interaction with GR is found at transcriptional, translational, and post-translational levels (summarized in Figure 1; Nader et al., 2010). The molecular clock machinery works as an interlocked transcriptional-translational-feedback loop (Takahashi, 2017). The positive members of the loop: BMAL1 (brain and muscle aryl hydrocarbon receptor nuclear translocator-like 1) and CLOCK (circadian locomotor output cycles kaput) heterodimerize and activate the transcription of their repressors *Per1/2* (*Period 1/2*), *Cry1/2* (*Cryptochrome 1/2*) through binding of E-Box promoter elements. Upon translation, PER and CRY form complexes in the cytosol, translocate into the nucleus and repress CLOCK/BMAL1 activity, shutting down their own transcription. After clearance of PER/CRY complexes, the inhibition of CLOCK/BMAL1 is released and a new circadian (~24 h) cycle begins. The cycle is further stabilized by accessory loops in which CLOCK/BMAL1 drive the circadian expression of Dec 1/2 and nuclear receptors of the ROR and the REV-ERB family (Takahashi, 2017).

As mentioned above, GR through its ability to respond to GCs' circadian oscillations, is an ideal coupling partner of the molecular clock (Lambrou et al., 2021). Activated GR is able to influence the transcription of various clock genes via binding to GREs in their promoter regions, among them *Per2, Rev-ERBß, Dec2, NPAS2,* and *E4BP4/NFIL3* (So et al., 2009; Nader et al., 2010). The clock gene *Per1* contains both, E-Box and GRE elements in its promoter; it is therefore responsive to both, BMAL1/CLOCK and GR binding (Conway-Campbell et al., 2010). Moreover, the nuclear receptor *Rev-ERBα* is repressed by GR activity through negative GREs present in its promoter (Surjit et al., 2011).

The clock machinery and GR also interact at the protein level. It has been shown that Rev-ERBα, GRs and HSP90 interact in the cytosol (Okabe et al., 2016). Moreover, Rev-ERBα and GR distribute differentially between the nuclei and the cytosol depending on the phase of the clock, suggesting a possible influence of each other with regard to intracellular trafficking (Surjit et al., 2011; Okabe et al., 2016). The above-mentioned interaction has been shown in cultured fibroblast, whether this mechanism is also present in brain cells needs to be determined. CLOCK harbors a histone-acetyl-transferase activity which is able to alter the affinity of GR to GREs through acetylation of lysine clusters in its hinge region (Nader et al., 2010). Also, CRY proteins are able to decrease GR's transactivation potential by interacting directly with GR (Lamia et al., 2011). These multiple and reciprocal molecular interactions stress the relevance of both pathways for the cellular and systemic regulation of circadian rhythms.

3. Glucocorticoids during circadian system development

During pregnancy, maternal physiology including the circadian system has to adapt to fulfill fetal requirements. During the first two thirds of pregnancy, the embryo/fetus is protected by the placenta from excessive levels of GCs by expressing (among others) the enzyme 11β-Hydroxysteroid dehydrogenase (11β-HSD2) which inactivates GCs converting them into an inactive metabolite, cortisone (O'Donnell et al., 2012). Even though only 10% of maternal GCs reach the fetus, a circadian rhythmicity of GCs can still be detected in fetal blood (Astiz et al., 2020). During the last third of pregnancy, there is a gradual

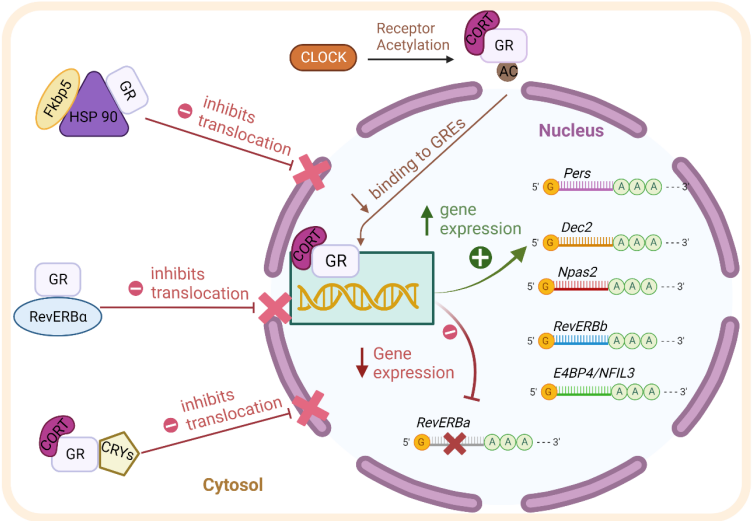

FIGURE 1
Scheme of the reciprocal molecular interaction between GR and the clock machinery at transcriptional, translational, and post-translational levels as described in detail in the text. BMAL1: brain and muscle aryl hydrocarbon receptor nuclear translocator-like 1. CLOCK: circadian locomotor output cycles kaput. *Pers: Periods. Dec2: differentially expressed in Chondrocytes 2. Npas2: Neuronal PAS Domain-Containing Protein 2. RevErb-beta: Nuclear Receptor Subfamily 1 Group D Member 2.* AC: acetyl group. GR: Glucocorticoid receptor. RevERb-Alpha: Nuclear Receptor Subfamily 1 Group D Member 1. CRY1/2 (Cryptochrome 1/2). HSP90: Heat shock protein 90. FKBP5: FK506-binding protein 5. CORT: Corticosterone.

increase of GC levels in fetal blood (Atkinson and Waddell, 1995) that helps the fetus to continue developing and growing (Fowden et al., 2022). This is partly due to a down-regulation of 11β-HSD2 (Wieczorek et al., 2019). Therefore, even if GC concentration changes over pregnancy, the circadian rhythmicity is always present, and since GR is expressed at high levels in the fetal hypothalamus (including the SCN during that period), it could be a key signal driving the development and maturation of the circadian system and its coupling to the HPA axis (Astiz et al., 2020; Greiner et al., 2022).

Indeed, extensive evidence shows that maternal stress or circadian rhythm disruption (e.g., through altered photoperiod, sleep deprivation, shift work) leads to a higher risk of developing metabolic, behavioral, and sleep disorders later in life (Moisiadis and Matthews, 2014b; Vilches et al., 2014; Marín, 2016; Mendez et al., 2016; Logan and McClung, 2019; Lužná et al., 2020). Interestingly, due to the close SCN-HPA axis relationship most of the experimental paradigms assessing the long-term effects of maternal stress used in nocturnal rodents entail some degree of circadian disruption because animals are subjected to different manipulations during their normal rest/light phase. Reciprocally, circadian disruption paradigms entail a certain degree of activation of the stress system. This issue was disentangled recently by our lab, when we demonstrated that the offspring from mothers exposed to GCs during the rest phase show worse circadian and stress-related behavioral phenotypes than those from mothers exposed to the same GC concentration, but during the active phase. This means that the effect of prenatal GCs activating epigenetic mechanisms and programming offspring behavior depends on the maternal exposure time (Astiz et al., 2020). We have found that when GC exposure happens, GR in the fetal hypothalamus is activated only if the signal reaches the tissue during the inactive phase. This time-dependent sensitivity to GCs in the fetal hypothalamus was gated by an autonomous function of the fetal molecular clock (Astiz et al., 2020). Then, the maturation of the clock and stress axis of the newborn seems to depend not only on maternal GCs but also on GR sensitivity, which is time-dependent.

4. Glucocorticoids and the adult circadian system

From a physiological point of view, an efficient synchronization of the circadian system would require that central or peripheral signals feedback to the SCN to adjust its function according to the internal environment. In the adult, SCN hypothalamic efferences reach the sub-PVN, PVN, supraoptic nuclei (SON), dorsomedial nucleus (DMH), and the arcuate nucleus (ARC) among many others (Saeb-Parsy et al., 2000; Kalsbeek et al., 2004; Postnova et al., 2013; Buijs et al., 2017) and some of those connections are reciprocal (e.g., with the ARC). However, the SCN clock is quite resistant to re-setting signals. This property, so far attributed to the robust network feature of the SCN circuit, might be important to prevent the impact of *Zeitgeber* noise such as sporadic light exposure, acute stress, or miss-timed food intake on the central pacemaker (Schibler et al., 2015).

GCs, as one of the main outputs of the circadian system, might feedback to the SCN, however, it is still under discussion whether the influence is direct or indirect (Balsalobre et al., 2000). In the early 90s, it was demonstrated that SCN neurons are among the few cell types in adult rodents that do not express GR (Rosenfeld et al., 1988). Interestingly, experiments manipulating GC circadian phase have shown that, GCs have a key role in circadian resynchronization of locomotor activity after jetlag, indicating a clear influence on the SCN (Kiessling et al., 2010). Furthermore, either the removal of the adrenal glands or the restitution of the hormone within physiological limits in adrenalectomized rats, demonstrated that glucocorticoids are involved in plastic rearrangements of the SCN circuit (Maurel et al., 2000). These ultrastructural arrangements have been observed over the 24 h cycle characterized by day/night changes of the glial, axon terminal, and/or somato-dendritic coverage of neurons expressing arginine vasopressin (AVP) or vasoactive intestinal peptide (VIP) (Becquet et al., 2008).

As mentioned before, we know now that astrocytes play a key role as time-keepers of the adult SCN. Astrocytes express the molecular clock machinery with self-sustained circadian rhythms that persist even in constant environmental conditions (Prolo et al., 2005; Marpegan et al., 2009; Barca-Mayo et al., 2017). The molecular clock in SCN astrocytes is entrainable by neuronal signals (Marpegan et al., 2009), temperature changes (Prolo et al., 2005), and they reciprocally modulate neuronal rhythms (Barca-Mayo et al., 2017). Additionally, several astroglial functions are under circadian control such as, intracellular Ca^{2+} waves (Brancaccio et al., 2017) and the release of gliotransmitters, ATP (Burkeen et al., 2011) and glutamate (Svobodova et al., 2018) and even their morphological changes during the day (Becquet et al., 2008). Interestingly, we have found GR expression in the SCN of adult mice colocalizing with glial fibrillary acidic protein (GFAP) a marker of mature astrocytes (Figure 2) confirming previous observations (Moriya et al., 2000; Leone et al., 2006). Although this needs further investigation it opens the possibility that not only neurons but also astrocytes might play an essential role in the complex cooperation between the SCN, the HPA axis and the systemic coordination of circadian rhythms.

5. Perspective

In summary, accumulating evidence suggests that GCs play an important role in the development and maturation of the circadian system. This, in turn, feeds back on stress axis regulation in the adult. Glial clocks may play an important role in this context, but experimental evidence for this is still sparse. To causally address such interaction, it would be important to study clock system development in animals with alterations in glial clock function and how glial disruption affects clock and stress regulation in the offspring. With regard to humans, the relevance of perinatal rhythms for shaping circadian system regulation and stress responses offers tremendous potential for therapeutic interventions. Can stabilization of GC rhythms during the end of pregnancy lead to increased resilience of the offspring against stress and stress-associated disorders, and what type of interventions beyond GC treatment are efficient in this context? To which extent is GC perinatal programming reversible later in life, and—against the background of the broad impact of stress hormones on physiological functions—what other systems are affected? Finally, how does GC programming affect glial function later in life, and what does this mean for neuro-immunologic

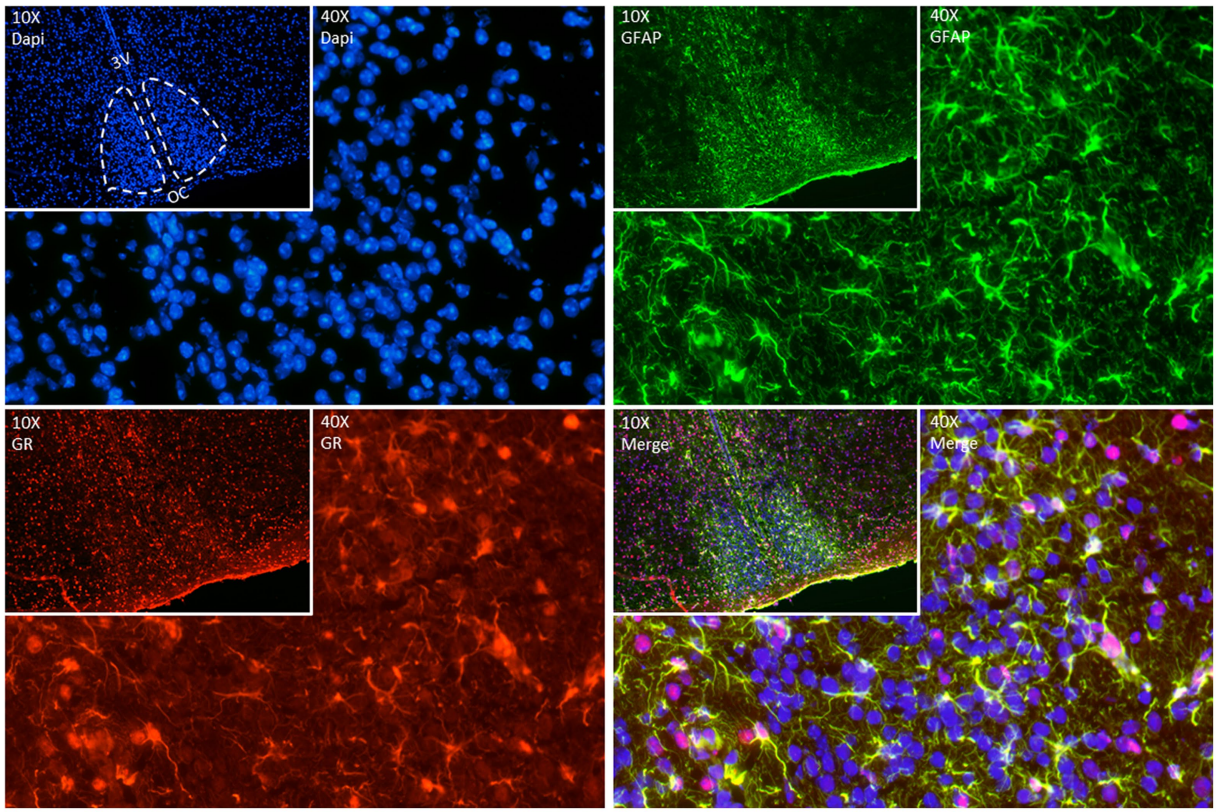

FIGURE 2
Representative double fluorescence immunostainings in the adult SCN. GFAP (green) used as an astrocyte marker, GR (red) and DAPI (blue) as a nuclear marker. Brain was collected from a 90-day old mouse at ZT (Zeitgeber time) 7, immediately frozen on dry ice, and sectioned (12μm) in a cryostat. After fixation (20min at room temperature (RT)), sections were blocked with goat serum 4% in phosphate buffer (PBS) containing 0.4% of Triton X-100 for 1h at RT. Sections were incubated with anti-GR (Abcam Ab183127, 1:200 in blocking) for 2 nights at 4°C. Sections were incubated afterwards with anti-GFAP (ThermoFisher 14–9,892-82, 1:200 in blocking) for 1 night at 4°C. The day after, sections were incubated with secondary antibodies – goat anti-rabbit Alexa 594 (ThermoFisher A11012, 1:500) and goat anti-mouse Alexa 488 (ThermoFisher A11029, 1:500) in a dark chamber for 2h at RT. DAPI staining was performed to stain nuclei by incubating slides with 300nM DAPI (ThermoFisher D1306) in PBS for 2min in the dark. Images of immunofluorescent staining were made using Nikon Ts2R-FL (10X (insets) and 40X magnification).

disorders? First steps in this direction have been taken with the studies on perinatal GC treatments (Astiz et al., 2020). It will be interesting to further decipher the underlying mechanisms of GC-fetal rhythm interaction and search for additional factors that impinge on this crosstalk.

Author contributions

All authors listed have made a substantial, direct, and intellectual contribution to the work and approved it for publication.

Funding

This work was supported by the German Research Foundation (DFG) grant AS547-1/2 (to ML and MA) and OS353-10/1 (to HO), by Spanish Research Grants PID2021-122694OB-I00 funded by Ministerio de Ciencia e Innovacion (MCIN) to MA and KH, by Achucarro Basque Center for Neuroscience and Basque Foundation of Science (Ikerbasque) to MA, and by the Federation of the European Biochemical Societies (FEBS) Summer Fellowship 2022 (to KH).

Acknowledgments

The authors would like to thank Beatrix Mahnke and Cecile Demarez, students at the Institute of Neurobiology, University of Lübeck for their contribution optimizing the immunofluorescence protocol.

Conflict of interest

The authors declare that the research was conducted in the absence of any commercial or financial relationships that could be construed as a potential conflict of interest.

Publisher's note

References

Antunica-Noguerol, M., Budziński, M. L., Druker, J., Gassen, N. C., Sokn, M. C., Senin, S., et al. (2016). The activity of the glucocorticoid receptor is regulated by SUMO conjugation to FKBP51. *Cell Death Differ.* 23, 1579–1591. doi: 10.1038/cdd.2016.44

Astiz, M., Heyde, I., Fortmann, M. I., Bossung, V., Roll, C., Stein, A., et al. (2020). The circadian phase of antenatal glucocorticoid treatment affects the risk of behavioral disorders. *Nat. Commun.* 11:3593. doi: 10.1038/s41467-020-17429-5

Astiz, M., and Oster, H. (2018). Perinatal programming of circadian clock-stress crosstalk. *Neural Plast.* 2018, 1–12. doi: 10.1155/2018/5689165

Atkinson, H. C., and Waddell, B. J. (1995). The hypothalamic-pituitary-adrenal axis in rat pregnancy and lactation: circadian variation and interrelationship of plasma adrenocorticotropin and corticosterone. *Endocrinology* 136, 512–520. doi: 10.1210/endo.136.2.7835284

Balsalobre, A., Brown, S. A., Marcacci, L., Tronche, F., Kellendonk, C., Reichardt, H. M., et al. (2000). Resetting of circadian time in peripheral tissues by glucocorticoid signaling. *Science (New York, N.Y.)* 289, 2344–2347. doi: 10.1126/science.289.5488.2344

Barca-Mayo, O., Pons-Espinal, M., Follert, P., Armirotti, A., Berdondini, L., and De Pietri Tonelli, D. (2017). Astrocyte deletion of Bmal1 alters daily locomotor activity and cognitive functions via GABA signalling. *Nat. Commun.* 8:14336. doi: 10.1038/ncomms14336

Becquet, D., Girardet, C., Guillaumond, F., François-Bellan, A.-M., and Bosler, O. (2008). Ultrastructural plasticity in the rat suprachiasmatic nucleus. Possible involvement in clock entrainment. *Glia* 56, 294–305. doi: 10.1002/glia.20613

Biebl, M. M., and Buchner, J. (2019). Structure, function, and regulation of the Hsp90 machinery. *Cold Spring Harb. Perspect. Biol.* 11:a034017. doi: 10.1101/cshperspect.a034017

Binder, E. B. (2009). The role of FKBP5, a co-chaperone of the glucocorticoid receptor in the pathogenesis and therapy of affective and anxiety disorders. *Psychoneuroendocrinology* 34, S186–S195. doi: 10.1016/j.psyneuen.2009.05.021

Brancaccio, M., Edwards, M. D., Patton, A. P., Smyllie, N. J., Chesham, J. E., Maywood, E. S., et al. (2019). Cell-autonomous clock of astrocytes drives circadian behavior in mammals. *Science (New York, N.Y.)* 363, 187–192. doi: 10.1126/science.aat4104

Brancaccio, M., Patton, A. P., Chesham, J. E., Maywood, E. S., and Hastings, M. H. (2017). Astrocytes control circadian timekeeping in the Suprachiasmatic nucleus via Glutamatergic signaling. *Neuron* 93, 1420–1435.e5. doi: 10.1016/j.neuron.2017.02.030

Buijs, F. N., Guzmán-Ruiz, M., León-Mercado, L., Basualdo, M. C., Escobar, C., Kalsbeek, A., et al. (2017). Suprachiasmatic nucleus interaction with the arcuate nucleus; essential for organizing physiological rhythms. *ENeuro* 4:ENEURO.0028-17.2017. doi: 10.1523/ENEURO.0028-17.2017

Buijs, R. M., Kalsbeek, A., van der Woude, T. P., van Heerikhuize, J. J., and Shinn, S. (1993). Suprachiasmatic nucleus lesion increases corticosterone secretion. *Am. J. Phys.* 264, R1186–R1192. doi: 10.1152/ajpregu.1993.264.6.R1186

Burkeen, J. F., Womac, A. D., Earnest, D. J., and Zoran, M. J. (2011). Mitochondrial calcium signaling mediates rhythmic extracellular ATP accumulation in suprachiasmatic nucleus astrocytes. *J. Neurosci. Off. J. Soc. Neurosci.* 31, 8432–8440. doi: 10.1523/JNEUROSCI.6576-10.2011

Busada, J. T., and Cidlowski, J. A. (2017). Mechanisms of glucocorticoid action during development. *Curr. Top. Dev. Biol.* 125, 147–170. doi: 10.1016/bs.ctdb.2016.12.004

Carmona-Alcocer, V., Rohr, K. E., Joye, D. A. M., and Evans, J. A. (2020). Circuit development in the master clock network of mammals. *Eur. J. Neurosci.* 51, 82–108. doi: 10.1111/ejn.14259

Čečmanová, V., Houdek, P., Šuchmanová, K., Sládek, M., and Sumová, A. (2019). Development and entrainment of the fetal clock in the Suprachiasmatic nuclei: the role of glucocorticoids. *J. Biol. Rhythm.* 34, 307–322. doi: 10.1177/0748730419835360

Collins, B., Pierre-Ferrer, S., Muheim, C., Lukacsovich, D., Cai, Y., Spinnler, A., et al. (2020). Circadian VIPergic neurons of the Suprachiasmatic nuclei sculpt the sleep-wake cycle. *Neuron* 108, 486–499.e5. doi: 10.1016/j.neuron.2020.08.001

Conway-Campbell, B. L., Sarabdjitsingh, R. A., McKenna, M. A., Pooley, J. R., Kershaw, Y. M., Meijer, O. C., et al. (2010). Glucocorticoid Ultradian rhythmicity directs cyclical gene pulsing of the clock gene period 1 in rat hippocampus. *J. Neuroendocrinol.* 22, 1093–1100. doi: 10.1111/j.1365-2826.2010.02051.x

Criado-Marrero, M., Rein, T., Binder, E. B., Porter, J. T., Koren, J., and Blair, L. J. (2018). Hsp90 and FKBP51: complex regulators of psychiatric diseases. *Philos. Trans. R. Soc. Lond. Ser. B Biol. Sci.* 373:20160532. doi: 10.1098/rstb.2016.0532

Daskalakis, N. P., Meijer, O. C., and de Kloet, E. R. (2022). Mineralocorticoid receptor and glucocorticoid receptor work alone and together in cell-type-specific manner: implications for resilience prediction and targeted therapy. *Neurobiology of Stress* 18:100455. doi: 10.1016/j.ynstr.2022.100455

Dibner, C., Schibler, U., and Albrecht, U. (2010). The mammalian circadian timing system: organization and coordination of central and peripheral clocks. *Annu. Rev. Physiol.* 72, 517–549. doi: 10.1146/annurev-physiol-021909-135821

Fowden, A. L., Vaughan, O. R., Murray, A. J., and Forhead, A. J. (2022). Metabolic consequences of glucocorticoid exposure before birth. *Nutrients* 14:2304. doi: 10.3390/nu14112304

Fries, G. R., Gassen, N. C., and Rein, T. (2017). The FKBP51 glucocorticoid receptor co-chaperone: regulation, function, and implications in health and disease. *Int. J. Mol. Sci.* 18:2614. doi: 10.3390/ijms18122614

Fuller, P. J., Yang, J., and Young, M. J. (2019). "Chapter three—mechanisms of mineralocorticoid receptor signaling" in *Vitamins and Hormones*. ed. G. Litwack, vol. *109* (Academic Press), 37–68.

Fuller, P. J., Yao, Y., Yang, J., and Young, M. J. (2012). Mechanisms of ligand specificity of the mineralocorticoid receptor. *J. Endocrinol.* 213, 15–24. doi: 10.1530/JOE-11-0372

George, C. L., Birnie, M. T., Flynn, B. P., Kershaw, Y. M., Lightman, S. L., and Conway-Campbell, B. L. (2017). Ultradian glucocorticoid exposure directs gene-dependent and tissue-specific mRNA expression patterns in vivo. *Mol. Cell. Endocrinol.* 439, 46–53. doi: 10.1016/j.mce.2016.10.019

Greiner, P., Houdek, P., Sládek, M., and Sumová, A. (2022). Early rhythmicity in the fetal suprachiasmatic nuclei in response to maternal signals detected by omics approach. *PLoS Biol.* 20:e3001637. doi: 10.1371/journal.pbio.3001637

Groeneweg, F. L., Karst, H., de Kloet, E. R., and Joëls, M. (2012). Mineralocorticoid and glucocorticoid receptors at the neuronal membrane, regulators of nongenomic corticosteroid signalling. *Mol. Cell. Endocrinol.* 350, 299–309. doi: 10.1016/j.mce.2011.06.020

Hannibal, J., Møller, M., Ottersen, O. P., and Fahrenkrug, J. (2000). PACAP and glutamate are co-stored in the retinohypothalamic tract. *J. Comp. Neurol.* 418, 147–155. doi: 10.1002/(SICI)1096-9861(20000306)418:2<147::AID-CNE2>3.0.CO;2-#

Hastings, M. H., Maywood, E. S., and Brancaccio, M. (2018). Generation of circadian rhythms in the suprachiasmatic nucleus. *Nat. Rev. Neurosci.* 19, 453–469. doi: 10.1038/s41583-018-0026-z

Ibuka, N., Inouye, S. I., and Kawamura, H. (1977). Analysis of sleep-wakefulness rhythms in male rats after suprachiasmatic nucleus lesions and ocular enucleation. *Brain Res.* 122, 33–47. doi: 10.1016/0006-8993(77)90660-6

Kabrita, C. S., and Davis, F. C. (2008). Development of the mouse suprachiasmatic nucleus: determination of time of cell origin and spatial arrangements within the nucleus. *Brain Res.* 1195, 20–27. doi: 10.1016/j.brainres.2007.12.020

Kalsbeek, A., Buijs, R. M., van Heerikhuize, J. J., Arts, M., and van der Woude, T. P. (1992). Vasopressin-containing neurons of the suprachiasmatic nuclei inhibit corticosterone release. *Brain Res.* 580, 62–67. doi: 10.1016/0006-8993(92)90927-2

Kalsbeek, A., La Fleur, S., Van Heijningen, C., and Buijs, R. M. (2004). Suprachiasmatic GABAergic inputs to the paraventricular nucleus control plasma glucose concentrations in the rat via sympathetic innervation of the liver. *J. Neurosci. Off. J. Soc. Neurosci.* 24, 7604–7613. doi: 10.1523/JNEUROSCI.5328-03.2004

Kalsbeek, A., Heerikhuize, J. J.Van, Wortel, J., and Buijs, R. M. (1996). A diurnal rhythm of stimulatory input to the Hypothalamo–pituitary–adrenal system as revealed by timed Intrahypothalamic administration of the vasopressin V1Antagonist. *J. Neurosci.*, 16 , 5555–5565, doi: 10.1523/JNEUROSCI.16-17-05555.1996

Kalsbeek, A., Yi, C.-X., Cailotto, C., la Fleur, S. E., Fliers, E., and Buijs, R. M. (2011). Mammalian clock output mechanisms. *Essays Biochem.* 49, 137–151. doi: 10.1042/bse0490137

Kiessling, S., Eichele, G., and Oster, H. (2010). Adrenal glucocorticoids have a key role in circadian resynchronization in a mouse model of jet lag. *J. Clin. Invest.* 120, 2600–2609. doi: 10.1172/JCI41192

Klengel, T., Mehta, D., Anacker, C., Rex-Haffner, M., Pruessner, J. C., Pariante, C. M., et al. (2013). Allele-specific FKBP5 DNA demethylation mediates gene–childhood trauma interactions. *Nat. Neurosci.* 16, 33–41. doi: 10.1038/nn.3275

Koch, C. E., Begemann, K., Kiehn, J. T., Griewahn, L., Mauer, J., Hess, M. E., et al. (2020). Circadian regulation of hedonic appetite in mice by clocks in dopaminergic neurons of the VTA. *Nat. Commun.* 11:3071. doi: 10.1038/s41467-020-16882-6

Kolber, B. J., Wieczorek, L., and Muglia, L. J. (2008). Hypothalamic-pituitary-adrenal axis dysregulation and behavioral analysis of mouse mutants with altered glucocorticoid or mineralocorticoid receptor function. *Stress (Amsterdam, Netherlands)* 11, 321–338. doi: 10.1080/10253890701821081

Lambrou, G. I., Kino, T., Koide, H., Ng, S. S. M., Geronikolou, S. A., Bacopoulou, F., et al. (2021). Bioinformatics analyses of spatial peripheral circadian clock-mediated gene expression of glucocorticoid receptor-related genes. *Adv. Exp. Med. Biol.* 1338, 67–79. doi: 10.1007/978-3-030-78775-2_9

Lamia, K. A., Papp, S. J., Yu, R. T., Barish, G. D., Uhlenhaut, N. H., Jonker, J. W., et al. (2011). Cryptochromes mediate rhythmic repression of the glucocorticoid receptor. *Nature* 480, 552–556. doi: 10.1038/nature10700

Landgraf, D., Achten, C., Dallmann, F., and Oster, H. (2015). Embryonic development and maternal regulation of murine circadian clock function. *Chronobiol. Int.* 32, 416–427. doi: 10.3109/07420528.2014.986576

Lehman, M. N., Silver, R., Gladstone, W. R., Kahn, R. M., Gibson, M., and Bittman, E. L. (1987). Circadian rhythmicity restored by neural transplant.

Immunocytochemical characterization of the graft and its integration with the host brain. *J. Neurosci. Off. J. Soc. Neurosci.* 7, 1626–1638.

Leone, M. J., Marpegan, L., Bekinschtein, T. A., Costas, M. A., and Golombek, D. A. (2006). Suprachiasmatic astrocytes as an interface for immune-circadian signalling. *J. Neurosci. Res.* 84, 1521–1527. doi: 10.1002/jnr.21042

Liston, C., Cichon, J. M., Jeanneteau, F., Jia, Z., Chao, M. V., and Gan, W.-B. (2013). Circadian glucocorticoid oscillations promote learning-dependent synapse formation and maintenance. *Nat. Neurosci.* 16, 698–705. doi: 10.1038/nn.3387

Logan, R. W., and McClung, C. A. (2019). Rhythms of life: circadian disruption and brain disorders across the lifespan. *Nat. Rev. Neurosci.* 20, 49–65. doi: 10.1038/s41583-018-0088-y

Lužná, V., Houdek, P., Liška, K., and Sumová, A. (2020). Challenging the integrity of rhythmic maternal signals revealed gene-specific responses in the fetal Suprachiasmatic nuclei. *Front. Neurosci.* 14:613531. doi: 10.3389/fnins.2020.613531

Marín, O. (2016). Developmental timing and critical windows for the treatment of psychiatric disorders. *Nat. Med.* 22, 1229–1238. doi: 10.1038/nm.4225

Marpegan, L., Krall, T. J., and Herzog, E. D. (2009). Vasoactive intestinal polypeptide entrains circadian rhythms in astrocytes. *J. Biol. Rhythm.* 24, 135–143. doi: 10.1177/0748730409332042

Maurel, D., Sage, D., Mekaouche, M., and Bosler, O. (2000). Glucocorticoids up-regulate the expression of glial fibrillary acidic protein in the rat suprachiasmatic nucleus. *Glia* 29, 212–221. doi: 10.1002/(sici)1098-1136(20000201)29:3<212::aid-glia3>3.0.co;2-6

Mazaira, G. I., and Galigniana, M. D. (2019). Reconstitution of the steroid receptor Heterocomplex. *Methods Mol. Biol. (Clifton, N.J.)* 1966, 125–135. doi: 10.1007/978-1-4939-9195-2_10

Mendez, N., Halabi, D., Spichiger, C., Salazar, E. R., Vergara, K., Alonso-Vasquez, P., et al. (2016). Gestational Chronodisruption impairs circadian physiology in rat male offspring, increasing the risk of chronic disease. *Endocrinology* 157, 4654–4668. doi: 10.1210/en.2016-1282

Moisiadis, V. G., and Matthews, S. G. (2014a). Glucocorticoids and fetal programming part 1: outcomes. *Nat. Rev. Endocrinol.* 10, 391–402. doi: 10.1038/nrendo.2014.73

Moisiadis, V. G., and Matthews, S. G. (2014b). Glucocorticoids and fetal programming part 2: mechanisms. *Nat. Rev. Endocrinol.* 10, 403–411. doi: 10.1038/nrendo.2014.74

Moore, R. Y., and Eichler, V. B. (1972). Loss of a circadian adrenal corticosterone rhythm following suprachiasmatic lesions in the rat. *Brain Res.* 42, 201–206. doi: 10.1016/0006-8993(72)90054-6

Moriya, T., Yoshinobu, Y., Kouzu, Y., Katoh, A., Gomi, H., Ikeda, M., et al. (2000). Involvement of glial fibrillary acidic protein (GFAP) expressed in astroglial cells in circadian rhythm under constant lighting conditions in mice. *J. Neurosci. Res.* 60, 212–218. doi: 10.1002/(SICI)1097-4547(20000415)60:2<212::AID-JNR10>3.0.CO;2-P

Munekawa, K., Tamada, Y., Iijima, N., Hayashi, S., Ishihara, A., Inoue, K., et al. (2000). Development of astroglial elements in the suprachiasmatic nucleus of the rat: with special reference to the involvement of the optic nerve. *Exp. Neurol.* 166, 44–51. doi: 10.1006/exnr.2000.7490

Nader, N., Chrousos, G. P., and Kino, T. (2010). Interactions of the circadian CLOCK system and the HPA axis. *Trends Endocrinol. Metab.* 21, 277–286. doi: 10.1016/j.tem.2009.12.011

Nagai, K., Nishio, T., Nakagawa, H., Nakamura, S., and Fukuda, Y. (1978). Effect of bilateral lesions of the suprachiasmatic nuclei on the circadian rhythm of food-intake. *Brain Res.* 142, 384–389. doi: 10.1016/0006-8993(78)90648-0

Nicolaides, N. C., Chrousos, G., and Kino, T. (2000). "Glucocorticoid receptor" in *Endotext*. eds. K. R. Feingold, B. Anawalt, A. Boyce, G. Chrousos, W. W. de Herder and K. Dhatariyaet al. (MDText.com, Inc.) Available at: http://www.ncbi.nlm.nih.gov/books/NBK279171/

O'Donnell, K. J., Bugge Jensen, A., Freeman, L., Khalife, N., O'Connor, T. G., and Glover, V. (2012). Maternal prenatal anxiety and downregulation of placental 11β-HSD2. *Psychoneuroendocrinology* 37, 818–826. doi: 10.1016/j.psyneuen.2011.09.014

Oakley, R. H., Whirledge, S. D., Petrillo, M. G., Riddick, N. V., Xu, X., Moy, S. S., et al. (2021). Combinatorial actions of glucocorticoid and mineralocorticoid stress hormone receptors are required for preventing neurodegeneration of the mouse hippocampus. *Neurobiol. Stress* 15:100369. doi: 10.1016/j.ynstr.2021.100369

Okabe, T., Chavan, R., Fonseca Costa, S. S., Brenna, A., Ripperger, J. A., and Albrecht, U. (2016). REV-ERBα influences the stability and nuclear localization of the glucocorticoid receptor. *J. Cell Sci.* 129, 4143–4154. doi: 10.1242/jcs.190959

Olejníková, L., Polidarová, L., and Sumová, A. (2018). Stress affects expression of the clock gene Bmal1 in the suprachiasmatic nucleus of neonatal rats via glucocorticoid-dependent mechanism. *Acta Physiol. (Oxf.)* 223:e13020. doi: 10.1111/apha.13020

Oster, H., Damerow, S., Kiessling, S., Jakubcakova, V., Abraham, D., Tian, J., et al. (2006). The circadian rhythm of glucocorticoids is regulated by a gating mechanism residing in the adrenal cortical clock. *Cell Metab.* 4, 163–173. doi: 10.1016/j.cmet.2006.07.002

Oyamada, N., Sone, M., Miyashita, K., Park, K., Taura, D., Inuzuka, M., et al. (2008). The role of mineralocorticoid receptor expression in brain remodeling after cerebral ischemia. *Endocrinology* 149, 3764–3777. doi: 10.1210/en.2007-1770

Pevet, P., and Challet, E. (2011). Melatonin: both master clock output and internal time-giver in the circadian clocks network. *J. Physiol. Paris* 105, 170–182. doi: 10.1016/j.jphysparis.2011.07.001

Pezük, P., Mohawk, J. A., Wang, L. A., and Menaker, M. (2012). Glucocorticoids as entraining signals for peripheral circadian oscillators. *Endocrinology* 153, 4775–4783. doi: 10.1210/en.2012-1486

Postnova, S., Fulcher, R., Braun, H. A., and Robinson, P. A. (2013). A minimal physiologically based model of the HPA axis under influence of the sleep-wake cycles. *Pharmacopsychiatry* 46 Suppl 1, S36–S43. doi: 10.1055/s-0033-1333763

Pratt, W. B., and Toft, D. O. (1997). Steroid receptor interactions with heat shock protein and immunophilin chaperones. *Endocr. Rev.* 18, 306–360. doi: 10.1210/edrv.18.3.0303

Prolo, L. M., Takahashi, J. S., and Herzog, E. D. (2005). Circadian rhythm generation and entrainment in astrocytes. *J. Neurosci. Off. J. Soc. Neurosci.* 25, 404–408. doi: 10.1523/JNEUROSCI.4133-04.2005

Reddy, T. E., Pauli, F., Sprouse, R. O., Neff, N. F., Newberry, K. M., Garabedian, M. J., et al. (2009). Genomic determination of the glucocorticoid response reveals unexpected mechanisms of gene regulation. *Genome Res.* 19, 2163–2171. doi: 10.1101/gr.097022.109

Rimmele, U., Meier, F., Lange, T., and Born, J. (2010). Suppressing the morning rise in cortisol impairs free recall. *Learn. Mem.* 17, 186–190. doi: 10.1101/lm.1728510

Romero, M. T., Lehman, M. N., and Silver, R. (1993). Age of donor influences ability of suprachiasmatic nucleus grafts to restore circadian rhythmicity. *Brain Res. Dev. Brain Res.* 71, 45–52. doi: 10.1016/0165-3806(93)90103-h

Rosenfeld, P., Van Eekelen, J. A. M., Levine, S., and De Kloet, E. R. (1988). Ontogeny of the type 2 glucocorticoid receptor in discrete rat brain regions: an immunocytochemical study. *Dev. Brain Res.* 42, 119–127. doi: 10.1016/0165-3806(88)90207-6

Saeb-Parsy, K., Lombardelli, S., Khan, F. Z., McDowall, K., Au-Yong, I. T., and Dyball, R. E. (2000). Neural connections of hypothalamic neuroendocrine nuclei in the rat. *J. Neuroendocrinol.* 12, 635–648. doi: 10.1046/j.1365-2826.2000.00503.x

Schibler, U., Gotic, I., Saini, C., Gos, P., Curie, T., Emmenegger, Y., et al. (2015). Clock-talk: interactions between central and peripheral circadian oscillators in mammals. *Cold Spring Harb. Symp. Quant. Biol.* 80, 223–232. doi: 10.1101/sqb.2015.80.027490

Sekaran, S., Lupi, D., Jones, S. L., Sheely, C. J., Hattar, S., Yau, K.-W., et al. (2005). Melanopsin-dependent photoreception provides earliest light detection in the mammalian retina. *Curr. Biol.* 15, 1099–1107. doi: 10.1016/j.cub.2005.05.053

Silver, R., LeSauter, J., Tresco, P. A., and Lehman, M. N. (1996). A diffusible coupling signal from the transplanted suprachiasmatic nucleus controlling circadian locomotor rhythms. *Nature* 382, 810–813. doi: 10.1038/382810a0

So, A. Y.-L., Bernal, T. U., Pillsbury, M. L., Yamamoto, K. R., and Feldman, B. J. (2009). Glucocorticoid regulation of the circadian clock modulates glucose homeostasis. *Proc. Natl. Acad. Sci. U. S. A.* 106, 17582–17587. doi: 10.1073/pnas.0909733106

Son, G. H., Chung, S., Choe, H. K., Kim, H.-D., Baik, S.-M., Lee, H., et al. (2008). Adrenal peripheral clock controls the autonomous circadian rhythm of glucocorticoid by causing rhythmic steroid production. *Proc. Natl. Acad. Sci. U. S. A.* 105, 20970–20975. doi: 10.1073/pnas.0806962106

Surjit, M., Ganti, K. P., Mukherji, A., Ye, T., Hua, G., Metzger, D., et al. (2011). Widespread negative response elements mediate direct repression by agonist- Liganded glucocorticoid receptor. *Cells* 145, 224–241. doi: 10.1016/j.cell.2011.03.027

Svobodova, I., Bhattaracharya, A., Ivetic, M., Bendova, Z., and Zemkova, H. (2018). Circadian ATP release in Organotypic cultures of the rat Suprachiasmatic nucleus is dependent on P2X7 and P2Y receptors. *Front. Pharmacol.* 9:192. doi: 10.3389/fphar.2018.00192

Takahashi, J. S. (2017). Transcriptional architecture of the mammalian circadian clock. *Nat. Rev. Genet.* 18, 164–179. doi: 10.1038/nrg.2016.150

Tso, C. F., Simon, T., Greenlaw, A. C., Puri, T., Mieda, M., and Herzog, E. D. (2017). Astrocytes regulate daily rhythms in the Suprachiasmatic nucleus and behavior. *Curr. Biol.* 27, 1055–1061. doi: 10.1016/j.cub.2017.02.037

Vilches, N., Spichiger, C., Mendez, N., Abarzua-Catalan, L., Galdames, H. A., Hazlerigg, D. G., et al. (2014). Gestational chronodisruption impairs hippocampal expression of NMDA receptor subunits Grin1b/Grin3a and spatial memory in the adult offspring. *PLoS One* 9:e91313. doi: 10.1371/journal.pone.0091313

Wieczorek, A., Perani, C. V., Nixon, M., Constancia, M., Sandovici, I., Zazara, D. E., et al. (2019). Sex-specific regulation of stress-induced fetal glucocorticoid surge by the mouse placenta. *Am. J. Physiol. Endocrinol. Metab.* 317, E109–E120. doi: 10.1152/ajpendo.00551.2018

frontiers | Frontiers in Neuroscience

TYPE Original Research
PUBLISHED 12 May 2023
DOI 10.3389/fnins.2023.1173537

OPEN ACCESS

EDITED BY
Daisuke Ono,
Nagoya University, Japan

REVIEWED BY
Koji L. Ode,
The University of Tokyo, Japan
Alicia Costa,
Universidad de la República, Uruguay

*CORRESPONDENCE
Arisa Hirano
✉ hirano.arisa.gt@u.tsukuba.ac.jp
Takeshi Sakurai
✉ sakurai.takeshi.gf@u.tsukuba.ac.jp

RECEIVED 24 February 2023
ACCEPTED 21 April 2023
PUBLISHED 12 May 2023

CITATION
Masuda K, Katsuda Y, Niwa Y, Sakurai T and Hirano A (2023) Analysis of circadian rhythm components in EEG/EMG data of aged mice. *Front. Neurosci.* 17:1173537. doi: 10.3389/fnins.2023.1173537

Analysis of circadian rhythm components in EEG/EMG data of aged mice

Kosaku Masuda[1,2], Yoko Katsuda[1,2], Yasutaka Niwa[1,2,3], Takeshi Sakurai[1,2]* and Arisa Hirano[1,2]*

[1]Institute of Medicine, University of Tsukuba, Tsukuba, Ibaraki, Japan, [2]International Institute for Integrative Sleep Medicine (WPI-IIIS), University of Tsukuba, Tsukuba, Ibaraki, Japan, [3]Graduate School of Medicine, Hirosaki University, Hirosaki, Aomori, Japan

Aging disrupts circadian clocks, as evidenced by a reduction in the amplitude of circadian rhythms. Because the circadian clock strongly influences sleep–wake behavior in mammals, age-related alterations in sleep–wake patterns may be attributable, at least partly, to functional changes in the circadian clock. However, the effect of aging on the circadian characteristics of sleep architecture has not been well assessed, as circadian behaviors are usually evaluated through long-term behavioral recording with wheel-running or infrared sensors. In this study, we examined age-related changes in circadian sleep–wake behavior using circadian components extracted from electroencephalography (EEG) and electromyography (EMG) data. EEG and EMG were recorded from 12 to 17-week-old and 78 to 83-week-old mice for 3days under light/dark and constant dark conditions. We analyzed time-dependent changes in the duration of sleep. Rapid eye movement (REM) and non-REM (NREM) sleep significantly increased during the night phase in old mice, whereas no significant change was observed during the light phase. The circadian components were then extracted from the EEG data for each sleep–wake stage, revealing that the circadian rhythm in the power of delta waves during NREM sleep was attenuated and delayed in old mice. Furthermore, we used machine learning to evaluate the phase of the circadian rhythm, with EEG data serving as the input and the phase of the sleep–wake rhythm (environmental time) as the output. The results indicated that the output time for the old mice data tended to be delayed, specifically at night. These results indicate that the aging process significantly impacts the circadian rhythm in the EEG power spectrum despite the circadian rhythm in the amounts of sleep and wake attenuated but still remaining in old mice. Moreover, EEG/EMG analysis is useful not only for evaluating sleep–wake stages but also for circadian rhythms in the brain.

KEYWORDS

sleep, aging, circadian rhythms, EEG, machine learning

1. Introduction

Many biological processes exhibit circadian rhythms that help organisms adapt to environmental cycles. These rhythms are regulated by the circadian clock, which is altered with aging (Hood and Amir, 2017). In mice, a long free-running period of the behavioral rhythm and a decrease in the ability to entrain environmental cycles have been observed (Nakamura et al., 2011; Sellix et al., 2012). Aging also affects sleep–wake behavior in animals, including humans

(Mander et al., 2017). In mice, the amount of sleep during the dark period generally increases, whereas wakefulness decreases with age (Wimmer et al., 2013; Panagiotou et al., 2017; McKillop et al., 2018). In addition to the sleep/wake ratio, the electroencephalography (EEG) power changes with age, suggesting that aging induces both quantitative and qualitative changes in sleep.

Sleep–wake patterns are strongly governed by the circadian clock, as evidenced by the considerable effect of mutations in the core clock genes on sleep–wake rhythms (Wisor et al., 2002; Laposky et al., 2005; Mang et al., 2016). Conversely, sleep deprivation and other sleep interventions also perturb circadian rhythms, as demonstrated by studies investigating the impact of such interventions on behavioral and physiological characteristics (Wisor et al., 2008; Hoekstra et al., 2021; Lu et al., 2021). These findings suggest a bidirectional relationship between sleep and the circadian clock, both of which have a profound mutual influence on each other. Nonetheless, sleep and circadian behavioral rhythms are commonly studied independently. Circadian behavior is often exemplified by the use of long-term activity recordings using wheels or infrared sensors under constant dark conditions (DD) to measure behavioral rhythms in rodents. Although such methods can capture free-running wheel-running/spontaneous activity rhythms or phase responses to stimulation, they present significant challenges in accurately tracking sleep–wake stages, such as wakefulness, rapid eye movement (REM) sleep, and non-REM (NREM) sleep, as well as in assessing qualitative changes in sleep.

In contrast, sleep evaluation typically involves EEG and electromyography (EMG). EEG represents brain activity patterns that are obtained from electrodes positioned near the surface of the mouse brain (dura mater) and is an important indicator for discerning sleep stages. However, analyzing EEG/EMG data is more time-consuming and complex than simply counting wheel-running activity sessions, which makes it challenging to use EEG/EMG to assess sleep for a long duration. Consequently, analysis evaluating circadian rhythms of sleep amount and quality using EEG/EMG has been relatively uncommon. Previous studies have evaluated diurnal variations in delta power during NREM sleep as an indicator of sleepiness, revealing periodic changes throughout the day (Wisor et al., 2008; Wimmer et al., 2013). Nevertheless, there have been limited comprehensive analyses of circadian fluctuations in the EEG power spectrum, and the impact of aging on these circadian components remains largely unknown.

In this study, we conducted a precise evaluation of circadian rhythms in sleep–wake patterns of aged mice, with a particular focus on the EEG power spectrum. We first confirmed that changes in sleep–wake patterns are associated with aging, as previously shown. We extracted circadian components from the EEG power spectrum of each sleep–wake stage and observed that time-dependent changes in the power spectrum during NREM sleep were significantly attenuated in aged mice. Furthermore, we developed a machine learning-based method to reconstruct circadian phases from short-term (1 h) EEG data, which enabled us to assess age-mediated circadian phase alterations at a higher time resolution. Specifically, we found that the circadian phase was significantly delayed at all sleep–wake stages in aged mice. Our method represents a promising high-throughput approach for evaluating the circadian phase and sleep scoring in future studies.

2. Materials and methods

2.1. Animals

All animal experiments were approved by the Animal Experiment and Use Committee of the University of Tsukuba and adhered to NIH guidelines. C57BL/6J wild-type male mice, purchased from The Jackson Laboratory, were used for EEG measurements. The young ($n = 13$) and aged ($n = 20$) mice were 12–17 weeks and 78–83 weeks old, respectively. Food and water were provided *ad libitum*.

2.2. Surgery

Male mice were anesthetized by isoflurane inhalation (Pfizer, United States) and fixed to a stereotaxic frame. The electrodes were implanted on the mouse cortex. Two stainless-steel screws for EEG recording were placed, each at +1.4 mm AP and + 1.2 mm ML from the bregma and − 2.6 mm AP and + 1.2 mm ML from the lambda and connected to a 4-pin headmount. Two insulated silver wires for EMG recording, connected to the same headmount, were inserted into the neck muscles bilaterally. An anchor screw was then positioned on the skull. The entire assembly was fixed to the skull with dental cement. The mouse skin was sutured using a sanitized thread.

2.3. EEG/EMG recording

EEG/EMG was recorded from freely moving mice as described previously (Hasegawa et al., 2022). Mice were entrained to a 12:12 light–dark (LD) cycle with lights turning on at 8:00 am and off at 8:00 pm. They were single-housed in a recording chamber for at least 3 days to habituate to the environment. EEG and EMG were recorded for 3 days under the LD condition 1–3 weeks after the electrode implantation surgery. The EEG/EMG signals were amplified and filtered (EEG: 0.5–250 Hz, EMG: 16–250 Hz). 50 Hz EEG and EMG signals were also filtered since the power supply frequency in Japan (50 Hz) possibly causes artificial noise signals. The EEG and EMG signals were acquired using SleepSignRecorder (KISSEI COMTEC, Nagano, Japan) at a sampling rate of 128 Hz, which is the same frequency as used in the previous study for the neural network model described later (Tezuka et al., 2021). Eight young mice and 10 aged mice were kept in the LD condition for 4 days after the measurement and then transferred to DD. The EEG and EMG of these mice were measured again from the second day in DD for 3 days. Environmental time is presented as zeitgeber time (ZT) under both LD and DD conditions.

2.4. Automated sleep–wake stage scoring using a neural network model

Sleep–wake stages were determined based on the UTSN-L model, which is a neural network model for automatic sleep–wake stage scoring developed in a previous study (Tezuka et al., 2021) using EEG/EMG data for 3 days in LD or DD. This model is a convolutional neural network using a one-channel EEG (raw

signal and spectrum) and zeitgeber time, and shows 90% overall accuracy. This model classifies every 10 s-EEG data into one of the following sleep–wake stages: wakefulness (WAKE), REM sleep, or NREM sleep. Because this model also uses past EEG data for prediction, it does not output results for the first 100 s. Therefore, the sleep–wake stages for the first 100 s were manually classified. The parameters for the model trained in a previous study[1] were also used for neural network scoring in this study. Because this model uses only EEG data, wakefulness was determined again by the threshold of EMG power after scoring. First, the $\log_{10}$ value of the standard deviation of the EMG power every 10 s was calculated as the amplitude. The threshold value was determined by applying Otsu's binarization (Otsu, 1979) to the amplitudes for all time periods. The epochs in which the EMG amplitude exceeded the threshold were determined as WAKE, regardless of the result of the neural network scoring. After sleep–wake stage scoring, the hourly averages of sleep/wake amounts were calculated, and the amplitude, phase, and period of the rhythm of each sleep–wake stage were determined by cosine fitting. Cosine fitting was performed with the least squares method using Python (lmfit).[2]

2.5. Calculation of circadian components in EEG power spectra

Fourier transform was performed for the EEG data every 10 s to obtain the EEG power spectra at each epoch, which corresponds to sleep–wake stage scoring. EEG power spectra were obtained for every 0.1 Hz from 0 to 16 Hz. The standard deviation of the EMG data every 10 s was calculated and defined as the EMG amplitude. The hourly average EEG power spectra and EMG amplitude for each sleep–wake stage were then calculated. Next, to determine the amplitude and phase of the EEG power rhythms, we obtained the amplitude A and the peak time t_p of the EEG power at each frequency. The EEG power was normalized as follows:

$$EEG_{norm,i,f} = \left(EEG_{hourly,i,f} - EEG_{ave,f}\right) / EEG_{ave,f} \quad (1)$$

$$EEG_{ave,f} = \frac{1}{T}\sum_{i=1}^{T} EEG_{hourly,i,f} \quad (2)$$

where $EEG_{hourly,i,f}$ and $EEG_{norm,i,f}$ are the hourly averaged EEG power and normalized EEG power at the i time point at the frequency f, respectively, $EEG_{ave,f}$ is the average EEG power, and T is the measurement length ($T = 72$ h). This calculation was performed for all frequencies. The first Fourier component was then obtained using the following equation:

$$COS = \frac{2}{T}\sum_{i=1}^{T} EEG_{norm,i} \cos\left(2\pi \frac{i\Delta t}{\tau}\right),$$
$$SIN = \frac{2}{T}\sum_{i=1}^{T} EEG_{norm,i} \sin\left(2\pi \frac{i\Delta t}{\tau}\right), \quad (3)$$

where $\tau = 24$ h and the average interval $\Delta t = 1$ h. Using COS and SIN, the amplitudes A and peak time t_p were determined as follows:

$$A = \sqrt{COS^2 + SIN^2}, \quad (4)$$

$$t_p = \arctan 2\left(SIN, COS\right) / 2\pi * 24 \quad (5)$$

We applied these calculations to EEG power rhythms at each frequency and sleep–wake stage.

2.6. Estimation of circadian time using EEG power spectra

We constructed phase estimation models using machine learning for the correspondence between the EEG power spectra of each sleep–wake stage and environmental time. The models were constructed using the normalized EEG power spectra of each sleep–wake stage as the input and the environmental time as the output. The spectral distribution was normalized by dividing each spectrum by the sum of the spectral densities. The environmental time is represented as a point on a circular unit, that is, $\left\{\cos\left(ZT / 24 * 2\pi\right), \sin\left(ZT / 24 * 2\pi\right)\right\}$, where ZT represents zeitgeber time, and the model was constructed for the x and y components. The subjective circadian time was estimated from the angle between x and y, that is, estimated time = $\arctan 2\left(y, x\right) / 2\pi * 24$. We used linear regression, the k-nearest neighbor method, a support vector machine, and a random forest algorithm as the regression models. Similarly, we estimated the subjective circadian time using the hourly averages of the spectrum without distinguishing sleep–wake stages and the spectral distribution of all sleep–wake stages as input. The Python library "scikitlearn" (version 1.2.0)[3] was used to construct each model. Default parameters were used for all the hyperparameters of each regression model. In the random forest algorithm, the importance of each input for estimation was also calculated using this library.

We evaluated the accuracy of the models by leave-one-out cross-validation using the LD condition of young mice as a control. First, we selected one of the mice, trained the model using the EEG data of the other mice, and predicted the subjective time of the selected mouse based on the trained model. This process was repeated for all mice to verify the accuracy of the model. Here, the accuracy of the estimation model was defined as the mean value of $\cos\left\{\left(\text{Estimated time} - ZT\right) / 24 * 2\pi\right\}$. When the estimation error is

1 https://github.com/tarotez/sleepstages

2 https://lmfit.github.io/lmfit-py

3 https://github.com/scikit-learn/scikit-learn

small, this value approaches 1, and when the estimated time is in reverse phase, i.e., Estimated time $-ZT=12$, it approaches -1. Therefore, the closer this value is to 1, the more accurate the prediction. For mice other than young and in the LD condition, prediction models were constructed based on data from all young mice in the LD condition, and the subjective time was predicted based on that model.

3. Results

3.1. Sleep–wake patterns in young and aged mice

In this study, we employed a neural network model (Tezuka et al., 2021) to analyze the sleep–wake stages of young (12–17 weeks old) and old mice (78–83 weeks old) under LD and DD conditions (Figure 1). To evaluate the accuracy of the automated scoring, a portion of the EEG data was manually scored (Supplementary Figure S1). The results indicated that during the dark period (ZT12-24), the duration of NREM and REM sleep increased, and wakefulness time decreased in old mice, whereas small changes were observed during the light period under LD conditions (Figure 2; Supplementary Figure S2). Young mice showed a sharp increase in wakefulness after the light-to-dark transition (ZT12), whereas the change was more gradual in aged mice. These results are consistent with those of previous studies (Wimmer et al., 2013; Panagiotou et al., 2017; McKillop et al., 2018). Likewise, in old mice under DD, there was an increase in the amount of sleep and a decrease in wakefulness during the subjective night. The amplitude of the sleep–wake rhythm, as calculated by their amounts, was decreased, and the phase was slightly delayed in old mice when the phase was calculated using the amounts of NREM and REM sleep (Supplementary Figures S3, S4). Additionally, old mice showed a large distribution in the peak time of each stage, suggesting a variation in the degree of circadian phase disturbance among aged individuals.

3.2. Circadian rhythm components in EEG

We utilized Fourier transformation to calculate EEG power spectra from data collected every 10 s and subsequently determined the average power spectra for each sleep–wake stage. The spectra varied between the light and dark phases for each sleep–wake stage (Figure 3), indicating that sleep quality was time-dependent. However, aged mice exhibited less pronounced variations in the EEG power spectra during NREM sleep between the light and dark periods than young mice. Similar fluctuations in the spectra were also observed between the subjective day (ZT0-12) and night (ZT12-24) under DD conditions (Supplementary Figure S5), implying the involvement of the circadian clock.

We calculated the hourly averaged EEG power and presented selected examples of EEG power rhythms at a specific frequency, where the changes in EEG power were large between day and night (Figure 4). Diurnal fluctuations in EEG power were evident across all sleep–wake stages in both the LD and DD conditions. The delta wave, generally regarded as a <4 Hz wave in NREM sleep that reflects drowsiness, exhibited reduced variability in aged mice during both LD and DD (Figure 4). Moreover, the rhythm amplitudes of EEG power

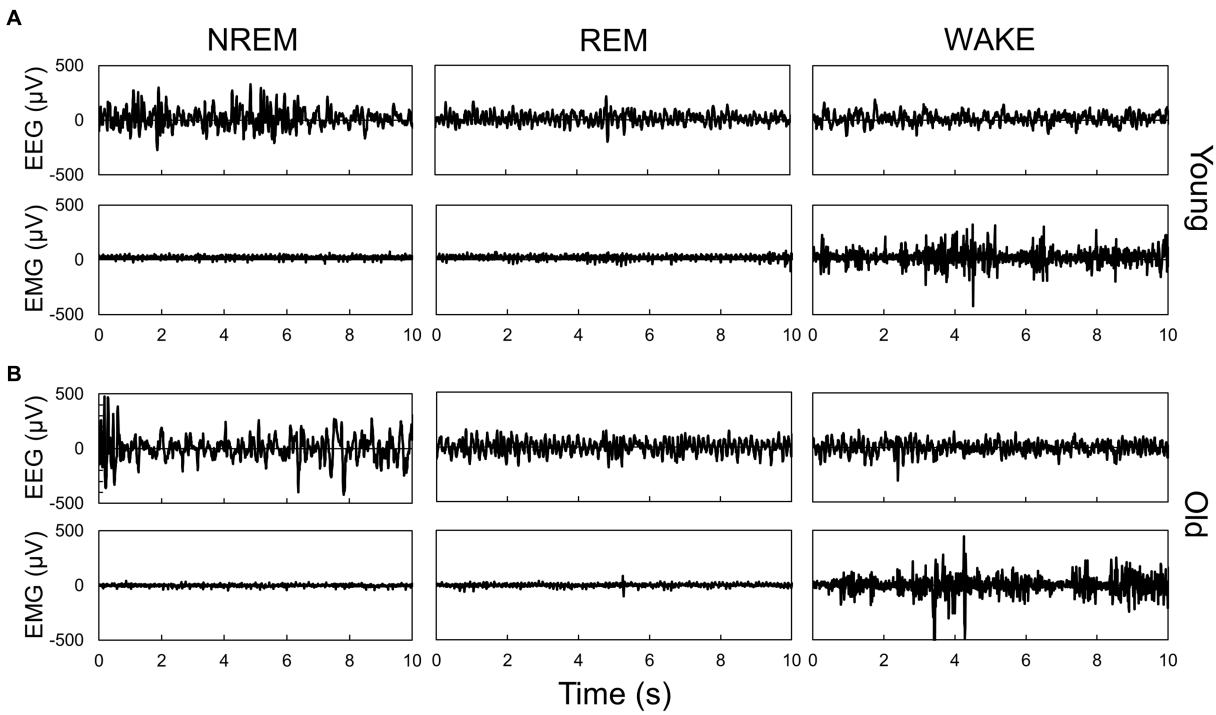

FIGURE 1
Representative EEG and EMG signals during each sleep–wake stage in young **(A)** and old **(B)** mice. Sleep–wake stage was determined by the neural network model. Each panel shows typical signals during each stage, which were scored by the neural network model.

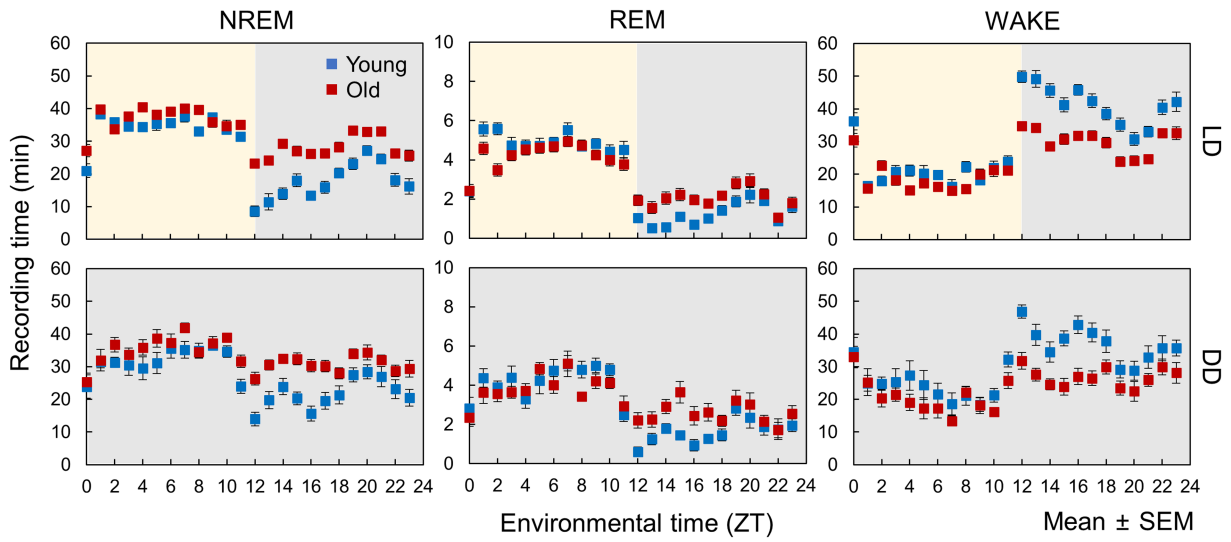

FIGURE 2
Sleep–wake patterns in young and old mice. Each point is the amount of each sleep–wake stage per hour (n=13 in young mice and 20 in old mice in LD, 8 in young mice and 10 in old mice in DD conditions). Error bars indicate standard error. Blue and red dots represent values for young and old mice, respectively. Yellow and gray areas indicate light and dark conditions, respectively. The results of the comparison of young and old mice by t-test at each time point are shown in Supplementary Figure S2.

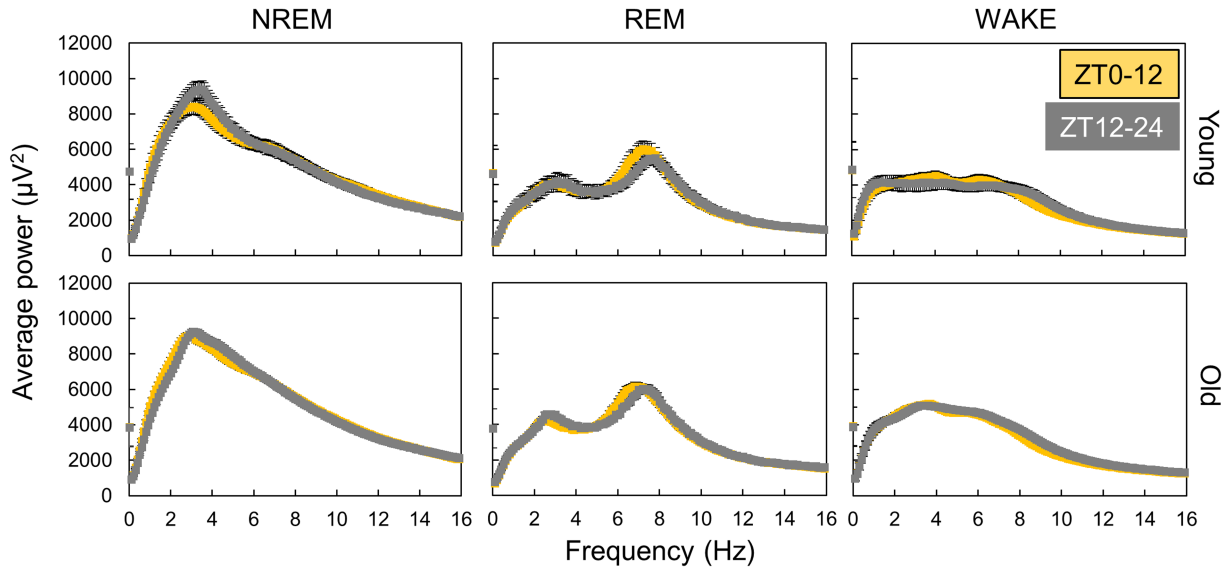

FIGURE 3
Variation in EEG power spectra during day and night. The points are the average of power spectra during day (ZT0-12) and night (ZT12-24) obtained by Fourier transform from EEG data every 10s (n=13 in young mice and 20 in old mice in LD). The interval of frequency is 0.1Hz. Error bars indicate standard error. Yellow and gray areas indicate light and dark conditions, respectively.

at 9 Hz during wakefulness in old mice were smaller than those of young mice in LD but not in DD, suggesting that light input may influence EEG power spectra and that this effect can be attenuated by aging.

To clarify the changes in circadian rhythm components in EEG with age, we calculated the amplitude and peak time of EEG power and EMG amplitude rhythms at each sleep–wake stage and frequency (Figure 5; Supplementary Figure S6). In the LD condition, EEG power at different frequencies peaked at different environmental times, in which the peak time continuously fluctuated according to the frequency (Figure 5A; Supplementary Figure S7A). The peak times of the specific frequencies also varied among sleep–wake stages. Peak times of EEG power rhythms tended to be distributed in the middle of the light or dark period (ZT = 6 or 18). However, some frequencies, such as 2 Hz in NREM, showed a peak around ZT0, suggesting that the rhythm of EEG power was not a result of the response to the light–dark transition but was regulated by an intrinsic signal from the circadian clock. The amplitude of the EEG power rhythms varied

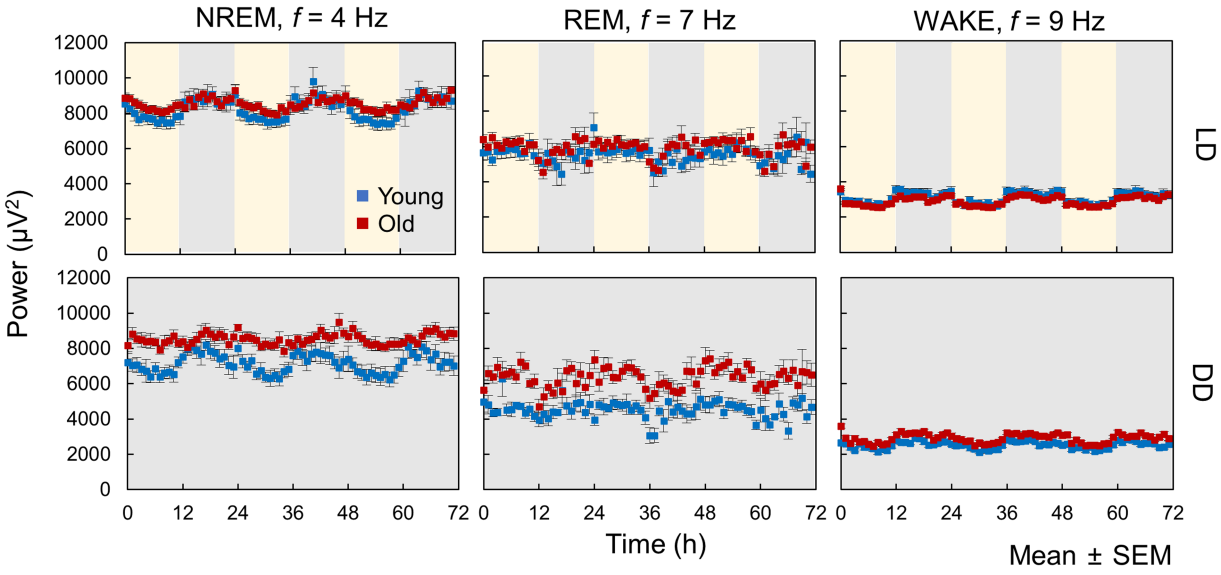

FIGURE 4
Circadian oscillation in EEG power. These data represent hourly averages of EEG power at 4Hz for NREM, 7Hz for REM, and 9Hz for WAKE (n=13 in young mice and 20 in old mice in LD, 8 in young mice and 10 in old mice in DD conditions). Error bars indicate standard error. Blue and red dots represent values for young and old mice, respectively. Yellow and gray areas indicate light and dark conditions, respectively.

among frequencies at each sleep–wake stage (Figure 5B; Supplementary Figure S6B). Compared with that in young mice, the peak time in old mice was delayed at most frequencies in NREM sleep and significantly shifted around 5 Hz in wakefulness. Interestingly, the peak time calculated by the amount of wakefulness showed no significant difference between the two groups (Supplementary Figure S3), indicating that the circadian sleep phase cannot be precisely evaluated only by the duration of sleep–wake stages. In contrast, the amplitude of EEG power rhythms at 4 Hz in NREM was significantly decreased in old mice (Figure 5B), as previously shown (Figure 4). In DD, the EEG power rhythms also exhibited amplitudes and peak times similar to those in the LD condition (Figures 5C,D). These results indicate that the rhythms in EEG power were autonomous and independent of light signals, in other words, regulated by the circadian clock. We also observed that the effects of aging were distinct at different sleep–wake stages.

3.3. Estimation of circadian time in aged mice

The evaluation of circadian rhythms typically involves determining the amplitude and phase (peak time) of the rhythm per cycle using methods such as cosine fitting. However, changes in circadian rhythms can be time-dependent, and a method that obtains a single phase and amplitude from the rhythm of multiple cycles may not capture the time-dependent changes in circadian rhythm. Notably, in old mice, sleep amounts significantly increased during only the night period (Figure 1), showing time-specific alternation. In contrast, recent studies have suggested a method to estimate the subjective time in individuals from RNA-seq data obtained at a single time point (Hesse et al., 2020). The molecular timetable method, a fundamental time estimation method that employs mRNA expression data, estimates subjective time by identifying which rhythmic genes are at peak or trough expression (Ueda et al., 2004). For example, if the Period genes that exhibit peak expression around CT12 are at their highest, the samples' subjective time is estimated as CT12. As depicted in Figure 4, the EEG power spectra showed different peak times depending on the frequency. In other words, each spectral distribution is presumed to possess a unique shape at each circadian time, enabling the estimation of mice's subjective time through spectral distributions.

In this study, we developed a circadian time estimation model based on the EEG power spectrum. To build the model, we used several fundamental machine learning algorithms, such as linear regression, k-nearest neighbor method, ridge regression, support vector machine, and random forest algorithm, to identify the most effective method for predicting the phase. The inputs were set to hourly normalized power spectra in NREM sleep, REM sleep, or wakefulness, hourly normalized power spectra without distinguishing sleep–wake stages, and all sets of spectra in each sleep–wake stage. We used normalized power spectra to reduce experimental errors in the EEG power, and the circadian rhythm component seen in Section 3.2 was also observed in the normalized power spectra (Supplementary Figures S8–S10). The outputs were set to the environmental time.

First, to assess the accuracy of each model, we conducted leave-one-out cross-validation using data from young mice in the LD condition (Figure 6A). Among the various machine learning algorithms, the random forest algorithm showed superior performance for all input types. The best performance was achieved when the sets of EEG power spectra and information on the sleep–wake stages were used. Feature importance analysis revealed that frequencies with larger circadian amplitudes, such as 4 Hz in NREM sleep (Figure 5), showed higher importance (Figure 6B). The estimation of circadian time can be broadly categorized into discriminating between day and night (SIN) and morning and evening

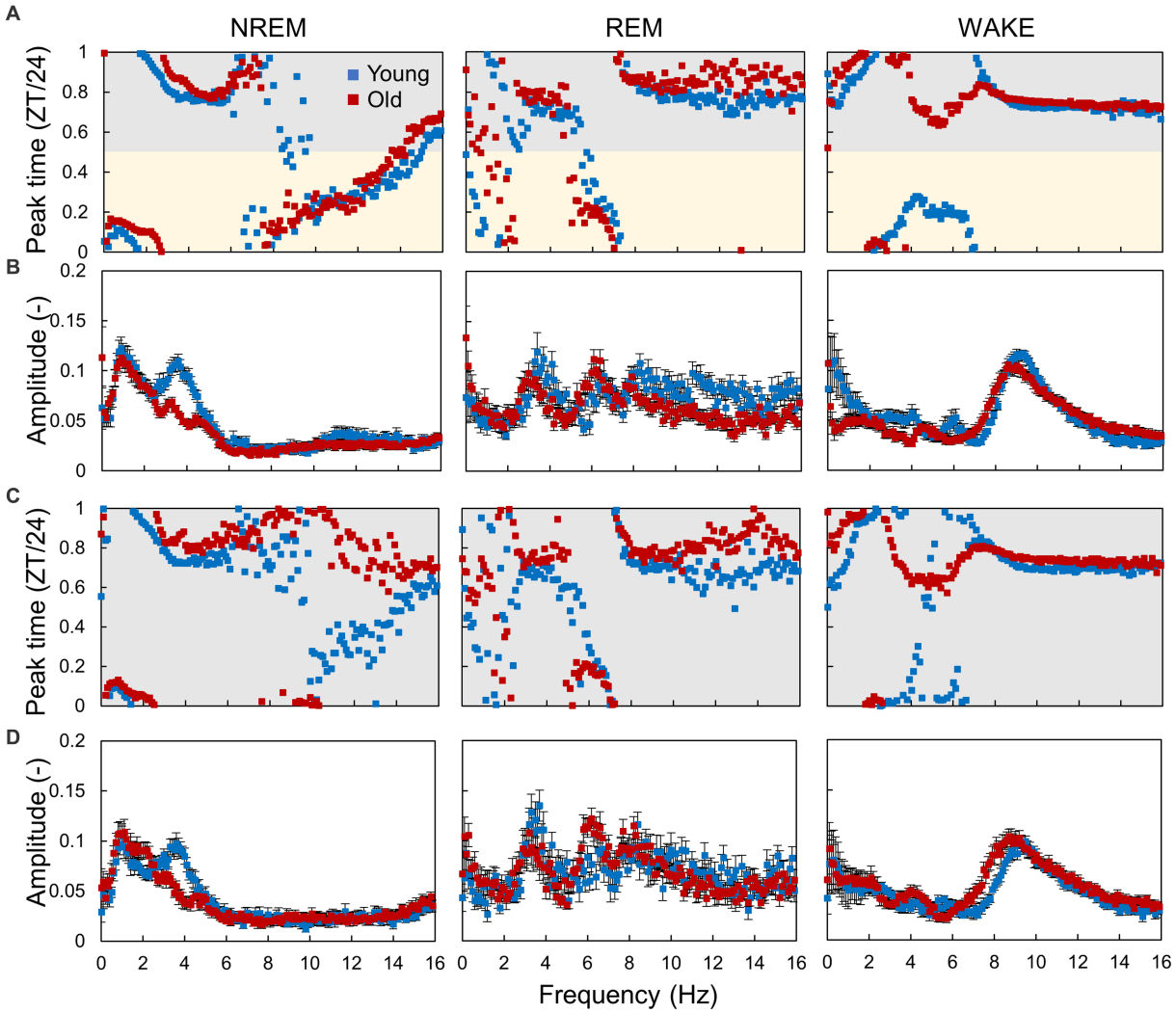

FIGURE 5
Circadian rhythm components in EEG power. **(A,B)** Peak time **(A)** and amplitude **(B)** of the EEG power rhythm at each frequency obtained from the hourly EEG power spectra in LD conditions. **(C,D)** Peak time **(C)** and amplitude **(D)** of the EEG power rhythm in DD conditions. Error bars indicate standard error. Blue and red dots represent values for young and old mice, respectively. Yellow and gray areas indicate light and dark conditions, respectively. The interval of each frequency is 0.1Hz. The results of the comparison of young and old mice by Mardia–Watson–Wheeler test for peak time and *t*-test for amplitude at each time point are shown in Supplementary Figure S6.

(COS), and the EEG spectrum in NREM was the most important factor for both discriminations (Figure 6C). This indicates that the shape of the EEG spectrum in NREM changes more prominently depending on the phase of the circadian rhythm than in the other sleep–wake stages.

Next, we used an estimation model constructed using the random forest algorithm, utilizing data from young mice under LD conditions, to forecast subject times (Figure 7A). Initially, we compared the actual time and estimated time by employing data from young mice in LD and DD conditions. The estimated times were close to the actual times, whereas there was a substantial shift in the light–dark transition (ZT11-12), which was smaller in DD than in LD. Under the DD condition, where light does not cause an effect, the EEG spectrum may gradually alter in a time-dependent manner around ZT12. We further carried out the estimation by employing the model established from young mice in the DD condition, yielding similar results (Supplementary Figure S11). These results indicate that the estimation model created from data from young mice can be used to assess the spontaneous circadian rhythm of mice.

Finally, we compared the subject time between young and old mice (Figure 7; Supplementary Figure S12). Under LD conditions, although a small effect was observed during the light period, the old mice showed a large delay in circadian time during the night period. The results obtained under the DD condition also showed a phase delay during the subjective night period but a small advancement during the light period. These results indicate that the circadian phase underwent a delay with aging; however, this change was dependent on the environmental time. To check the accuracy of these results, we also trained the model on the dataset of old mice in LD and predict the circadian phase in young and old mice (Supplementary Figure S13). The results showed a similar delay of the estimated time in old mice in the subjective dark period in DD, and an overall time delay in

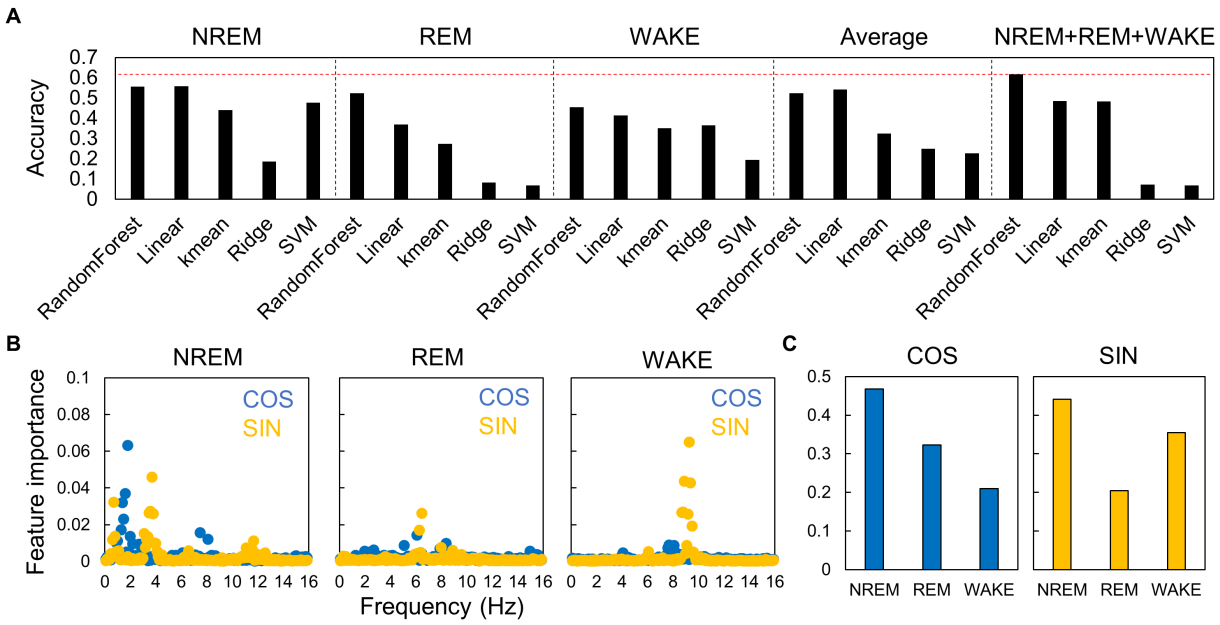

FIGURE 6
Accuracy of estimation of circadian phase using EEG power spectra in different algorithms. **(A)** Accuracy of the models constructed by each algorithm. The accuracies are shown for each sleep–wake stage, for hourly spectral averages that do not distinguish between sleep–wake stages, and for spectra of all stages. The red dotted line indicates the highest value. Each value is the average of five trials. SVM, support vector machine. **(B)** Importance of each frequency at each sleep–wake stage for time estimation. Blue dots (COS) represent the importance of morning/evening discrimination, and yellow points (SIN) represent the importance of day/night discrimination. **(C)** Importance of each sleep–wake stage for time estimation.

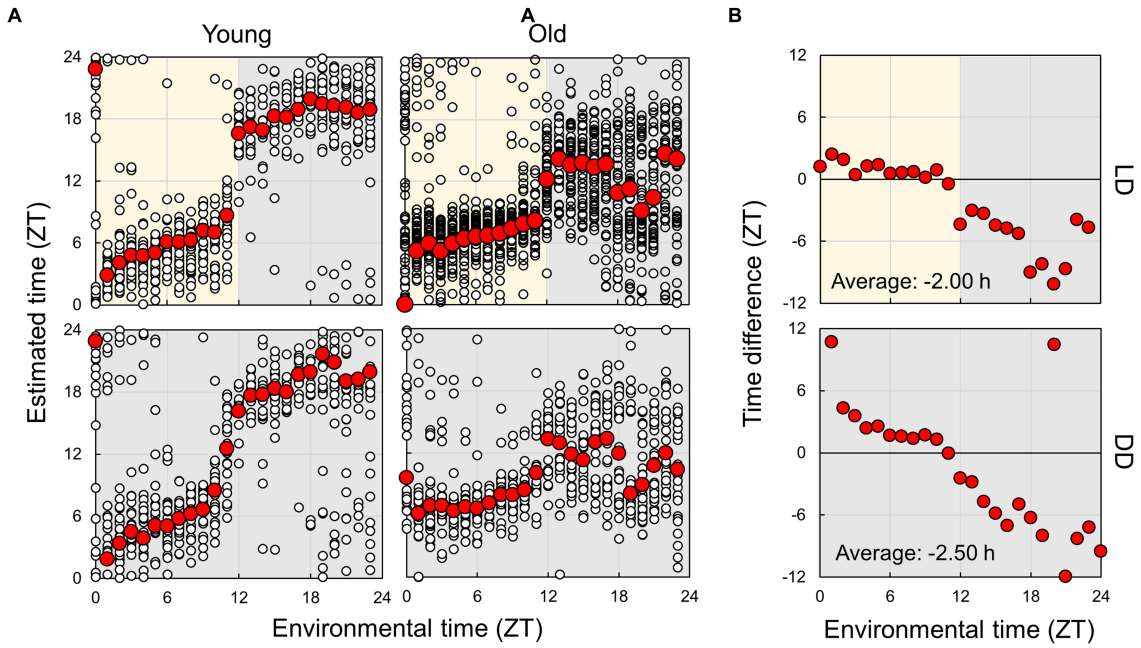

FIGURE 7
Estimation of subjective circadian phase based on EEG power spectra. **(A)** Estimated subjective time of mice in each condition using the model built based on the EEG of young mice in LD conditions. Blank circles represent the individual data, and red points represent the mean value of each time. **(B)** Difference in estimated time between young and old mice. The values shown in the figures are averages of time differences. Yellow and gray areas indicate light and dark conditions, respectively. The results of the comparison of young and old mice by Mardia–Watson–Wheeler test at each time point are shown in Supplementary Figure S8.

LD. This confirmed that the circadian rhythm of old mice tend to be delayed. However, the phase delay in the dark period was modest compared to the results of the model trained using the dataset of young mice. We also estimated the subject time based on the spectrum of each sleep–wake stage. We observed that the phase in old mice was delayed at night during NREM sleep, although the circadian times were strongly disturbed during REM and wakefulness at night (Figure 8; Supplementary Figure S14). In particular, the circadian fluctuation in the amount of REM sleep was not largely affected (Figure 2); nevertheless, the phase estimated by the spectral power was disturbed during REM sleep (Figure 8).

4. Discussion

In this study, we analyzed the sleep–wake patterns of young and aged mice and extracted the circadian rhythm component of each EEG power spectrum to simultaneously assess sleep and circadian rhythms modulated by aging. First, we confirmed the reduction in the amplitude of rhythms in sleep–wake patterns with aging owing to a decrease in wakefulness during the dark period (Figure 2; Wimmer et al., 2013; Panagiotou et al., 2017; McKillop et al., 2018). Subsequently, we extracted the circadian rhythm components in the EEG power spectra at each stage. The presence of spontaneous rhythms in EEG power spectra, even under constant dark conditions (Figures 3–5), suggests regulation by the internal clock. The peak time and amplitude of the EEG power rhythms varied according to the frequencies and sleep–wake stages. Notably, in aged mice, the amplitude of the circadian rhythm in the EEG tended to be attenuated, particularly during NREM sleep and wakefulness. Furthermore, we employed machine learning to evaluate the modulation of circadian rhythms in aged mice with a high temporal resolution (Figure 7). We showed that the phase of circadian rhythm was delayed in aged mice only during the dark period, and the delay was more obvious during REM sleep and wakefulness than in NREM sleep. These results confirm that the attenuation and phase delay of circadian rhythms with aging occurred at the EEG level and that the effects of aging on circadian rhythm and sleep–wake behavior depend on sleep–wake stages (wakefulness, NREM or REM) and time of day (circadian phase), respectively.

We extracted circadian rhythm components from the EEG power spectrum. The results showed different circadian rhythms among sleep–wake stages. Previous studies also showed that the delta power (0.5–4 Hz) rhythm of NREM has a peak around ZT0 (Wisor et al., 2008; Wimmer et al., 2013), and the 5–7 Hz rhythm of REM and WAKE has a peak around ZT6 (Yasenkov and Deboer, 2010). These results are consistent with our results (Figure 5). In aged mice, the amplitude of the EEG power rhythm was attenuated, especially at 4 Hz (delta wave), during NREM. Delta power is an indicator of sleepiness or sleep quality because the lack of sleep, such as sleep deprivation, strengthens it (Åkerstedt and Gillberg, 1990; Wisor et al., 2008). Thus, it is predicted to be rhythmic, lagging behind the sleep–wake pattern, as shown in our results (Figure 5).

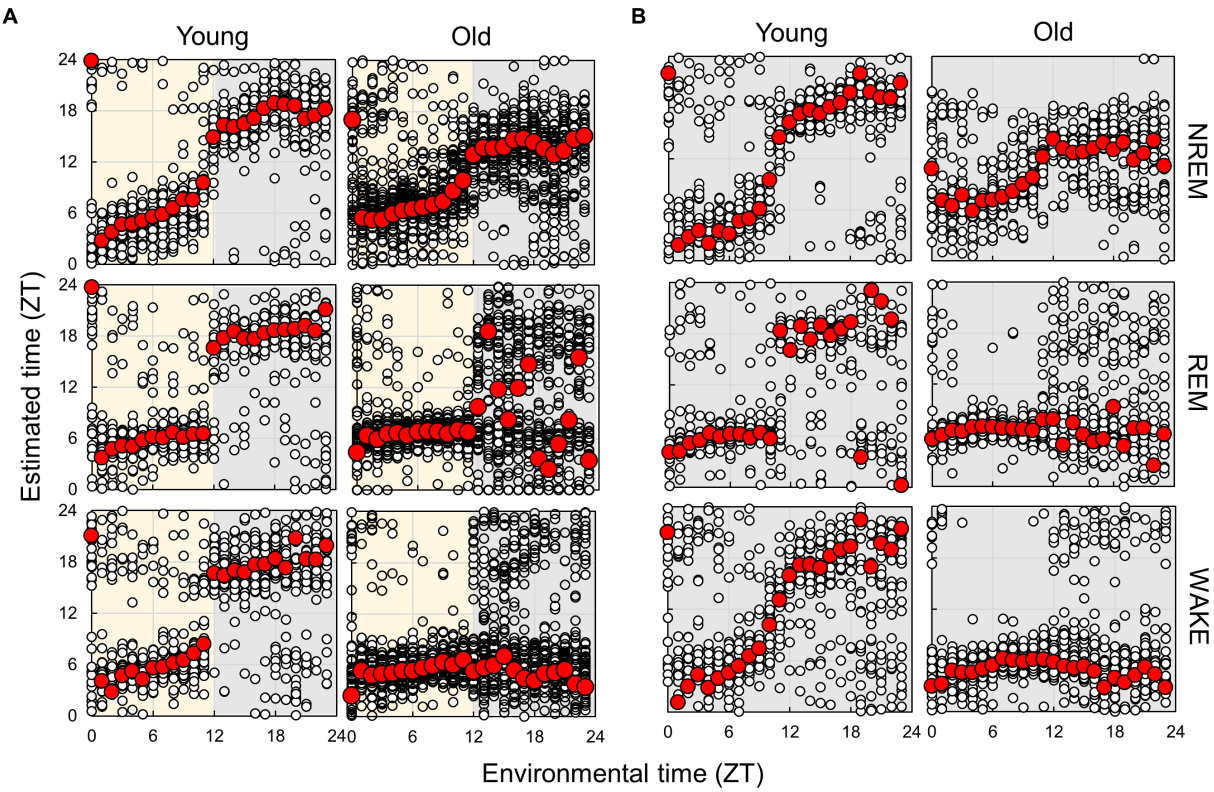

FIGURE 8
Subjective circadian phase in each sleep–wake stage in LD **(A)** and DD **(B)** conditions. Blank circles represent the individual data, and red points represent the mean value of each time. The time difference between young and old mice and the results of the comparison of young and old mice by Mardia–Watson–Wheeler test at each time point are shown in Supplementary Figures S13, S14.

However, although delta wave usually refers to between 0.5–4 Hz wave, the peak time of the EEG power rhythm and the effect of aging vary even between them (Figure 5). 0.5 Hz wave showed the peak during the light phase and was not affected by aging. On the other hand, the rhythm of 4 Hz wave power peaks in the middle of the night and was significantly attenuated by aging. Therefore, it is likely that these delta powers are largely influenced by sleep pressure, but also affected by other factors such as the circadian clock. The amount of sleep in the old mice increased at night, and the amplitude of the rhythm of the sleep–wake pattern decreased (Figure 2). These results indicate an association between circadian rhythm attenuation and aging and sleep disorders in the elderly. Moreover, disturbances in circadian rhythm in old mice also appeared at night, which is the active period for these animals (Figure 8). Although it remains unknown whether these changes are caused by changes in either circadian rhythm or sleep, the fact that age-associated changes in circadian rhythm and sleep–wake behavior are time-dependent suggests the need for time-dependent treatment of sleep and circadian rhythm disorders.

Although many studies have analyzed EEG for sleep analysis, few studies have focused on the phase of the circadian rhythm. In general, manual EEG analysis is time-consuming and can create bias by the analyst, making it difficult to evaluate circadian rhythms using the same criteria. Thus, we used the neural network model developed in a previous study (Tezuka et al., 2021) for sleep–wake stage scoring. One intent of this analysis was to demonstrate that circadian rhythms can be analyzed using large-scale EEG data. By combining automated sleep–wake stage scoring with circadian time prediction, it is possible to analyze circadian rhythms for large-scale data from various EEG databases without any bias. Notably, because the estimation method does not require long-term (over 1 d) recording of EEG to output the circadian phase, short-term EEG data, which were not intended to examine circadian rhythms, can be subjected to re-analysis using our method. We utilized this model in the current study because one of its features is the use of environmental time as one of its inputs, which reduces the time-dependent sleep scoring errors. In addition, because the model is capable of real-time analysis of sleep–wake stages, real-time circadian rhythm phase analysis would also be possible using our methods. Newer models have been proposed for machine learning EEG analysis; therefore, the accuracy of circadian rhythm phase estimation may also be improved using the latest models (Craik et al., 2019; Phan and Mikkelsen, 2022;Koyanagi et al., 2023). We propose that automated and spontaneous evaluation of sleep and circadian rhythms can be useful for high-throughput mutant screening, in which sleep and circadian rhythms are usually evaluated by separate screenings.

We estimated the subjective circadian time of mice using machine learning, and the estimated times were proportional to the environmental time under both LD and DD conditions. This indicates that EEG rhythms at each sleep–wake stage were not merely responses to light–dark transitions but clock-driven spontaneous rhythms and that it is possible to evaluate the phase of circadian rhythms without a long measurement period, as in behavioral analysis. However, even in young control mice, the estimation results were disturbed during the second half of the dark period. This may result from the increase in sleep amount at this time. The method of averaging hourly spectra may not provide sufficient data to evaluate the differences in sleepiness between light and dark periods. Therefore, it is necessary to develop methods that utilize higher-temporal-resolution data for time prediction. For example, previous studies have shown the existence of circadian periodicity in fractal structures in EEG (Croce et al., 2018). A more detailed extraction of circadian rhythm components in EEG will enable the evaluation of circadian rhythm phases with higher accuracy and temporal resolution. Apart from EEG and EMG, mice exhibit various other biological rhythms such as body temperature and endocrine rhythms. Simultaneous measurement of these rhythms with EEG can improve our understanding of circadian rhythm changes associated with aging, and potentially enhance our ability to predict circadian rhythms. The circadian time estimated for the old mice were highly disturbed during the night period (Figures 7, 8). However, the disruption was more modest when based on the old mice dataset (Supplementary Figure S13). It is assumed that when the old mice dataset was used for training, EEG powers that had no or weak rhythms in the old mice were not used for the estimation, leading to a more stable estimated circadian time in the old mice. In other words, the loss of the circadian rhythm component in the old mice might have caused the delay in the estimated time during nighttime in the old mice. Therefore, further development of analysis methods may be necessary to estimate the circadian phase reliably, regardless of the dataset used for training.

As demonstrated by previous studies and the present study, aging has a significant impact on circadian rhythm and sleep. Moreover, circadian rhythm disturbances and sleep disorders also accelerate aging (Kondratov et al., 2006; Sadeghmousavi et al., 2020; Carroll et al., 2021; Acosta-Rodríguez et al., 2022). Therefore, because aging, circadian rhythm, and sleep are mutually influential, it is difficult to evaluate them individually. Furthermore, circadian behavior has been conventionally analyzed using the quantitative fluctuation of behavior (such as counts of wheel-running and amounts of sleep) but not from the qualitative aspect. In the present study, we reconstructed the circadian phases during each sleep–wake stage separately based on spectrum analysis (Figure 8). The results showed that the circadian phases in the aged mice were delayed during NREM sleep, although significantly disrupted during REM sleep and wakefulness, indicating that aging affects circadian rhythms during each stage; however, these mechanisms may be independent. The present study indicates that analysis of circadian rhythms using EEG is useful to more deeply understand the effect of factors such as aging, which affect both sleep–wake and circadian rhythms.

Data availability statement

The original contributions presented in the study are included in the article/Supplementary material, further inquiries can be directed to the corresponding authors.

Ethics statement

The animal study was reviewed and approved by the Animal Experiment and Use Committee of the University of Tsukuba.

Author contributions

KM and AH designed this study. YK and YN performed the experiments. KM analyzed the data. KM, YN, TS, and AH wrote the manuscript. All authors discussed the results and implications and commented on the manuscript.

Funding

This study was partially supported by Grant-in-Aid for JSPS Fellows (no. 22J00270 to KM), for Scientific Research (no. 22K15157 to KM) provided by the Japan Society for the Promotion of Science (JSPS), the Moonshot Research Development Program (no. AGL03337 to AH) provided by Japan Agency for Medical Research and Development (AMED), and Research grant (AH) (The Naito Foundation, Japan).

Conflict of interest

The authors declare that the research was conducted in the absence of any commercial or financial relationships that could be construed as a potential conflict of interest.

Publisher's note

Supplementary material

The Supplementary material for this article can be found online at: https://www.frontiersin.org/articles/10.3389/fnins.2023.1173537/full#supplementary-material

References

Acosta-Rodríguez, V., Rijo-Ferreira, F., Izumo, M., Xu, P., Wight-Carter, M., Green, C. B., et al. (2022). Circadian alignment of early onset caloric restriction promotes longevity in male C57BL/6J mice. *Science* 376, 1192–1202. doi: 10.1126/science.abk0297

Åkerstedt, T., and Gillberg, M. (1990). Subjective and objective sleepiness in the active individual. *Int. J. Neurosci.* 52, 29–37. doi: 10.3109/00207459008994241

Carroll, J. E., Ross, K. M., Horvath, S., Okun, M., Hobel, C., Rentscher, K. E., et al. (2021). Postpartum sleep loss and accelerated epigenetic aging. *Sleep Health* 7, 362–367. doi: 10.1016/j.sleh.2021.02.002

Craik, A., He, Y., and Contreras-Vidal, J. L. (2019). Deep learning for electroencephalogram (EEG) classification tasks: a review. *J. Neural Eng.* 16:031001. doi: 10.1088/1741-2552/ab0ab5

Croce, P., Quercia, A., Costa, S., and Zappasodi, F. (2018). Circadian rhythms in fractal features of EEG signals. *Front. Physiol.* 9:1567. doi: 10.3389/fphys.2018.01567

Hasegawa, E., Miyasaka, A., Sakurai, K., Cherasse, Y., Li, Y., and Sakurai, T. (2022). Rapid eye movement sleep is initiated by basolateral amygdala dopamine signaling in mice. *Science* 375, 994–1000. doi: 10.1126/science.abl6618

Hesse, J., Malhan, D., Yalçin, M., Aboumanify, O., Basti, A., and Relógio, A. (2020). An optimal time for treatment—predicting circadian time by machine learning and mathematical modelling. *Cancers* 12:3103. doi: 10.3390/cancers12113103

Hoekstra, M. M., Jan, M., Katsioudi, G., Emmenegger, Y., and Franken, P. (2021). The sleep-wake distribution contributes to the peripheral rhythms in PERIOD-2. *Elife* 10:e69773. doi: 10.7554/eLife.69773

Hood, S., and Amir, S. (2017). The aging clock: circadian rhythms and later life. *J. Clin. Invest.* 127, 437–446. doi: 10.1172/JCI90328

Kondratov, R. V., Kondratova, A. A., Gorbacheva, V. Y., Vykhovanets, O. V., and Antoch, M. P. (2006). Early aging and age-related pathologies in mice deficient in BMAL1, the core componentof the circadian clock. *Genes Dev.* 20, 1868–1873. doi: 10.1101/gad.1432206

Koyanagi, I., Tezuka, T., Yu, J., Srinivasan, S., Naoi, T., Yasugaki, S., et al. (2023). Fully automatic REM sleep stage-specific intervention systems using single EEG in mice. *Neurosci. Res.* 186, 51–58. doi: 10.1016/j.neures.2022.10.001

Laposky, A., Easton, A., Dugovic, C., Walisser, J., Bradfield, C., and Turek, F. (2005). Deletion of the mammalian circadian clock gene BMAL1/Mop3 alters baseline sleep architecture and the response to sleep deprivation. *Sleep* 28, 395–410. doi: 10.1093/sleep/28.4.395

Lu, Y., Liu, B., Ma, J., Yang, S., and Huang, J. (2021). Disruption of circadian transcriptome in lung by acute sleep deprivation. *Front. Genet.* 12:664334. doi: 10.3389/fgene.2021.664334

Mander, B. A., Winer, J. R., and Walker, M. P. (2017). Sleep and human aging. *Neuron* 94, 19–36. doi: 10.1016/j.neuron.2017.02.004

Mang, G. M., La Spada, F., Emmenegger, Y., Chappuis, S., Ripperger, J. A., Albrecht, U., et al. (2016). Altered sleep homeostasis in rev-erb α knockout mice. *Sleep* 39, 589–601. doi: 10.5665/sleep.5534

McKillop, L. E., Fisher, S. P., Cui, N., Peirson, S. N., Foster, R. G., Wafford, K. A., et al. (2018). Effects of aging on cortical neural dynamics and local sleep homeostasis in mice. *J. Neurosci.* 38, 3911–3928. doi: 10.1523/JNEUROSCI.2513-17.2018

Nakamura, T. J., Nakamura, W., Yamazaki, S., Kudo, T., Cutler, T., Colwell, C. S., et al. (2011). Age-related decline in circadian output. *J. Neurosci.* 31, 10201–10205. doi: 10.1523/JNEUROSCI.0451-11.2011

Otsu, N. (1979). A threshold selection method from gray-level histograms. *IEEE Trans. Syst. Man Cybern.* 9, 62–66. doi: 10.1109/TSMC.1979.4310076

Panagiotou, M., Vyazovskiy, V. V., Meijer, J. H., and Deboer, T. (2017). Differences in electroencephalographic non-rapid-eye movement sleep slow-wave characteristics between young and old mice. *Sci. Rep.* 7:43656. doi: 10.1038/srep43656

Phan, H., and Mikkelsen, K. (2022). Automatic sleep staging of EEG signals: recent development, challenges, and future directions. *Physiol. Meas.* 43:04TR01. doi: 10.1088/1361-6579/ac6049

Sadeghmousavi, S., Eskian, M., Rahmani, F., and Rezaei, N. (2020). The effect of insomnia on development of Alzheimer's disease. *J. Neuroinflammation* 17:289. doi: 10.1186/s12974-020-01960-9

Sellix, M. T., Evans, J. A., Leise, T. L., Castanon-Cervantes, O., Hill, D. D., DeLisser, P., et al. (2012). Aging differentially affects the re-entrainment response of central and peripheral circadian oscillators. *J. Neurosci.* 32, 16193–16202. doi: 10.1523/JNEUROSCI.3559-12.2012

Tezuka, T., Kumar, D., Singh, S., Koyanagi, I., Naoi, T., and Sakaguchi, M. (2021). Real-time, automatic, open-source sleep stage classification system using single EEG for mice. *Sci. Rep.* 11:11151. doi: 10.1038/s41598-021-90332-1

Ueda, H. R., Chen, W., Minami, Y., Honma, S., Honma, K., Iino, M., et al. (2004). Molecular-timetable methods for detection of body time and rhythm disorders from single-time-point genome-wide expression profiles. *Proc. Natl. Acad. Sci. U. S. A.* 101, 11227–11232. doi: 10.1073/pnas.0401882101

Wimmer, M. E., Rising, J., Galante, R. J., Wyner, A., Pack, A. I., and Abel, T. (2013). Aging in mice reduces the ability to sustain sleep/wake states. *PLoS One* 8:e81880. doi: 10.1371/journal.pone.0081880

Wisor, J. P., O'Hara, B. F., Terao, A., Selby, C. P., Kilduff, T. S., Sancar, A., et al. (2002). A role for cryptochromesin sleep regulation. *BMC Neurosci.* 3:20. doi: 10.1186/1471-2202-3-20

Wisor, J. P., Pasumarthi, R. K., Gerashchenko, D., Thompson, C. L., Pathak, S., Sancar, A., et al. (2008). Sleep deprivation effects on circadian clock gene expression in the cerebral cortex parallel electroencephalographic differences among mouse strains. *J. Neurosci.* 28, 7193–7201. doi: 10.1523/JNEUROSCI.1150-08.2008

Yasenkov, R., and Deboer, T. (2010). Circadian regulation of sleep and the sleep EEG under constant sleep pressure in the rat. *Sleep* 33, 631–641. doi: 10.1093/sleep/33.5.631

frontiers | Frontiers in Neuroscience

TYPE Original Research
PUBLISHED 16 May 2023
DOI 10.3389/fnins.2023.1178457

OPEN ACCESS

EDITED BY
Rae Silver,
Columbia University, United States

REVIEWED BY
Jennifer Anne Evans,
Marquette University, United States
Marco Brancaccio,
Imperial College London, United Kingdom

*CORRESPONDENCE
Stephan Michel
✉ S.H.Michel@lumc.nl

†These authors have contributed equally to this work and share first authorship

RECEIVED 02 March 2023
ACCEPTED 24 April 2023
PUBLISHED 16 May 2023

CITATION
Olde Engberink AHO, de Torres Gutiérrez P, Chiosso A, Das A, Meijer JH and Michel S (2023) Aging affects GABAergic function and calcium homeostasis in the mammalian central clock. *Front. Neurosci.* 17:1178457. doi: 10.3389/fnins.2023.1178457

Aging affects GABAergic function and calcium homeostasis in the mammalian central clock

Anneke H. O. Olde Engberink†, Pablo de Torres Gutiérrez†, Anna Chiosso, Ankita Das, Johanna H. Meijer and Stephan Michel*

Laboratory for Neurophysiology, Department of Cell and Chemical Biology, Leiden University Medical Center, Leiden, Netherlands

Introduction: Aging impairs the function of the central circadian clock in mammals, the suprachiasmatic nucleus (SCN), leading to a reduction in the output signal. The weaker timing signal from the SCN results in a decline in rhythm strength in many physiological functions, including sleep–wake patterns. Accumulating evidence suggests that the reduced amplitude of the SCN signal is caused by a decreased synchrony among the SCN neurons. The present study was aimed to investigate the hypothesis that the excitation/inhibition (E/I) balance plays a role in synchronization within the network.

Methods: Using calcium (Ca^{2+}) imaging, the polarity of Ca^{2+} transients in response to GABA stimulation in SCN slices of old mice (20–24 months) and young controls was studied.

Results: We found that the amount of GABAergic excitation was increased, and that concordantly the E/I balance was higher in SCN slices of old mice when compared to young controls. Moreover, we showed an effect of aging on the baseline intracellular Ca^{2+} concentration, with higher Ca^{2+} levels in SCN neurons of old mice, indicating an alteration in Ca^{2+} homeostasis in the aged SCN. We conclude that the change in GABAergic function, and possibly the Ca^{2+} homeostasis, in SCN neurons may contribute to the altered synchrony within the aged SCN network.

KEYWORDS

excitatory/inhibitory balance, suprachiasmatic nucleus, calcium imaging, old mice, circadian, chloride transporters

1. Introduction

In mammals, the suprachiasmatic nucleus (SCN) functions as a master circadian clock that drives 24 h rhythms in both physiology and behavior. Based on molecular feedback loops, individual SCN neurons generate ~24 h rhythms in gene expression and cellular processes that in turn regulate electrical activity rhythms (Buhr and Takahashi, 2013; Hastings et al., 2018). This circadian rhythmicity is maintained when the SCN neurons are isolated, demonstrating that single cells function as cell autonomous oscillators (Welsh et al., 1995, 2010; Reppert and Weaver, 2002). Through synchronization and coupling, these individual SCN neurons produce a coherent output signal in ensemble electrical activity with a peak in the subjective day and a trough in the subjective night, which is conveyed to other brain areas and the periphery (Ramkisoensing and Meijer, 2015). Misalignment of single cell oscillators leads to a disruption or loss of SCN rhythm at the tissue level and consequently to malfunction of peripheral clocks.

This can have detrimental effects on human health and is associated with, for instance, cancer, cardiovascular, metabolic, and immune disorders (Roenneberg and Merrow, 2016; Patke et al., 2019). Aging promotes such circadian dysfunction by impacting the clock machinery on different levels (Buijink and Michel, 2021). Vice versa, the dysfunctional circadian clock has detrimental effects on the course of aging and is a risk factor for age-related diseases (Kondratova and Kondratov, 2012; Fonseca Costa and Ripperger, 2015). Understanding age-related mechanisms of clock dysfunction can therefore help identifying targets to intervene in this vicious cycle.

In both humans and animal models, age-related changes often lead to a reduction in behavioral activity levels and fragmented sleep–wake rhythms (Dijk and Duffy, 1999; Hofman and Swaab, 2006; Farajnia et al., 2012), a longer latency to re-entrain to shifted light–dark schedules (Biello, 2009; Froy, 2011), and the inability to adapt to a different photoperiod (Buijink et al., 2020). These behavioral deficits are likely the effect of age-related attenuation of the timing signal generated by the SCN network (Oster et al., 2003; Farajnia et al., 2014a).

Both *in vivo* and *ex vivo* studies showed a significant reduction in the amplitude of the ensemble electrical activity rhythm of the aged SCN (Satinoff et al., 1993; Watanabe et al., 1995; Nakamura et al., 2011; Farajnia et al., 2012), which can partly be explained by decreased synchronization within the SCN network. *Ex vivo* electrophysiological recordings of subpopulations in SCN slices of aged mice showed redistribution of phases with a second cluster in the middle of the night. In contrast, peaks in SCN electrical activity in young control slices only clustered around the middle of the day (Farajnia et al., 2012).

An important neurotransmitter that plays a role in synchronization within the SCN network is γ-aminobutyric acid (GABA), which is expressed in almost all SCN neurons (Moore and Speh, 1993; Abrahamson and Moore, 2001). Although the precise role for GABA in the process of synchronization is still under debate (Ono et al., 2020), the number of GABAergic synaptic terminals in the SCN are diminished by 26% due to aging (Palomba et al., 2008) and GABAergic postsynaptic currents are reduced in frequency and amplitude (Nygard et al., 2005; Farajnia et al., 2012). Interestingly, GABA has the ability to act both as an inhibitory and excitatory neurotransmitter in SCN neurons and therefore contributes to plasticity in the excitatory/inhibitory (E/I) balance within the SCN (Albus et al., 2005; Choi et al., 2008). A narrow control over the E/I balance in neuronal networks is known to be critical for proper brain function and E/I imbalance—often caused by a reduction in GABAergic activity—has been correlated with aging-related deficits and the pathogenesis of several neurodegenerative diseases (Rissman and Mobley, 2011; Legon et al., 2016; Tran et al., 2019; Bruining et al., 2020). The possible effects of aging on the polarity of GABAergic signaling and the corresponding E/I balance in the SCN have not yet been studied.

Here, we investigated the aging effect on the GABAergic E/I balance by measuring intracellular calcium levels. Specifically, we determined the polarity of Ca^{2+} transients in response to GABA stimulation in SCN slices of old mice (20–24 months) and young controls during the day, and tested our hypothesis that aging leads to an increment in excitatory responses to GABA. We confirmed that the E/I balance shifted towards more excitation in SCN slices of old mice compared to young controls. Furthermore, we found an effect of aging on the baseline intracellular Ca^{2+} concentration ($[Ca^{2+}]_i$) and intracellular Ca^{2+}. The cells measured from the SCN slices of old mice showed a higher $[Ca^{2+}]_i$ during the day compared to the cells from the young controls. Analysis of Ca^{2+} transients' kinetics in response to depolarizations showed slower increase reaching higher peak amplitudes in old SCN neurons, suggesting higher buffer capacity, but also larger Ca^{2+} influx compared to young. This may contribute to high basal $[Ca^{2+}]_i$ and dysfunctional Ca^{2+} signaling in the old SCN neurons amplifying the effect of increased E/I ratios.

2. Materials and methods

2.1. Animals

Young (2–4 months, $N = 11$) and old (20–24 months, $N = 9$) male C57BL/6 mice (Janvier Labs, Saint-Berthevin, France) were housed in a climate controlled environment (21°C, 40%–50% humidity) with full-spectrum diffused lighting with an intensity between 50 and 100 lux (Osram truelight TL) and *ad libitum* access to food and water throughout the experiment. The mice were kept in groups of 2–4 mice on an equinoctial photoperiod of 12:12 h light–dark (LD 12:12) cycle. Mice older than 20 months received, in addition to the regular food, hydration and nutritional gels as supportive care. The animals were kept under these conditions for at least 4 weeks prior to the *ex vivo* experiments. *Ex vivo* experiments were performed within a 4-h interval centered around the middle of the day, zeitgeber time (ZT) 6.

2.2. Slice preparation

After decapitation, brains were quickly removed and placed into modified ice-cold artificial cerebrospinal fluid (ACSF), containing (in mM): NaCl 116.4, KCl 5.4, NaH_2PO_4 1.0, $MgSO_4$ 0.8, $CaCl_2$ 1, $MgCl_2$ 4, $NaHCO_3$ 23.8, glucose 15.1, and 5 mg/L gentamycine (Sigma Aldrich, Munich, Germany) and saturated with 95% O_2–5% CO_2. Coronal hypothalamic slices containing the SCN (250 µm) were cut using a vibratome (VT 1000S, Leica Microsystems, Wetzlar, Germany) and sequentially maintained in a holding chamber containing regular, oxygenated ACSF ($CaCl_2$ increased to 2 mM and without $MgCl_2$). The slices were incubated in a water bath (37°C) for 30 min and were then maintained at room temperature until the start of the recordings.

2.3. Ca^{2+} imaging

Neurons in brain slices were bulk-loaded with the ratiometric, membrane permeable Ca^{2+} indicator dye fura-2-acetoxymethyl ester (Fura-2-AM, Teflabs, Austin, United States). First, the slices were transferred from the holding chamber to a 35 mm petri dish and reviewed under the microscope. The side of the slide that contained (the larger part of) the SCN was placed up and the ACSF was removed from the petri dish. One drop of highly concentrated Fura-2-AM (998 µM) was placed on the SCN of each slice for 1 min after which 1 mL of a mix of ACSF containing 7 µM Fura-2-AM was added to the slices. The slices stayed in this mixture for 1 h on room temperature while maintained saturated with 95% O_2–5% CO_2. The slices were then rinsed four times with fresh ACSF before being transferred back into the holding chamber where they stayed another hour on room

temperature. After this loading protocol, the slices were moved (one by one) to a recording chamber (RC-26G, Warner Instruments, Hamden, CT, United States) mounted on the fixed stage of an upright fluorescence microscope (Axioskop 2-FS Plus, Carl Zeiss Microimaging, Oberkochen, Germany) and constantly perfused with oxygenated ACSF (2.5 mL/min) at room temperature. The indicator dye was excited alternatively at wavelengths of 340 and 380 nm by means of a monochromator (Polychrome V, TILL Photonics; now FEI Munich GmbH, Munich, Germany). Emitted light (505 nm) was collected by a 40x objective and detected by a cooled CCD camera (Sensicam, TILL Photonics; now FEI Munich GmbH, Munich, Germany), and images were acquired at 2 s intervals. It can be expected that Fura-2 will label neurons as well as astrocytes, however the morphology of Fura-2-filled SCN astrocytes is distinct from SCN neurons (Svobodova et al., 2018), and the threshold for Ca^{2+} responses to elevated K^+ application is higher in astrocytes (Duffy and MacVicar, 1994). We are therefore confident that our recordings were performed on SCN neurons. The slices settled in the recording chamber for at least 5 min before the start of the recordings. After 1 min of baseline recording, GABA (Sigma Aldrich, Munich, Germany;200 µM, 15 s) was applied locally using an eight-channel pressurized focal application system (ALA-VM8, ALA scientific instruments, NY, United States), and Ca^{2+} transients were recorded. After two GABA pulses, 1 min apart, and another minute of recording in which the Ca^{2+} transients returned to baseline, ACSF containing elevated levels of K^+ ("high K^+" 20 mM, 15 s) was applied to identify healthy neurons, but also to determine the Ca^{2+} buffer capacity of the cell. Cells with at least 10% increase in $[Ca^{2+}]_i$ in response to K^+ were considered to be healthy. The experiments as well as the analysis were accomplished using imaging software (TILLvision, TILL Photonics; now FEI Munich GmbH, Munich, Germany).

2.4. Data analysis and statistics

Single-wavelength images were background subtracted and ratio images (340/380) were generated. Regions of interest were generated to define cells and mean ratio values were determined, from which the intracellular Ca^{2+} concentration was calculated. Neuronal Ca^{2+} responses were further analyzed using IGOR Pro (WaveMetrics, Portland, OR, United States). Cells with an amplitude less than 10% of baseline values in response to elevated levels of K^+, or cells with instable (rising or falling) baselines or baselines >600 nM were excluded from analyses. These criteria will eliminate cells that are severely dysfunction or in apoptosis, but we still expect to be able to record aging-related changes in the SCN slices. Previous work has shown that aging induces rather specific loss of neuronal function (i.e., circadian modulation of ion channel activity) but not overall diminishing of neurons or even GABAergic signaling (Farajnia et al., 2012). The transient responses in Ca^{2+} concentration within the first seconds after the stimulation were evaluated, with responses smaller than ±10% of baseline values defined as non-responding cells. GABA-evoked responses showing Ca^{2+} transients with a decrease in amplitude of more than 10% from baseline were considered inhibitory and responses with an increase of more than 10% from baseline were defined as excitatory. Cells that showed both excitatory and inhibitory responses after a single GABA stimulation were defined as biphasic. Per animal, one to three SCN slices were analyzed and the Ca^{2+} responses to GABA application were measured in typically 60–160 cells. For each animal, the distribution of the different types of responses and the E/I ratio were determined. To calculate the mean E/I ratio, the number of cells that responded excitatory was divided by the number of cells that responded inhibitory per animal (i.e., slices from 1 animal were pooled) and averaged per group. In total we measured 924 cells in 27 slices from 9 old mice and 1,204 cells in 26 slices from 11 young mice.

Ca^{2+} transients in response to high-K^+ application were analyzed using a custom-made Python script (3.8.10). Basal intracellular Ca^{2+} concentration ($[Ca^{2+}]_i$) before the GABA application was represented by the mean of 10 measurements before treatment. The amplitude of $[Ca^{2+}]_i$ transients was defined as the difference between peak and baseline value. Values extending more than three times the standard variation in the data set were excluded. The time constant of the rising phase (tau) was calculated by fitting an exponential curve into the interval between the start of the high-K^+ rise (defined as the first value 2.5 standard deviations above the baseline) and the maximum value of $[Ca^{2+}]_i$ for the high-K^+ transient. Fitted curves with an r-squared value lower than 0.95 were excluded.

Statistical analyses were performed using GraphPad Prism (San Diego, CA, United States) and IBM SPSS statistics version 25 (Armonk, NY, United States). The effect of age on the GABAergic response types, $[Ca^{2+}]_i$ baselines and high K^+ responses were tested using generalized estimating equations (GEE) models, with brain slice as a grouping variable. The resulting p-values underwent Bonferroni correction to account for multiple testing. When single variable comparisons were drawn between the two age groups, two-sided, unpaired t-tests with Welch's correction were performed. Differences with $p \leq 0.05$ were considered significant.

3. Results

3.1. GABAergic excitation increased in old SCN

We investigated the effect of aging on the GABAergic activity in SCN neurons by recording GABA-induced single cell Ca^{2+} transients in SCN slices from old (20–24 months) and young (2–4 months) mice (Figure 1A). In each SCN slice, we recorded a combination of transient increases, decreases, or no changes in $[Ca^{2+}]_i$ in response to GABA application (non-responders). In another subset of SCN neurons we recorded a biphasic response to GABA. The amplitude of the GABAergic responses did not differ between the old and the young SCN neurons (Supplementary Figure S1, inhibition; old: −66.53 ± 5.39 nM, $n = 433$, young: −59.87 ± 1.82 nM, $n = 691$, $p = 1.0$, excitation; old: 58.90 ± 4.32 nM, $n = 313$, young: 62.73 ± 5.03 nM, $n = 322$, $p = 1.00$). The percentages of the different GABAergic response types differed between old and young animals. Old SCN slices exhibited significantly more excitatory responses to GABA as compared to SCN slices of young controls (Figure 1B; Supplementary Figure S2, old: 32.99 ± 3.17%, $n = 9$, young: 23.41 ± 2.29%, $n = 11$, $p = 0.044$). This increase in GABAergic excitation leads to an increase in the E/I balance in old SCN slices, as compared to young SCN slices (Figure 1C, old: 0.80 ± 0.12, $n = 9$, young: 0.48 ± 0.07, $n = 11$, $p = 0.034$). These results show that aging affects the polarity of responses to GABA.

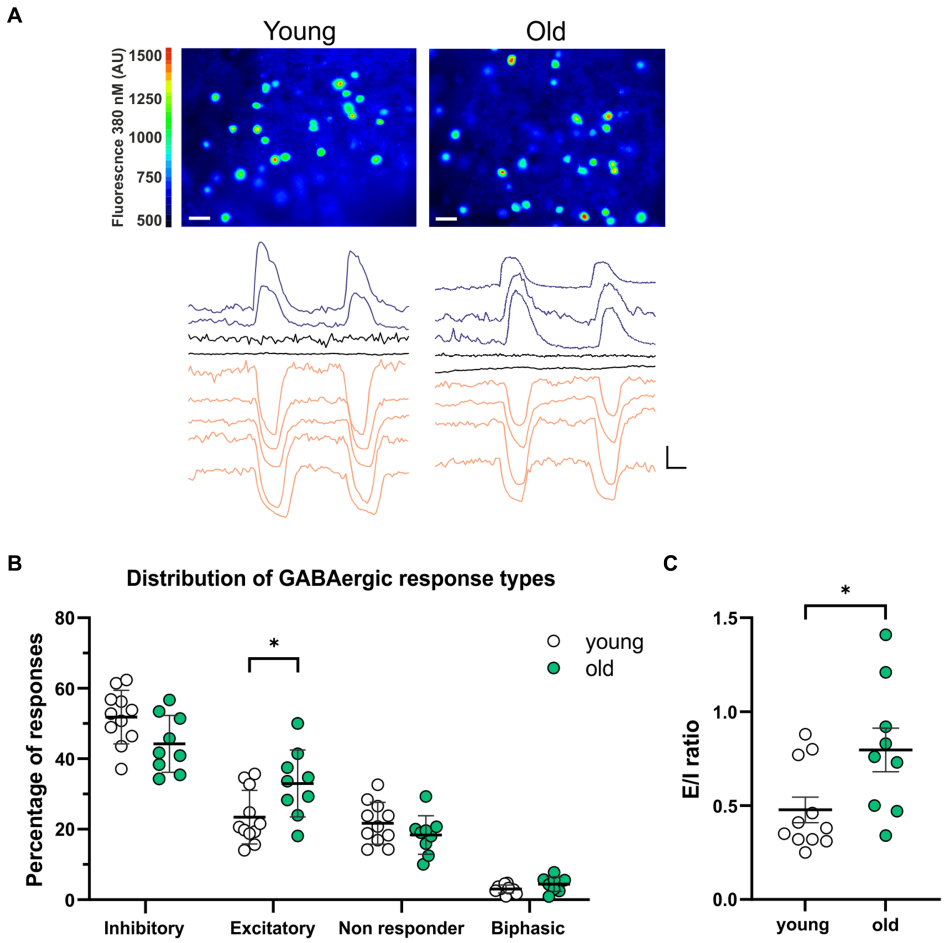

FIGURE 1
More GABAergic excitation in SCN slices from old mice. **(A)** Upper panels: examples of fura-2-AM loaded SCN neurons in slices from young (left) and old (right) mice. Color scale indicates fluorescence at 380 nm excitation in arbitrary units (Scale bar, 20 μm). Lower panels: example traces of Ca^{2+} transients in response to two GABA administrations recorded from one SCN slice from a young (left) and old (right) mouse. Excitatory responses are shown in blue, inhibitory responses in orange and non-responding cells in black (Scale bars, 50 nM, 20 s). **(B)** The percentages of inhibitory, excitatory, non-responding, and biphasic cells. Each dot represents the mean percentage of responses per response type per SCN. Every single dot in one response type category adds up to 100% together with the corresponding dots in the other categories. **(C)** E/I ratio's in young and old mice, determined by dividing the number of excitatory responses by the number of inhibitory responses measured from each SCN. Open dots represent values from young mice ($n = 11$) and filled, green dots represent values from old ($n = 9$) mice. Bars indicate mean ± SEM. *$p < 0.05$, **$p < 0.01$; distribution of GABAergic response types: GEE with Bonferroni correction **(B)**, E/I ratio: unpaired t-test with Welch's correction **(C)**.

3.2. Age-related increase in GABAergic excitation mainly in posterior part of the SCN

Several studies have shown that the amount of GABAergic excitation varies between the different SCN areas in rats (Albus et al., 2005; Choi et al., 2008; Irwin and Allen, 2009). Therefore, we tested whether there were regional differences in the distribution of the GABAergic response types along the anteroposterior and the dorsoventral axis. We defined regions by earlier described landmarks like the shape of the optic chiasm and the distance to the 3rd ventricle (Morin et al., 2006; see Supplementary Figure S3).

When comparing young and old, the posterior part of the SCN was the only region showing significant differences with more GABAergic excitation and less inhibition (Figures 2C,D, excitation; old: 45.05 ± 6.24%, $N = 9$, young: 19.98 ± 4.14%, $N = 5$, $p = 0.001$, inhibition; old: 36.81 ± 5.53%, $N = 9$, young: 60.62 ± 4.89%, $N = 5$, $p = 0.04$).The calculated E/I balance was also significantly different between young and old in the posterior SCN slices (Figure 2E, old: 1.08 ± 0.20, $N = 8$, young: 0.36 ± 0.10, $N = 5$, $p = 0.003$). No differences in GABAergic responses or E/I balance were observed in the central part of the SCN slices of young and old mice (Figures 2B,E, E/I ratio; old: 0.79 ± 0.19, $N = 10$, young: 0.73 ± 0.12, $N = 10$, $p = 0.767$). There were also no significant differences in GABAergic responses between the dorsal and ventral SCN, both for the old and young mice (Figure 3).

3.3. Altered Ca^{2+} homeostasis in old SCN neurons

To examine whether the baseline $[Ca^{2+}]_i$ changes with aging, we compared $[Ca^{2+}]_i$ (determined by the average $[Ca^{2+}]_i$ in a 20 s interval before GABA application) in SCN neurons from old and young mice during the day. We found higher baseline $[Ca^{2+}]_i$ levels in

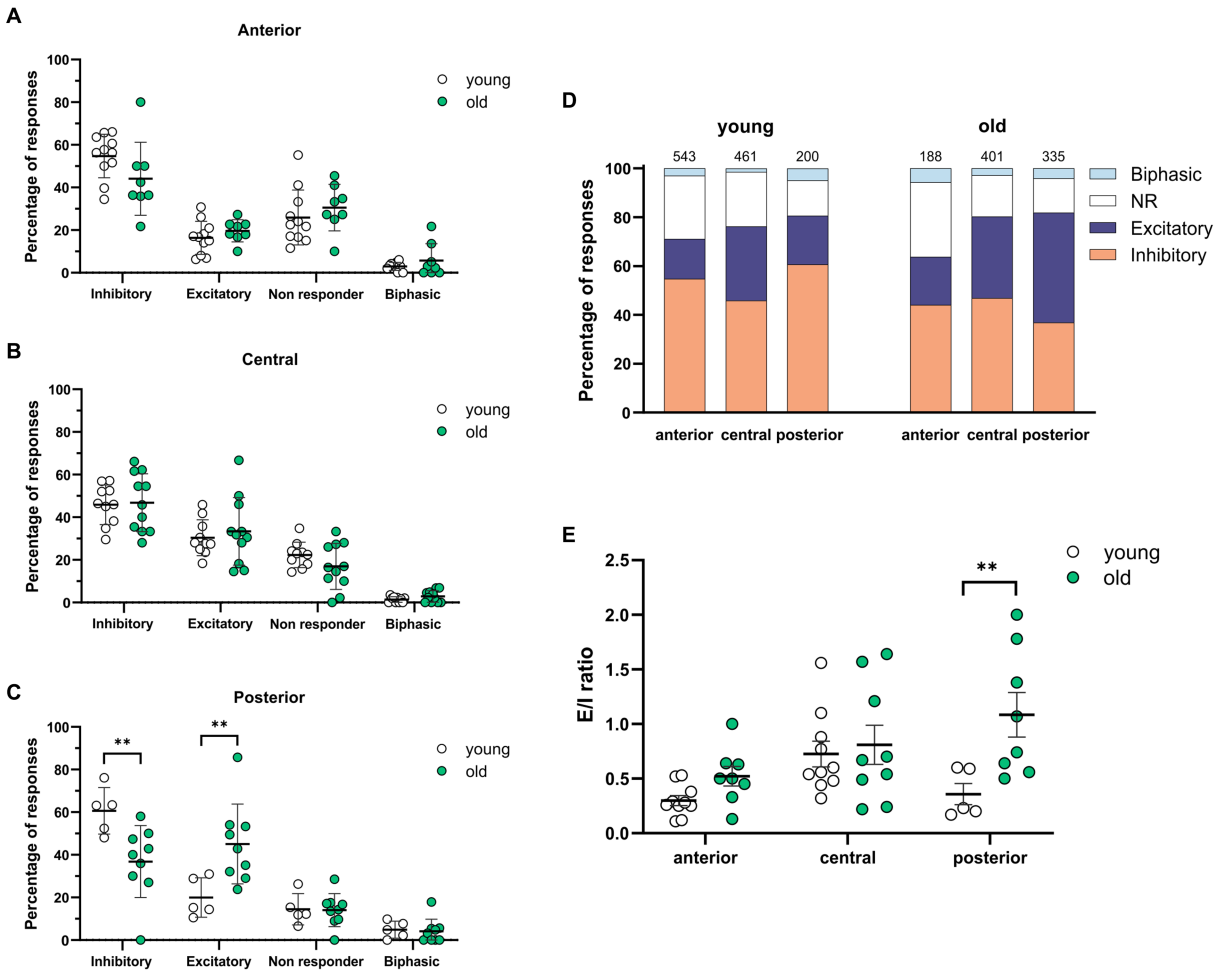

FIGURE 2
Spatial differences in GABAergic responses along the anteroposterior axis. **(A–C)** The percentages of inhibitory, excitatory, non-responding, and biphasic cells in the anterior **(A)**, central **(B)**, and posterior **(C)** part of the young and old SCN. Each dot represents the mean percentage of responses per response type per SCN. Every single dot in one response type category adds up to 100% together with the corresponding dots in the other categories. **(D)** Distribution of GABAergic response types for the anterior, central, and posterior part of the young (left) and the old (right) SCN. Orange represents the percentage of inhibitory responses, dark blue represents excitatory responses, white represents non-responding cells, and light blue represents biphasic responses. The value on top of the bar shows the total number of cells measured. **(E)** E/I ratios per SCN region in young and old mice, determined by dividing the number of excitatory responses by the number of inhibitory responses measured from different parts of the SCN along the anteroposterior axis. Open dots represent values from young mice and filled, green dots represent values from old mice. Bars indicate mean ± SEM. $^{**}p < 0.01$; distribution of GABAergic response types: GEE with Bonferroni correction **(A,B,C,E)**.

cells of the old SCN, when compared to the young SCN neurons (Figure 4A, old: 150.17 ± 3.78 nM, $n = 924$, young: 132.09 ± 2.28 nM, $n = 1{,}204$, $p < 0.0001$). We also wondered if GABAergic response types were correlated to different baseline levels of $[Ca^{2+}]_i$. Interestingly, the age-related increase in basal $[Ca^{2+}]_i$ was restricted to cells responding to GABA with either inhibition or excitation, but not found in non-responding cells or cells with a biphasic response to GABA. Baseline $[Ca^{2+}]_i$ was higher in old SCN neurons that exhibited GABAergic inhibitory as well as excitatory responses, when compared to young SCN neurons (Figure 4B, inhibition; old: 160.80 ± 6.80 nM, $n = 419$, young: 134.10 ± 2.78 nM, $n = 632$, $p = 0.000092$, excitation; old: 135.10 ± 4.75 nM, $n = 296$, young; 116.10 ± 3.88 nM, $n = 270$, $p = 0.004$).

These results suggest that Ca^{2+} homeostasis in the SCN neurons is affected by age and the GABAergic response type is correlated to the baseline $[Ca^{2+}]_i$ in young and old SCN. To further investigate this, we analyzed the kinetics and amplitude of the high-K^+ response, which can be influenced by alteration in the intracellular Ca^{2+} buffering system. We found that the rise time of the Ca^{2+} influx increased in aging SCN neurons (Figure 5C; Young; median = 9.48 s, IQR = 8.92 s. Old; median = 10.24, IQR = 11,06, $p = 0.045$), while there were no differences in amplitude of the peak response (Figure 5B, $p = 0.205$). However, we found regional differences in amplitude of Ca^{2+} transients between young and old SCN with larger impact in the central and dorsal regions on the amplitude of the response (Figures 5D,E, central: $p = 0.006$; dorsal: $p = 0.018$). We could not find a significant change in rise time in the subregions (anterior: $p = 1.0$; central: $p = 0.609$; posterior: $p = 0.795$). This implies an increased buffering capacity of the SCN causing the slower rise, but also an increased net Ca^{2+} influx in the central subregion leading to a larger response during excitation of the neurons.

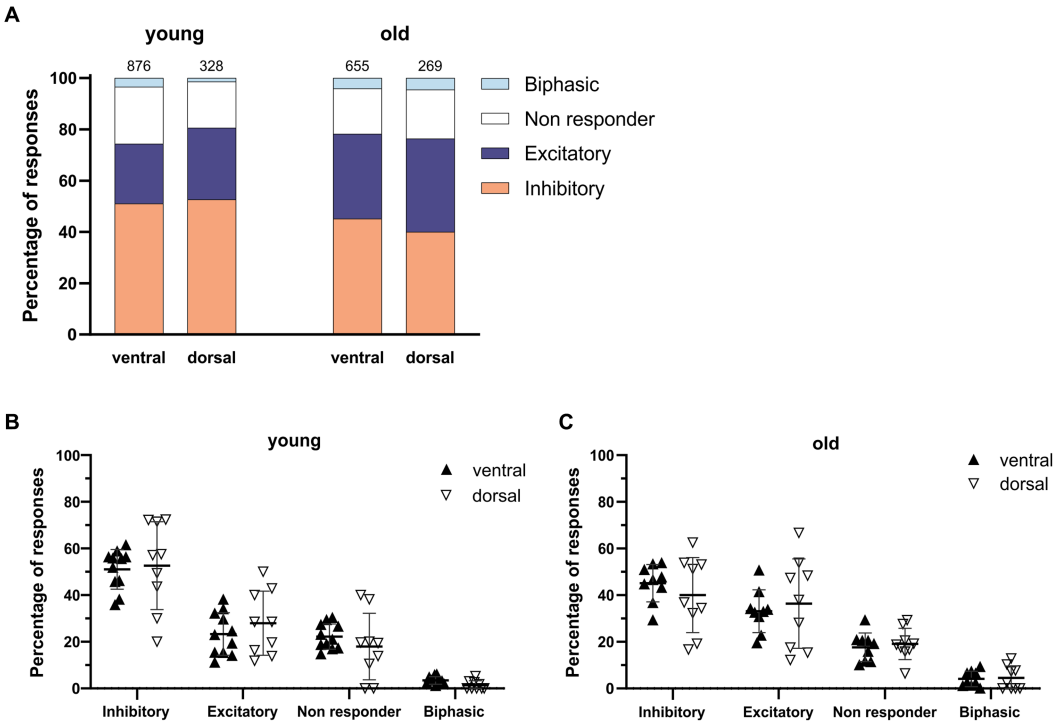

FIGURE 3
GABAergic responses along the dorsoventral axis. **(A)** Distribution of GABAergic response types for the ventral and dorsal part of the young (left) and the old (right) SCN. Orange represents the percentage of inhibitory responses, dark blue represents excitatory responses, white represents non-responding cells, and light blue represents biphasic responses. The value on top of the bar represents the total number of cells measured. **(B,C)** The percentages of inhibitory, excitatory, non-responding, and biphasic cells in the dorsal and ventral part of the young **(B)** and old **(C)** SCN. Each dot represents the mean percentage of responses per response type per SCN sub-region. Every single dot in one response type category adds up to 100% together with the corresponding dots in the other categories. Filled triangles represent values from the ventral part and open triangles represent values from the dorsal part of the SCN. Bars indicate mean ± SEM. GEE for each category with Bonferroni correction **(B,C)** n. s.

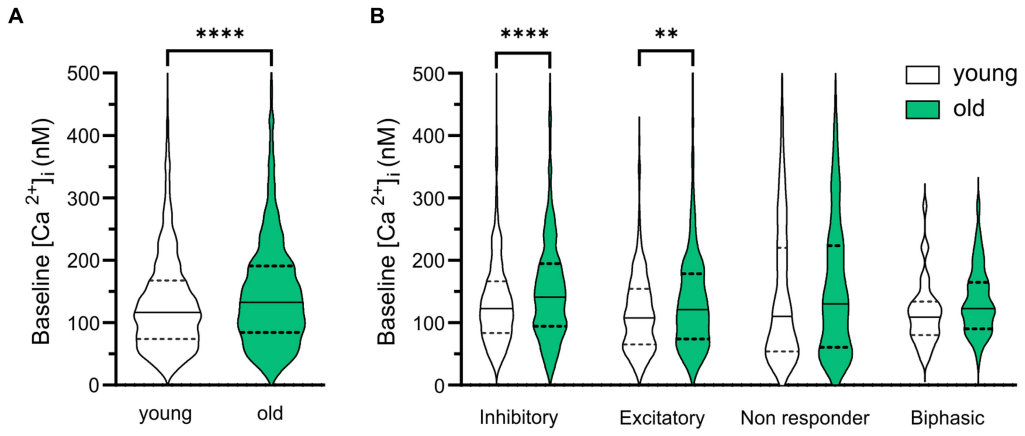

FIGURE 4
Baseline $[Ca^{2+}]_i$ is higher in old SCN neurons. **(A)** Violin plots show baseline $[Ca^{2+}]_i$ levels (nM) from all SCN neurons measured in slices from young ($n = 1{,}204$) and old ($n = 924$) mice. **(B)** Violin plots show baseline $[Ca^{2+}]_i$ levels (nM) from all SCN neurons measured categorized per GABAergic response type. White violins represent data from young mice and grey violins represent data from old mice. Violin plots show median and quartiles, $^{**}p < 0.01$, $^{****}p < 0.0001$, unpaired *t*-test with Welch's correction **(A)**, GEE with Bonferroni correction **(B)**.

4. Discussion

In this study we examined the effect of aging on the GABAergic E/I balance and on intracellular Ca^{2+} levels in the mammalian pacemaker. Our results demonstrate that aging affects the response polarity, and thus the function, of GABA, which is the most abundant neurotransmitter in the SCN. We measured significantly more GABAergic excitatory responses in SCN slices from old mice when

10.3389/fnins.2023.1178457

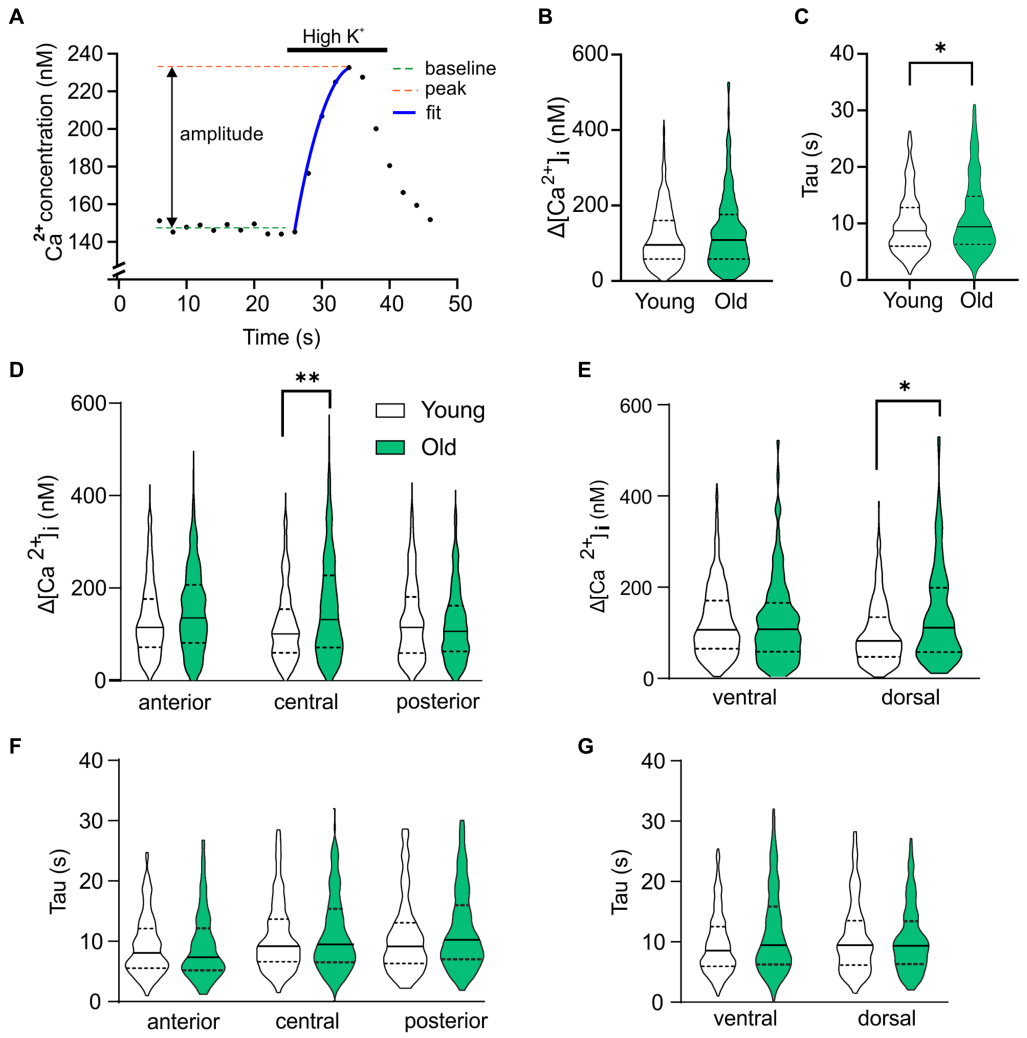

FIGURE 5
Age-dependent changes in Ca^{2+} homeostasis. **(A)** Example of depolarization-induced Ca^{2+} transient to explain the parameters analyzed and plotted in **(B–G)**. **(B)** Violin plot showing the amplitude of the Ca^{2+} response to depolarization caused by elevated extracellular K^+ for all cells recorded. **(C)** Rise time of the depolarization-induced Ca^{2+} transient is significantly increased in old SCN neurons compared to young controls. **(D,E)** Analysis of subregions show significant higher amplitude of High K^+ response in old neurons of posterior and dorsal SCN compared to young controls. **(F,G)** Time constant of rise in $[Ca^{2+}]_i$ is significantly increased in ventral neurons of SCN neurons from old mice compared to young controls. *p<0.05, **p<0.01, independent samples t-test **(B,C)**, GEE with Bonferroni correction **(D–G)**.

compared to slices from young controls. Particularly, in the posterior part of the old SCN we found significantly more excitation and significantly less inhibition compared to the young SCN. Accordingly, we recorded increased E/I ratios in SCN slices from old mice. We also demonstrate that the baseline $[Ca^{2+}]_i$ is higher in SCN cells from old mice, compared to young mice. This is interesting considering that Ca^{2+} is an important intracellular signaling molecule and critical for molecular rhythm generation (Lundkvist et al., 2005). Given previous studies on the aging SCN, we are confident that our data reflect the impact on aging on neuronal physiology and we try to exclude pathological phenomena by our exclusion criteria. However, the aging process is a continuum and the border to pathology is not always clear-cut. The number of cells unresponsive to GABA application was not significantly different between young and old animals, suggesting that aging did not severely compromise GABAergic signaling *per se* and our results are reflecting specific aging-dependent changes like reported earlier for circadian modulation of ion channel activity (Farajnia et al., 2012). Still, additional experiments for future studies could include perforated patch recordings for determining E/I (Farajnia et al., 2014b) and Fura-2 titration via a patch electrode to measure the calcium homeostasis in more detail (Neher, 1995).

GABA is known to elicit both inhibitory and excitatory responses in the central clock (Choi et al., 2008; Irwin and Allen, 2009; Farajnia et al., 2014b) and the polarity of GABAergic activity can switch depending on the subregion of the SCN (Albus et al., 2005; Choi et al., 2008; Irwin and Allen, 2009; DeWoskin et al., 2015; Myung et al., 2015). We found spatial differences in the distribution of the different GABAergic response types, with a significant increase in excitatory responses along the anteroposterior axis in the old, but not the young SCN (Figures 2A–D). In slices from both young and old mice, we did not find a difference in the polarity of the GABAergic responses between the ventral and dorsal SCN (Figure 3). The lack of regional

differences in GABAergic responses between anterior, central, and posterior SCN slices of young controls, or between dorsal and ventral SCN slices is comparable to a previous study examining the effect of photoperiod on the GABAergic responses in the mouse SCN (Farajnia et al., 2014b). The spatial organization that we observed in C57BL/6 mice differed from the spatial pattern previously observed in rat, in which there are regional differences found along the dorsoventral axis (Albus et al., 2005; Choi et al., 2008; Irwin and Allen, 2009). We have no explanation for this difference, but it adheres to anatomical differences that are also observed between mice and rats with more defined dorsal and ventral subregions in the rat and more interspersed neuropeptide distribution in the mouse SCN (Morin et al., 2006).

The reported increase in GABAergic excitation in the old SCN suggests an increase in $[Cl^-]_i$, since the polarity of the GABAergic signal depends in part on the $[Cl^-]_i$ and the relationship between the chloride equilibrium potential (E_{Cl}^-) and the membrane potential (V_m) (Kaila, 1994; Ben-Ari, 2002). Protein expression of the cation-chloride co-transporter responsible for the influx of chloride, the NKCC1, displays circadian rhythmicity in hamsters under constant conditions and is regulated by environmental lighting conditions, as NKCC1 protein levels in the SCN of hamsters housed in constant light are higher than of hamsters entrained to 14:10 LD cycles or under constant darkness (McNeill et al., 2020). There is no clear consensus on the distribution of co-transporter expression in the SCN. NKCC1 protein expression is shown to be higher in the dorsal part of the rat SCN at night, with no differences in subregion during the day (Choi et al., 2008), however, in hamsters exposed to constant darkness or 14:10 LD cycles, NKCC1 expression is higher in the ventral SCN compared to the dorsal part (McNeill et al., 2020). Another study shows higher $[Cl^-]_i$ during the day than during the night in both the ventral and dorsal mouse SCN neurons. Additionally, the KCCs—the extruders of chloride—play a major role in $[Cl^-]_i$ regulation, while NKCC1 has a relatively minor role (Klett and Allen, 2017). Our results suggest that the—relative or absolute—expression of NKCC1 and/or KCC2 may also be affected by aging, since we demonstrated an alteration in the polarity of the GABAergic response in the old SCN.

4.1. E/I balance and synchronization within the SCN network

The increase in excitatory responses in the old SCN may be part of mechanisms that contribute to the degree of synchronization within the SCN network. Both *in vivo* and *ex vivo* studies showed a significant reduction in the amplitude of the ensemble electrical activity rhythms of the aged SCN that is likely the consequence of decreased synchronization within the SCN network (Satinoff et al., 1993; Watanabe et al., 1995; Nakamura et al., 2011; Farajnia et al., 2012). *Ex vivo* electrophysiological recordings showed changes in neuronal phase distribution in SCN slices of aged mice (Farajnia et al., 2012) and these alterations at the network level underlie the diminished SCN output signal. Although the mechanisms that regulate neuronal phase distribution in the SCN are still unknown, there are studies suggesting that an increase in E/I balance might be responsible for modulating the phase distribution (Farajnia et al., 2014b; Rohr et al., 2019). GABA is expressed in almost all SCN neurons and is, because of its dual action as inhibitor and activator, an important contributor to the E/I balance in the SCN (Albus et al., 2005; Choi et al., 2008). Even though evidence suggest that GABA is involved in phase adjustment and synchronization of the SCN network, no consensus exists on the precise role of GABA in network synchronization (Ono et al., 2020). Our results contribute to this debate by showing increased levels of GABAergic excitation in an SCN network that is in a more desynchronized state (Farajnia et al., 2012), suggesting GABA regulation is involved in phase distribution. Other studies also suggest that GABA does not promote synchrony, or works as a destabilizer or phase desynchronizer within the SCN, but these studies do not distinguish between GABAergic inhibition or excitation (Aton et al., 2006; Freeman et al., 2013). Whether there is an actual causal link between either the E/I balance and synchronization still needs further investigation.

Alterations in the SCN network are involved in aging, as well as in the adaptation to photoperiods. As with aging, exposure to a long day photoperiod causes more phase dispersal in the SCN (VanderLeest et al., 2007; Brown and Piggins, 2009; Buijink et al., 2016) and a switch in the polarity of GABAergic activity from inhibition to excitation in many SCN neurons (Farajnia et al., 2014b). Farajnia et al. proposes that the relation between GABAergic inhibition and excitation may contribute to the photoperiod-induced phase adjustments within the network. Our results show an increase in the number of excitatory GABAergic responses and an increase in the E/I balance in the old SCN (Figure 1), similar to the changes in the SCN of mice entrained to a long photoperiod, and thus our data support this hypothesis.

4.2. Plasticity in E/I balance in the SCN

The polarity of the GABAergic response in the SCN, and thus the E/I balance, can vary depending on time of day or the photoperiod to which the animals are exposed (Albus et al., 2005; Choi et al., 2008; Farajnia et al., 2014b). In addition, a recent study showed that lighting conditions affect the circadian regulation and levels of NKCC1 protein expression, and thus the action of GABA (McNeill et al., 2020). The plasticity in GABAergic function is thought to support adaptation to environmental conditions. It is not clear whether the excitatory action of GABA in aging is also functional by contributing to a compensatory mechanism to reorganize the neuronal network of the SCN, or else, is a consequence of a loss of function in the aging SCN. Moreover, it remains to be investigated whether there is still plasticity in the E/I balance in the SCN of old mice, or if the increase that we show here is static and irreversibly changed in the SCN network. In an recent study we were able to show that the aging SCN is still able to adapt its molecular clock to different photoperiods as well as the young, suggesting that the SCN network is still flexible in aging (Buijink et al., 2020).

4.3. Aging and intracellular Ca^{2+} homeostasis in the SCN

One important intracellular component involved in phase adjustment is Ca^{2+}, which we determined in our baseline measurements before GABA application. Because of the use of a ratiometric dye, we were able to compare baseline $[Ca^{2+}]_i$ of SCN neurons from slices of old and young mice. Our results show that the baseline $[Ca^{2+}]_i$ is higher in SCN cells from old mice, compared to

young controls (Figure 4) which is in accordance with previous studies in other brain areas (Galla et al., 2020; Uryash et al., 2020; Mozolewski et al., 2021). In both young and old SCN slices, the neurons that showed GABAergic inhibition exhibited the highest baseline calcium levels. GABA induced Ca^{2+} transients can depend on baseline $[Ca^{2+}]_i$ (Irwin and Allen, 2009). A possible cause for the relationship between baseline $[Ca^{2+}]_i$ and GABAergic response type could be the different levels of electrical activity of the neuron. At a higher firing rate, the $[Ca^{2+}]_i$ baseline would be increased due to influx of Ca^{2+} through voltage-activated Ca^{2+} channels and an inhibitory input would have a larger effect compared to a silent neuron. Also, it is plausible that a neuron with a low or high $[Ca^{2+}]_i$ may not be able to further lower or raise $[Ca^{2+}]_i$ after a GABAergic stimulus, respectively.

In addition, we measured changes in kinetics of depolarization induced Ca^{2+} transients. Old neurons in the SCN showed a slower rise in $[Ca^{2+}]_i$, but also can reach a higher response peak (Figure 5). Similar results were found using patch clamp recordings in old hippocampal neurons in rats (Oh et al., 2013), suggesting an increase in buffer capacity in aged neurons, but also a larger influx of Ca^{2+} exhausting the homeostatic capacity in longer excitations and driving $[Ca^{2+}]_i$ to high levels.

Our evidence implies that both baseline calcium levels and calcium homeostasis are altered in the old SCN, which could further impair cellular phase adjustments. Even though Ca^{2+} is one of the most essential and well-studied signaling molecules, surprisingly little is known about the influence of aging on the Ca^{2+} signaling or Ca^{2+} homeostasis in the SCN. Studies in other brain areas have focused on the contribution of plasma membrane Ca^{2+} pumps, intracellular stores like the endoplasmic reticulum, and the mitochondria in aged neurons or neurodegenerative disorders (Supnet and Bezprozvanny, 2010; Zaidi et al., 2018; Calvo-Rodriguez et al., 2020; Trombetta-Lima et al., 2021). It should be noted though, that the SCN neurons can already tolerate higher levels of $[Ca^{2+}]_i$ when compared to other brain areas (Diekman et al., 2013). Given the essential role of calcium in both intracellular signaling pathways and rhythm generation and its association with multiple neurodegenerative disorders (Foster, 2007; Berridge, 2013), restoring calcium signaling in old SCN neurons could be an interesting target for therapy.

Additionally, maintenance of an adequate balance of excitation and inhibition could benefit healthy aging. Several studies have shown a shift in E/I balance, with heightened neuronal activity in the hippocampus or prefrontal cortex due to decreased inhibitory networks (Legon et al., 2016; Tran et al., 2019). This loss of inhibition, and thus an increased E/I ratio, was correlated to aging and the pathogenesis of neurodegenerative disorders (Rissman and Mobley, 2011; Bruining et al., 2020). Moreover, the E/I ratio increased in aged rats with impaired memory function, however aged rats with unimpaired memory function had similar hippocampal E/I ratios as young controls, showing that a proper balance between inhibition and excitation is crucial for maintaining memory performance during aging (Tran et al., 2019) and stresses the importance of an adequate balance in the aged brain. Our study demonstrates that the E/I balance of the neuronal network of the central clock is also challenged by aging with potential consequences for clock function. The stabilization of SCN E/I ratio to a healthy range in aging will not only benefit SCN network properties, but may also counteract the detrimental effects of the clock on neurodegenerative diseases (Leng et al., 2019; Fifel and De Boer, 2021).

Data availability statement

The raw data supporting the conclusions of this article will be made available by the authors, without undue reservation.

Ethics statement

All animal experiments were performed in accordance with the regulations of the Dutch law on animal welfare, and the institutional ethics committee for animal procedures of the Leiden University Medical Center (Leiden, Netherlands) approved the protocol (AVD 1160020185524; PE. 18.113.07).

Author contributions

AHOE, SM, and JHM designed the study. AHOE, PdTG, and AC performed the experiments. PdTG developed analysis tools for calcium transients. AHOE, PdTG, AC, and AD performed the analysis of the data. AHOE, SM, JHM, and PdTG wrote the manuscript. All authors contributed to the article and approved the submitted version.

Funding

This study was supported by funding from Velux Stiftung (project grant 1029 to SM) and by funding from ERC (adv grant 834513 to JHM). This study is part of the doctoral thesis by AHOE (Olde Engberink, 2022).

Acknowledgments

The authors thank Mayke Tersteeg for her technical assistance and help with animal caretaking. The authors also thank Ruben Schalk, Tom de Boer, and Roula Tsonaka for their help with the statistics.

Conflict of interest

The authors declare that the research was conducted in the absence of any commercial or financial relationships that could be construed as a potential conflict of interest.

Publisher's note

Supplementary material

The Supplementary material for this article can be found online at: https://www.frontiersin.org/articles/10.3389/fnins.2023.1178457/full#supplementary-material

References

Abrahamson, E. E., and Moore, R. Y. (2001). Suprachiasmatic nucleus in the mouse: retinal innervation, intrinsic organization and efferent projections. *Brain Res.* 916, 172–191. doi: 10.1016/S0006-8993(01)02890-6

Albus, H., Vansteensel, M. J., Michel, S., Block, G. D., and Meijer, J. H. (2005). A GABAergic mechanism is necessary for coupling dissociable ventral and dorsal regional oscillators within the circadian clock. *Curr. Biol.* 15, 886–893. doi: 10.1016/j.cub.2005.03.051

Aton, S. J., Huettner, J. E., Straume, M., and Herzog, E. D. (2006). GABA and Gi/o differentially control circadian rhythms and synchrony in clock neurons. *Proc. Natl. Acad. Sci. U. S. A.* 103, 19188–19193. doi: 10.1073/pnas.0607466103

Ben-Ari, Y. (2002). Excitatory actions of gaba during development: the nature of the nurture. *Nat. Rev. Neurosci.* 3, 728–739. doi: 10.1038/nrn920

Berridge, M. J. (2013). Dysregulation of neural calcium signaling in Alzheimer disease, bipolar disorder and schizophrenia. *Prion* 7, 2–13. doi: 10.4161/pri.21767

Biello, S. M. (2009). Circadian clock resetting in the mouse changes with age. *Age (Dordr.)* 31, 293–303. doi: 10.1007/s11357-009-9102-7

Brown, T. M., and Piggins, H. D. (2009). Spatiotemporal heterogeneity in the electrical activity of suprachiasmatic nuclei neurons and their response to photoperiod. *J. Biol. Rhythm.* 24, 44–54. doi: 10.1177/0748730408327918

Bruining, H., Hardstone, R., Juarez-Martinez, E. L., Sprengers, J., Avramiea, A. E., Simpraga, S., et al. (2020). Measurement of excitation-inhibition ratio in autism spectrum disorder using critical brain dynamics. *Sci. Rep.* 10:9195. doi: 10.1038/s41598-020-65500-4

Buhr, E. D., and Takahashi, J. S. (2013). "Molecular components of the mammalian circadian clock" in *Circadian Clocks*. eds. A. Kramer and M. Merrow (Berlin, Heidelberg: Springer), 3–27.

Buijink, M. R., Almog, A., Wit, C. B., Roethler, O., Olde Engberink, A. H., Meijer, J. H., et al. (2016). Evidence for weakened intercellular coupling in the mammalian circadian clock under long photoperiod. *PLoS One* 11:e0168954. doi: 10.1371/journal.pone.0168954

Buijink, M. R., and Michel, S. (2021). A multi-level assessment of the bidirectional relationship between aging and the circadian clock. *J. Neurochem.* 157, 73–94. doi: 10.1111/jnc.15286

Buijink, M. R., Olde Engberink, A. H. O., Wit, C. B., Almog, A., Meijer, J. H., Rohling, J. H. T., et al. (2020). Aging affects the capacity of photoperiodic adaptation downstream from the central molecular clock. *J. Biol. Rhythm.* 35, 167–179. doi: 10.1177/0748730419900867

Calvo-Rodriguez, M., Hernando-Pérez, E., López-Vázquez, S., Núñez, J., Villalobos, C., and Núñez, L. (2020). Remodeling of intracellular Ca(2+) homeostasis in rat hippocampal neurons aged in vitro. *Int. J. Mol. Sci.* 21:1549. doi: 10.3390/ijms21041549

Choi, H. J., Lee, C. J., Schroeder, A., Kim, Y. S., Jung, S. H., Kim, J. S., et al. (2008). Excitatory actions of GABA in the suprachiasmatic nucleus. *J. Neurosci.* 28, 5450–5459. doi: 10.1523/JNEUROSCI.5750-07.2008

DeWoskin, D., Myung, J., Belle, M. D., Piggins, H. D., Takumi, T., and Forger, D. B. (2015). Distinct roles for GABA across multiple timescales in mammalian circadian timekeeping. *Proc. Natl. Acad. Sci. U. S. A.* 112, E3911–E3919. doi: 10.1073/pnas.1420753112

Diekman, C. O., Belle, M. D., Irwin, R. P., Allen, C. N., Piggins, H. D., and Forger, D. B. (2013). Causes and consequences of hyperexcitation in central clock neurons. *PLoS Comput. Biol.* 9:e1003196. doi: 10.1371/journal.pcbi.1003196

Dijk, D. J., and Duffy, J. F. (1999). Circadian regulation of human sleep and age-related changes in its timing, consolidation and EEG characteristics. *Ann. Med.* 31, 130–140. doi: 10.3109/07853899908998789

Duffy, S., and MacVicar, B. A. (1994). Potassium-dependent calcium influx in acutely isolated hippocampal astrocytes. *Neuroscience* 61, 51–61. doi: 10.1016/0306-4522(94)90059-0

Farajnia, S., Deboer, T., Rohling, J. H., Meijer, J. H., and Michel, S. (2014a). Aging of the suprachiasmatic clock. *Neuroscientist* 20, 44–55. doi: 10.1177/1073858413498936

Farajnia, S., Michel, S., Deboer, T., vanderLeest, H. T., Houben, T., Rohling, J. H., et al. (2012). Evidence for neuronal desynchrony in the aged suprachiasmatic nucleus clock. *J. Neurosci.* 32, 5891–5899. doi: 10.1523/JNEUROSCI.0469-12.2012

Farajnia, S., van Westering, T. L. E., Meijer, J. H., and Michel, S. (2014b). Seasonal induction of GABAergic excitation in the central mammalian clock. *Proc. Natl. Acad. Sci. U. S. A.* 111, 9627–9632. doi: 10.1073/pnas.1319820111

Fifel, K., and De Boer, T. (2021). The circadian system in Parkinson's disease, multiple system atrophy, and progressive supranuclear palsy. *Handb. Clin. Neurol.* 179, 301–313. doi: 10.1016/B978-0-12-819975-6.00019-4

Fonseca Costa, S. S., and Ripperger, J. A. (2015). Impact of the circadian clock on the aging process. *Front. Neurol.* 6:43. doi: 10.3389/fneur.2015.00043

Foster, T. C. (2007). Calcium homeostasis and modulation of synaptic plasticity in the aged brain. *Aging Cell* 6, 319–325. doi: 10.1111/j.1474-9726.2007.00283.x

Freeman, G. M., Krock, R. M., Aton, S. J., Thaben, P., and Herzog, E. D. (2013). GABA networks destabilize genetic oscillations in the circadian pacemaker. *Neuron* 78, 799–806. doi: 10.1016/j.neuron.2013.04.003

Froy, O. (2011). Circadian rhythms, aging, and life span in mammals. *Physiology (Bethesda)* 26, 225–235. doi: 10.1152/physiol.00012.2011

Galla, L., Redolfi, N., Pozzan, T., Pizzo, P., and Greotti, E. (2020). Intracellular calcium dysregulation by the Alzheimer's disease-linked protein Presenilin 2. *Int. J. Mol. Sci.* 21:770. doi: 10.3390/ijms21030770

Hastings, M. H., Maywood, E. S., and Brancaccio, M. (2018). Generation of circadian rhythms in the suprachiasmatic nucleus. *Nat. Rev. Neurosci.* 19, 453–469. doi: 10.1038/s41583-018-0026-z

Hofman, M. A., and Swaab, D. F. (2006). Living by the clock: the circadian pacemaker in older people. *Ageing Res. Rev.* 5, 33–51. doi: 10.1016/j.arr.2005.07.001

Irwin, R. P., and Allen, C. N. (2009). GABAergic signaling induces divergent neuronal Ca2+ responses in the suprachiasmatic nucleus network. *Eur. J. Neurosci.* 30, 1462–1475. doi: 10.1111/j.1460-9568.2009.06944.x

Kaila, K. (1994). Ionic basis of GABAA receptor channel function in the nervous system. *Prog. Neurobiol.* 42, 489–537. doi: 10.1016/0301-0082(94)90049-3

Klett, N. J., and Allen, C. N. (2017). Intracellular chloride regulation in AVP+ and VIP+ neurons of the suprachiasmatic nucleus. *Sci. Rep.* 7:10226. doi: 10.1038/s41598-017-09778-x

Kondratova, A. A., and Kondratov, R. V. (2012). The circadian clock and pathology of the ageing brain. *Nat. Rev. Neurosci.* 13, 325–335. doi: 10.1038/nrn3208

Legon, W., Punzell, S., Dowlati, E., Adams, S. E., Stiles, A. B., and Moran, R. J. (2016). Altered prefrontal excitation/inhibition balance and prefrontal output: markers of aging in human memory networks. *Cereb. Cortex* 26, 4315–4326. doi: 10.1093/cercor/bhv200

Leng, Y., Musiek, E. S., Hu, K., Cappuccio, F. P., and Yaffe, K. (2019). Association between circadian rhythms and neurodegenerative diseases. *Lancet Neurol.* 18, 307–318. doi: 10.1016/S1474-4422(18)30461-7

Lundkvist, G. B., Kwak, Y., Davis, E. K., Tei, H., and Block, G. D. (2005). A calcium flux is required for circadian rhythm generation in mammalian pacemaker neurons. *J. Neurosci.* 25, 7682–7686. doi: 10.1523/JNEUROSCI.2211-05.2005

McNeill, J. K., Walton, J. C., Ryu, V., and Albers, H. E. (2020). The excitatory effects of GABA within the suprachiasmatic nucleus: regulation of Na-K-2Cl cotransporters (NKCCs) by environmental lighting conditions. *J. Biol. Rhythm.* 35, 275–286. doi: 10.1177/0748730420924271

Moore, R. Y., and Speh, J. C. (1993). GABA is the principal neurotransmitter of the circadian system. *Neurosci. Lett.* 150, 112–116. doi: 10.1016/0304-3940(93)90120-A

Morin, L. P., Shivers, K. Y., Blanchard, J. H., and Muscat, L. (2006). Complex organization of mouse and rat suprachiasmatic nucleus. *Neuroscience* 137, 1285–1297. doi: 10.1016/j.neuroscience.2005.10.030

Mozolewski, P., Jeziorek, M., Schuster, C. M., Bading, H., Frost, B., and Dobrowolski, R. (2021). The role of nuclear Ca2+ in maintaining neuronal homeostasis and brain health. *J. Cell Sci.* 134:jcs254904. doi: 10.1242/jcs.254904

Myung, J., Hong, S., DeWoskin, D., De Schutter, E., Forger, D. B., and Takumi, T. (2015). GABA-mediated repulsive coupling between circadian clock neurons in the SCN encodes seasonal time. *Proc. Natl. Acad. Sci. U. S. A.* 112, E3920–E3929. doi: 10.1073/pnas.1421200112

Nakamura, T. J., Nakamura, W., Yamazaki, S., Kudo, T., Cutler, T., Colwell, C. S., et al. (2011). Age-related decline in circadian output. *J. Neurosci.* 31, 10201–10205. doi: 10.1523/JNEUROSCI.0451-11.2011

Neher, E. (1995). The use of fura-2 for estimating Ca^{2+} buffers and Ca^{2+} fluxes. *Neuropharmacology* 34, 1423–1442. doi: 10.1016/0028-3908(95)00144-U

Nygard, M., Hill, R. H., Wikstrom, M. A., and Kristensson, K. (2005). Age-related changes in electrophysiological properties of the mouse suprachiasmatic nucleus in vitro. *Brain Res. Bull.* 65, 149–154. doi: 10.1016/j.brainresbull.2004.12.006

Oh, M. M., Oliveira, F. A., Waters, J., and Disterhoft, J. F. (2013). Altered calcium metabolism in aging CA1 hippocampal pyramidal neurons. *J. Neurosci.* 33, 7905–7911. doi: 10.1523/JNEUROSCI.5457-12.2013

Olde Engberink, A. H. O. (2022). A balanced clock—network plasticity in the central mammalian clock. Doctoral Dissertation, University of Leiden, The Netherlands.

Ono, D., Honma, K. I., and Honma, S. (2020). GABAergic mechanisms in the suprachiasmatic nucleus that influence circadian rhythm. *J. Neurochem.* 157, 31–41. doi: 10.1111/jnc.15012

Oster, H., Baeriswyl, S., Van Der Horst, G. T., and Albrecht, U. (2003). Loss of circadian rhythmicity in aging mPer1−/-mCry2−/− mutant mice. *Genes Dev.* 17, 1366–1379. doi: 10.1101/gad.256103

Palomba, M., Nygård, M., Florenzano, F., Bertini, G., Kristensson, K., and Bentivoglio, M. (2008). Decline of the presynaptic network, including GABAergic terminals, in the aging suprachiasmatic nucleus of the mouse. *J. Biol. Rhythm.* 23, 220–231. doi: 10.1177/0748730408316998

Patke, A., Young, M. W., and Axelrod, S. (2019). Molecular mechanisms and physiological importance of circadian rhythms. *Nat. Rev. Mol. Cell Biol.* 21, 67–84. doi: 10.1038/s41580-019-0179-2

Ramkisoensing, A., and Meijer, J. H. (2015). Synchronization of biological clock neurons by light and peripheral feedback systems promotes circadian rhythms and health. *Front. Neurol.* 6:128. doi: 10.3389/fneur.2015.00128

Reppert, S. M., and Weaver, D. R. (2002). Coordination of circadian timing in mammals. *Nature* 418, 935–941. doi: 10.1038/nature00965

Rissman, R. A., and Mobley, W. C. (2011). Implications for treatment: GABAA receptors in aging, down syndrome and Alzheimer's disease. *J. Neurochem.* 117, 613–622. doi: 10.1111/j.1471-4159.2011.07237.x

Roenneberg, T., and Merrow, M. (2016). The circadian clock and human health. *Curr. Biol.* 26, R432–R443. doi: 10.1016/j.cub.2016.04.011

Rohr, K. E., Pancholi, H., Haider, S., Karow, C., Modert, D., Raddatz, N. J., et al. (2019). Seasonal plasticity in GABAA signaling is necessary for restoring phase synchrony in the master circadian clock network. *Elife* 8:e49578. doi: 10.7554/eLife.49578

Satinoff, E., Li, H., Tcheng, T. K., Liu, C., McArthur, A. J., Medanic, M., et al. (1993). Do the suprachiasmatic nuclei oscillate in old rats as they do in young ones? *Am. J. Phys.* 265, R1216–R1222.

Supnet, C., and Bezprozvanny, I. (2010). Neuronal calcium signaling, mitochondrial dysfunction, and Alzheimer's disease. *J. Alzheimers Dis.* 20 Suppl 2, S487–S498. doi: 10.3233/JAD-2010-100306

Svobodova, I., Bhattaracharya, A., Ivetic, M., Bendova, Z., and Zemkova, H. (2018). Circadian ATP release in organotypic cultures of the rat suprachiasmatic nucleus is dependent on P2X7 and P2Y receptors. *Front. Phamacol.* 9:192. doi: 10.3389/fphar.2018.00192

Tran, T., Bridi, M., Koh, M. T., Gallagher, M., and Kirkwood, A. (2019). Reduced cognitive performance in aged rats correlates with increased excitation/inhibition ratio in the dentate gyrus in response to lateral entorhinal input. *Neurobiol. Aging* 82, 120–127. doi: 10.1016/j.neurobiolaging.2019.07.010

Trombetta-Lima, M., Sabogal-Guáqueta, A. M., and Dolga, A. M. (2021). Mitochondrial dysfunction in neurodegenerative diseases: a focus on iPSC-derived neuronal models. *Cell Calcium* 94:102362. doi: 10.1016/j.ceca.2021.102362

Uryash, A., Flores, V., Adams, J. A., Allen, P. D., and Lopez, J. R. (2020). Memory and learning deficits are associated with ca(2+) dyshomeostasis in normal aging. *Front. Aging Neurosci.* 12:224. doi: 10.3389/fnagi.2020.00224

VanderLeest, H. T., Houben, T., Michel, S., Deboer, T., Albus, H., Vansteensel, M. J., et al. (2007). Seasonal encoding by the circadian pacemaker of the SCN. *Curr. Biol.* 17, 468–473. doi: 10.1016/j.cub.2007.01.048

Watanabe, A., Shibata, S., and Watanabe, S. (1995). Circadian rhythm of spontaneous neuronal activity in the suprachiasmatic nucleus of old hamster in vitro. *Brain Res.* 695, 237–239. doi: 10.1016/0006-8993(95)00713-Z

Welsh, D. K., Logothetis, D. E., Meister, M., and Reppert, S. M. (1995). Individual neurons dissociated from rat suprachiasmatic nucleus express independently phased circadian firing rhythms. *Neuron* 14, 697–706. doi: 10.1016/0896-6273(95)90214-7

Welsh, D. K., Takahashi, J. S., and Kay, S. A. (2010). Suprachiasmatic nucleus: cell autonomy and network properties. *Annu. Rev. Physiol.* 72, 551–577. doi: 10.1146/annurev-physiol-021909-135919

Zaidi, A., Adewale, M., McLean, L., and Ramlow, P. (2018). The plasma membrane calcium pumps-the old and the new. *Neurosci. Lett.* 663, 12–17. doi: 10.1016/j.neulet.2017.09.066

frontiers | Frontiers in Neuroscience

TYPE Original Research
PUBLISHED 19 May 2023
DOI 10.3389/fnins.2023.1177458

OPEN ACCESS

EDITED BY
Daisuke Ono,
Nagoya University, Japan

REVIEWED BY
Jun Yan,
Chinese Academy of Sciences (CAS), China
Andrew Philip Patton,
University of Cambridge, United Kingdom

*CORRESPONDENCE
Jennifer A. Evans
✉ jennifer.evans@marquette.edu

†These authors have contributed equally to this work

‡PRESENT ADDRESSES
Vania Carmona-Alcocer,
Department of Biomedical Sciences,
University of Windsor, Windsor
ON, Canada
Lindsey S. Brown,
Princeton Neuroscience Institute,
Princeton University, Princeton, NJ,
United States
Kayla E. Rohr,
Department of Psychiatry,
University of California, San Diego, San Diego,
CA, United States

RECEIVED 01 March 2023
ACCEPTED 21 April 2023
PUBLISHED 19 May 2023

CITATION
Carmona-Alcocer V, Brown LS, Anchan A, Rohr KE and Evans JA (2023) Developmental patterning of peptide transcription in the central circadian clock in both sexes. *Front. Neurosci.* 17:1177458. doi: 10.3389/fnins.2023.1177458

Developmental patterning of peptide transcription in the central circadian clock in both sexes

Vania Carmona-Alcocer[1†‡], Lindsey S. Brown[2†‡], Aiesha Anchan[1], Kayla E. Rohr[1†] and Jennifer A. Evans[1*]

[1]Department of Biomedical Science, Marquette University, Milwaukee, WI, United States, [2]Harvard John A. Paulson School of Engineering and Applied Sciences, Harvard University, Allston, MA, United States

Introduction: Neuropeptide signaling modulates the function of central clock neurons in the suprachiasmatic nucleus (SCN) during development and adulthood. Arginine vasopressin (AVP) and vasoactive intestinal peptide (VIP) are expressed early in SCN development, but the precise timing of transcriptional onset has been difficult to establish due to age-related changes in the rhythmic expression of each peptide.

Methods: To provide insight into spatial patterning of peptide transcription during SCN development, we used a transgenic approach to define the onset of *Avp* and *Vip* transcription. *Avp-Cre* or *Vip-Cre* males were crossed to Ai9$^{+/+}$ females, producing offspring in which the fluorescent protein tdTomato (tdT) is expressed at the onset of *Avp* or *Vip* transcription. Spatial patterning of *Avp-tdT* and *Vip-tdT* expression was examined at critical developmental time points spanning mid-embryonic age to adulthood in both sexes.

Results: We find that *Avp-tdT* and *Vip-tdT* expression is initiated at different developmental time points in spatial subclusters of SCN neurons, with developmental patterning that differs by sex.

Conclusions: These data suggest that SCN neurons can be distinguished into further subtypes based on the developmental patterning of neuropeptide expression, which may contribute to regional and/or sex differences in cellular function in adulthood.

KEYWORDS

circadian, suprachiasmatic nucleus, development, neuropeptide transcription, sex differences, spatial mapping

Introduction

Daily rhythms in mammals are programmed by the circadian timekeeping system (Mohawk et al., 2012), which ensures that behavior and physiology are well matched to environmental conditions over the solar day. In nearly every biological system, cell physiology is modulated by autoregulatory genetic feedback loops controlling circadian rhythms in gene expression (Buhr and Takahashi, 2013). At the system level, clock tissues in the body are coordinated by a central clock in the suprachiasmatic nucleus (SCN), which is necessary for daily rhythms in behavior and physiology (Hastings et al., 2018). As the central pacemaker, the SCN processes photic inputs from the retina, sustains tissue-level rhythms through local communication, and provides outputs to coordinate cellular rhythms in downstream targets. Neural network mechanisms that support SCN timekeeping are essential for achieving internal and external coordination of the circadian system in an ever-changing environment.

The SCN is a heterogenous network of cellular clocks that displays self-sustained circadian rhythms in metabolism, electrical activity, gene/protein expression, and peptide release

(Hastings et al., 2018). SCN neurons express the neurotransmitter GABA and can be distinguished into different subpopulations based on peptide expression (Antle et al., 2003). Two types of SCN neurons have been studied in mammals in depth (Abrahamson and Moore, 2001; Moore et al., 2002; Ono et al., 2021). Located in the SCN shell and core respectively, AVP and VIP neurons provide network signals that regulate daily rhythms in behavior and physiology (Vosko et al., 2007; Kalsbeek et al., 2010; Ono et al., 2021). In addition to regional patterns of peptide expression, SCN neurons display cellular rhythms with spatial gradients that repeat across the network each circadian cycle (Hamada et al., 2004; Evans et al., 2011; Enoki et al., 2012; Brancaccio et al., 2013). Spatial gradients in clock function are stereotyped across individual animals, are evident in a variety of cellular processes, and can be modulated by experience (Inagaki et al., 2007; Evans et al., 2013). How neural identity maps onto differences in cellular function in the SCN network is a key question in the field.

The importance of the SCN clock during adulthood is well established, but the process by which SCN circuits form is not fully understood (Landgraf et al., 2014; Bedont and Blackshaw, 2015; Carmona-Alcocer et al., 2020). Across mammalian species, SCN neurogenesis occurs over the third to fourth quarter of gestation (Shimada and Nakamura, 1973; Altman and Bayer, 1978; Davis et al., 1990; Antle et al., 2005; Kabrita and Davis, 2008). The onset of daily rhythms in SCN activity has been detected as early as the end of neurogenesis and as late as the first few days after birth (Reppert, 1992; Shimomura et al., 2001; Sladek et al., 2004; Ohta et al., 2006; Wreschnig et al., 2014; Carmona-Alcocer et al., 2018). Despite these early milestones, postnatal development is critical for SCN circuit formation (Landgraf et al., 2014; Bedont and Blackshaw, 2015; Carmona-Alcocer et al., 2020). Both *Avp* and *Vip* transcripts are detected in the mouse SCN during late embryonic development (Okamura et al., 1983; Vandunk et al., 2011), but transcript and peptide levels increase over the first 3 weeks after birth (Hyodo et al., 1992; Ban et al., 1997; Herzog et al., 2000). Previous work suggests that the roles of AVP and VIP in the regulation of SCN function vary over development (Wreschnig et al., 2014; Ono et al., 2016; Carmona-Alcocer et al., 2018; Mazuski et al., 2020), but how these peptide circuits mature remains unclear.

One outstanding question concerns spatial patterning of SCN circuits during development. Spatiotemporal gradients in SCN neurogenesis have been reported, with SCN core neurons appearing before those in the SCN shell in mice, rats, and hamsters (Altman and Bayer, 1978; Davis et al., 1990; Antle et al., 2005; Kabrita and Davis, 2008). In the mouse, SCN shell neurons are generated in the middle-posterior regions before those in the anterior pole (Okamura et al., 1983; Kabrita and Davis, 2008). These studies suggest that SCN neurons in different regions of the network develop at different times, but it remains unclear if spatial patterning occurs for other milestones in cellular development (e.g., differentiation). Interestingly, previous work suggests that the onset of *Vip* transcription occurs in two distinct subclusters of SCN neurons that differ in spatial location and cellular function in adulthood (Ban et al., 1997). One obstacle in understanding SCN peptide development is that rhythms in SCN transcripts can change as the network matures (Isobe and Muramatsu, 1995; Ban et al., 1997; Shimomura et al., 2001; Houdek and Sumova, 2014). The resulting need to conduct a circadian time course at each developmental age has limited insight into spatial patterning during SCN development.

Here we use a genetic approach to test if SCN neurons display spatial patterning of peptide transcription during development. This approach uses Cre to permanently label cells with a fluorescent reporter at the time of *Avp* and *Vip* transcription (Harris et al., 2014; Taniguchi, 2014), thus circumventing the need to conduct a circadian time course to detect expression of the peptide itself. Using this genetic approach, we tracked *Avp* and *Vip* transcription across the entire SCN at key stages of pre-and post-natal development. We find that genetically labeled cells in each peptide class appear in spatially distinct subclusters over development. In addition, we find that biological sex influences developmental patterning of *Avp* and *Vip* labeling in a manner that differs for each SCN peptide class. Collectively, these data suggest that SCN neurons can be distinguished into further subclasses based on developmental patterning of neuropeptide transcription.

Materials and methods

Mice lines and general husbandry

Mice were bred and raised under a 24-h light–dark cycle with 12 h of light and 12 h of darkness [LD12:12: lights off: 1800 CST defined as Zeitgeber Time 12 (ZT12)]. Throughout life, ambient temperature was maintained at 22°C ± 2°C, and mice had *ad libitum* access to water and food (Teklad Rodent Diet 8,604). These studies used mice derived from crossing *Ai9*$^{+/+}$ females (Madisen et al., 2010) with *Avp*-IRES2-Cre$^{+/-}$ males (Harris et al., 2014), JAX# 023530, C57Bl/6 background) or *Vip*-IRES-Cre$^{+/+}$ males (Taniguchi, 2014), JAX# 010908, C57Bl/Jx129S background). In the heterozygous progeny of this cross (i.e., *Avp-Cre*$^{+/-}$; *Ai9*$^{+/-}$ and *Vip-Cre*$^{+/-}$; *Ai9*$^{+/-}$), Cre recombinase is expressed under the *Avp/Vip* promoter, causing cell-specific expression of the red fluorescent protein, tdTomato (tdT) at the onset of peptide transcription. For convenience, we refer to these as *Avp-tdT* and *Vip-tdT* mice. All procedures were conducted according to the NIH Guide for the Care and Use of Animals and were approved by the Institutional Animal Care and Use Committees at Marquette University.

Experimental breeding

To genetically label *Avp and Vip* neurons over specific developmental ages, male *Avp-Cre* or *Vip-Cre* mice were paired overnight with nulliparious female *Ai9*$^{+/+}$ mice. On the morning following cohabitation, successful mating was verified by the presence of vaginal plugs and designated Embryonic Day 1 (E01). Pregnant dams were tracked throughout pregnancy, and the day of birth was designated Postnatal Day 0 (P00). Sex and genotype of offspring were determined by PCR amplification of *Sly/Xlr* (McFarlane et al., 2013) and *Cre*$^{+/-}$ (Jackson Laboratory, oligo primers # 18475, 18,474, 10,362), respectively. Both male and female mice were used in all experiments, with biological sex confirmed by genotyping (McFarlane et al., 2013).

Brain collection, tissue processing, and microscopy

To evaluate specificity of labeling, brains were collected from *Ai9*$^{+/+}$, *Avp-tdT* and *Vip-tdT* mice of both sexes and sectioned in the coronal plane (40 µm) prior to mounting onto microscope slides for cell counting. To evaluate the correspondence between tdT labeling and peptide expression in adulthood, *Avp-tdT* and *Vip-tdT* mice of both sexes (n = 4-5/sex/genotype, P84, 22 weeks of age) received 1 µl colchicine injection into the third ventricle (0.5 µL/min) to slow microtubule transport and measure cumulative peptide expression over the circadian cycle. Brains were collected 48 h later (ZT06) and fixed in 4% paraformaldehyde overnight, cryoprotected in 20% sucrose for 4 days, and then sectioned in the coronal plane (25 µm). Free-floating slices were washed 6 times in PBS, blocked for 1 h in normal donkey serum, incubated for 48 h at 4°C with primary antibodies (Rabbit anti-AVP, Millipore AB1565, 1:1 K; Rabbit anti-VIP, Sigma HPA017324, 1:500), washed 6 times in PBS, incubated for 2 h at room temperature with secondary antibodies (Alexa Fluor 488, Donkey anti-rabbit, JIR 711–545-152, 1:500), and then washed 6 times in PBS before mounting in Prolong Anti-Fade medium with DAPI (Thermo Fisher, Cat# P36935) and cover slipped. For each experiment, slices were imaged by collecting 10X Z-stack images on a Nikon A1R+ confocal microscope (Nikon Instruments, Melville, NY, United States). The anterior, middle, and posterior SCN slice was identified for each sample and used for data analyses. Using ImageJ, a hyperstack projection of the Z-stack for each slice from each sample was created, and the total number of tdT+ and/or AVP/VIP+ cells was counted using the 3D Object Counter module.

To evaluate developmental patterns of *Avp-tdT* and *Vip-tdT* expression, brains were collected at E16, E18, E19, P01, P03, P05, P10 or P84 (i.e., Adult, n = 3–7 mice/sex/genotype, at least 2 litters collected at each age). For embryonic ages, pregnant females were anesthetized with isoflurane and euthanized by cervical dislocation before pups were extracted from the uterus and decapitated. Postnatal mice were euthanized by decapitation, whereas adult mice were anesthetized and euthanized as described for dams. Brains were collected in the middle of the photophase (ZT06), except E19 brains were collected 1 h before lights-off. Brains were fixed in 4% paraformaldehyde overnight at 4°C, cryoprotected in 20% sucrose for 48 h and 30% sucrose for 72 h at 4°C, then sectioned in the coronal plane (40 µm). All slices through the entire SCN were retained as one series and thaw-mounted onto microscope slides or saved as free-floating slices (P84). Nuclear staining was achieved by embedding slices in DAPI-containing mounting media (Abcam, Cat# ab104135) before cover-slipping. As described above, confocal images of tdT expression were collected. Using ImageJ, SCN images were aligned across samples in the XY plane using the Python OpenCV package and verified manually using SCN DAPI-determined boundaries. tdT+ cells were counted using a hyperstack as above, and the XYZ location of each cell was recorded (Supplementary Figure S1). Each SCN slice was mapped to the corresponding slice in the adult data based on preserved morphology across ages (Supplementary Figures S2A,B). Sex did not influence SCN area over development (Supplementary Figure S2C). tdT+ cells were counted using a hyperstack as above, and the XYZ location of each cell was recorded (Supplementary Figure S1). Cell counts were analyzed based on anteroposterior SCN region (anterior, middle, posterior SCN). In addition, cell clusters were identified using k-means clustering (Python scikit-learn), with the optimal number of clusters determined by the location of the elbow in the sum of squared distances (Nugent and Meila, 2010). At each developmental timepoint, cells were assigned to one of the spatial clusters identified in P84 adult samples. To visualize cellular density in different SCN regions, cellular coordinates were used to determine the number of neighboring cells within a 50 µm radius for each sample (Supplementary Figures S3A–C).

Data analyses

Statistical analyses were performed with JMP software (SAS Institute). Data are represented in figures and tables as mean ± SEM. When datasets contained within-subject factors (Slice Position, Cell Cluster), a mixed linear model was used to parse out random effects driven by individual differences among mice. When models only contained between-subject factors (Sex, Cell Type, Age), a full-factorial ANOVA was used to assess main effects and interactions. *Post-hoc* tests were performed with Tukey's HSD or Least Square Mean contrasts to control for family-wise error. Statistical significance was set at $p < 0.05$.

Results

Genetic approach for labeling SCN neurons by neuropeptide class

To evaluate spatial patterning of SCN development, we employed a genetic strategy (Figure 1A). Driven by the *Avp-* or *Vip*-promoter, Cre recombinase induced tdTomato (tdT) expression in *Avp-tdT* and *Vip-tdT* mice. As expected, tdT expression in the SCN was Cre-dependent, with very little recombination in *Ai9*$^{+/+}$ mice (Figure 1B, Supplementary Figure S4). Next, co-expression of tdT and AVP/VIP peptide expression was evaluated in adult mice using *in vivo* intracranial colchicine injections and immunohistochemistry (Figures 1C–F, Supplementary Figures S5A–D). AVP-IHC+ neurons outnumbered VIP-IHC+ neurons (Figure 1D, Cre: $F(1,15) = 175$, $p < 0.0001$), as expected based on previous work in the mouse (Abrahamson and Moore, 2001). However, the number of *Avp-tdT*+ and *Vip-tdT*+ SCN cells were more similar [Figure 1D, Cre: $F(1,15) = 4.1$, $p = 0.06$]. Approximately 30% *Vip-tdT*+ neurons were co-labeled by IHC, compared to 70% of *Avp-tdT*+ neurons [Figure 1E, Cre: $F(1,15) = 112.5$, $p < 0.0001$]. On the other hand, over 80% of VIP-IHC+ neurons were co-labeled with tdT, compared to only 43% of AVP-IHC+ neurons [Figure 1F, Cre: $F(1,15) = 105.8$, $p < 0.0001$]. Failure of Cre-mediated recombination in the *Avp-tdT* model appeared to be highest in the dorsal middle SCN (Figure 1C, Supplementary Figures S5A,E). Importantly, sex did not influence measures of tdT/AVP/VIP labeling or co-expression (Supplementary Figures S5C–F). These results indicate that this genetic approach does not fully capture peptide expression in the adult SCN, but that tdT can be used in both sexes.

Mapping *Avp-tdT*+ and *Vip-tdT*+ neurons in the adult SCN

As a next step toward constructing a developmental atlas, we mapped the spatial location of *Avp-tdT* and *Vip-tdT* SCN neurons

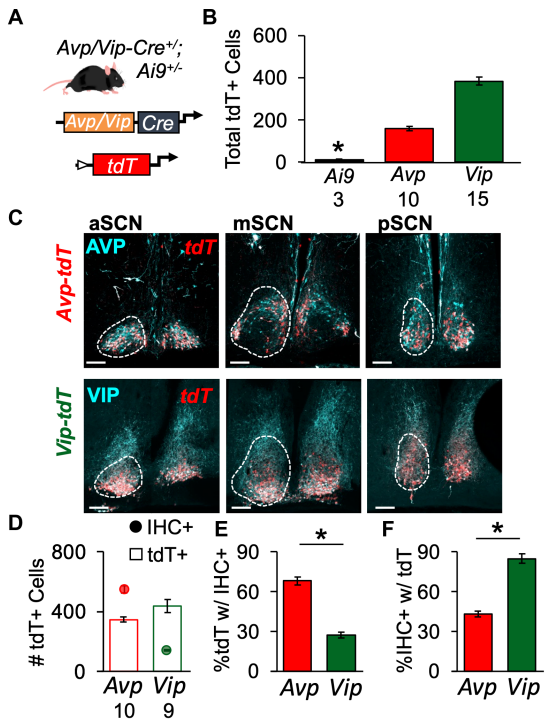

FIGURE 1
Genetic strategy to label spatial location of SCN peptide classes. **(A)** Schematic illustrating genetic approach to label *Avp*- and *Vip*-expressing SCN neurons with tdT. **(B)** tdT labeling is Cre-dependent in the SCN. Also see Supplementary Figure S4. Cre: $F(2,22)=24.1$, $p<0.0001$; Sex: $F(1,22)=0.3$, $p>0.5$; Cre*Sex: $F(2,22)=0.6$, $p>0.5$. **(C)** Representative SCN slices illustrating tdT and AVP/VIP expression in a male *Avp-tdT* or *Vip-tdT* SCN. Scale bars=100µm. **(D)** Total number of labeled neurons collapsed across three SCN slices. AVP/VIP IHC: Cre: $F(1,15)=175$, $p<0.0001$; Sex: $F(1,15)=0.2$, $p>0.6$; Cre*Sex: $F(1,15)=0.3$, $p>0.5$. tdT+: Cre: $F(1,15)=4.12$, $p=0.06$; Sex: $F(1,15)=2.3$, $p>0.1$; Cre*Sex: $F(1,15)=2.9$, $p>0.1$. **(E)** More *Avp-tdT+* neurons express AVP compared to *Vip-tdT+* neurons that express VIP. Cre: $F(1,15)=112.5$, $p<0.0001$; Sex: $F(1,15)=3.2$, $p=0.09$; Cre*Sex: $F(1,15)=0.1$, $p>0.8$. **(F)** More *Vip-tdT+* express tdT compared to *Avp-tdT+* neurons. Cre: $F(1,15)=105.8$, $p<0.0001$; Sex: $F(1,15)=1.6$, $p>0.2$; Cre*Sex: $F(1,15)=0.2$, $p>0.6$. Numbers below *x*-axis in panels **(B,D)** indicate sample sizes for each group. Contrasts comparing genotype, *$p<0.05$.

in adulthood using a more comprehensive approach. All *Avp-tdT+* and *Vip-tdT+* cells were counted throughout the anteroposterior SCN in each sex (Figure 2A, Supplementary Figure S1). When counted across all SCN slices, *Vip-tdT+* cells outnumbered *Avp-tdT+* cells [Figure 2B, Cre: $F(1,9)=18.1$, $p<0.005$], with more *Vip-tdT+* cells in females than males [Figure 2B, Sex: $F(1,9)=7.3$, $p<0.05$, Contrasts, $p<0.05$]. When parsed by SCN slice position, females displayed more *Avp-tdT+* cells than males in the anterior and posterior SCN, and females displayed more *Vip-tdT+* cells than males in the middle SCN (Figure 2C, Contrasts, $p<0.05$).

To complement anatomical division of anteroposterior regions, we used k means clustering based on the cellular coordinates for each sample. For both cell types and sexes, the best fit was achieved by $k=3$ spatial clusters, as determined by the elbow location for total cell dispersion (i.e., Inertia, Figure 3A) and cell dispersion normalized to the total cell counts/sample (Distance, Supplementary Figure S6A). Spatial mapping of k means revealed one posterior cluster and two clusters that were positioned more anterior, which differed in lateral-medial location (Figure 3B). As expected, there was greater dispersion of *Avp-tdT+* than *Vip-tdT+* neurons at $k=3$ (Figure 3B, Supplementary Figure S6B), with differences in both inertia and distance [Inertia-Cre: $F(1,9)=17.5$, $p<0.005$; Distance-Cre: $F(1,9)=17.5$, $p<0.005$, Contrasts, $p<0.05$]. There were no significant sex differences in cell dispersion [Inertia-Sex: $F(1,9)=4.8$, $p=0.06$; Distance- Sex: $F(1,9)=0.1$, $p>0.7$]. Nevertheless, more subtle sex differences were detected in the number and location of cells in specific clusters (Figures 3B,C). Specifically, females displayed a larger number of lateral *Avp-tdT+* cells relative to males (Figure 3C, Contrasts, $p<0.01$), and the lateral cluster for both cell types was positioned more anterior in the female SCN (Figure 3B).

To evaluate spatial patterns of cell density, next we mapped the number of neighboring cells within a 50 µm radius of each cellular coordinate (Figure 4A, Supplementary Videos S1–S4). Cell density maps were aggregated for all samples, with and without normalization to the total number of cells in each sample (Figures 4B,C, Supplementary Figures S7, S8). For both cell types, the overall morphology was similar across sex (Figures 4B,C, Supplementary Figures S7, S8). Compared to males, between-sample variability in cell density and total cell counts was larger in female *Avp-tdT* SCN neurons [Supplementary Figure S3B, Levene's test $F(1,5)=10.52$, $p<0.05$], and *Avp-tdT+* cell density was similar when normalized to the total number of cells in each sample (Figures 4B,C, Supplementary Figures S7, S8). For *Vip-tdT+* neurons, variability in cell density and total cell counts did not differ by sex [Supplementary Figure S3C, Levene's test $F(1,4)=0.38$, $p>0.7$]. Collectively, these results suggest that spatial patterning of cellular density for *Avp-tdT+* and *Vip-tdT+* populations does not markedly differ between male and female SCN in adulthood.

SCN development of *Avp-tdT* and *Vip-tdT* expression

To evaluate SCN developmental patterning, we applied these mapping approaches to samples collected from age E18-P10 (Figures 5A,B). Gestational weight, litter size, and gains in pup weight did not differ by genotype (Supplementary Figures S9A–C). Sex did not influence growth in SCN area (Supplementary Figure S2C). Overall, *Avp-tdT* mice had smaller SCN than *Vip-tdT* mice [Supplementary Figure S9D, Cre: $F(1,84)=8.53$, $p<0.005$], but this was only statistically significant at P05 (Supplementary Figure S9D, Contrasts, $p<0.01$). These data indicate that the presence of *Avp-tdT* and *Vip-tdT* transgenes did not interfere with gross measures of development.

Over development, the total number of *Avp-tdT+* and *Vip-tdT+* cells increased, with differences across cell type [Figure 5C, Age: $F(7,99)=411.9$, $p<0.0001$, Cre: $F(1,99)=89.6$, $p<0.001$, Cre*Age: $F(7,99)=11.3$, $p<0.0001$]. In addition, sex influenced the developmental appearance of *Avp-tdT+* and *Vip-tdT+* cells [Supplementary Figure S10A, Age*Sex: $F(7,99)=5.17$, $p<0.0001$]. Effects of cell-type and sex persisted when cell counts were normalized to sex-specific adult values [Figure 5D, Age: $F(7,99)=409.4$, $p<0.0001$, Sex: $F(1,99)=50.18$, $p<0.0001$, Age*Sex: $F(7,99)=8.27$, $p<0.0001$, Cre*Age: $F(7,99)=2.88$, $p<0.01$], indicating that these effects were not driven by differences in the total number of cells. In each sex, a very

10.3389/fnins.2023.1177458

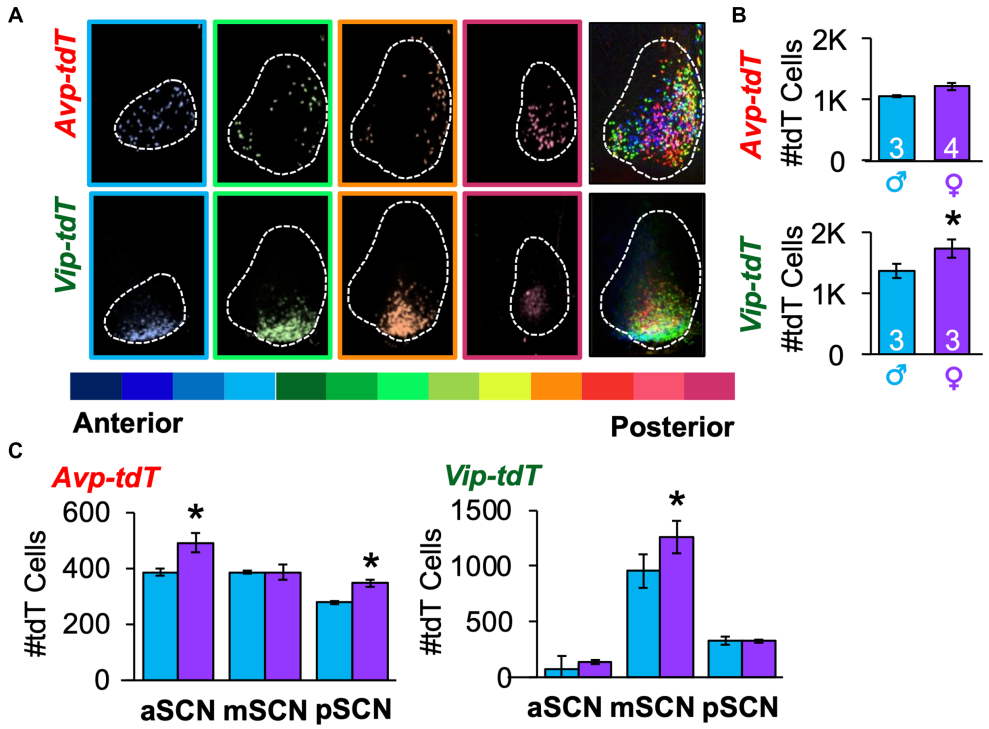

FIGURE 2
Spatial mapping of SCN neurons in each peptide class in adulthood. **(A)** A representative subset of SCN slices collected through the anteroposterior axis from a female *Avp-tdT* or *Vip-tdT* mouse. Each slice is color-coded by slice position, with cells in all SCN slices superimposed in rightmost panel. The full set of SCN slices from this mouse is illustrated in Supplementary Figure S1A. **(B)** Total number of SCN *Avp-tdT+* and *Vip-tdT+* neurons in each sex. Cre: $F(1,9)=18.1$, $p<0.005$, Sex: $F(1,9)=7.3$, $p<0.05$; Sex*Cre: $F(1,9)=1.1$, $p>0.3$. **(C)** Sex influences the number of *Avp-tdT+* and *Vip-tdT+* neurons in different anteroposterior SCN regions. *Avp-tdT* - Sex: $F(1,5)=5.6$, $p=0.06$; Position: $F(2,10)=25.1$, $p=0.0001$; Sex*Position: $F(2,10)=4.5$, $p<0.05$. *Vip-tdT* – Sex: $F(1,4)=3.6$, $p>0.1$; Position: $F(2,8)=63.3$, $p<0.0001$; Sex*Position: $F(2,8)=1.5$, $p>0.2$. aSCN, mSCN, and pSCN: Anterior, middle, and posterior SCN. Contrasts comparing male and female data for each cell type, *$p<0.05$.

small number of *Avp-tdT+* and *Vip-tdT+* cells were detected at E18 (Supplementary Figure S10A, *Avp* = 1.2 ± 0.1%, *Vip* = 1.9% ± 0.2% relative to adult). Population size for both cell types increased progressively after birth. When collapsed by sex, *Avp-tdT+* cells appeared between P01–P05, after which it stabilized to adult levels. In contrast, the relative number of *Vip-tdT+* cells increased from P01-P03 and P05-P10. At P05, there was a greater percentage of *Avp-tdT+* cells compared to *Vip-tdT+* cells (Figure 5C, Contrasts, $p<0.005$). For each cell type, males displayed an accelerated appearance of *tdT+* cells (Figure 5D). Relative to females, males had more *Avp-tdT+* cells from P01–P05 and more *Vip-tdT+* cells from P01-P10 (Figure 5D, Contrasts, $p<0.05$). The number of labeled cells decreased to adult levels in males, and females displayed a more linear appearance of total cells for each peptide class (Figure 5D).

To evaluate spatial patterning, the number of cells in each class was analyzed in the anterior, middle, and posterior SCN. Age influenced cellular patterning in a manner that interacted with SCN region and sex (Figure 6, Supplementary Figure S10). Specifically, *Avp-tdT+* cells appeared in a posterior-to-anterior pattern over P01–P05, with larger regional differences in males (Figures 6A,B, Contrasts, $p<0.05$). In the posterior SCN of males, *Avp-tdT+* cells exceeded adult levels from P03–P05 (Figure 6B). Regional patterning was also detected for *Vip-tdT+* cells, which was likewise influenced by sex (Figures 6C,D, Contrasts, $p<0.05$). *Vip-tdT+* cells increased steadily in the middle SCN, with a larger proportion in males at P03 (Figure 6D, Contrasts, $p<0.05$). At P05, both sexes displayed an increased proportion of *Vip-tdT+* cells in the posterior SCN that exceeded adult levels (Figure 6D). Last, the appearance of *Vip-tdT+* cells in the anterior SCN was delayed in females, with a lower percentage relative to males at P05 and P10 (Figure 6D, Contrasts, $p<0.05$). These results suggest that there are regional gradients in the onset of peptide transcription that differ by cell type, region, and sex.

For each cell type, cell dispersion within k-means clusters increased as the SCN grew with age (Figure 7A). Cellular dispersion was greater in *Avp-tdT+* than *Vip-tdT+* cells (Figures 7B,C, Supplementary Figure S11B, Contrasts, $p<0.05$). *Avp-tdT+* cells displayed a stepwise pattern of increasing cell dispersion over P03–P10 (Figure 7A), likely since this cell type spans the anteroposterior extent of the SCN. Developmental patterning of cellular appearance and density was influenced by sex (Figures 8, 9). The spatial location of clusters was largely similar in each sex across development (Figure 8A), but sex influenced the appearance of cells in different clusters (Figures 8B,C). In male SCN, there was a greater number of *Avp-tdT+* cells in the posterior cluster at P05 and in the lateral cluster over P03–P10 relative to females (Figure 8B, Contrasts, $p<0.05$). In addition, males had more *Vip-tdT+* cells in the lateral cluster from P01–P10 and in the posterior cluster at P10 (Figure 8C, Contrasts, $p<0.05$). In contrast, females displayed more *Avp-tdT+* cells in the medial cluster at P03 and more *Vip-tdT+* cells in the medial cluster at P10 (Figures 8B,C, Contrasts, $p<0.05$). Overall, male SCN displayed

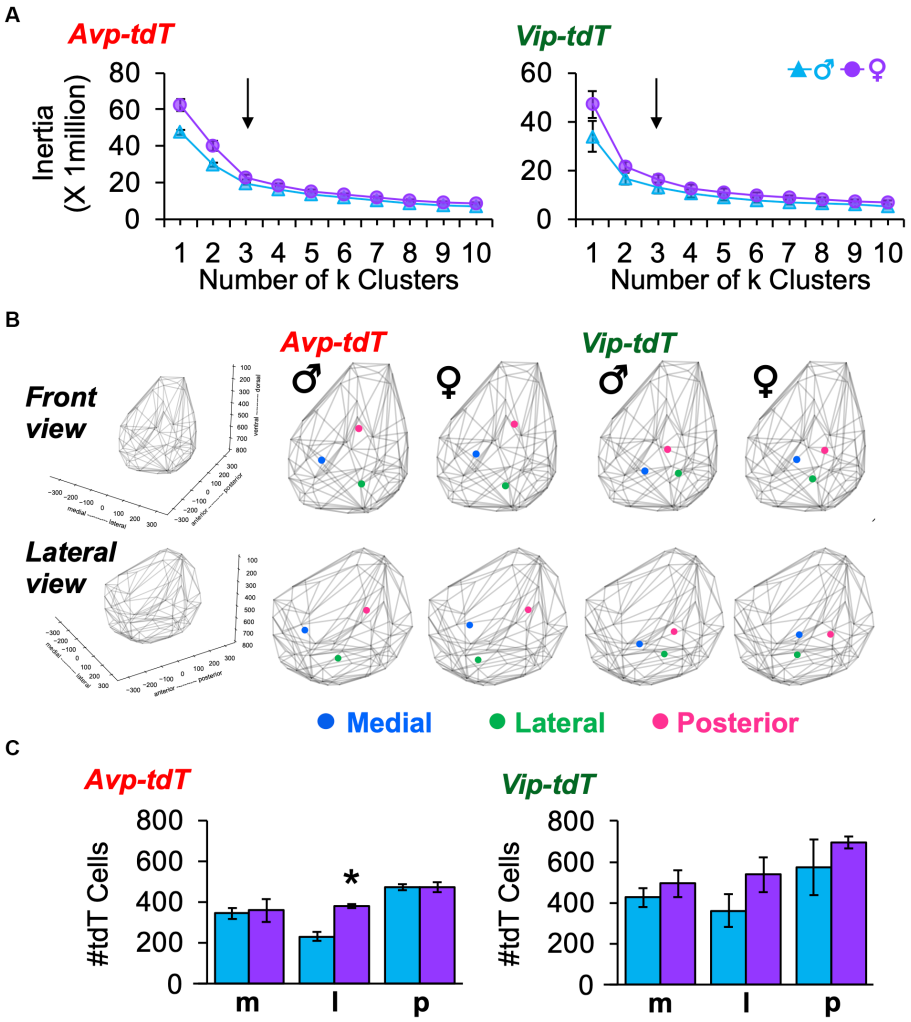

FIGURE 3
K means clustering of SCN neurons in each peptide class in adulthood. **(A)** Elbow plots illustrating measures of cell dispersion in each sex. Arrow indicates optimal number of clusters. **(B)** Spatial location of cluster centers in each sex in the front and lateral views. Lattice frames illustrate SCN boundaries determined using the position of all tdT identified cells observed across adult samples of both genotypes. **(C)** Number of labeled cells in each cluster divided by sex. Cre: $F(1, 9)=18.1$, $p<0.005$, Cluster: $F(2,18)=10.4$, $p=0.001$, Sex: $F(1,9)=7.3$, $p<0.05$, Cell*Cluster: $F(2,18)=0.2$, $p>0.8$, Cell*Sex: $F(1,9)=1.1$, $p>0.3$, Cluster*Sex: $F(2,18)=1.3$, $p>0.3$, Cell*Cluster*Sex: $F(2,18)=0.2$, $p>0.8$. m, medial; l, lateral; p, posterior. Contrasts comparing male and female data for each cell type, *$p<0.05$.

higher cell density for *Avp-tdT*+ and *Vip-tdT*+ cells at P05 relative to females (Figure 9). Collectively, these results indicate that the developmental patterning of SCN *Avp-tdT*+ and *Vip-tdT*+ cells differs by sex.

Discussion

Hypothalamus anatomy is conserved across vertebrates, guided by molecular mechanisms that determine nuclei that contain a large diversity of neuron subtypes (Xie and Dorsky, 2017; Benevento et al., 2022). Relative to early induction, less is known about how these peptide circuits are built and remodeled. In the SCN, AVP and VIP neurons regulate the timing of sleep, stress, and reproductive rhythms. How peptide circuits in the SCN network are patterned over development may have profound impacts on clock function in adulthood. Using a genetic approach to track SCN development of peptide circuits, our results suggest that SCN patterning varies by cell type, regional subcluster, and sex. The genetic and/or hormonal factors that guide spatial patterning of SCN peptide circuits warrant further research.

Genetic labeling provides insight into cellular appearance over development without the need for surgical or chemical interventions that could interfere with gestation and rearing, but this approach is not without limitations. Both *Avp-tdT* and *Vip-tdT* expression were Cre-dependent consistent with previous work describing these genetic models (Harris et al., 2014; Taniguchi, 2014). We find that 70% of *Avp-tdT*+ neurons were AVP-IHC+, but less than 30% of *Vip-tdT*+ neurons were VIP-IHC+. Low VIP co-expression could reflect transient *Vip* transcription over development in a large subset of these cells, which would suggest that the VIP cell population may expand and contract over development. However, this observation could also reflect threshold limits of IHC and/or expression of VIP-related peptides that are not recognized by the antibody used

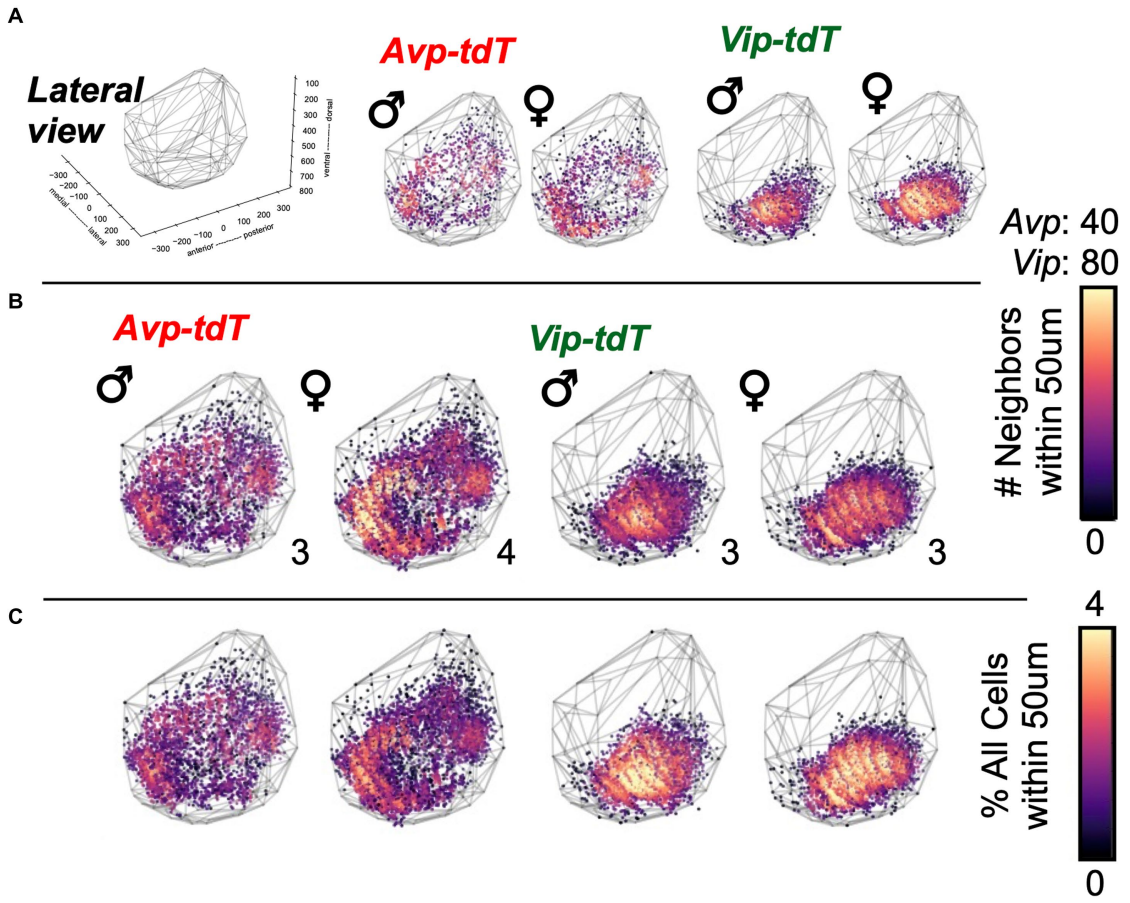

FIGURE 4
Cell density plots for SCN neurons in each peptide class in adult males and females. **(A)** Representative samples illustrating cell density in individual mice of each sex. All samples are illustrated in Supplementary Figures S3B,C. **(B–C)** Cell density plots aggregated across samples illustrating total number of neighboring cells **(B)** and the percentage of neighboring cells normalized to total SCN cells in each sample **(C)**. Number in bottom right corner for each map indicates the number of aggregated samples. Other orientations are illustrated in Supplementary Figures S7–S8 and Videos S1–S4.

here (Lee et al., 2013; Southey et al., 2014). On the other hand, over 80% of VIP+ cells were labeled with *Vip-tdT*, but only 43% of AVP+ cells were labeled by *Avp-tdT*. This has been noted in previous work using this genetic model (Jamieson, 2020), and our data indicate that the dorsal region of the middle SCN displays the highest rate of AVP and *Avp-tdT* discordance. Failure of Cre-mediated recombination may reflect cellular variation in epigenetic landscape or genetic history (i.e., loss of Cre during cell division), as suggested in previous work (Jamieson, 2020). Interestingly, low co-expression of AVP and *Avp-tdT* labeling also occurs in this genetic model after adult-specific viral transduction (Jamieson, 2020), which suggests that this observation is not a developmental artifact. Further, we used colchicine to visualize total protein expression over the daily cycle, yet our estimates of colocalization are similar to this previous work (Jamieson, 2020). Collectively, these data indicate that each mouse model used here does not fully capture peptide expression in adulthood, thus limiting the ability to comprehensively map each peptide population during development. However, these validation data also provide an interesting complement to our developmental results by suggesting that neurons in each peptide class may be divided into subclusters. Another known caveat of Cre models is that the transgene can interfere with native peptide expression (Cheng et al., 2019; Joye et al., 2020; Rohr et al., 2020). Importantly, peptide levels in heterozygous *Avp-tdT* and *Vip-tdT* mice do not differ from wildtype mice during early development, and circadian behavior does not differ between these two groups during adulthood (Joye et al., 2020; Rohr et al., 2020). However, it is difficult to dismiss that a non-significant decrease in peptide expression could alter SCN patterning. With these caveats in mind, we decided to employ this genetic approach to study SCN peptide development because it avoids the need to conduct a circadian time course at every age.

Consistent with previous work, we find developmental differences in the appearance of SCN neurons in these two peptide classes. *Avp-tdT*+ and *Vip-tdT*+ neurons were detected as early as E18, and cell number for each peptide class increased over the first 10 days after birth. Our results align well with previous work characterizing peptide development, despite the likely delays between transcription onset and tdT labeling. *Avp* and *Vip* transcripts are first detected in the mouse SCN at E17-18 and E18-19, respectively (Vandunk et al., 2011). AVP and VIP peptide levels increase over the first 2 days after birth (Hyodo et al., 1992; Carmona-Alcocer et al., 2018). SCN AVP cell numbers are stable after P06, but AVP peptide levels continue to increase from P06-P30 (Herzog et al., 2000), which would not be captured with the

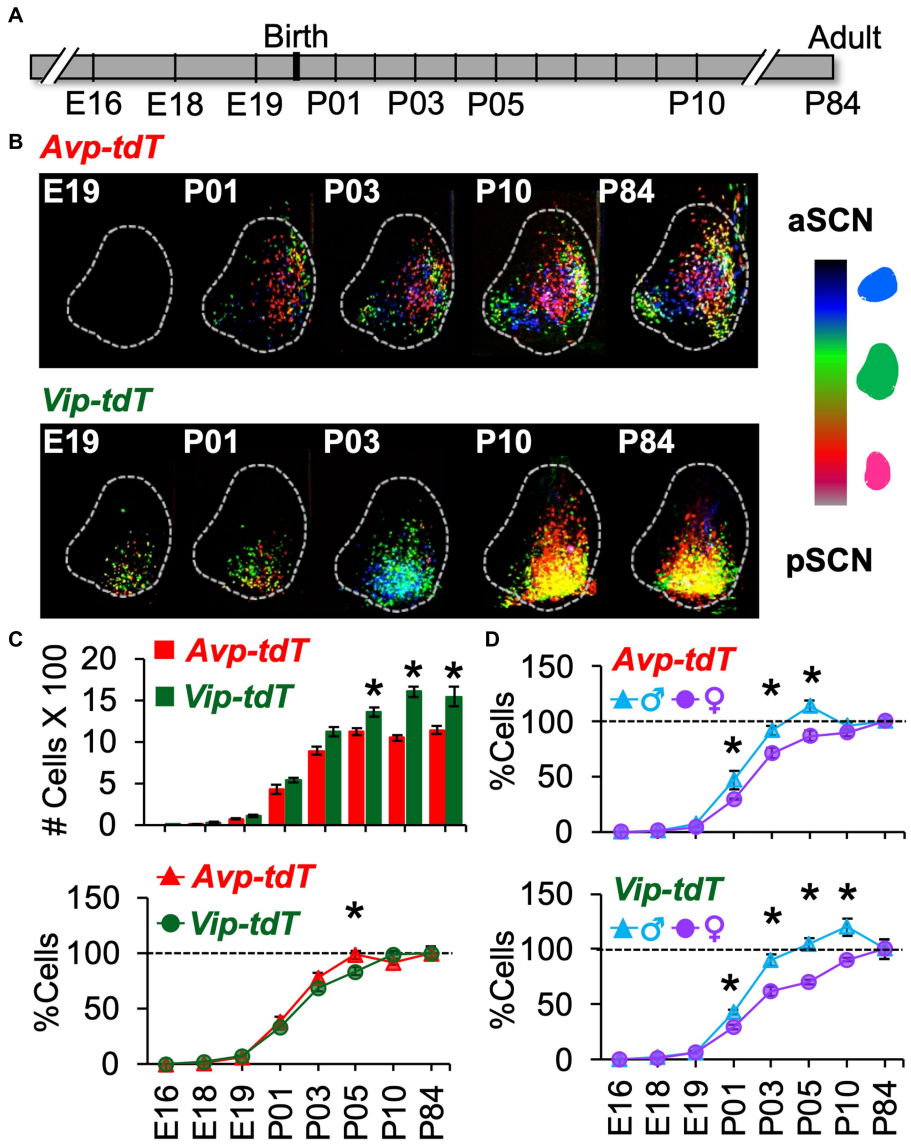

FIGURE 5
Developmental appearance of SCN *Avp-tdT+* and *Vip-tdT+* neurons. **(A)** Timeline illustrating ages of tissue collection. Breeding and pup development data are in Supplementary Figure S9. **(B)** Labeled cells aggregated across SCN slice positions for a representative mouse from each age group illustrating progressive appearance of *Avp-tdT+* and *Vip-tdT+* cells during postnatal development. **(C)** Top: Total number of SCN *Avp-tdT+* and *Vip-tdT+* cells across development. Cre: $F(1,99)=89.6$, $p<0.001$, Age: $F(7,99)=411.9$, $p<0.0001$, Sex: $F(1,99)=0.7$, $p=0.4$, Cre*Age: $F(7,99)=11.3$, $p<0.0001$, Cre*Sex: $F(1,99)=0.01$, $p>0.9$, Age*Sex: $F(7,99)=5.2$, $p<0.0001$, Cre*Age*Sex: $F(7,99)=0.9$, $p>0.5$. Bottom: To compare developmental patterns across cell type, cell counts at each age were expressed as a percent relative to the number of labeled cells in adults. Cre: $F(1,99)=0.2$, $p>0.6$, Age: $F(7,99)=409.4$, $p<0.0001$, Sex: $F(1,99)=50.2$, $p<0.0001$, Cre*Age: $F(7,99)=2.9$, $p<0.01$, Cre*Sex: $F(1,99)=1.6$, $p>0.2$, Age*Sex: $F(7,99)=8.3$, $p<0.0001$, Cre*Age*Sex: $F(7,99)=1.1$, $p>0.3$. Total cell counts divided by sex, with magnification of E18-P01 data, are in Supplementary Figure S10A. **(D)** Percent labeled cells at each age divided by sex and cell type. *Avp-tdT+*: Age: $F(7,47)=204.3$, $p<0.0001$, Sex: $F(1,47)=16.4$, $p<0.0005$, Age*Sex: $F(7,47)=3.0.1$, $p<0.01$. *Vip-tdT+*: Age: $F(7,52)=222.5$, $p<0.0001$, Sex: $F(1,52)=36.0$, $p<0.0001$, Age*Sex: $F(7,52)=6.7$, $p<0.0001$. Contrasts comparing genotype or sex in each cell type, *$p<0.05$.

present approach. Interesting, VIP cell numbers increase between P06 and P30 (Herzog et al., 2000), which we also observed in the present work. It remains unclear what molecular factors drive ontogenetic patterning in these two different SCN peptide classes. The expression of transcription factors during embryogenesis (e.g., Lhx1, Shh, Six3, Six6) is important in early SCN specification (Bedont and Blackshaw, 2015; Carmona-Alcocer et al., 2020). Lhx1 and Foxd1 deletion decreases both *Avp* and *Vip* expression (Vandunk et al., 2011; Newman et al., 2018), suggesting common genetic programs direct cellular differentiation in both classes. Differences in the timing of developmental patterning across these two cell types may be linked to intrinsic and/or extrinsic factors. Over the first week of life, terminal differentiation, synaptogenesis, gliogenesis, and retinal innervation occurs in the SCN (Bedont and Blackshaw, 2015; Carmona-Alcocer et al., 2020), and later maturation of the VIP population may be linked to postnatal maturation of retinal inputs (McNeill et al., 2011). Both AVP and VIP influence SCN circuit formation and function during development (Ono et al., 2016; Bedont et al., 2018; Mazuski et al.,

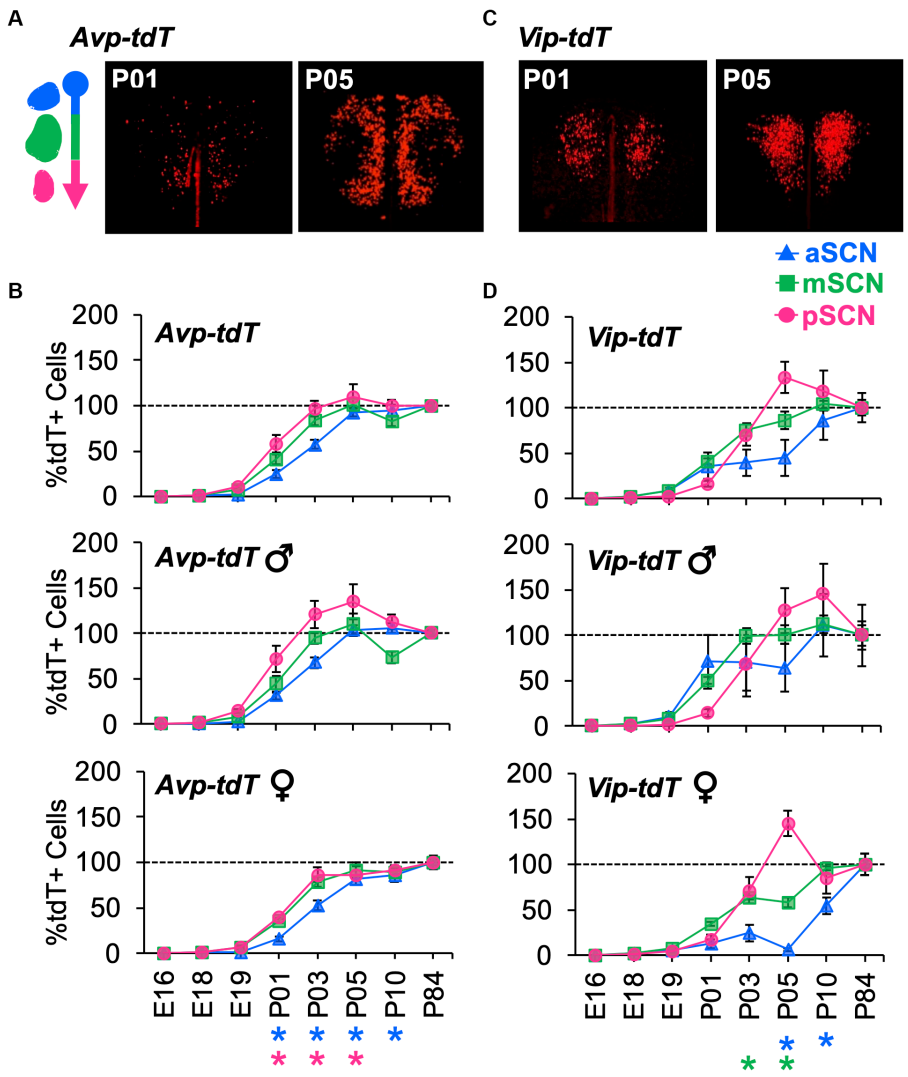

FIGURE 6
Developmental appearance of *Avp-tdT+* and *Vip-tdT+* neurons across the anteroposterior SCN. **(A)** Representative samples illustrating spatial patterning of *Avp-tdT+* development in the reconstructed horizontal plane. Coronal sections are illustrated in Supplementary Figure S10A. **(B)** Regional gradients in the developmental appearance of *Avp-tdT+* neurons are influenced by sex. Age: $F(7,47)=190.4$, $p<0.0001$, Sex: $F(1,47)=18.5$, $p<0.0001$, Position: $F(2,94)=14.7$, $p<0.001$, Age*Sex: $F(7,47)=3.3$, $p<0.01$, Age*Position: $F(14,94)=3.3$, $p<0.0005$, Sex*Position: $F(2,94)=4.2$, $p<0.02$, Age*Sex*Position: $F(14,94)=0.8$, $p>0.6$. **(C)** Representative samples illustrating spatial patterning *Vip-tdT+* development in the reconstructed horizontal plane. Coronal sections are illustrated in Supplementary Figure S10B. **(D)** Regional gradients in the developmental appearance of *Vip-tdT+* neurons are influenced by sex. Age: $F(7,53)=97.5$, $p<0.0001$, Sex: $F(1,53)=22.7$, $p<0.0001$, Position: $F(2,106)=3.3$, $p<0.05$, Age*Sex: $F(7,53)=4.0$, $p<0.005$, Age*Position: $F(14,106)=2.9$, $p<0.001$, Sex*Position: $F(2,106)=1.8$, $p>0.1$, Age*Sex*Position: $F(14,106)=0.7$, $p>0.7$. *Post hoc* contrasts comparing male and female data for each slice position are indicated by color-coded asterisks below the *x* axis of each female graph in panels **(B,D)**. *$p<0.05$.

2020); thus, the timing and patterning of these peptides may have important consequences for pacemaker function.

Notably, we find that SCN peptide classes can be further subdivided based on spatial patterning during development. For *Avp-tdT+* neurons, we find that there is a posterior–anterior gradient when analyzed by anatomical division based on slice position. Consistent with these results, k means clustering detected that the posterior *Avp-tdT+* cluster matured faster than other clusters in each sex, with development of one of the more anterior *Avp-tdT+* clusters delayed in a sex-influenced manner. For *Vip-tdT+* neurons, we observed a rapid increase of cells in the posterior cluster. Consistent with this result, VIP neurons have been reported to increase in the middle and posterior SCN over P06 to P30 in the mouse SCN (Herzog et al., 2000). In rats, two developmental waves of *Vip* expression have been reported, with *Vip* transcription occurring in medial SCN cells earlier than lateral SCN cells (Ban et al., 1997; Kawamoto et al., 2003). These two spatially defined subclusters displayed different patterns of clock gene expression and photic sensitivity in adulthood (Ban et al., 1997; Kawamoto et al., 2003). Further, VIP neurons in adulthood can be divided into two subpopulations based on electrical firing (Mazuski et al., 2018) and *Grp* expression (Todd et al., 2020; Wen et al., 2020). Interestingly, recent work in the mouse has found two subsets of *Avp* cells that differ in the expression of *Cck* or *Nms* (Moffitt et al., 2018). Whether functional subclasses of SCN *Vip* and *Avp* cells map onto the regional subclusters found here would be interesting to examine in future work. It is also unclear how the current spatial gradients may

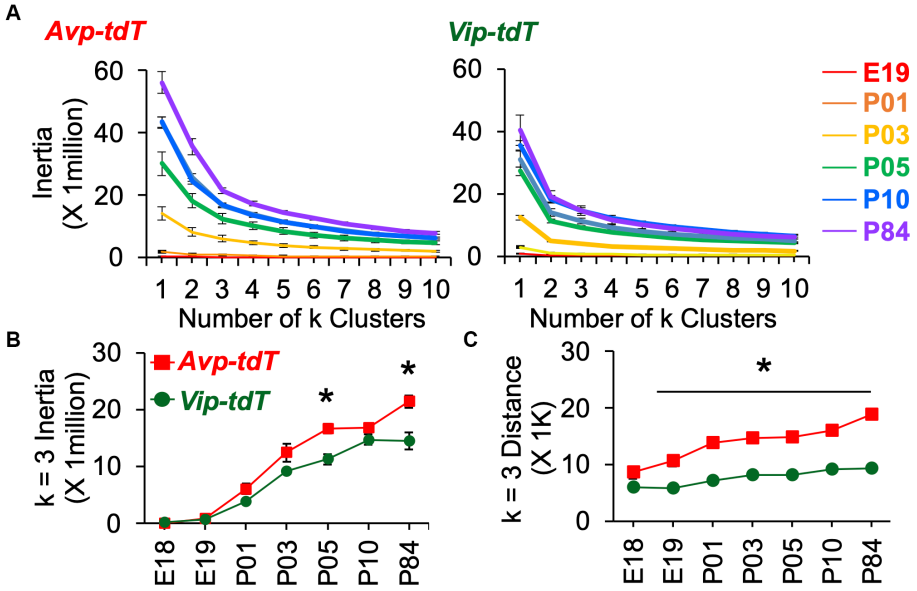

FIGURE 7
K means clustering of SCN neurons appearance across development. **(A)** Elbow plots illustrating measures of cell dispersion across age, collapsed across sex. **(B,C)** Measures of cell dispersion across age, collapsed across sex. Inertia and distance data are divided by sex in Supplementary Figure S11B. *Inertia*: Cre: $F(1,88)=34.4$, $p<0.001$, Age: $F(6,88)=124.7$, $p<0.0001$, Sex: $F(1,88)=0.2$, $p>0.6$, Cre*Age: $F(6,88)=4.0$, $p<0.005$, Cre*Sex: $F(1,88)=0.1$, $p>0.7$, Age*Sex: $F(6,88)=1.9$, $p=0.08$, Cre*Age*Sex: $F(6,88)=0.3$, $p>0.9$. *Distance*: Cre: $F(1,88)=408.4$, $p<0.001$, Age: $F(6,88)=33.1$, $p<0.0001$, Sex: $F(1,88)=2.1$, $p>0.1$, Cre*Age: $F(6,88)=6.7$, $p<0.001$, Cre*Sex: $F(1,88)=1.0$, $p>0.3$, Age*Sex: $F(6,88)=0.3$, $p>0.9$, Cre*Age*Sex: $F(6,88)=0.6$, $p>0.7$. Contrasts comparing genotype, *$p<0.05$.

relate to those found for SCN neurogenesis (Okamura et al., 1983; Kabrita and Davis, 2008). In the mouse, SCN neurogenesis occurs over embryonic days 11–16 (E11–16), with a peak at E14 (Shimada and Nakamura, 1973; Kabrita and Davis, 2008). SCN core neurons are generated at an earlier age (peak at E12) than shell neurons (peak E13.5) in the mouse (Kabrita and Davis, 2008). In the hamster, AVP neurons are generated over a longer period of gestation than VIP and GRP neurons in the SCN core, with posterior-to-anterior gradients (Antle et al., 2005). The degree to which onset of neuropeptide expression is timed by neurogenesis and/or extrinsic cues present in the microenvironment (Xie and Dorsky, 2017; Benevento et al., 2022) remains an open question.

Last, our results suggest that developmental patterning of peptide circuits is influenced by sex. The male SCN displayed postnatal increases in *Avp-tdT*+ and *Vip-tdT*+ cell number and density that were not maintained into adulthood. The number of *Vip-tdT*+ cells at P05–P10 exceeded adult levels in male SCN by 20%, and the number of *Avp-tdT*+ neurons at P05 exceeded adult levels in male SCN by 14%. Given that tdT labeling is permanent, this observation suggests a loss of SCN cells in males. The majority of SCN apoptosis occurs over P01-P07 in mice, but an estimated 20% of cells are lost between P07 and adulthood (Ahern et al., 2013; Bedont et al., 2014; Mosley et al., 2017). In contrast, the female SCN displayed a more linear patterning of *Avp-tdT*+ and *Vip-tdT*+ cell appearance, with increasing numbers of both cell types between P10 and P84. In addition, the more anterior *Avp-tdT*+ cluster that matured last differed by sex, with the lateral cluster appearing last in females and the medial cluster appearing last in males. Interestingly, the lateral cluster had significantly more *Avp-tdT*+ neurons in adult females than males due to the increase in cell number after P10. Likewise, the *Vip-tdT*+ cluster that matured last differed by sex, again being the lateral cluster in females and the medial cluster in males. Cell number in the lateral *Vip-tdT*+ cluster also differed by sex due to post-P10 increases in cell numbers in females. Collectively, these data indicate that SCN development is not complete by P10, raising the possibility that puberty represents another time of SCN development (Bakker and Baum, 2008).

Whether these sex differences are driven by genetic and/or hormonal factors remains to be tested, but it is tempting to speculate that sex steroids are organizing development of SCN circuits. The critical period in the mouse is E18-P01, with testosterone levels decreasing rapidly at birth and the sensitive period in females extending to P07 (McCarthy et al., 2018). The mouse SCN expresses receptors for sex steroids that are regionally clustered in adulthood (Joye and Evans, 2021), potentially contributing to the spatial gradients in peptide development observed here. Sex differences in SCN neurogenesis have been reported in mice (Abizaid et al., 2004). Specifically, females display more SCN neurogenesis at E18, and testosterone administration to pregnant dams reduces SCN neurogenesis at this late stage of gestation (Abizaid et al., 2004). This suggests that neurogenesis closes earlier in males (Shimada and Nakamura, 1973; Kabrita and Davis, 2008) due to sex steroid signaling. Last, the peak in SCN apoptosis occurs at P03 in males and P05 in females with equivalent postnatal SCN volume (Ahern et al., 2013). To our knowledge, sex steroid receptor expression over early SCN development has not been examined in the mouse, but androgen receptors are expressed later in life in the slow-maturing diurnal rodent *Octogon degus* (Lee et al., 2004). Overall, our work suggests

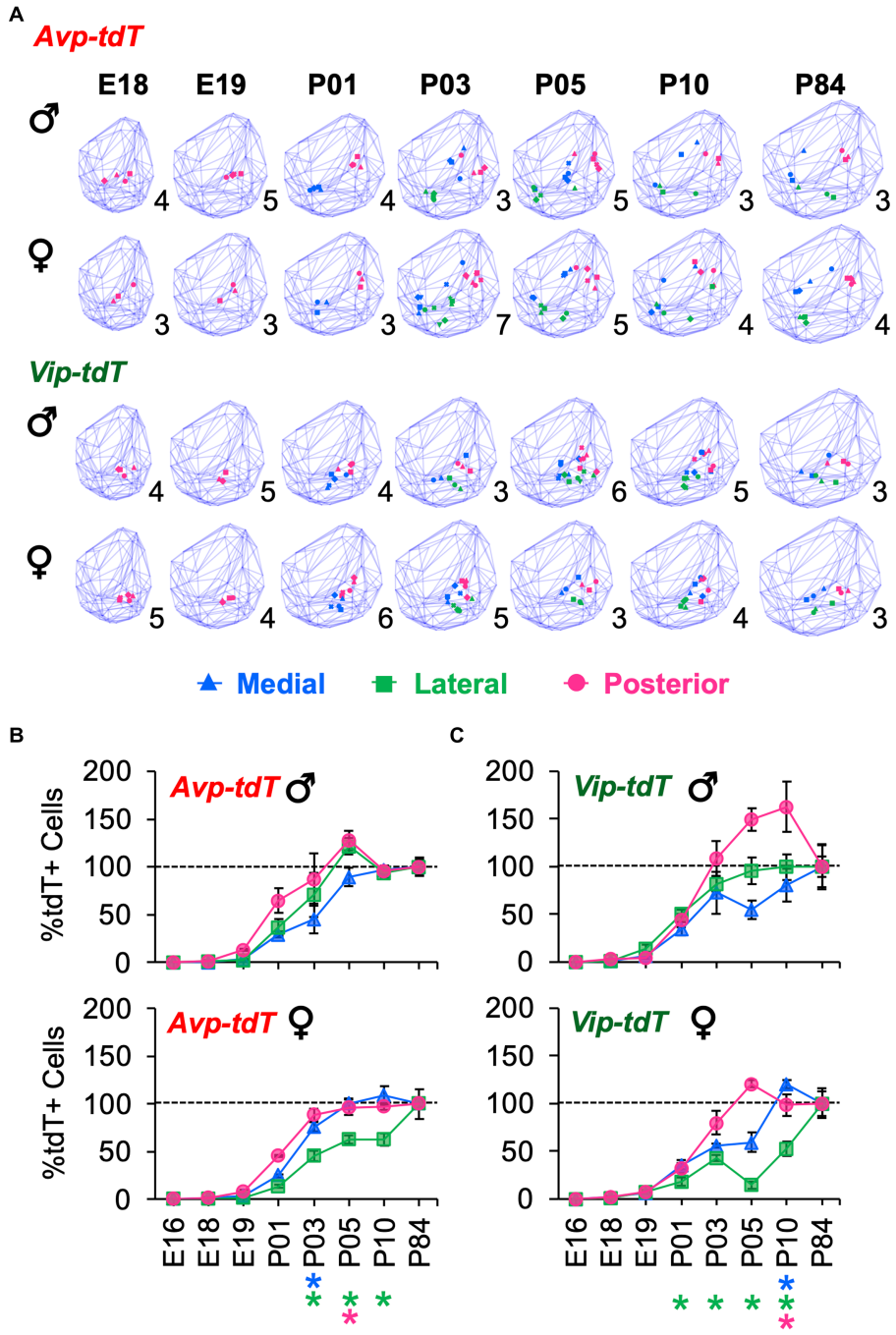

FIGURE 8
Sex differences in the development of SCN *Avp-tdT+* and *Vip-tdT+* cell clusters. **(A)** Spatial location of cellular clusters at each age for each cell type. Blue lattice frames illustrate SCN boundaries at each age. Number in bottom right corner for each map indicates number of samples. **(B,C)** Regional gradients in the developmental appearance of *Avp-tdT+* and *Vip-tdT* clusters are influenced by sex. Age: $F(6,88)=237.2$, $p<0.0001$, Cre: $F(1,88)=75.4$, $p<0.0001$, Cluster: $F(2,176)=144.5$, $p<0.0001$, Sex: $F(1,88)=0.1$, $p>0.8$, Age*Cre: $F(6,88)=7.4$, $p<0.0001$, Age*Cluster: $F(12,176)=14.7$, $p<0.0001$, Age*Sex: $F(6,88)=3.2$, $p<0.01$, Cre*Cluster: $F(2,176)=8.3$, $p<0.0005$, Cre*Sex: $F(1,88)=0.3$, $p>0.6$, Cluster*Sex: $F(2,176)=5.1$, $p<0.01$, Age*Cre*Cluster: (12,176)=4.4, $p<0.0001$, Age*Cluster*Sex: $F(12,176)=1.9$, $p<0.05$, Age*Cre*Cluster*Sex: $F(12,176)=1.5$, $p>0.1$. *Post hoc* contrasts comparing male and female data for each slice position are indicated by color-coded asterisks below the *x* axis of each female graph in Figures 6B,C. *$p<0.05$.

that SCN shape and peptide expression is influenced by sex, as reported in humans (Swaab et al., 1985, 1994). Future work is warranted to further explore how adult clock function in both sexes is influenced by SCN patterning during development and how this process is impacted by postnatal conditions, such as light exposure (Cambras et al., 1998, 2015; Ohta et al., 2006; Ciarleglio et al., 2011; Ono et al., 2013; Madahi et al., 2018).

A central question here concerned the spatial patterning of SCN maturation, which we have represented in 3D maps for two different peptide classes at critical developmental time points

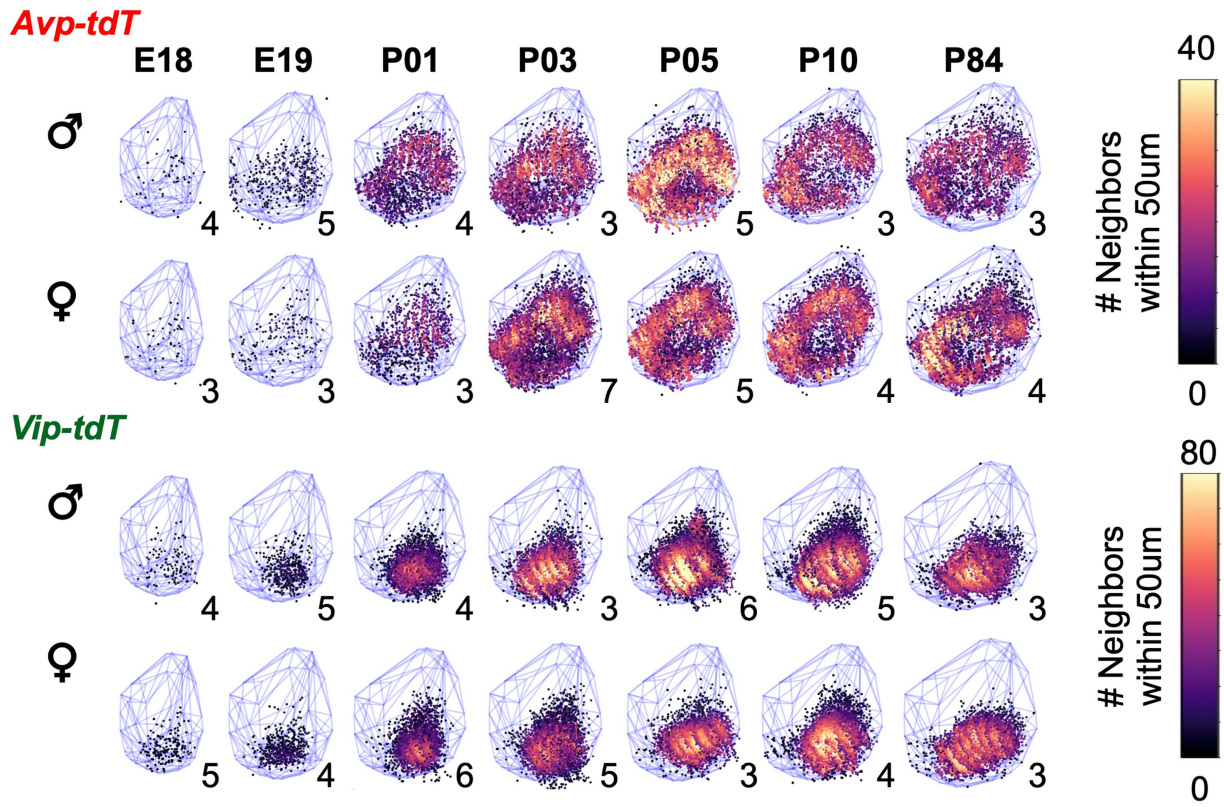

FIGURE 9
Sex differences in the developmental patterning of SCN *Vip-tdT* cell density plots aggregated across samples for each age illustrating total number of neighboring cells for each cell type in each sex. Blue lattice frames illustrate SCN boundaries at each age. Number in bottom right corner for each map indicates the number of aggregated samples. Additional orientations at select ages are shown in Supplementary Videos S1–S12.

spanning mid-embryonic age to adulthood in both sexes. Both AVP and VIP neurons provide local and long-range cues that regulate daily rhythms (Vosko et al., 2007; Kalsbeek et al., 2010; Mieda et al., 2016; Rohr et al., 2020; Shan et al., 2020). In addition to shell-core compartmentalization, cellular differences in clock function are also evident across the anteroposterior axis (Hamada et al., 2004; Yan et al., 2007; Evans et al., 2011; Yoshikawa et al., 2015, 2017). Do regional and sex differences in peptide development relate to differences in cellular clock function in adulthood? Does the spatial patterning of the SCN circuit extend to other developmental milestones (e.g., gliogenesis, axonal projections)? Do sexual dimorphisms in spatial patterning relate to sex differences in peptide expression and clock function in adulthood? More broadly, how do changes in the conditions present during the postnatal SCN developmental period influence circuit formation to modulate adult clock function? Future work investigating these questions may provide insight into the long-lasting effects of perinatal light exposure on health (Torrey et al., 2000; Madahi et al., 2018).

Data availability statement

The raw data supporting the conclusions of this article will be made available by the authors, without undue reservation.

Ethics statement

The animal study was reviewed and approved by the Institutional Animal Care and Use Committees at Marquette University.

Author contributions

JAE wrote the manuscript with contributions and approval of submitted version by all authors. All authors contributed to experimental design, performed research and analyzed data.

Funding

This work was supported by the National Institutes of Health, R01GM143545.

Acknowledgments

We thank the Marquette University Animal Resource Center for animal care. For their assistance, we also thank Alec Huber, Favio Saabedra, Jennifer John, and John Abel.

Conflict of interest

The authors declare that the research was conducted in the absence of any commercial or financial relationships that could be construed as a potential conflict of interest.

Publisher's note

All claims expressed in this article are solely those of the authors and do not necessarily represent those of their affiliated organizations, or those of the publisher, the editors and the reviewers. Any product that may be evaluated in this article, or claim that may be made by its manufacturer, is not guaranteed or endorsed by the publisher.

Supplementary material

The Supplementary material for this article can be found online at: https://www.frontiersin.org/articles/10.3389/fnins.2023.1177458/full#supplementary-material

References

Abizaid, A., Mezei, G., Sotonyi, P., and Horvath, T. L. (2004). Sex differences in adult suprachiasmatic nucleus neurons emerging late prenatally in rats. *Eur. J. Neurosci.* 19, 2488–2496. doi: 10.1111/j.0953-816X.2004.03359.x

Abrahamson, E. E., and Moore, R. Y. (2001). Suprachiasmatic nucleus in the mouse: retinal innervation, intrinsic organization and efferent projections. *Brain Res.* 916, 172–191. doi: 10.1016/S0006-8993(01)02890-6

Ahern, T. H., Krug, S., Carr, A. V., Murray, E. K., Fitzpatrick, E., Bengston, L., et al. (2013). Cell death atlas of the postnatal mouse ventral forebrain and hypothalamus: effects of age and sex. *J. Comp. Neurol.* 521, 2551–2569. doi: 10.1002/cne.23298

Altman, J., and Bayer, S. A. (1978). Development of the diencephalon in the rat. I. Autoradiographic study of the time of origin and settling patterns of neurons of the hypothalamus. *J. Comp. Neurol.* 182, 945–971. doi: 10.1002/cne.901820511

Antle, M. C., Foley, D. K., Foley, N. C., and Silver, R. (2003). Gates and oscillators: A network model of the brain clock. *J. Biol. Rhythm.* 18, 339–350. doi: 10.1177/0748730403253840

Antle, M. C., Lesauter, J., and Silver, R. (2005). Neurogenesis and ontogeny of specific cell phenotypes within the hamster suprachiasmatic nucleus. *Brain Res. Dev. Brain Res.* 157, 8–18. doi: 10.1016/j.devbrainres.2005.02.017

Bakker, J., and Baum, M. J. (2008). Role for estradiol in female-typical brain and behavioral sexual differentiation. *Front. Neuroendocrinol.* 29, 1–16. doi: 10.1016/j.yfrne.2007.06.001

Ban, Y., Shigeyoshi, Y., and Okamura, H. (1997). Development of vasoactive intestinal peptide mRNA rhythm in the rat suprachiasmatic nucleus. *J. Neurosci.* 17, 3920–3931. doi: 10.1523/JNEUROSCI.17-10-03920.1997

Bedont, J. L., and Blackshaw, S. (2015). Constructing the suprachiasmatic nucleus: a watchmaker's perspective on the central clockworks. *Front. Syst. Neurosci.* 9:74:74. doi: 10.3389/fnsys.2015.00074

Bedont, J. L., Legates, T. A., Slat, E. A., Byerly, M. S., Wang, H., Hu, J., et al. (2014). Lhx1 controls terminal differentiation and circadian function of the suprachiasmatic nucleus. *Cell Rep.* 7, 609–622. doi: 10.1016/j.celrep.2014.03.060

Bedont, J. L., Rohr, K. E., Bathini, A., Hattar, S., Blackshaw, S., Sehgal, A., et al. (2018). Asymmetric vasopressin signaling spatially organizes the master circadian clock. *J. Comp. Neurol.* 526, 2048–2067. doi: 10.1002/cne.24478

Benevento, M., Hokfelt, T., and Harkany, T. (2022). Ontogenetic rules for the molecular diversification of hypothalamic neurons. *Nat. Rev. Neurosci.* 23, 611–627. doi: 10.1038/s41583-022-00615-3

Brancaccio, M., Maywood, E. S., Chesham, J. E., Loudon, A. S., and Hastings, M. H. (2013). A Gq-Ca2+ axis controls circuit-level encoding of circadian time in the suprachiasmatic nucleus. *Neuron* 78, 714–728. doi: 10.1016/j.neuron.2013.03.011

Buhr, E. D., and Takahashi, J. S. (2013). Molecular components of the mammalian circadian clock. *Handb. Exp. Pharmacol.* 217, 3–27. doi: 10.1007/978-3-642-25950-0_1

Cambras, T., Canal, M. M., Cernuda-Cernuda, R., Garcia-Fernandez, J. M., and Diez-Noguera, A. (2015). Darkness during early postnatal development is required for normal circadian patterns in the adult rat. *Chronobiol. Int.* 32, 178–186. doi: 10.3109/07420528.2014.960048

Cambras, T., Vilaplana, J., Torres, A., Canal, M. M., Casamitjana, N., Campuzano, A., et al. (1998). Constant bright light (LL) during lactation in rats prevents arrhythmicity due to LL. *Physiol. Behav.* 63, 875–882. doi: 10.1016/S0031-9384(98)00006-7

Carmona-Alcocer, V., Abel, J. H., Sun, T. C., Petzold, L. R., Doyle, F. J., Simms, C. L., et al. (2018). Ontogeny of circadian rhythms and synchrony in the suprachiasmatic nucleus. *J. Neurosci.* 38, 1326–1334. doi: 10.1523/JNEUROSCI.2006-17.2017

Carmona-Alcocer, V., Rohr, K. E., Joye, D. A. M., and Evans, J. A. (2020). Circuit development in the master clock network of mammals. *Eur. J. Neurosci.* 51, 82–108. doi: 10.1111/ejn.14259

Cheng, A. H., Fung, S. W., and Cheng, H. M. (2019). Limitations of the Avp-IRES2-Cre (JAX #023530) and Vip-IRES-Cre (JAX #010908) models for chronobiological investigations. *J. Biol. Rhythm.* 34, 634–644. doi: 10.1177/0748730419871184

Ciarleglio, C. M., Axley, J. C., Strauss, B. R., Gamble, K. L., and Mcmahon, D. G. (2011). Perinatal photoperiod imprints the circadian clock. *Nat. Neurosci.* 14, 25–27. doi: 10.1038/nn.2699

Davis, F. C., Boada, R., and Ledeaux, J. (1990). Neurogenesis of the hamster suprachiasmatic nucleus. *Brain Res.* 519, 192–199. doi: 10.1016/0006-8993(90)90077-O

Enoki, R., Kuroda, S., Ono, D., Hasan, M. T., Ueda, T., Honma, S., et al. (2012). Topological specificity and hierarchical network of the circadian calcium rhythm in the suprachiasmatic nucleus. *Proc. Natl. Acad. Sci. U. S. A.* 109, 21498–21503. doi: 10.1073/pnas.1214415110

Evans, J. A., Leise, T. L., Castanon-Cervantes, O., and Davidson, A. J. (2011). Intrinsic regulation of spatiotemporal organization within the suprachiasmatic nucleus. *PLoS One* 6:e15869. doi: 10.1371/journal.pone.0015869

Evans, J. A., Leise, T. L., Castanon-Cervantes, O., and Davidson, A. J. (2013). Dynamic interactions mediated by nonredundant signaling mechanisms couple circadian clock neurons. *Neuron* 80, 973–983. doi: 10.1016/j.neuron.2013.08.022

Hamada, T., Antle, M. C., and Silver, R. (2004). Temporal and spatial expression patterns of canonical clock genes and clock-controlled genes in the suprachiasmatic nucleus. *Eur. J. Neurosci.* 19, 1741–1748. doi: 10.1111/j.1460-9568.2004.03275.x

Harris, J. A., Hirokawa, K. E., Sorensen, S. A., Gu, H., Mills, M., Ng, L. L., et al. (2014). Anatomical characterization of Cre driver mice for neural circuit mapping and manipulation. *Front Neural Circuits* 8:76. doi: 10.3389/fncir.2014.00076

Hastings, M. H., Maywood, E. S., and Brancaccio, M. (2018). Generation of circadian rhythms in the suprachiasmatic nucleus. *Nat. Rev. Neurosci.* 19, 453–469. doi: 10.1038/s41583-018-0026-z

Herzog, E. D., Grace, M. S., Harrer, C., Williamson, J., Shinohara, K., and Block, G. D. (2000). The role of clock in the developmental expression of neuropeptides in the suprachiasmatic nucleus. *J. Comp. Neurol.* 424, 86–98. doi: 10.1002/1096-9861(20000814)424:1<86::AID-CNE7>3.0.CO;2-W

Houdek, P., and Sumova, A. (2014). In vivo initiation of clock gene expression rhythmicity in fetal rat suprachiasmatic nuclei. *PLoS One* 9:e107360. doi: 10.1371/journal.pone.0107360

Hyodo, S., Yamada, C., Takezawa, T., and Urano, A. (1992). Expression of provasopressin gene during ontogeny in the hypothalamus of developing mice. *Neuroscience* 46, 241–250. doi: 10.1016/0306-4522(92)90024-V

Inagaki, N., Honma, S., Ono, D., Tanahashi, Y., and Honma, K. (2007). Separate oscillating cell groups in mouse suprachiasmatic nucleus couple photoperiodically to the onset and end of daily activity. *Proc. Natl. Acad. Sci. U. S. A.* 104, 7664–7669. doi: 10.1073/pnas.0607713104

Isobe, Y., and Muramatsu, K. (1995). Day-night differences in the contents of vasoactive intestinal peptide, gastrin-releasing peptide and Arg-vasopressin in the suprachiasmatic nucleus of rat pups during postnatal development. *Neurosci. Lett.* 188, 45–48. doi: 10.1016/0304-3940(95)11391-9

Jamieson, B. (2020). *The role of SCN AVP neurons in modulating RP3V kisspeptin neuron activity in physiological and pathological reproductive states*. Dunedin University of Otago.

Joye, D. A. M., and Evans, J. A. (2021). Sex differences in daily timekeeping and circadian clock circuits. *Semin. Cell Dev. Biol.* 126, 45–55. doi: 10.1016/j.semcdb.2021.04.026

Joye, D. A. M., Rohr, K. E., Keller, D., Inda, T., Telega, A., Pancholi, H., et al. (2020). Reduced VIP expression affects circadian clock function in VIP-IRES-CRE mice (JAX 010908). *J. Biol. Rhythm.* 35, 340–352. doi: 10.1177/0748730420925573

Kabrita, C. S., and Davis, F. C. (2008). Development of the mouse suprachiasmatic nucleus: determination of time of cell origin and spatial arrangements within the nucleus. *Brain Res.* 1195, 20–27. doi: 10.1016/j.brainres.2007.12.020

Kalsbeek, A., Fliers, E., Hofman, M. A., Swaab, D. F., and Buijs, R. M. (2010). Vasopressin and the output of the hypothalamic biological clock. *J. Neuroendocrinol.* 22, 362–372. doi: 10.1111/j.1365-2826.2010.01956.x

Kawamoto, K., Nagano, M., Kanda, F., Chihara, K., Shigeyoshi, Y., and Okamura, H. (2003). Two types of VIP neuronal components in rat suprachiasmatic nucleus. *J. Neurosci. Res.* 74, 852–857. doi: 10.1002/jnr.10751

Landgraf, D., Koch, C. E., and Oster, H. (2014). Embryonic development of circadian clocks in the mammalian suprachiasmatic nuclei. *Front. Neuroanat.* 8:143. doi: 10.3389/fnana.2014.00143

Lee, T. M., Hummer, D. L., Jechura, T. J., and Mahoney, M. M. (2004). Pubertal development of sex differences in circadian function: an animal model. *Ann. N. Y. Acad. Sci.* 1021, 262–275. doi: 10.1196/annals.1308.031

Lee, J. E., Zamdborg, L., Southey, B. R., Atkins, N. Jr., Mitchell, J. W., Li, M., et al. (2013). Quantitative peptidomics for discovery of circadian-related peptides from the rat suprachiasmatic nucleus. *J. Proteome Res.* 12, 585–593. doi: 10.1021/pr300605p

Madahi, P. G., Ivan, O., Adriana, B., Diana, O., and Carolina, E. (2018). Constant light during lactation programs circadian and metabolic systems. *Chronobiol. Int.* 35, 1153–1167. doi: 10.1080/07420528.2018.1465070

Madisen, L., Zwingman, T. A., Sunkin, S. M., Oh, S. W., Zariwala, H. A., Gu, H., et al. (2010). A robust and high-throughput Cre reporting and characterization system for the whole mouse brain. *Nat. Neurosci.* 13, 133–140. doi: 10.1038/nn.2467

Mazuski, C., Abel, J. H., Chen, S. P., Hermanstyne, T. O., Jones, J. R., Simon, T., et al. (2018). Entrainment of circadian rhythms depends on firing rates and neuropeptide release of VIP SCN neurons. *Neuron* 99, 555–563. doi: 10.1016/j.neuron.2018.06.029

Mazuski, C., Chen, S. P., and Herzog, E. D. (2020). Different roles for VIP neurons in the neonatal and adult Suprachiasmatic nucleus. *J. Biol. Rhythm.* 35, 465–475. doi: 10.1177/0748730420932073

Mccarthy, M. M., Herold, K., and Stockman, S. L. (2018). Fast, furious and enduring: sensitive versus critical periods in sexual differentiation of the brain. *Physiol. Behav.* 187, 13–19. doi: 10.1016/j.physbeh.2017.10.030

Mcfarlane, L., Truong, V., Palmer, J. S., and Wilhelm, D. (2013). Novel PCR assay for determining the genetic sex of mice. *Sex. Dev.* 7, 207–211. doi: 10.1159/000348677

Mcneill, D. S., Sheely, C. J., Ecker, J. L., Badea, T. C., Morhardt, D., Guido, W., et al. (2011). Development of melanopsin-based irradiance detecting circuitry. *Neural Dev.* 6:8. doi: 10.1186/1749-8104-6-8

Mieda, M., Okamoto, H., and Sakurai, T. (2016). Manipulating the cellular circadian period of arginine vasopressin neurons alters the behavioral circadian period. *Curr. Biol.* 26, 2535–2542. doi: 10.1016/j.cub.2016.07.022

Moffitt, J. R., Bambah-Mukku, D., Eichhorn, S. W., Vaughn, E., Shekhar, K., Perez, J. D., et al. (2018). Molecular, spatial, and functional single-cell profiling of the hypothalamic preoptic region. *Science* 362:eaau5324. doi: 10.1126/science.aau5324

Mohawk, J. A., Green, C. B., and Takahashi, J. S. (2012). Central and peripheral circadian clocks in mammals. *Annu. Rev. Neurosci.* 35, 445–462. doi: 10.1146/annurev-neuro-060909-153128

Moore, R. Y., Speh, J. C., and Leak, R. K. (2002). Suprachiasmatic nucleus organization. *Cell Tissue Res.* 309, 89–98. doi: 10.1007/s00441-002-0575-2

Mosley, M., Shah, C., Morse, K. A., Miloro, S. A., Holmes, M. M., Ahern, T. H., et al. (2017). Patterns of cell death in the perinatal mouse forebrain. *J. Comp. Neurol.* 525, 47–64. doi: 10.1002/cne.24041

Newman, E. A., Kim, D. W., Wan, J., Wang, J., Qian, J., and Blackshaw, S. (2018). Foxd1 is required for terminal differentiation of anterior hypothalamic neuronal subtypes. *Dev. Biol.* 439, 102–111. doi: 10.1016/j.ydbio.2018.04.012

Nugent, R., and Meila, M. (2010). An overview of clustering applied to molecular biology. *Methods Mol. Biol.* 620, 369–404. doi: 10.1007/978-1-60761-580-4_12

Ohta, H., Mitchell, A. C., and Mcmahon, D. G. (2006). Constant light disrupts the developing mouse biological clock. *Pediatr. Res.* 60, 304–308. doi: 10.1203/01.pdr.0000233114.18403.66

Okamura, H., Fukui, K., Koyama, E., Tsutou, H. L., Tsutou, T., Terubayashi, H., et al. (1983). Time of vasopressin neuron origin in the mouse hypothalamus: examination by combined technique of immunocytochemistry and [3H]thymidine autoradiography. *Brain Res.* 285, 223–226. doi: 10.1016/0165-3806(83)90055-X

Ono, D., Honma, S., and Honma, K. (2013). Postnatal constant light compensates Cryptochrome1 and 2 double deficiency for disruption of circadian behavioral rhythms in mice under constant dark. *PLoS One* 8:e80615. doi: 10.1371/journal.pone.0080615

Ono, D., Honma, S., and Honma, K. (2016). Differential roles of AVP and VIP signaling in the postnatal changes of neural networks for coherent circadian rhythms in the SCN. *Sci. Adv.* 2:e1600960. doi: 10.1126/sciadv.1600960

Ono, D., Honma, K. I., and Honma, S. (2021). Roles of neuropeptides, VIP and AVP, in the mammalian central circadian clock. *Front. Neurosci.* 15:650154. doi: 10.3389/fnins.2021.650154

Reppert, S. (1992). "Pre-natal development of a hypothalamic biological clock" in *Progress in Brain Reserach*. eds. D. Swabb, M. Hofman, M. Mirmiran, R. Ravid and F. Van Leeuwen (Amsterdam: Elsevier Science Pulishers BV)

Rohr, K. E., Telega, A., Savaglio, A., and Evans, J. A. (2020). Vasopressin regulates daily rhythms and circadian clock circuits in a manner influenced by sex. *Horm. Behav.* 127:104888. doi: 10.1016/j.yhbeh.2020.104888

Shan, Y., Abel, J. H., Li, Y., Izumo, M., Cox, K. H., Jeong, B., et al. (2020). Dual-color single-cell imaging of the suprachiasmatic nucleus reveals a circadian role in network synchrony. *Neuron* 108, 164–179. doi: 10.1016/j.neuron.2020.07.012

Shimada, M., and Nakamura, T. (1973). Time of neuron origin in mouse hypothalamic nuclei. *Exp. Neurol.* 41, 163–173. doi: 10.1016/0014-4886(73)90187-8

Shimomura, H., Moriya, T., Sudo, M., Wakamatsu, H., Akiyama, M., Miyake, Y., et al. (2001). Differential daily expression of Per1 and Per2 mRNA in the suprachiasmatic nucleus of fetal and early postnatal mice. *Eur. J. Neurosci.* 13, 687–693. doi: 10.1046/j.0953-816x.2000.01438.x

Sladek, M., Sumova, A., Kovacikova, Z., Bendova, Z., Laurinova, K., and Illnerova, H. (2004). Insight into molecular core clock mechanism of embryonic and early postnatal rat suprachiasmatic nucleus. *Proc. Natl. Acad. U. S. A.* 101, 6231–6236. doi: 10.1073/pnas.0401149101

Southey, B. R., Lee, J. E., Zamdborg, L., Atkins, N. Jr., Mitchell, J. W., Li, M., et al. (2014). Comparing label-free quantitative peptidomics approaches to characterize diurnal variation of peptides in the rat suprachiasmatic nucleus. *Anal. Chem.* 86, 443–452. doi: 10.1021/ac4023378

Swaab, D. F., Fliers, E., and Partiman, T. S. (1985). The suprachiasmatic nucleus of the human brain in relation to sex, age and senile dementia. *Brain Res.* 342, 37–44. doi: 10.1016/0006-8993(85)91350-2

Swaab, D. F., Zhou, J. N., Ehlhart, T., and Hofman, M. A. (1994). Development of vasoactive intestinal polypeptide neurons in the human suprachiasmatic nucleus in relation to birth and sex. *Brain Res. Dev. Brain Res.* 79, 249–259. doi: 10.1016/0165-3806(94)90129-5

Taniguchi, H. (2014). Genetic dissection of GABAergic neural circuits in mouse neocortex. *Front. Cell. Neurosci.* 8:8. doi: 10.3389/fncel.2014.00008

Todd, W. D., Venner, A., Anaclet, C., Broadhurst, R. Y., De Luca, R., Bandaru, S. S., et al. (2020). Suprachiasmatic VIP neurons are required for normal circadian rhythmicity and comprised of molecularly distinct subpopulations. *Nat. Commun.* 11:4410. doi: 10.1038/s41467-020-17197-2

Torrey, E. F., Miller, J., Rawlings, R., and Yolken, R. H. (2000). Seasonal birth patterns of neurological disorders. *Neuroepidemiology* 19, 177–185. doi: 10.1159/000026253

Vandunk, C., Hunter, L. A., and Gray, P. A. (2011). Development, maturation, and necessity of transcription factors in the mouse suprachiasmatic nucleus. *J. Neurosci.* 31, 6457–6467. doi: 10.1523/JNEUROSCI.5385-10.2011

Vosko, A. M., Schroeder, A., Loh, D. H., and Colwell, C. S. (2007). Vasoactive intestinal peptide and the mammalian circadian system. *Gen. Comp. Endocrinol.* 152, 165–175. doi: 10.1016/j.ygcen.2007.04.018

Wen, S., Ma, D., Zhao, M., Xie, L., Wu, Q., Gou, L., et al. (2020). Spatiotemporal single-cell analysis of gene expression in the mouse suprachiasmatic nucleus. *Nat. Neurosci.* 23, 456–467. doi: 10.1038/s41593-020-0586-x

Wreschnig, D., Dolatshad, H., and Davis, F. C. (2014). Embryonic development of circadian oscillations in the mouse hypothalamus. *J. Biol. Rhythm.* 29, 299–310. doi: 10.1177/0748730414545086

Xie, Y., and Dorsky, R. I. (2017). Development of the hypothalamus: conservation, modification and innovation. *Development* 144, 1588–1599. doi: 10.1242/dev.139055

Yan, L., Karatsoreos, I., Lesauter, J., Welsh, D. K., Kay, S., Foley, D., et al. (2007). Exploring spatiotemporal organization of SCN circuits. *Cold Spring Harb. Symp. Quant. Biol.* 72, 527–541. doi: 10.1101/sqb.2007.72.037

Yoshikawa, T., Inagaki, N. F., Takagi, S., Kuroda, S., Yamasaki, M., Watanabe, M., et al. (2017). Localization of photoperiod responsive circadian oscillators in the mouse suprachiasmatic nucleus. *Sci. Rep.* 7:8210. doi: 10.1038/s41598-017-08186-5

Yoshikawa, T., Nakajima, Y., Yamada, Y., Enoki, R., Watanabe, K., Yamazaki, M., et al. (2015). Spatiotemporal profiles of arginine vasopressin transcription in cultured suprachiasmatic nucleus. *Eur. J. Neurosci.* 42, 2678–2689. doi: 10.1111/ejn.13061

frontiers | Frontiers in Neuroscience

TYPE Original Research
PUBLISHED 14 June 2023
DOI 10.3389/fnins.2023.1166137

OPEN ACCESS

EDITED BY
Jeff Jones,
Washington University in St. Louis,
United States

REVIEWED BY
Alessio Delogu,
King's College London, United Kingdom
Sergio I. Hidalgo,
University of California,
Davis, United States

*CORRESPONDENCE
Joseph S. Takahashi
✉ joseph.takahashi@utsouthwestern.edu

RECEIVED 14 February 2023
ACCEPTED 23 May 2023
PUBLISHED 14 June 2023

CITATION
Schirmer AE, Kumar V, Schook A, Song EJ, Marshall MS and Takahashi JS (2023) *Cry1* expression during postnatal development is critical for the establishment of normal circadian period.
Front. Neurosci. 17:1166137.
doi: 10.3389/fnins.2023.1166137

Cry1 expression during postnatal development is critical for the establishment of normal circadian period

Aaron E. Schirmer[1,2], Vivek Kumar[1,3], Andrew Schook[1], Eun Joo Song[1], Michael S. Marshall[1,4,5] and Joseph S. Takahashi[1,6,7]*

[1]Department of Neurobiology, Northwestern University, Evanston, IL, United States, [2]Department of Biology, Northeastern Illinois University, Chicago, IL, United States, [3]The Jackson Laboratory, Bar Harbor, ME, United States, [4]Department of Pathology, Massachusetts General Hospital, Boston, MA, United States, [5]Harvard Medical School, Boston, MA, United States, [6]Department of Neuroscience, Peter O'Donnell Jr. Brain Institute, University of Texas Southwestern Medical Center, Dallas, TX, United States, [7]Howard Hughes Medical Institute, University of Texas Southwestern Medical Center, Dallas, TX, United States

The mammalian circadian system generates an approximate 24-h rhythm through a complex autoregulatory feedback loop. Four genes, *Period1* (*Per1*), *Period2* (*Per2*), *Cryptochrome1* (*Cry1*), and *Cryptochrome2* (*Cry2*), regulate the negative feedback within this loop. Although these proteins have distinct roles within the core circadian mechanism, their individual functions are poorly understood. Here, we used a tetracycline trans-activator system (tTA) to examine the role of transcriptional oscillations in *Cry1* and *Cry2* in the persistence of circadian activity rhythms. We demonstrate that rhythmic *Cry1* expression is an important regulator of circadian period. We then define a critical period from birth to postnatal day 45 (PN45) where the level of *Cry1* expression is critical for setting the endogenous free running period in the adult animal. Moreover, we show that, although rhythmic *Cry1* expression is important, in animals with disrupted circadian rhythms overexpression of *Cry1* is sufficient to restore normal behavioral periodicity. These findings provide new insights into the roles of the Cryptochrome proteins in circadian rhythmicity and further our understanding of the mammalian circadian clock.

KEYWORDS

cryptochrome, circadian rhythms, period length, development, gene expression

Introduction

Many biological, physiological, and behavioral processes oscillate with a daily (approximately 24-h) rhythm. These circadian rhythms provide synchrony between an organism and its external environment, allowing the organism to adapt its physiology and behavior to changing environmental conditions (Pittendrigh, 1960). In the mammalian circadian system, light information is detected by specialized ganglion cells in the retina and is then transmitted along the retinal hypothalamic tract to the suprachiasmatic nucleus (SCN) of the hypothalamus (Johnson et al., 1988; Moore et al., 1995; Provencio et al., 2002). The SCN acts as the central circadian pacemaker, regulating circadian rhythms in mammalian behavior and physiology (Low-Zeddies and Takahashi, 2001; Takahashi et al., 2008; Welsh et al., 2010).

Individual cells and groups of cells within the mature SCN have cell-autonomous circadian periods (Welsh et al., 1995; Herzog et al., 1998) and oscillate with different phases (Quintero

et al., 2003; Shan et al., 2020). These rhythms are determined by a cell-autonomous molecular clock that is the result of interlocking transcriptional regulatory feedback loops that come together to produce an approximate 24-h cycle (Takahashi, 2017; Cox and Takahashi, 2019). The positive elements in the primary feedback loop are two transcription factors, CLOCK and BMAL1 (Vitaterna et al., 1994; King et al., 1997; Bunger et al., 2000), whereas the negative elements consist of the PER1 and PER2 proteins (members of the PAS protein family) and CRY1 and CRY2 proteins (members of the vitamin B2-based blue light photoreceptor/photolyase protein family; Kume et al., 1999; van der Horst et al., 1999; Zheng et al., 1999; Cermakian et al., 2001). The PER proteins dimerize with the CRY proteins to inhibit the CLOCK and BMAL1 complex, preventing *Per* and *Cry* gene expression (Cox and Takahashi, 2019).

All four of the negative feedback loop proteins are necessary for the core circadian mechanism (Griffin et al., 1999; van der Horst et al., 1999; Vitaterna et al., 1999; Zheng et al., 1999; Bae et al., 2001). However, mice lacking *Cry1* have a short circadian period, while mice lacking *Cry2* have a lengthened period (van der Horst et al., 1999; Vitaterna et al., 1999), suggesting that the CRY proteins have different modes of action within the molecular clock. One limitation of null mouse lines is that they permanently remove genes in an irreversible manner throughout the lifespan of the entire organism. Thus, very little is known about the importance of these proteins in the development of the SCN.

In this study, we used a tetracycline-controlled transactivator (tTA) system to investigate the developmental impact of *Cry1* and *Cry2* expression. We created tg(tetO:*Cry1*) and tg(tetO:*Cry2*) mice, which in combination with pre-existing tg(Scg2:tTA) mice (Hong et al., 2007) allow for inducible, brain-specific overexpression of *Cry1* or *Cry2*, respectively. We first assessed the persistence and maintenance of circadian behavioral rhythms in mice overexpressing *Cry1* or *Cry2* specifically in the brain. Surprisingly, we found that oscillations in *Cry1* and *Cry2* expression are not essential for the persistence of circadian rhythmicity but play an important role in maintaining the period of circadian behavioral rhythms. Next, in order to better understand the role of the molecular clockwork in SCN development, the tTA system was used to overexpress *Cry1* throughout the brain at various points through development. We uncovered a novel role for *Cry1* in the development of free running period and defined a critical period of *Cry1* expression lasting from birth until postnatal day 45 (PN45). Finally, to test the hypothesis that rhythmicity of *Cry1* (not just expression) is necessary for a functional circadian clock, *Cry1* was constitutively expressed in *Cry1/Cry2* null and double null mice to assess its impact on circadian locomotor activity. We found that *Cry1* overexpression in the brain is able to partially rescue behavioral rhythmicity of *Cry1/Cry2* null mice. Together, our findings demonstrate that *Cry1* expression is important for the maintenance of circadian period but is not essential for the persistence of circadian rhythmicity *per se*.

Materials and methods

Generation of the tetO:*Cry1* vector

The tetO:*Cry1* vector was constructed using Gateway technology (Invitrogen, Carlsbad, CA). All reactions were performed as described in Invitrogen's Gateway cloning manual, except at half of the recommended volumes. BP and LR clonase (Invitrogen) were used to transfer a full length *Cry1* cDNA from ATTC (GenBank accession number BCO22174) from pCMV-Sport6 into a pTRE2ppDEST destination vector to facilitate cloning of gateway compatible cDNAs. To do this, the pTRE2 vector (Clontech) was modified by the addition of a gateway destination cassette and four rare restriction endonuclease sites. The gateway destination cassette contained attR sites and positive (Cmr) and negative (ccdB) selection markers required for gateway recombinant cloning. The rare 8 base pair restriction endonucleases PmeI (New England BioLabs, Beverly, MA) and PacI (New England BioLabs) were added into the 5′ end of the tetO sequence and the 3′ end of the poly A by site-directed mutagenesis to allow for removal of the tetO-transgene from the vector backbone for injection into oocytes. All recombinants were transformed into DH5α cells, and positive transformants were selected for on LB + Km 25 μg/mL plates. The presence of the correct fragment in the transformants from both reactions were verified by digestion with BsrG1 (New England BioLabs), followed by gel electrophoresis on a 1% agarose gel in 1X TBE. The vector was then purified on a cesium chloride gradient.

Generation of the tetO:*Cry2* vector

The tg(tetO:*Cry2*) vector was created from a full length *Cry2* cDNA from ATTC (GenBank accession number BC054794) in the pYX-Asc vector. Due to the incompatibility of the pYX-Asc vector with the Gateway system, the *Cry2* cDNA was first cloned from pYX-Asc into pTRE2pp to convert it to a Gateway compatible vector. pYX-Asc was linearized with AscI (New England BioLabs) and the ends were blunted with T4 DNA polymerase. The fragment was purified on a 1% agarose gel in 1X TBE and the 5.6 kb fragment was extracted using a Qiagen gel extraction kit (Cat. NO. 28706) by the methods described in the QIAquick Spin Handbook (Cat. NO. 28706). Simultaneously, digests were conducted on the pYX-Asc fragment with NotI (New England BioLabs) and the pTRE2pp vector with PvuII (blunt end, New England BioLabs) and NotI. Both of these fragments (a *Cry2* 3.9 kb and a pTRE2 3.8 kb fragment) were gel purified using the Qiagen gel extraction kit. The two purified fragments were then ligated with T4 DNA Ligase (New England BioLabs). The products of the ligation were transformed into DH5α cells and purified on LB + Amp 100 μg/mL plates. The presence of the correct fragments in the transformants and the purification of these fragments were conducted in the same manner as described above for tg(tetO:*Cry1*).

Creation of tg(tetO:*Cry1*) and tg(tetO:*Cry2*) mice

Using standard transgenic techniques, vectors were linearized with PmeI (New England BioLabs) and microinjected as previously described (Antoch et al., 1997). Transgenic mice were identified by PCR analysis of gDNA using a tetO-specific forward primer (CGCCTGGAGACGCCATCC) and a *Cry1* (ATGAATGGAGG CTGCCGAGG) or *Cry2* (AGGTGTCGTCATGGTTCTCC) specific reverse primer which yield a 400 bp and 748 bp band, respectively. PCR reactions were carried out using 1 μL of extracted gDNA in

11.1 µL water, 0.1 µL of AmpliTaq (Applied Biosystems, Carlsbad, CA), 1.6 µL of 1.25 mM dNTP, 2.0 µL 10X GeneAmp PCR Buffer I (Applied Biosystems), 4.0 µL 5 M Betaine, and 0.1 µL of each primer at a concentration of 100 mM to create a 20 µL reaction. The Thermocycling profile was as follows: 95° for 5 min, followed by 33 cycles of 95° for 15 s, 55° for 30 s, and 72° for 15 s, which was followed by a single extension step of 72° for 2 min. Each individual transgenic mouse resulting from the microinjection was backcrossed to WT C57BL/6J mice to create the individual hemizygous tetO lines. All mice were maintained in groups of five under standard controlled environmental conditions, with a 12-h light and 12-h dark (12:12 LD) cycle (lights on at 5 am standard time) and free access to food and water unless otherwise stated.

Conditional overexpression of *Cry* genes driven by tg(Scg2:Tta)

Both tg(tetO:*Cry1*) and tg(tetO:*Cry2*) lines were crossed to a pre-existing driver line to overexpress *Cry1* and *Cry2* in the brain (Hong et al., 2007). Hemizygous tg(Scg2:tTA) mice were crossed with the hemizygous tetO transgenic lines to produce F1 double-transgenic mice, as well as single transgenic and WT controls, as described previously with DTg *Per2* mice (Chen et al., 2009; Supplementary Figure 1A).

Validation of *Cry* overexpression in double-transgenic mice

Both tg(tetO:*Cry1*) and tg(tetO:*Cry2*) lines were validated by *in situ* hybridization and qPCR to determine expression from the transgene. *In situ* hybridization was conducted as previously described (Sangoram et al., 1998). Briefly, 20 µm coronal sections encompassing the SCN were thaw mounted on gelatin-coated slides. Sections were fixed for 5 min in 4% paraformaldehyde in PBS, treated for 10 min in 0.1 M triethanolamine/acetic anhydride, and then dehydrated through an ethanol series. Slides were hybridized overnight at 47 °C in a hybridization solution composed of 50% formamide, 300 mM NaCl, 10 mM Tris HCL (pH 8.0), 1 mM EDTA, 1X Denhardt's, 10% dextran sulfate, 10 mM DTT and containing 5×10^7 cpm/mL of the relevant ^{33}P-labled probe. The *Cry1* riboprobe was generated from nucleotides 1,015–1,320 of accession number BC022174 while the *Cry2* riboprobe was generated from nucleotides 1,256–1,559 of accession number BC054794. For both probes the nucleotide sequence was PCR amplified and cloned into the pCR 2.1-topo vector (Invitrogen). To prepare the probe, the vector was linearized with HindIII; and the transcription reaction was initiated from the T7 promoter/priming site. The relative expression was quantified using NIH "Image" software version 1.34 s on a Macintosh computer as previously described (Panda et al., 2002).

Rearing tg(tetO:*Cry1* L1) animals on doxycycline

Hemizygous tg(tetO:*Cry1*) animals were crossed to hemizygous tg(Scg2:tTA) animals to produce double-transgenic, single-transgenic, and WT control animals. All breeding cages were maintained under standard controlled environmental conditions, with a 12:12 LD cycle (lights on at 5 am standard time) with free access to food and water containing 10 µg/mL doxycycline. Doxycycline treatment was started when animals were placed into breeding cages and was continued through conception, gestation, birth, and postnatal development of the pups. Pups were weaned from their mothers at approximately 21 days of age and were maintained in groups of five under the same environmental conditions with free access to food and water containing 10 µg/mL doxycycline until behavior testing.

Time course of *Cry1* developmental effects

Groups of mice were raised on water and switched to 10 µg/mL doxycycline at points from embryonic day 0 to postnatal day 231. Other groups were reared on 10 µg/mL doxycycline and converted to water from embryonic day 0 to postnatal day 104. Animals were then maintained under the appropriate condition (either on 10 µg/mL doxycycline or on water depending on the paradigm) until the 36th day of the wheel running experiment where they were once again switched to the opposite condition. The timing of the change was based on the date of birth (postnatal day 0).

Rescue of *Cry1/Cry2* double null animals

Cry1−/− / *Cry2*−/− / tg(Scg2:tTA) / tg(tetO:Cry1) animals were produced by systematically crossing the single-transgenic animals to a congenic C57BL/6J background containing the *Cry1*−/− and *Cry2*−/− alleles. The transactivator line was produced by crossing a hemizygous tg(Scg2:tTA) female to a *Cry1*−/− / *Cry2*−/− male to produce G1 mice. G1s were selected based on PCR amplification of a 500 bp band from genomic DNA (Forward Primer-CAAGTGTAT GGCCAGATCTCAA; Reverse Primer-AGACAAGCTTGATGCAA ATGAG; 38 cycles with an annealing temperature of 57° followed by a single 72° step (for 5 min) demonstrating the presence of tg(Scg2:tTA). Once *Cry1*± / *Cry2*± / tg(Scg2:tTA) animals were created, they were intercrossed to a siblings of identical genotype to produce *Cry1*−/− / *Cry2*−/− / tg(Scg2:tTA) mice. The operator line was produced by crossing hemizygous tg(tetO:*Cry1*) L1 females with a *Cry1*−/− / *Cry2*−/− male to produce the G1 generation. G1s were selected based on PCR amplification of genomic DNA for the presence of tg(tetO:*Cry1*) to create *Cry1*± / *Cry2*± / tg(tetO:*Cry1*) animals. These animals were intercrossed to siblings of the same genotype to produce the G1F2 generation. *Cry1/2* Genotyping was conducted as previously described (Vitaterna et al., 1999). The transactivator *Cry1*−/− / *Cry2*± / tg(Scg2:tTA) G1F2s were then crossed with the operator *Cry1*−/− / *Cry2*−/− / tg(tetO:Cry1) G1F2s to produce *Cry1*−/− /*Cry2*−/− / tg(Scg2:tTA) / tg(tetO:*Cry1*) mice.

Circadian activity analysis

Circadian locomotor activity was analyzed for double-transgenic, single-transgenic, and WT-control animals for all tg(tetO:*Cry1*) and tg(tetO:*Cry2*) lines. Wheel-running activity was recorded and analyzed as described previously (Yoo et al., 2004). Briefly, activity (wheel

revolutions) was recorded continuously by a PC system ClockLab (Actimetrics, Wilmette, IL) and displayed and analyzed using ClockLab software (Actimetrics, Wilmette, IL). Period was calculated using a Chi-square periodogram (Sokolove and Bushell, 1978) with a six-minute resolution between hours 10 and 36 (ClockLab). The relative power of the circadian component from 18 to 30 h was determined from a normalized Fast Fourier transformation using a Blackman-Harris window (ClockLab). For *Cry1* developmental studies, animals were maintained for 7 days in a 12:12 LD cycle on 10 μg/mL doxycycline followed by constant darkness for 28 days on 10 μg/mL doxycycline and 25 days on water. The free running period was analyzed for days 10–25 (Doxycycline) and 45–60 (H_2O) respectively. For the rescue experiments, circadian locomotor activity was also analyzed for double-transgenic tg(tetO:*Cry1*) *Cry1/Cry2* double nulls, single-transgenic double nulls, and WT double nulls. Free running period and the relative power of the circadian components were calculated for days 10–25 (H_2O), days 45–60 (Doxycycline), and days 70–85 (H_2O). The period and relative power values were compared between groups by ANOVA and Tukey *post hoc* analysis.

Results

Overexpression of either *Cry1* or *Cry2* alters circadian behavioral rhythms

Both tg(tetO:*Cry1*) double-transgenic (DTg *Cry1*) and tg(tetO:*Cry2*) double-transgenic (DTg *Cry2*) mouse lines demonstrated constitutive overexpression of *Cry1* or *Cry2* in the SCN when compared to single-transgenic and WT controls (Supplementary Figures 1B–E). After this was confirmed, adult DTg *Cry1* and DTg *Cry2* mice were assayed for circadian locomotor rhythms in both constant darkness (DD) and constant light (LL) (Figure 1). DTg *Cry1* animals exhibited a free running period in DD that was significantly longer than WT and single-transgenic controls (Figures 1A,B). This long rhythm was also lower in amplitude than the WT and tetO single-transgenic controls (Average power for DTg *Cry1* = 0.019 ± 0.154, tetO = 0.129 ± 0.009, Scg2 = 0.079 ± 0.019, and WT = 0.150 ± 0.01). There was no additional lengthening of period in DTg *Cry1* mice in response to LL (Figure 1C). In contrast, DTg *Cry2* mice exhibited a free running period that was significantly shorter than WT and single-transgenic controls in both DD and LL (Figures 1D,E).

When the transgene was silenced by treatment with 10 μg/mL of doxycycline, DTg *Cry1* animals exhibited a significant period change and in some cases a phase shift was apparent in DD, although periods remained significantly longer than WT and single-transgenic animals on doxycycline (Figure 1B). Importantly, these changes were reversed by placing mice back on regular water (Figure 1B). In contrast, DTg *Cry2* mice on doxycycline returned to a period comparable to WT and single-transgenic controls (Figure 1D). Interestingly, in LL DTg *Cry2* mice on doxycycline had periods that remained shorter than the tetO single-transgenic and WT controls (Figure 1E). Taken together, these results suggest that oscillations/levels of *Cry1* and *Cry2* are important the maintenance of circadian period; however, they are not necessary for the persistence of circadian activity rhythms. Moreover, these data add to the evidence that *Cry1* and *Cry2* likely have different modes of action within the negative feedback loop of individual cells (Kume et al., 1999; Lee et al., 2001; Van Gelder et al., 2002).

Developmental *Cry1* overexpression establishes period length in adulthood

We next asked whether the sustained lengthening of period in the DTg *Cry1* mice in the absence of transgene expression (i.e., on doxycycline) was due to an effect from constitutive *Cry1* expression during development. DTg *Cry1* mice, along with single-transgenic and WT controls, were reared on 10 μg/mL doxycycline (silencing the transgene throughout development); and their locomotor activity rhythms were monitored as adults (Figure 2A). DTg *Cry1* mice reared and kept on doxycycline exhibited a period in DD that was significantly shorter than that of water-reared DTg *Cry1* mice and similar to that of WT and single-transgenic mice (Figures 2B,C). Interestingly, when the doxycycline was removed to allow overexpression of *Cry1* in adulthood, doxycycline reared, DTg *Cry1* mice maintained a period similar to WT (Figures 2B,C). These results suggest that it is the constitutive overexpression of *Cry1* during development that permanently alters the free running period in adult mice.

Cry1 expression is required for the postnatal establishment of circadian free-running period

Next, we sought to define the critical period of the developmental effects of silencing *Cry1*. DTg *Cry1* mice were reared on either water or doxycycline and then were converted to the opposite condition at various times during development. This experimental paradigm allowed for either the inactivation (water to doxycycline) or activation (doxycycline to water) of the *Cry1* transgene during various developmental stages. Circadian locomotor rhythms were then assayed to determine the free running period of the mice in adulthood. DTg mice with the transgene inactivated (water to doxycycline) before birth (PN0) displayed a phenotype similar to that of the doxycycline-reared animals (normal WT phenotype). Conversely, animals for which the transgene was inactivated after PN40 displayed a period similar to the water reared DTg *Cry1* mice (long period phenotype; Figure 3A). In the opposite experiment, DTg mice with the transgene activated (doxycycline to water) before birth (PN0) up until PN45 displayed a period similar to the water reared DTg *Cry1* mice (long period phenotype), whereas DTg mice with the transgene activated after PN45 displayed a phenotype similar to that of the doxycycline-reared animals (normal WT phenotype; Figure 3B). In both the activation and inactivation paradigms, when the switch occurred between PN0 and PN45, a gradient of phenotypes was seen: when *Cry1* expression was higher for longer, the free running period was longer. Thus, combining the data from these two experiments, we can define a critical period from PN0 to PN45 during which the free running period in the adult animal appears to be established.

Cry1 overexpression in the brain partially rescues circadian rhythms in arhythmic mice

Because the transgenes we utilized overexpress *Cry1* or *Cry2*, we assumed that the normal rhythmic expression of these genes is disrupted. Thus, to better understand whether rhythmicity of *Cry1*

10.3389/fnins.2023.1166137

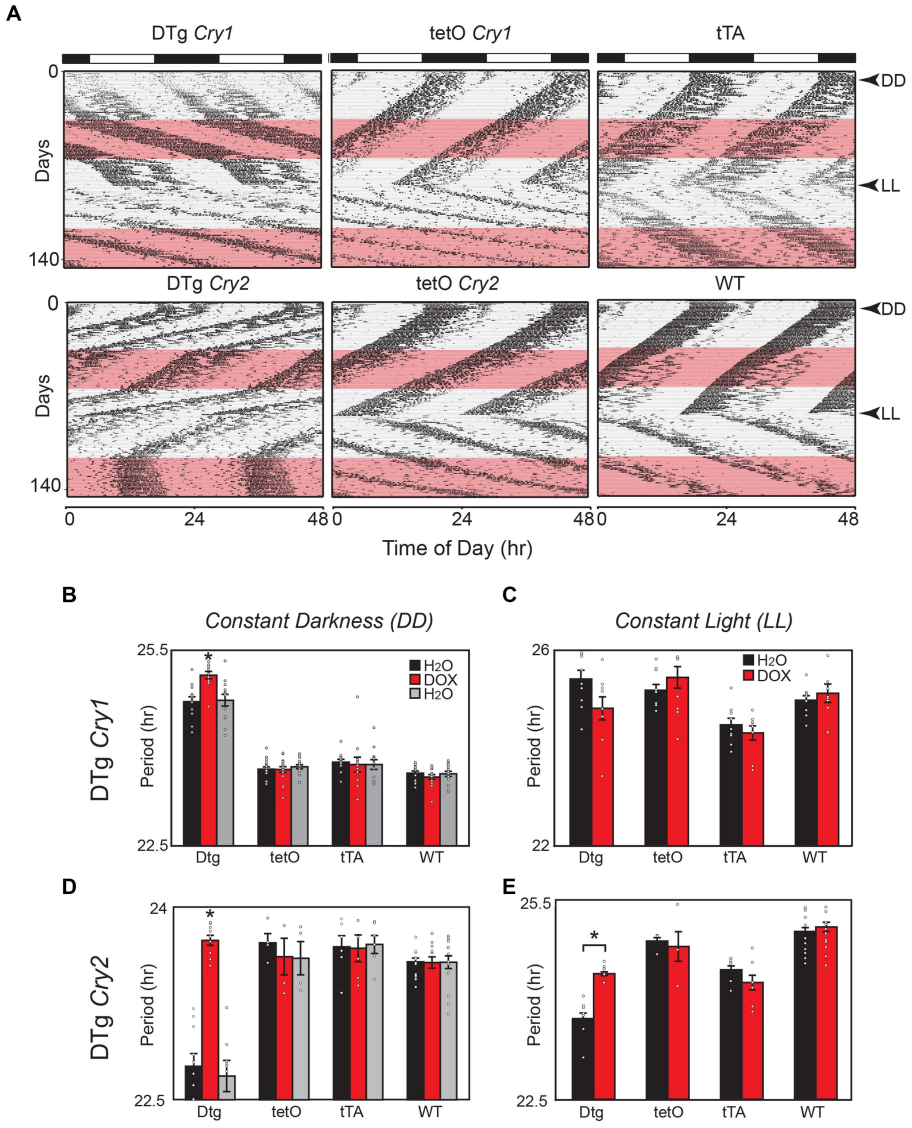

FIGURE 1
Overexpression of Cry1 and Cry2 in the brain alters circadian behavioral rhythms in mice. **(A)** Representative actograms for double-transgenic (DTg) Cry1 and *Cry2* mice with controls. The pink bar denotes the time of doxycycline administration in constant darkness (DD) and constant light (LL). **(B)** In DD, DTg *Cry1* mice have a clear lengthening in period. Once treated with doxycycline, the period continues to lengthen in DTg *Cry1* mice. DTg *Cry1, n*=13; tetO *Cry1, n*=18; tTA *Cry1, n*=12; WT, *n*=15; (**p*<0.05). **(C)** In LL, the DTg *Cry1* mice are similar to WT. DTg *Cry1, n*=10; tetO *Cry1, n*=10; tTA *Cry1, n*=12; WT, *n*=15; (* *p*<0.05). **(D)** In DD, DTg *Cry2* mice display a significantly shorter period. Once treated with doxycycline, the period is returned to WT levels in DTg *Cry2* mice. DTg *Cry2, n*=10; tetO *Cry2, n*=4; tTA *Cry2, n*=6; WT, *n*=15; (**p*<0.05). **(E)** In LL, DTg *Cry2* mice exhibited periods shorter than those seen in WT, while Doxycycline restores the period of DTg *Cry2* mice to levels equivalent with the tetO single-transgenic controls. DTg *Cry2, n*=4; tetO *Cry2,* n=5; tTA *Cry2, n*=12; *WT, n*=15; (**p*<0.05). Double-transgenic (DTg); Operator only Control (tetO); Transactivator only control (tTA); Wild type (WT).

(and not just expression) is required to establish circadian rhythms, *Cry1* was constitutively expressed (tg(tetO:*Cry1*) driven by tg(Scg2:tTA)) on a *Cry1*/*Cry2* double null background as well as on individual *Cry1*$^{-/-}$ and *Cry2*$^{-/-}$ background; and locomotor activity rhythms were assessed. Constitutive *Cry1* expression was found to partially rescue circadian locomotor activity rhythms on both the *Cry1*/*Cry2* double null and individual *Cry1*$^{-/-}$ mice, with period lengths comparable to WT mice (Figure 4A; Supplementary Figure 2). However, the amplitude of these rhythms never returned to WT levels (Figure 4B). Surprisingly, when constitutive *Cry1* expression was silenced with 10 μg/mL doxycycline mice on a *Cry1*/*Cry2* double null background, these mice showed lengthening of period in a manner similar to that seen in the DTg *Cry1* mice on a WT background (Figure 4A). A loss of circadian rhythmicity (as would be expected in single-transgenic and *Cry1*/*Cry2* double null mice) was never seen. Together with our other results, these findings strongly suggest that rhythmicity in *Cry1* expression is not necessary, but rather the overall level of *Cry1* expression is what drives period length.

Discussion

In this study, *Cry1* and *Cry2* were constitutively overexpressed in the brain leading to animals that were rhythmic, but with altered

10.3389/fnins.2023.1166137

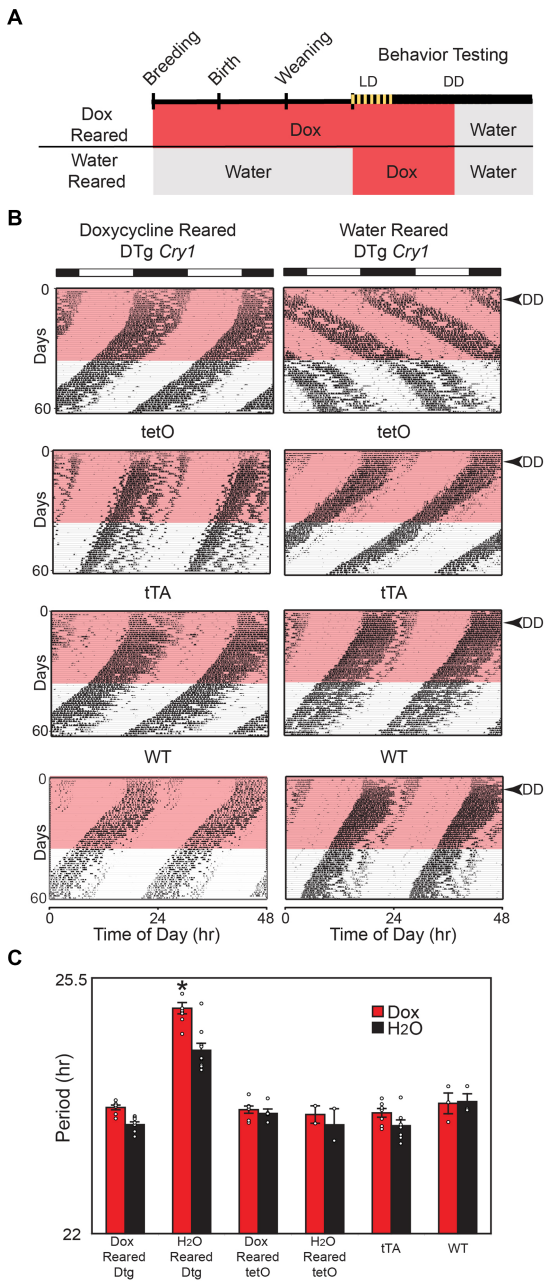

FIGURE 2
Cry1 overexpression during development is necessary for lengthening of period. **(A)** Schematic of experimental protocol. For the Dox Reared group, Doxycycline (10 μg/mL) was administered in drinking water when mice were placed into breeding cages and was continued through conception, gestation, birth, and postnatal development of pups. Pups were weaned from their mothers at approximately 21 days of age and were maintained on doxycycline up until the 28th day of behavioral testing, when they were switched to water for an additional 25 days. Water reared mice were also administered Doxycycline on days 0–35 of behavioral testing, then switched back to water for the remainder of the experiment. **(B)** Representative actograms of double-transgenic (DTg) *Cry1* mice and controls reared with or without 10 μg/mL doxycycline. The pink bar denotes the time of doxycycline administration during behavioral testing as adults. **(C)** Mean (± SEM) free running period in constant darkness (DD) on and off of doxycycline. The free running period was analyzed for days 10–25 (Dox) and 45–60 (H_2O). Doxycycline-reared (Dox Reared) DTg *Cry1* mice had a period similar to that of WT and single-transgenic control mice even when treated with doxycycline as adults, while water-reared (H_2O reared) DTg *Cry1* mice had a lengthened period both with water and doxycycline treatment (*p<0.05). Double-transgenic (DTg); Operator only Control (tetO); Transactivator only control (tTA); Wild type (WT).

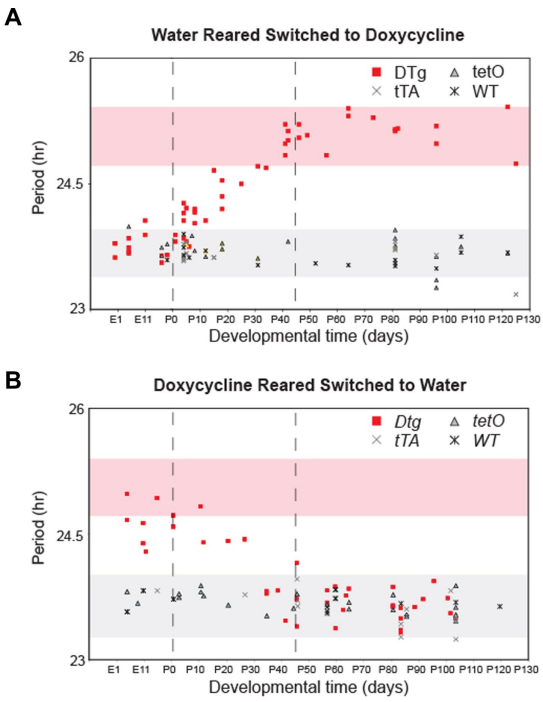

FIGURE 3
There is a postnatal critical period for Cry1 expression in the establishment of circadian period. Double-transgenic (DTg), single-transgenic, and WT controls were reared on water and converted to 10 μg/mL doxycycline at various developmental time points **(A)** or reared on doxycycline and were converted to water at various developmental time points **(B)**. Each point represents the period of a single adult animal in DD that was switched at a particular developmental time. The x-axis for both graphs is developmental time with PN0 being birth. Pink shading represents a 95% confidence interval around the average period for water reared DTg mice on doxycycline. Gray shading represents the 95% confidence interval around the average period for water reared WT and single-transgenic controls on doxycycline. Points outside of the two 95% confidence intervals are significantly different from water reared DTg mice and controls. Dotted lines indicate boundaries of the critical period for *Cry1* expression when considering data from both experiments.

periods. The constitutive overexpression of *Cry1* led to a lengthening of free running period, while constitutive overexpression of *Cry2* led to a shortening of free running period. These results make sense in light of the opposite phenotypes seen in *Cry1* and *Cry2* knockout mice (van der Horst et al., 1999; Vitaterna et al., 1999), but are none-the-less surprising, since the overexpression of these genes precludes the normal cycling of *Cry1* or *Cry2* gene expression. Interestingly, when *Cry2* overexpression was silenced with treatment of 10 μg/mL of doxycycline, the mice exhibited a period comparable to WT, while this same treatment in *Cry1* DTg mice continued to lengthen the free running period, suggesting a developmental role for *Cry1* in the establishment of circadian period. To test this hypothesis, we reared DTg *Cry1* mice from conception on doxycycline, and found that the constitutive overexpression of *Cry1* during development led to permanent alterations in free running period. Subsequently, we defined a critical period from birth to postnatal day 45 where the expression of *Cry1* permanently altered circadian period in adult mice.

There are several mechanisms that could explain how and why this developmental change is occurring. First, it possible that inactivity of the tetO transgene during development can lead to their functional silencing (Zhu et al., 2007). However, we show that activation as well

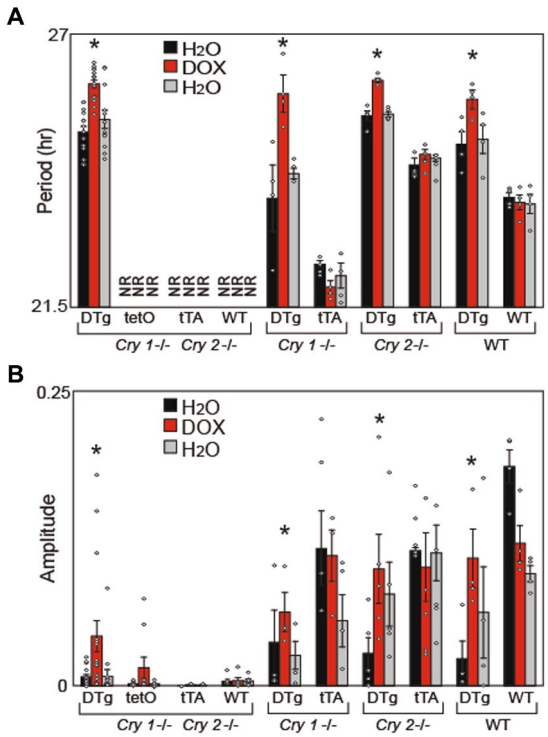

FIGURE 4
Cry1 Overexpression Rescues Circadian Rhythms in Cry1$^{-/-}$, Cry2$^{-/-}$, and Cry1$^{-/-}$/Cry2$^{-/-}$ Mice: **(A)** Average free running period (Period) and **(B)** FFT power (Amplitude) were calculated for all animals. Period, but not amplitude, was rescued in DTg on a *Cry1*$^{-/-}$ and *Cry1*$^{-/-}$ / *Cry2*$^{-/-}$ background. Values are presented as mean±SEM (*p<0.05); NR=non-rhythmic mice (from which we are unable to calculate a period). Double-transgenic (DTg); Operator only Control (tetO); Transactivator only control (tTA); Wild type (WT). DTg *Cry1*$^{-/-}$ / *Cry2*$^{-/-}$, n=20; tetO *Cry1*$^{-/-}$ / *Cry2*$^{-/-}$, n=10; tTA *Cry1*$^{-/-}$ / *Cry2*$^{-/-}$, n=3; WT *Cry1*$^{-/-}$ / *Cry2*$^{-/-}$, n=7; DTg *Cry1*$^{-/-}$, n=4; WT *Cry1*$^{-/-}$, n=4; DTg *Cry2*$^{-/-}$, n=5; WT *Cry2*$^{-/-}$, n=3; DTg WT, n=4; WT WT, n=4.

as inactivation of the transgene during development can lead to similar phenotypic effects that both fall within the same critical period, suggesting that the effects are not due to functional silencing or transgene inactivation.

Another possible mechanism could be through epigenetic modifications. Rhythmic changes in histone acetylation at circadian clock gene promoters are associated with chromatin modifications (Etchegaray et al., 2003; Doi et al., 2006; Ripperger and Schibler, 2006; Koike et al., 2012). Interestingly, CRY1 has been found to interact with a histone acetyltransferase to alter CLOCK/BMAL1-mediated transcription (Etchegaray et al., 2003), potentially providing a direct mechanism for long-term CRY1 effects. Future studies using tissues derived from these mouse models could help elucidate the molecular impacts of developmental *Cry1* expression.

Although preliminary data (not shown) suggest that the gross morphology of the SCN is normal in our DTg mice, it is also possible that the cellular phenotypes in the SCN are altered. In addition, the level or oscillation of *Cry1* could developmentally alter the synaptic connectivity and coupling in the SCN. Heterogeneous cellular phenotypes are integrated in the adult SCN, decreasing cycle-to-cycle variability in order to determine the generation and expression of circadian rhythms (Low-Zeddies and Takahashi, 2001; Herzog et al., 2004). Moreover, loss of function in clock genes has the ability to impact neural firing and synchrony in the SCN (Schwartz et al., 1987; Albus et al., 2002; Ono et al., 2013; Shan et al., 2020). Importantly, oscillations in fetal SCN neurons are known to be present as early as embryonic day 17, before synaptic connections are developed (Reppert and Schwartz, 1984; Speh and Moore, 1993; Shimomura et al., 2001; Carmona-Alcocer et al., 2018), suggesting they may play an important role in synaptic connectivity. Theoretically, alteration of *Cry1* expression and oscillations in fetal SCN neurons during the critical period could alter the firing patterns and therefore change the synaptic connectivity and neural representation of period within the adult SCN (Sumova et al., 2012, Ono et al., 2013). Our data are consistent with this theory because the critical developmental period matches the peak of synaptogenesis in the maturing SCN (Honma, 2020). However, these synaptic changes are likely subtle, as we see no evidence gross alterations in SCN morphology (data not shown).

In other organisms, the rhythmic requirements of the negative elements of the primary feedback loop have been elucidated by constitutively expressing these negative elements on a null background (Aronson et al., 1994; Edwards et al., 2016). *Cry1*/*Cry2* double null mice lack circadian rhythmicity in constant darkness, while individual *Cry1* or *Cry2* null mice are rhythmic but have abnormal periodicity (van der Horst et al., 1999; Vitaterna et al., 1999; Bae et al., 2001). The results of our experiments demonstrate that constitutive, brain-specific expression of *Cry1* can partially rescue circadian locomotor rhythms on a *Cry1*/*Cry2* double null background and suggest that oscillations in *Cry1* are not necessary for the maintenance of circadian locomotor period. Although we did not examine CRY1 protein expression, our findings are consistent with recent experiments which showed that overexpression of CRY1 protein rescues SCN rhythms in *Cry1*/*Cry2* null mice (McManus et al., 2022). There are also similar findings with the constitutive expression of CRY1 in Rat-1 fibroblasts (Fan et al., 2007; Yamanaka et al., 2007) and in the liver of mice (Chen et al., 2009). Interestingly, the amplitude of the rhythms was not rescued back to WT, therefore oscillations in *Cry1* expression may be necessary for the maintenance of circadian amplitude.

Finally, both CRY1 and CRY2 have been shown to repress CLOCK/BMAL1 in distinct ways (Kume et al., 1999; Lee et al., 2001; Van Gelder et al., 2002). CRY1 is thought to be a potent inhibitor of the positive feedback loop by directly interacting with the CLOCK/BMAL1 complex (Griffin et al., 1999; Kume et al., 1999; Shearman et al., 2000); although, it may require PER to act as a scaffolding protein to facilitate this interaction (Chen et al., 2009) as it has been shown to impact nuclear shuttling of PER (Smyllie et al., 2022). In contrast, CRY2 is thought to associate strongly with the CLOCK protein (Griffin et al., 1999). Our results suggest a fine-tuning role of *Cry2* in the negative feedback loop (Griffin et al., 1999). In particular, our finding of an effect of LL in DTg *Cry2* mice suggests an alteration of the phase response curve, leading to the intriguing possibility that *Cry2* plays a role in mediating the response to light.

In summary, our data support a novel, developmental role for *Cry1* expression in the SCN and also call into question the necessity of *Cry1* rhythmic expression after a critical period in development. These findings further our understanding of the mechanisms behind the generation of circadian rhythmicity. However, more research is needed to further determine how the various molecular feedback loops work together to generate rhythmicity, as well as how these feedback loops are interacting with rhythm generating components such as neural network oscillations.

Data availability statement

The original contributions presented in the study are included in the article/Supplementary material, further inquiries can be directed to the corresponding author.

Ethics statement

The animal study was reviewed and approved by Institutional Animal Care and Use Committee, Northwestern University.

Author contributions

AES planned and performed behavior experiments, analyzed data, made figures and wrote the manuscript. VK provided technical assistance with cloning. AS performed *in situ* hybridization experiments. EJS performed microinjection for transgenic mouse lines. MSM performed mouse colony maintenance and collected data. JST planned and helped with data analysis and writing of the manuscript. All authors contributed to the article and approved the submitted version.

Funding

This work was supported by a Silvio O. Conte Center NIH Grant P50 MH074924 to JST. JST is an Investigator in the Howard Hughes Medical Institute.

Acknowledgments

The authors would like to thank Kimberly Cox at Efferent Manuscript Services, LLC, for assistance in preparing the manuscript for publication.

Conflict of interest

The authors declare that the research was conducted in the absence of any commercial or financial relationships that could be construed as a potential conflict of interest.

Publisher's note

Supplementary material

The Supplementary material for this article can be found online at: https://www.frontiersin.org/articles/10.3389/fnins.2023.1166137/full#supplementary-material

References

Albus, H., Bonnefont, X., Chaves, I., Yasui, A., Doczy, J., Van Der Horst, G. T., et al. (2002). Cryptochrome-deficient mice lack circadian electrical activity in the suprachiasmatic nuclei. *Curr. Biol.* 12, 1130–1133. doi: 10.1016/S0960-9822(02)00923-5

Antoch, M. P., Song, E. J., Chang, A. M., Vitaterna, M. H., Zhao, Y., Wilsbacher, L. D., et al. (1997). Functional identification of the mouse circadian clock gene by transgenic BAC rescue. *Cells* 89, 655–667. doi: 10.1016/S0092-8674(00)80246-9

Aronson, B. D., Johnson, K. A., Loros, J. J., and Dunlap, J. C. (1994). Negative feedback defining a circadian clock: autoregulation of the clock gene frequency. *Science* 263, 1578–1584. doi: 10.1126/science.8128244

Bae, K., Jin, X., Maywood, E. S., Hastings, M. H., Reppert, S. M., and Weaver, D. R. (2001). Differential functions of mPer1, mPer2, and mPer3 in the SCN circadian clock. *Neuron* 30, 525–536. doi: 10.1016/S0896-6273(01)00302-6

Bunger, M. K., Wilsbacher, L. D., Moran, S. M., Clendenin, C., Radcliffe, L. A., Hogenesch, J. B., et al. (2000). Mop3 is an essential component of the master circadian pacemaker in mammals. *Cells* 103, 1009–1017. doi: 10.1016/S0092-8674(00)00205-1

Carmona-Alcocer, V., Abel, J. H., Sun, T. C., Petzold, L. R., Doyle, F. J., Simms, C. L., et al. (2018). Ontogeny of circadian rhythms and synchrony in the Suprachiasmatic nucleus. *J. Neurosci.* 38, 1326–1334. doi: 10.1523/JNEUROSCI.2006-17.2017

Cermakian, N., Monaco, L., Pando, M. P., Dierich, A., and Sassone-Corsi, P. (2001). Altered behavioral rhythms and clock gene expression in mice with a targeted mutation in the Period1 gene. *EMBO J.* 20, 3967–3974. doi: 10.1093/emboj/20.15.3967

Chen, R., Schirmer, A., Lee, Y., Lee, H., Kumar, V., Yoo, S. H., et al. (2009). Rhythmic PER abundance defines a critical nodal point for negative feedback within the circadian clock mechanism. *Mol. Cell* 36, 417–430. doi: 10.1016/j.molcel.2009.10.012

Cox, K. H., and Takahashi, J. S. (2019). Circadian clock genes and the transcriptional architecture of the clock mechanism. *J. Mol. Endocrinol.* 63, R93–R102. doi: 10.1530/JME-19-0153

Doi, M., Hirayama, J., and Sassone-Corsi, P. (2006). Circadian regulator CLOCK is a histone acetyltransferase. *Cells* 125, 497–508. doi: 10.1016/j.cell.2006.03.033

Edwards, M. D., Brancaccio, M., Chesham, J. E., Maywood, E. S., and Hastings, M. H. (2016). Rhythmic expression of cryptochrome induces the circadian clock of arrhythmic suprachiasmatic nuclei through arginine vasopressin signaling. *Proc. Natl. Acad. Sci. U. S. A.* 113, 2732–2737. doi: 10.1073/pnas.1519044113

Etchegaray, J. P., Lee, C., Wade, P. A., and Reppert, S. M. (2003). Rhythmic histone acetylation underlies transcription in the mammalian circadian clock. *Nature* 421, 177–182. doi: 10.1038/nature01314

Fan, Y., Hida, A., Anderson, D. A., Izumo, M., and Johnson, C. H. (2007). Cycling of CRYPTOCHROME proteins is not necessary for circadian-clock function in mammalian fibroblasts. *Curr. Biol.* 17, 1091–1100. doi: 10.1016/j.cub.2007.05.048

Griffin, E. A., Staknis, D., and Weitz, C. J. (1999). Light-independent role of CRY1 and CRY2 in the mammalian circadian clock. *Science* 286, 768–771. doi: 10.1126/science.286.5440.768

Herzog, E. D., Aton, S. J., Numano, R., Sakaki, Y., and Tei, H. (2004). Temporal precision in the mammalian circadian system: a reliable clock from less reliable neurons. *J. Biol. Rhythm.* 19, 35–46. doi: 10.1177/0748730403260776

Herzog, E. D., Takahashi, J. S., and Block, G. D. (1998). Clock controls circadian period in isolated suprachiasmatic nucleus neurons. *Nat. Neurosci.* 1, 708–713. doi: 10.1038/3708

Hong, H. K., Chong, J. L., Song, W., Song, E. J., Jyawook, A. A., Schook, A. C., et al. (2007). Inducible and reversible clock gene expression in brain using the tTA system for the study of circadian behavior. *PLoS Genet.* 3:e33. doi: 10.1371/journal.pgen.0030033

Honma, S. (2020). Development of the mammalian circadian clock. *Eur. J. Neurosci.* 51, 182–193. doi: 10.1111/ejn.14318

Johnson, R. F., Moore, R. Y., and Morin, L. P. (1988). Loss of entrainment and anatomical plasticity after lesions of the hamster retinohypothalamic tract. *Brain Res.* 460, 297–313. doi: 10.1016/0006-8993(88)90374-5

King, D. P., Zhao, Y., Sangoram, A. M., Wilsbacher, L. D., Tanaka, M., Antoch, M. P., et al. (1997). Positional Cloning of the Mouse Circadian Clock Gene. *Cell* 89, 641–653.

Koike, N., Yoo, S. H., Huang, H. C., Kumar, V., Lee, C., Kim, T. K., et al. (2012). Transcriptional architecture and chromatin landscape of the core circadian clock in mammals. *Science* 338, 349–354. doi: 10.1126/science.1226339

Kume, K., Zylka, M. J., Sriram, S., Shearman, L. P., Weaver, D. R., Jin, X., et al. (1999). mCRY1 and mCRY2 are essential components of the negative limb of the circadian clock feedback loop. *Cells* 98, 193–205. doi: 10.1016/S0092-8674(00)81014-4

Lee, C., Etchegaray, J. P., Cagampang, F. R., Loudon, A. S., and Reppert, S. M. (2001). Posttranslational mechanisms regulate the mammalian circadian clock. *Cells* 107, 855–867. doi: 10.1016/S0092-8674(01)00610-9

Low-Zeddies, S. S., and Takahashi, J. S. (2001). Chimera analysis of the clock mutation in mice shows that complex cellular integration determines circadian behavior. *Cells* 105, 25–42. doi: 10.1016/S0092-8674(01)00294-X

Mcmanus, D., Polidarova, L., Smyllie, N. J., Patton, A. P., Chesham, J. E., Maywood, E. S., et al. (2022). Cryptochrome 1 as a state variable of the circadian clockwork of the suprachiasmatic nucleus: evidence from translational switching. *Proc. Natl. Acad. Sci. U. S. A.* 119:e2203563119. doi: 10.1073/pnas.2203563119

Moore, R. Y., Speh, J. C., and Card, J. P. (1995). The retinohypothalamic tract originates from a distinct subset of retinal ganglion cells. *J. Comp. Neurol.* 352, 351–366. doi: 10.1002/cne.903520304

Ono, D., Honma, S., and Honma, K. (2013). Cryptochromes are critical for the development of coherent circadian rhythms in the mouse suprachiasmatic nucleus. *Nat. Commun.* 4:1666. doi: 10.1038/ncomms2670

Panda, S., Sato, T. K., Castrucci, A. M., Rollag, M. D., Degrip, W. J., Hogenesch, J. B., et al. (2002). Melanopsin (Opn4) requirement for normal light-induced circadian phase shifting. *Science* 298, 2213–2216. doi: 10.1126/science.1076848

Pittendrigh, C. S. (1960). Circadian rhythms and the circadian organization of living systems. *Cold Spring Harb. Symp. Quant. Biol.* 25, 159–184. doi: 10.1101/SQB.1960.025.01.015

Provencio, I., Rollag, M. D., and Castrucci, A. M. (2002). Photoreceptive net in the mammalian retina. This mesh of cells may explain how some blind mice can still tell day from night. *Nature* 415:493.

Quintero, J. E., Kuhlman, S. J., and Mcmahon, D. G. (2003). The biological clock nucleus: a multiphasic oscillator network regulated by light. *J. Neurosci.* 23, 8070–8076. doi: 10.1523/JNEUROSCI.23-22-08070.2003

Reppert, S. M., and Schwartz, W. J. (1984). The suprachiasmatic nuclei of the fetal rat: characterization of a functional circadian clock using 14C-labeled deoxyglucose. *J. Neurosci.* 4, 1677–1682. doi: 10.1523/JNEUROSCI.04-07-01677.1984

Ripperger, J. A., and Schibler, U. (2006). Rhythmic CLOCK-BMAL1 binding to multiple E-box motifs drives circadian Dbp transcription and chromatin transitions. *Nat. Genet.* 38, 369–374. doi: 10.1038/ng1738

Sangoram, A. M., Saez, L., Antoch, M. P., Gekakis, N., Staknis, D., Whiteley, A., et al. (1998). Mammalian circadian autoregulatory loop: a timeless ortholog and mPer1 interact and negatively regulate CLOCK-BMAL1-induced transcription. *Neuron* 21, 1101–1113. doi: 10.1016/S0896-6273(00)80627-3

Schwartz, W. J., Gross, R. A., and Morton, M. T. (1987). The suprachiasmatic nuclei contain a tetrodotoxin-resistant circadian pacemaker. *Proc. Natl. Acad. Sci. U. S. A.* 84, 1694–1698. doi: 10.1073/pnas.84.6.1694

Shan, Y., Abel, J. H., Li, Y., Izumo, M., Cox, K. H., Jeong, B., et al. (2020). Dual-color single-cell imaging of the Suprachiasmatic nucleus reveals a circadian role in network synchrony. *Neuron* 108:e7, 164–179.

Shearman, L. P., Sriram, S., Weaver, D. R., Maywood, E. S., Chaves, I., Zheng, B., et al. (2000). Interacting molecular loops in the mammalian circadian clock. *Science* 288, 1013–1019. doi: 10.1126/science.288.5468.1013

Shimomura, K., Low-Zeddies, S. S., King, D. P., Steeves, T. D., Whiteley, A., Kushla, J., et al. (2001). Genome-wide epistatic interaction analysis reveals complex genetic determinants of circadian behavior in mice. *Genome Res.* 11, 959–980. doi: 10.1101/gr.171601

Smyllie, N. J., Bagnall, J., Koch, A. A., Niranjan, D., Polidarova, L., Chesham, J. E., et al. (2022). Cryptochrome proteins regulate the circadian intracellular behavior and localization of PER2 in mouse suprachiasmatic nucleus neurons. *Proc. Natl. Acad. Sci. U. S. A.* 119

Sokolove, P. G., and Bushell, W. N. (1978). The chi square periodogram: its utility for analysis of circadian rhythms. *J. Theor. Biol.* 72, 131–160. doi: 10.1016/0022-5193(78)90022-X

Speh, J. C., and Moore, R. Y. (1993). Retinohypothalamic tract development in the hamster and rat. *Brain Res. Dev. Brain Res.* 76, 171–181. doi: 10.1016/0165-3806(93)90205-O

Sumova, A., Sladek, M., Polidarova, L., Novakova, M., and Houdek, P. (2012). Circadian system from conception till adulthood. *Prog. Brain Res.* 199, 83–103. doi: 10.1016/B978-0-444-59427-3.00005-8

Takahashi, J. S. (2017). Transcriptional architecture of the mammalian circadian clock. *Nat. Rev. Genet.* 18, 164–179. doi: 10.1038/nrg.2016.150

Takahashi, J. S., Hong, H. K., Ko, C. H., and Mcdearmon, E. L. (2008). The genetics of mammalian circadian order and disorder: implications for physiology and disease. *Nat. Rev. Genet.* 9, 764–775. doi: 10.1038/nrg2430

Van Der Horst, G. T., Muijtjens, M., Kobayashi, K., Takano, R., Kanno, S., Takao, M., et al. (1999). Mammalian Cry1 and Cry2 are essential for maintenance of circadian rhythms. *Nature* 398, 627–630. doi: 10.1038/19323

Van Gelder, R. N., Gibler, T. M., Tu, D., Embry, K., Selby, C. P., Thompson, C. L., et al. (2002). Pleiotropic effects of cryptochromes 1 and 2 on free-running and light-entrained murine circadian rhythms. *J. Neurogenet.* 16, 181–203. doi: 10.1080/01677060215306

Vitaterna, M. H., King, D. P., Chang, A. M., Kornhauser, J. M., Lowrey, P. L., Mcdonald, J. D., et al. (1994). Mutagenesis and mapping of a mouse gene, clock, essential for circadian behavior. *Science* 264, 719–725. doi: 10.1126/science.8171325

Vitaterna, M. H., Selby, C. P., Todo, T., Niwa, H., Thompson, C., Fruechte, E. M., et al. (1999). Differential regulation of mammalian period genes and circadian rhythmicity by cryptochromes 1 and 2. *Proc. Natl. Acad. Sci. U. S. A.* 96, 12114–12119. doi: 10.1073/pnas.96.21.12114

Welsh, D. K., Logothetis, D. E., Meister, M., and Reppert, S. M. (1995). Individual neurons dissociated from rat suprachiasmatic nucleus express independently phased circadian firing rhythms. *Neuron* 14, 697–706. doi: 10.1016/0896-6273(95)90214-7

Welsh, D. K., Takahashi, J. S., and Kay, S. A. (2010). Suprachiasmatic nucleus: cell autonomy and network properties. *Annu. Rev. Physiol.* 72, 551–577. doi: 10.1146/annurev-physiol-021909-135919

Yamanaka, I., Koinuma, S., Shigeyoshi, Y., Uchiyama, Y., and Yagita, K. (2007). Presence of robust circadian clock oscillation under constitutive over-expression of mCry1 in rat-1 fibroblasts. *FEBS Lett.* 581, 4098–4102. doi: 10.1016/j.febslet.2007.07.053

Yoo, S. H., Yamazaki, S., Lowrey, P. L., Shimomura, K., Ko, C. H., Buhr, E. D., et al. (2004). PERIOD2::LUCIFERASE real-time reporting of circadian dynamics reveals persistent circadian oscillations in mouse peripheral tissues. *Proc. Natl. Acad. Sci. U. S. A.* 101, 5339–5346. doi: 10.1073/pnas.0308709101

Zheng, B., Larkin, D. W., Albrecht, U., Sun, Z. S., Sage, M., Eichele, G., et al. (1999). The mPer2 gene encodes a functional component of the mammalian circadian clock. *Nature* 400, 169–173. doi: 10.1038/22118

Zhu, P., Aller, M. I., Baron, U., Cambridge, S., Bausen, M., Herb, J., et al. (2007). Silencing and un-silencing of tetracycline-controlled genes in neurons. *PLoS One* 2:e533. doi: 10.1371/journal.pone.0000533

frontiers | Frontiers in Neuroscience

TYPE Original Research
PUBLISHED 20 July 2023
DOI 10.3389/fnins.2023.1222551

OPEN ACCESS

EDITED BY
Takahiro J. Nakamura,
Meiji University, Japan

REVIEWED BY
Shota Nishitani,
University of Fukui, Japan
Rika Numano,
Toyohashi University of Technology, Japan

*CORRESPONDENCE
Linghui Pan
✉ panlinghui@gxmu.edu.cn

†These authors have contributed equally to this work and share first authorship

RECEIVED 14 May 2023
ACCEPTED 05 July 2023
PUBLISHED 20 July 2023

CITATION
Yang F, Liu R, He S, Ruan S, He B, Li J and Pan L (2023) Being a morning man has causal effects on the cerebral cortex: a Mendelian randomization study.
Front. Neurosci. 17:1222551.
doi: 10.3389/fnins.2023.1222551

Being a morning man has causal effects on the cerebral cortex: a Mendelian randomization study

Fan Yang[1,2,3,4,5†], Ru Liu[1†], Sheng He[1,6], Sijie Ruan[2], Binghua He[2], Junda Li[1] and Linghui Pan[1,3,4,5*]

[1]Department of Anesthesiology, Guangxi Medical University Cancer Hospital, Nanning, Guangxi Province, China, [2]Department of Anesthesiology, Central Hospital of Shaoyang, Shaoyang, Hunan Province, China, [3]Guangxi Key Laboratory for Basic Science and Prevention of Perioperative Organ Disfunction, Nanning, Guangxi Province, China, [4]Guangxi Clinical Research Center for Anesthesiology, Nanning, Guangxi Province, China, [5]Guangxi Engineering Research Center for Tissue and Organ Injury and Repair Medicine, Nanning, Guangxi Province, China, [6]Department of Anesthesiology, The First Affiliated Hospital of Southern China University, Hengyang, China

Introduction: Numerous studies have suggested a connection between circadian rhythm and neurological disorders with cognitive and consciousness impairments in humans, yet little evidence stands for a causal relationship between circadian rhythm and the brain cortex.

Methods: The top 10,000 morningness-related single-nucleotide polymorphisms of the Genome-wide association study (GWAS) summary statistics were used to filter the instrumental variables. GWAS summary statistics from the ENIGMA Consortium were used to assess the causal relationship between morningness and variates like cortical thickness (TH) or surficial area (SA) on the brain cortex. The inverse-variance weighted (IVW) and weighted median (WM) were used as the major estimates whereas MR-Egger, MR Pleiotropy RESidual Sum and Outlier, leave-one-out analysis, and funnel-plot were used for heterogeneity and pleiotropy detecting.

Results: Regionally, morningness decreased SA of the rostral middle frontal gyrus with genomic control (IVW: $\beta = -24.916$ mm, 95% CI: −47.342 mm to −2.490 mm, $p = 0.029$. WM: $\beta = -33.208$ mm, 95% CI: −61.933 mm to −4.483 mm, $p = 0.023$. MR Egger: $\beta < 0$) and without genomic control (IVW: $\beta = -24.581$ mm, 95% CI: −47.552 mm to −1.609 mm, $p = 0.036$. WM: $\beta = -32.310$ mm, 95% CI: −60.717 mm to −3.902 mm, $p = 0.026$. MR Egger: $\beta < 0$) on a nominal significance, with no heterogeneity or no outliers.

Conclusions and implications: Circadian rhythm causally affects the rostral middle frontal gyrus; this sheds new light on the potential use of MRI in disease diagnosis, revealing the significance of circadian rhythm on the progression of disease, and might also suggest a fresh therapeutic approach for disorders related to the rostral middle frontal gyrus-related.

KEYWORDS

Mendelian randomization, circadian rhythm, brain cortex, causal effect, morningness

1. Introduction

Being either a morning or night person indicates the state of the circadian clock, a hierarchical network in mammals (Hu et al., 2016). The suprachiasmatic nucleus (SCN) in the hypothalamus acts as the main part of the central circadian clock, reactive with light and capable of resetting and containing the synchronous rhythm in peripheral tissues (Baxter and Ray, 2020). The innate circadian clock functions as a commander to coordinate physiological processes, like immunity, metabolism, and inflammation (Shivshankar et al., 2020) Disruption of the clock could be a risk for multiple outcomes, like obesity, diabetes, hyperlipidemia, cancer, and so on (Neves et al., 2022).

There is some solid evidence for a connection between circadian rhythm disorder and neurologic diseases such as Alzheimer's and Parkinson's disease (Gu et al., 2015; Weissova et al., 2016; Richmond and Davey Smith, 2022). It is also linked to mental illnesses such as bipolar disorder, depression, and anxiety, and to disorders such as autism (Walker et al., 2021; Martinez-Cayuelas et al., 2022; Takaesu et al., 2022; Ketchesin et al., 2023).

In addition, neurological diseases and psychosis frequently manifest with cognitive and consciousness impairments, varying in type and severity. Since the cerebral cortex is universally regarded as an advanced hub for cognition and consciousness, many neurological diseases and psychosis have been definitively linked to substantial structural alterations within the cerebral cortex. Examples include schizophrenia patients who had significant variations in 55 regions of cortical thickness, 23 regions of the volume, seven regions of the area, and 55 regions of local gyrification index than healthy individuals (Han et al., 2023). Children with autism spectrum disorder also experience a higher empathizing-systemizing difference than children without autism, which shares a significant negative association with the gyrification in the left lateral occipital cortex (Pan et al., 2023). Mild traumatic brain injury patients with posttraumatic headache experience a reduced headache impact and improved cognitive function in the acute to subacute phase, along with the restoration of cortical thickness of the left caudal anterior cingulate cortex and left insula and cortical surface area of the right superior frontal gyrus, and the restoration confirmed a key regulatory role by further mediation analysis (Xu et al., 2023). Parkinson's Disease was discovered to have an initial presentation of thinner occipital, parietal, and temporal cortices, extending toward rostrally located cortical regions with increased disease severity, after which the bilateral putamen and amygdala shrink consistently, during which poorer cognition is connected with widespread cortical thinning and lower volumes of core limbic structures (Laansma et al., 2021). In Vuksanovic's study, it was discovered that patients with Alzheimer's Disease bear the most severe cognitive impairment, while individuals with behavioral variant Fronto-Temporal Dementia exhibit more impairment compared to healthy elders. Meanwhile, patients with Alzheimer's disease and behavioral variant Fronto-Temporal Dementia maintain distinct patterns of cerebral cortex structural disturbance which deviate significantly from the changes observed in normal aging (Vuksanovic et al., 2019). It is also widely accepted that the entorhinal cortex act as the first brain area related to pathologic changes in Alzheimer's disease (Li et al., 2021).

The exploration of the links among alterations in cerebral cortex structures, cognition, and consciousness has long been a focal point of scientific interest, which may advance human understanding of our cerebral cortex. One of the aims of this study is to explore the cortical changes induced by circadian rhythm disorder in humans, providing a structural localization for future investigations into the impact of circadian rhythms on cognitive function and serving as a filter in the analysis of large-scale imaging data such as MRI to figure out how much the circadian rhythm matters in these kinds of diseases. Additionally, a potential adjunctive therapeutic approach may be possible, targeting the specific cortical changes—improving/stabilizing circadian rhythms—although further validation is still required. To achieve the goal, it is not sufficient to merely identify the correlation between cortical structure and circadian rhythm since it is still unclear whether circadian rhythm disorders lead to changes in the brain or if the structural changes in the brain impact the rhythmic behavior in verse.

Mendelian randomization (MR) has recently received a lot more attention for its ability to infer credible causal relationships between exposures and outcomes (Richmond and Davey Smith, 2022). By fully utilizing the random assortment of genetic variants during the maturation of germ cells, MR analysis could gather the genetic variations relatively independently of environmental factors as instrumental variables (IVs), using it to divide the outcome cohort into subgroups, reaching the goal of randomization (Burgess and Thompson, 2015). Since the random assortment of genetic variants occurs before birth, a long time before the outcome onset, MR analysis has the ability to minimize biases of residual confounding and reverse causation (Bowden and Holmes, 2019).

Considering the uncertain causal association between being a morning person and the cerebral cortex, we performed an MR analysis to address this, aiming at exploring the related gyrus for further analysis and research.

2. Methods

2.1. Study design

In this study, a two-sample MR analysis was carried out to examine the causal effect between being a morning person and the structural changes of the cerebral cortex. The basic three MR assumptions urged to be met were (1) IVs should be in a robust correlation with exposure, (2) IVs should not respond to potential confounders, and (3) IVs could never affect the outcome except through exposure. To fulfill the assumptions, first, Europeans were determined to be the major subjects to minimize the potential confounders of ancestry. Then, cohorts in exposure and outcome were carefully selected to avoid the overlap of participants. Third, the PhenoScanner[1] was chosen to be the reference library for ruling out related genetic variants.

2.2. Exposure GWAS-being a morning person

In this study, the top 10,000 morningness-related single-nucleotide polymorphisms (SNPs) of the Genome-wide association study (GWAS) summary statistics were used for a two-sample MR

1 www.phenoscanner.medschl.cam.ac.uk

analysis (Hu et al., 2016). GWAS for morningness was performed on the 23andMe participant cohort (Eriksson et al., 2010). Morningness was defined by asking the participants twice if they are naturally night people or morning people in surveys that were either comprehensive with multiple questions on a subject matter or quick questions. Using the responses, participants were classified as night people, morning people, or missing. If one answer was missing, the other answer was used as the phenotype value. If one answer indicated being a morning person but the other indicated being a night person, the phenotype value would be treated as missing. As a result, 89,283 individuals were divided into morning person or night person, with the relatives dropped out, and European ancestry accounting for over 97%, referring to the European populations in threeHapMap 2 (Falush et al., 2007). Then, age, gender, and the top five PCs were used as covariates to account for population structure. Ultimately, Genome-wide Complex Trait Analysis (Yang et al., 2011) revealed that genetic variants could account for approximately 21% (95% CI: 13 to 29%) of the variability in the likelihood of being a morning person.

2.3. Outcome GWAS-the cerebral cortex

The brain cerebral cortex structural GWAS data was obtained from the ENIGMA Consortium (Grasby et al., 2020). In total, 51,665 individuals joined the project, nearly 94% of which were born with European ancestry, coming from 60 cohorts all over the world. Cortical measurements of surface area (SA) and thickness (TH) were obtained from brain magnetic resonance imaging (MRI) scans. The scans were segmented into 34 regions based on the Desikan-Killiany atlas (Desikan et al., 2006), resulting in a total of 70 phenotypes, including both regional and global SA and TH. Firstly, Grasby's group filtered out 33,992 participants of European ancestry from cohorts for the next analysis to control the biases (cohort information was listed in Supplementary Table S1). Secondly, GWAS analyses were independently performed on the 70 imaging phenotypes, namely 34 measurements for TH, 34 measurements for SA, total TH, and total SA. In regional GWAS analysis, global measures of SA and TH were used as covariates. Finally, once quality control was finished, the data were meta-analyzed using METAL (Willer et al., 2010). As a result, 34% (SE = 3%) of the variation in total surface area and 26% (SE = 2%) in average thickness could be explained by common genetic variants in the GWAS summary statistics.

2.4. Selection of genetic instruments

Genetic instruments were filtered with the following criteria: (1) the GWAS-correlated value of p was set as $5*10^{-8}$; (2) SNPs were aggregated by linkage disequilibrium (LD) r2 of <0.001, and < 1 MB from the index variant; (3) considering F statistic was able to quantify the strength of genetic instruments, SNPs with F statistics <10 were excluded; (4) harmonizing processes were conducted next to exclude ambiguous and palindromic SNPs; (5) after a first MR analysis, MR-pleiotropy residual sum and outlier (MR-PRESSO) process was used to check the SNPs with potential pleiotropy and to summarize a new value of *p* with outlier-corrected by removing the potential pleiotropy related SNPs, was after which, based on the new value of *p* and distortion test value of *p*, it was determined whether a second MR analysis should be necessary to verify robustness; and (6) PhenoScanner was used to see if the SNPs connected with the potential risk factors, including body mass index, obesity, smoking, drinking, neuropsychiatric disease, hypertension, and hyperlipemia, after which a second MR analysis would begin after removing SNPs associated with any of these potential confounders (Figure 1).

2.5. Mendelian randomization analyses

This study used random-effect inverse-variance weighted (IVW), MR-Egger, and weighted median as the major MR methods to address the variant heterogeneity and the pleiotropy effect. There are three assumptions that IVW needs to reach: (1) genetic variates need to be highly associated with exposure (Relevance hypothesis), (2) genetic variates should have nothing to do with confounding factors (Independence hypothesis), and (3) genetic variates could affect the outcome by exposure but nothing else (Exclusivity hypothesis). To sum up, it would be biased even if only one genetic variant is invalid (Burgess et al., 2013). Different from IVW, MR-Egger could be more robust to pleiotropy, and broadly used by allowing IVs to have a pleiotropic effect because there are only two assumptions for MR-Egger: (1) pleiotropic effect of IVs for outcome ought to be independent of the association between IVs and exposure, which is called the instrument strength independent of direct effect (InSIDE), relatively relaxing the constriction of exclusivity hypothesis (Bowden et al., 2015); and (2) there should be no measurement error (NOME) in correlation analysis between IVs and exposure. On the other hand, since the weighted median method uses the median IVs, it is robust to pleiotropy when >50% of the weight comes from valid IVs, which would result in a smaller type I error rate than IVW (Bowden et al., 2016). In the present study, IVW was chosen to be the main statistical method, because the cortical cortex structure-related SNPs were removed, outliers identified with MR-PRESSO were checked, and the InSIDE assumption of MR-Egger was difficult to confirm. Meanwhile, MR-Egger and weighted median were used to test the IVW estimates' robustness as they could provide more robust estimates in a broader set of scenarios, despite being less efficient (wider CIs). Taking everything into account, it would be defined as robust in the present study when the statistics matched the following criteria: (1) the estimates from IVW and weighted median were both statistically significant, for the MR-Egger was so strict in bias control that it increased type II error rate inverse; and (2) BETA, which could be regarded as the slope of the regression of the SNP-outcome effects on the SNP-exposure effects, should be positive or negative at the same time in the three methods. Once the BETAs were inconsistent, a tightened instrument value of *p* threshold would be used, and then the MR analysis should be re-performed (Chen et al., 2020).

For significant estimates, the MR-Egger intercept test and leave-one-out analyses were used for further assessing horizontal pleiotropy. To identify heterogeneity, Cochran's Q test was checked also.

2.6. Statistics

All analyses were performed using the packages TwoSampleMR (version 0.5.6) and MRPRESSO (version 1.0) in R (version 4.2.2) packages. Considering there were 136 MR estimates for region-level

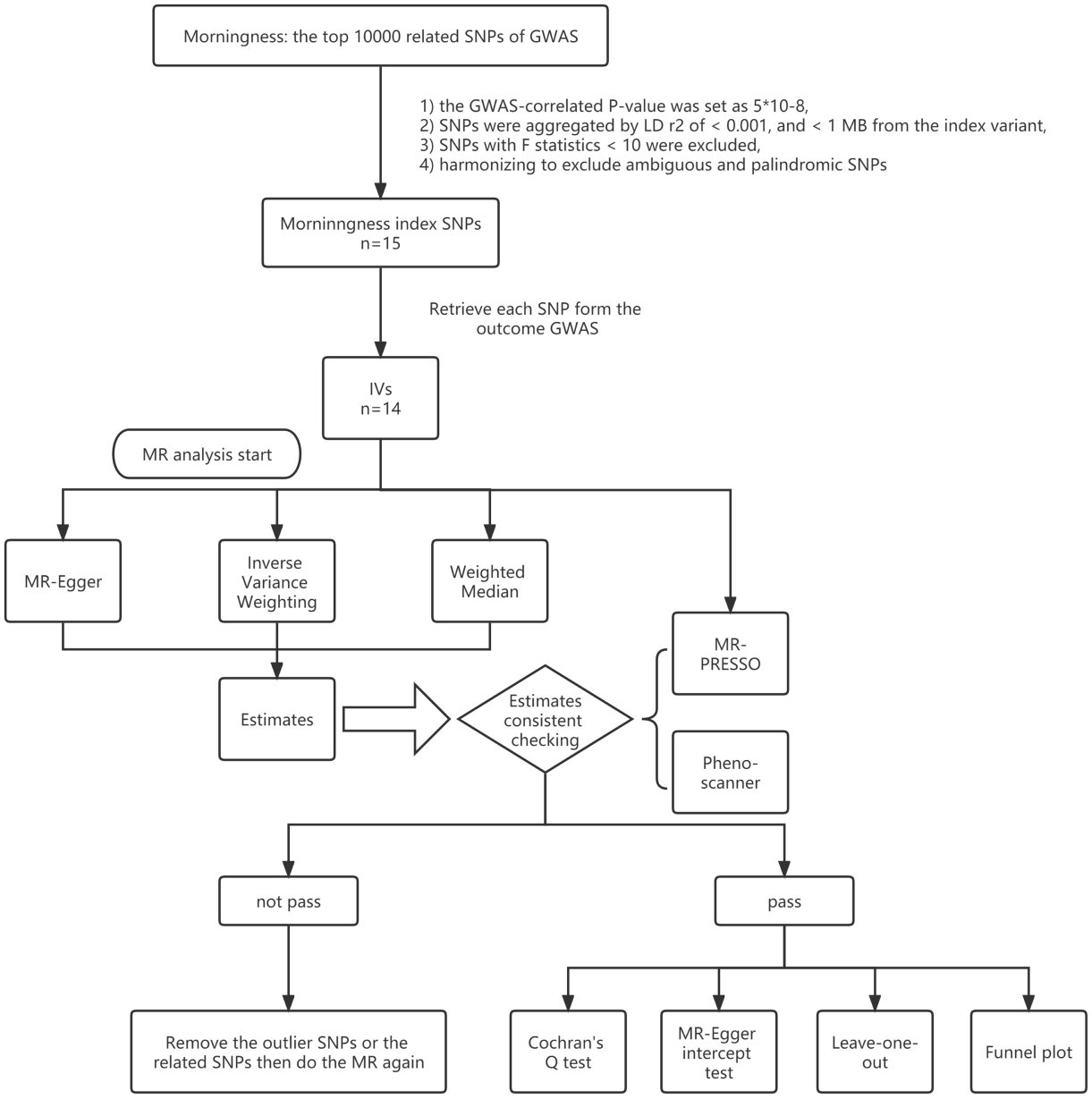

FIGURE 1
Study flame chart of the Mendelian randomization study to reveal the causal relationship between morningness and the brain cortical structure.

analyses and four MR estimates for global-level analyses, a Bonferroni-corrected value of p was set as 0.05/140 ($3.57*10^{-4}$), while a value of p less than 0.05 and greater than $3.57*10^{-4}$ was considered nominally significant.

3. Results

There were 15 SNPs recognized for morningness (Supplementary Table S2), but rs3972456 was missing in the outcome-related GWAS summary statistics. The remaining 14 SNPs passed the filter procedures and were selected as IVs preliminarily, with F statistics for these genetic instruments all larger than the selected value 10, indicating a strong prediction.

Then, a comprehensive MR study was conducted to determine whether genetically predicted morningness connected with the 70 phenotypes with or without genomic control (GC). On a global level, no evidence existed for morningness causing changes in total SA or total TH, and the value of ps for the MR-Egger intercept were > 0.05. But when testing the causal relationship of morningness and total SA with/without GC, heterogeneity was observed with an IVW-related Cochran Q-derived p-value <0.05, and outliers were identified with MR-PRESSO global-test p-value <0.05, which could be explained as acceptable by the use of the random-effects IVW as the main result and unnecessary for a second MR analysis because of the MR-PRESSO outlier-corrected p-value and distortion-test p-value >0.05. On a regional level, it was the only estimate of nominal significance that morningness decreased SA of the rostral middle frontal gyrus

TABLE 1 Significant Mendelian randomization estimates and the stability test results on the causal relationship of morningness and genetically predicted cortical structure.

Estimates		Rostral middle frontal average surface area _ noGC_wSA	Rostral middle frontal average surface area _ wGC_wSA
Inverse variance weighted (IVW)	N	13	13
	p-value	0.02943364	0.03596496
	SE	11.44181	11.71996
	BETA	−24.91603	−24.58055
	95% CI (BETA)	−47.34198 ~ −2.490075	−47.55168 ~ −1.609424
	OR	$1.51*10^{-11}$	$2.11*10^{-11}$
	95% CI (OR)	$2.75*10^{-21}$ ~ 0.08290378	$2.23*10^{-21}$ ~ 0.20000277
MR Egger	N	13	13
	p-value	0.1593967	0.1711283
	SE	27.49301	28.15703
	BETA	−41.49536	−41.22712
	95% CI (BETA)	−95.38165 ~ 12.39093	−96.41489 ~ 13.96066
	OR	$9.52*10^{-19}$	$1.25*10^{-18}$
	95% CI (OR)	$3.77*10^{-42}$ ~ 240610.1	$1.34*10^{-42}$ ~ 1156210.5
Weighted median	N	13	13
	p-value	0.02345826	0.02579779
	SE	14.65553	14.49354
	BETA	−33.20779	−32.30962
	95% CI (BETA)	−61.93263 ~ −4.482948	−60.71697 ~ −3.902274
	OR	$3.78*10^{-15}$	$9.29*10^{-15}$
	95% CI (OR)	$1.27*10^{-27}$ ~ 0.01130005	$4.28*10^{-27}$ ~ 0.02019594
Q-*p* value	IVW	0.9856199	0.9816331
	MR Egger	0.9833395	0.9789087
Pleiotropy	Egger intercept	1.772061	1.764273
	p-value	0.5289046	0.5208585
MR_PRESSO	Outlier corrected p	0.4098818	0.4041901
	Global Test p	0.0075	0.0033
	DistortionTest p	0.6848	0.6911

The significant estimate is defined as $p < 3.57*10^{-4}$ in IVW and weighted median, and the nominal significant estimate is defined as $p < 0.05$ in IVW and weighted median. *N*, number of SNPs; Q-*p* value, Cochran's Q-derived *p* value; noGC, without genomic control applied; wSA, the total surface area included as a covariate.

(RMFG) with GC (IVW: β = −25.647 mm, 95% CI: −47.794 mm to −3.499 mm, $p = 0.023$. Weighted median: β = −34.769 mm, 95% CI: −47.794 mm to −6.550 mm, $p = 0.016$. MR Egger: β < 0) and without GC (IVW: β = −25.971 mm, 95% CI: −62.986 mm to −4.349 mm, $p = 0.019$. Weighted median: β = −33.677 mm, 95% CI: −62.509 mm to −4.845 mm, $p = 0.022$. MR Egger: β < 0), with the *p*-values for MR-Egger intercept >0.05, and no heterogeneity or outliers (Supplementary Tables S3–S6). For the remaining estimates on the regional level, it was not necessary to run a second MR analysis, even though heterogeneity was observed in some cases but no outliers were found or the MR-PRESSO outlier-corrected *p*-values were > 0.05.

To figure out whether the nominal significant estimate could be violated by risk factors, Phenoscanner was used to check the IVs, finding that SNP rs13394871 was associated with body mass index (BMI), while others were associated with chronotype (Details of the instrumental variables are displayed in Supplementary Tables S7, S8). After removing rs13394871, estimates were consistent with the previous result. No causal relationship was verified on a global level, while on a regional level, only the nominally significant estimate remained, that morningness decreased SA of the RMFG with GC (IVW: β = −24.916 mm, 95% CI: −47.342 mm to −2.490 mm, $p = 0.029$. Weighted median: β = −33.208 mm, 95% CI: −61.933 mm to −4.483 mm, $p = 0.023$. MR Egger: β < 0) and without GC (IVW: β = −24.581 mm, 95% CI: −47.552 mm to −1.609 mm, $p = 0.036$. Weighted median: β = −32.310 mm, 95% CI: −60.717 mm to −3.902 mm, $p = 0.026$. MR Egger: β < 0), with the *p*-values for MR-Egger intercept >0.05, and no heterogeneity or outliers (Table 1, Figure 2 and Supplementary Tables S9–S12), indicating that the causal relationship between morningness and SA of the RMFG decreasing was not violated by potential risk factors.

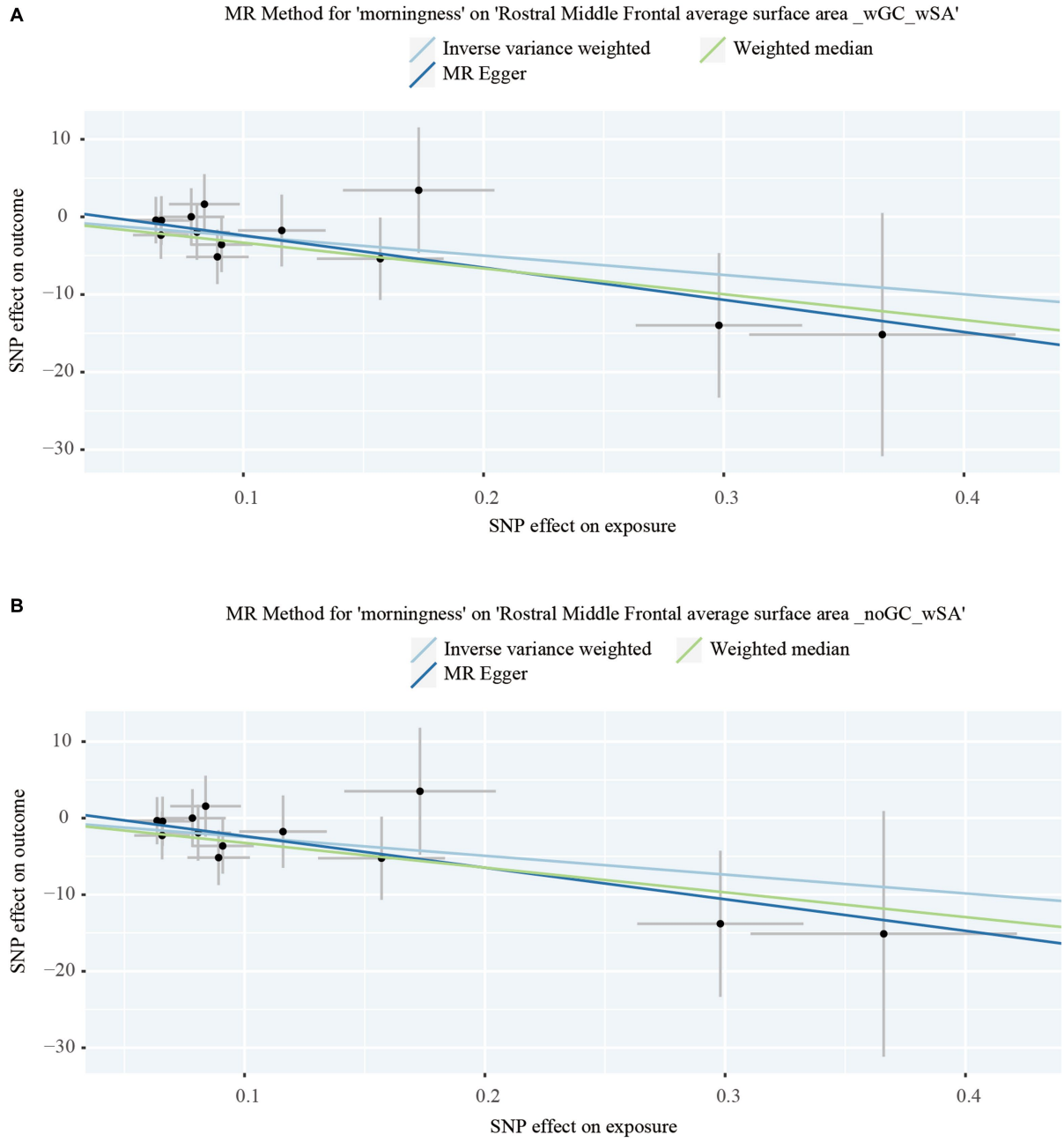

FIGURE 2
Dot plots of the significant Mendelian randomization statistics. **(A)** Statistics of morningness on the rostral middle frontal average surface area with genomic control applied and the total surface area included as a covariate; **(B)** statistics of morningness on the rostral middle frontal average surface area with the total surface area included as a covariate but genomic control not applied.

For significant estimates, leave-one-out analyses were used for further assessing horizontal pleiotropy, suggesting the estimates were not violated and biased by every single SNP (Figure 3).

4. Discussion

To the best of our knowledge, this is the first time a large-scale MR analysis has been carried out on the causal relationship between the state of circadian rhythm and changes in brain structure. Our study supports the causal relationship and provides novel information on the regional alterations ascribed to circadian rhythm.

Chronobiology began with Kleitman discovering its existence and is defined by Horne and Ostberg's questionnaire (Kleitman, 1939; Horne and Ostberg, 1976). In Hu's study, which supplied the exposure GWAS data source in the present study, to be a morning person is used as a substitute for rhythm following the steps of light, while a night one refers to a state in the opposite (Hu et al., 2016). Meanwhile, the present study points out that morningness decreases SA of the RMFG on a nominally significant level by systematically assessing the causality of morningness and cerebral cortex. That is to say, circadian rhythm disorder may cause an increase in rostral middle frontal gyrus surface area, but we cannot summarize a clear conclusion on whether the SA and TH of other gyri could be increased or decreased at the

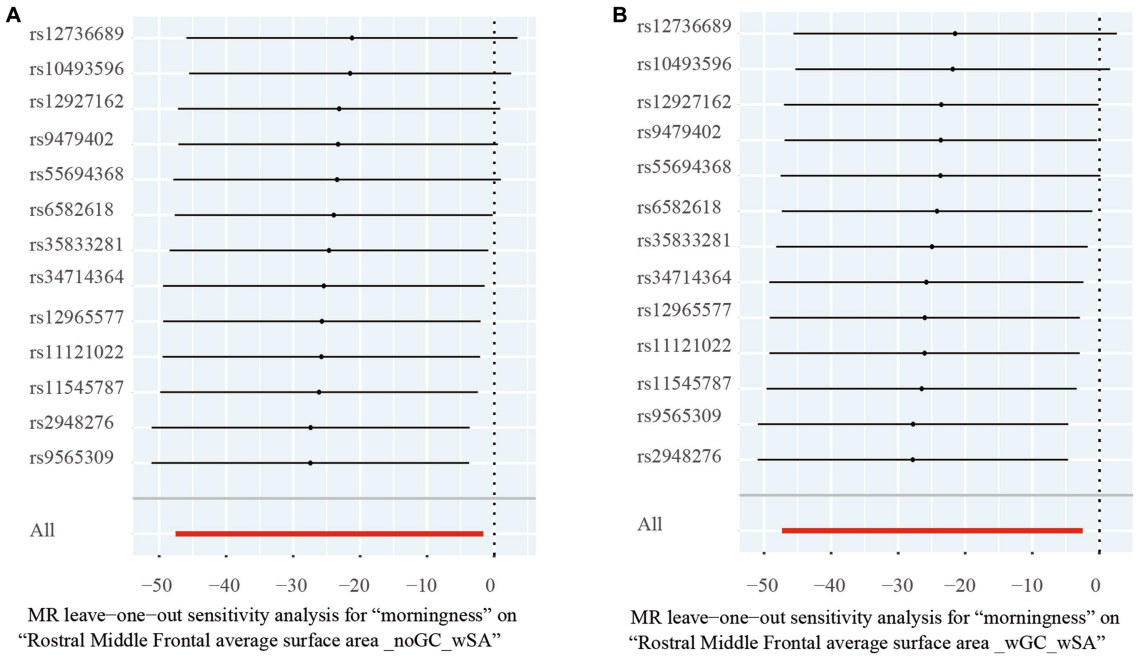

FIGURE 3
Leave-one-out analysis of the significant Mendelian randomization statistics. **(A)** Statistics of morningness on the rostral middle frontal average surface area with genomic control applied and total surface area included as a covariate; **(B)** statistics of morningness on the rostral middle frontal average surface area with the total surface area included as a covariate but genomic control not applied.

same time because the *p*-value of the causal relationship between morningness and SA of the RMFG is less than 0.05 but cannot pass the Bonferroni correction.

As the radial unit hypothesis posits, the increase of cortical SA is driven by the proliferation of neural progenitor cells, whereas TH is determined by the neurogenic divisions, which is a widely accepted hypothesis in neurology (Rakic, 1988, 1995, 2009), Grasby's study goes further to suggest that SA is affected by genetic variants located in the regulatory element of progenitor cells in fetal brain tissue rather than adult brain tissue, whereas TH is associated with the regulatory elements which are close to genes implicating cell differentiation, migration, adhesion, and myelination in adult brain tissue (Grasby et al., 2020). In other words, SA is more innate, while TH is determined later and environmentally. Consequently, it becomes mainstream to use SA and TH as the basic neuroimaging instruments to discover underlying neurobiological mechanisms of both congenital and acquired diseases. It seems to be that SA and TH are highly heritable, of which the variants represent a pathological process from different periods in neurodevelopment (Strike et al., 2019).

However, it turns out to be the environmental factors that are more important. Whether through interventional studies or observational studies, whether it be normal physiological alterations, acute trauma, or psychogenic diseases with complex etiology and mechanisms, it has been verified that SA and TH both exhibit changes in response to environmental variations. For example, Voineskos has conducted a randomized placebo-controlled clinical trial clarifying the effects of antipsychotic medication on brain structure, finding that those who relapse receiving a placebo experienced decreases in cortical thickness compared with those who sustain remission (Voineskos et al., 2020). And Besiroglu has examined cortical TH and SA in 30 patients with obsessive–compulsive disorder (OCD), 21 unaffected siblings (SIB), and 30 controls, finding that both OCD and SIB groups show significantly lower cortical thickness in the right anterior insula compared to healthy controls and there are no significant differences in cortical thickness and surface area between the OCD and SIB groups (Besiroglu et al., 2022). When it comes to the normal physiological alterations, scientists point out that during pregnancy, an obvious change in cortical TH is discovered in mothers, suggesting brain structural adaptations for maternal love behavior (Hoekzema et al., 2017; Kim et al., 2018; Carmona et al., 2019; Zhang et al., 2019). Meanwhile, a study of 30 patients with acute mild traumatic brain injury (mTBI) and 27 matched healthy controls discovered a significant increase of cortical SA and volume in the right lateral occipital gyrus of acute-stage mTBI patients, but no significant changes in TH, which might explain a compensatory mechanism for cognitive dysfunction in acute-stage mTBI patients (Li et al., 2022).

In the Brodmann partition, RMFG refers to a part of the region on the outer superior surface of the frontal lobe that includes the superior and middle frontal gyri (Amunts and Zilles, 2015). The superior frontal gyrus is associated with advanced cognitive functions such as decision-making, reasoning, and planning, while the middle frontal gyrus is located posteriorly to the superior frontal gyrus and is also known as the precentral gyrus, involved in the planning, execution, and maintenance of working memory (Badre and D'esposito, 2009; Krudop and Pijnenburg, 2015). Therefore, the RMFG plays an important role in cognitive control and planning, and is shown to be associated with many neurological and psychiatric disorders such as attention deficit hyperactivity disorder, Alzheimer's disease, and schizophrenia. For example, in the research on depression in Parkinson's patients, it was found that thinning of the RMFG cortical area is associated with worsening depression. Many scientists have shown that the thickness of cortical layers in the RMFG region

correlate with familial Alzheimer's disease, depression severity in Parkinson's patients, and first-episode schizophrenia (Quan et al., 2013, 2020; Yin et al., 2022).

The RMFG is also regarded as an emotion regulation center (Koenigs and Grafman, 2009). Emotion sensitivity is verified in Leon's study, where he has followed the examination of 24 mothers who neglect their children (the neglect group, NG) and 21 mothers with non-neglectful caregiving (21 in the control group, CG); he discovers that there is a decrease in TH of the right rostral middle frontal gyrus and an increased SA in the right lingual and lateral occipital cortices for the NG (Leon et al., 2021). There are other existing forms of emotion regulation disorders as well. In a bipolar disorder-related study, the severity of the disease corresponds with the thinner TH of the RMFG, but an increase of the TH on the RMFG is discovered after a period of treatment (Hibar et al., 2018). And Hibar's research also answers the question on whether RMFG could be influenced by the postnatal environment. While most of the studies above are cross-section experiments, a prospective study reached the same answer that the SA of RMFG could be influenced by the postnatal environment by demonstrating that, with no difference in the childhood brain structure, socioeconomic status in childhood is associated with adulthood brain structure changes in cortical TH of the precentral gyrus, postcentral gyrus, and caudal middle frontal, and in cortical SA of the RMFG, caudal middle frontal gyrus, and superior frontal gyrus (Dufford et al., 2021). All the SES-related variations have been further related to differences in cognitive, affective, and socio-emotional outcomes (Johnson et al., 2016; Dufford et al., 2019).

Our research mainly focused on the impact of circadian rhythms on brain function. Based on the results of the present study, it was found that circadian rhythms are indeed causally related to the SA of RMFG. A pilot study, fitting with the present study to some degree, indicates that 40 min of aerobic exercise and 20 min of anaerobic exercise a day, maintaining for 6 months, increases cortical thickness in the left pericalcarine area, the left superior parietal area, right RMFG, and right lateral occipital gyrus (Bashir et al., 2021), as physical exercise is beneficial to mental health and sleep (Hartescu et al., 2015; Panagiotou et al., 2021). Due to the impact of NO2 pollution on illumination, a cross-sectional study shows that exposure to air pollution of NO2 is associated with brain structure variates, including increases in the RMFG volume, supramarginal gyrus volume, the transverse temporal volume of the left brain, and the pars opercularis volume of the right brain (Lo et al., 2022), and air pollution exposure of NO2 is also associated with an increase in arousal (Lo et al., 2021; Tung et al., 2021).

Most of the variates in cortical structure observed in neurological disorders and diseases have been reported for TH, perhaps suggesting that TH would be more sensitive to environmental factors, such as treatment, illness, and so on (Grasby et al., 2020). The present study defines a significant estimate relating to SA, but not TH, which could be explained by the phenotypic variance of the RMFG being affected by common variants more for SA (21%) than TH (6%) (Grasby et al., 2020). In addition, changes in SA should not be viewed as a miracle, in other words, they may necessitate a longer duration like in Dufford's study (Dufford et al., 2021), reflecting a chronic process, but they do make sense. Eero Vuoksimaa's study suggests the same, wherein multivariate genetic analysis of 515 pairs of middle-aged twins reveals that the phenotypic and genetic association between neocortex volume and general cognitive ability is mainly driven by surface area rather than thickness (Vuoksimaa et al., 2015).

Notably, the present study confirms an estimate varied from the logical expectation. Being a morning person should be beneficial to our health as this suits the diurnal rhythm well, but in the present study, morningness was found to decrease the SA of the RMFG. Stomby's cross-sectional prospective study might have served an explanation with sleepless, by indicating that higher cortisol in elderly people with less sleep correlates with the decrease of SA on the RMFG (Stomby et al., 2016). However, for night people, compensatory hypertrophy could explain the increased SA of the RMFG, the same as the consequence of Li's study pointing out that patients with brain injury are discovered to have a significant increase of cortical SA and volume in the right lateral occipital gyrus (Li et al., 2022). All the evidence leads us to believe that the effects of circadian rhythm on the brain cortex may extend beyond what we currently understand, and urges further studies to elucidate the mechanism.

However, the core assumptions for MR analysis persist: (1) IVs need to be highly associated with exposure, (2) IVs should have nothing to do with confounding factors, and (3) IVs could affect the outcome by exposure but nothing else, MR analysis is faced challenges at its roots. Since the total phenotypic variation of the segregating population (VP) equals the sum of phenotypic variation coming from genetic variation (VG), variation related to environment factor (VE), and variation associated with the genetic and environmental factor interactions (VGE) (Andrew et al., 2010), there would be a statistical loss in the study using genetic variates as IVs for representing the phenotype of exposure.

In the present study, it was found that IVs could only account for approximately 21% of the morningness phenotype (Hu et al., 2016), but they still exhibited a nominally significant causal relationship with the decrease of SA in the RMFG. In other words, due to the high specificity and low sensitivity of the IVs, the conclusions derived from the present MR analysis have a low Type I error rate and a high Type II error rate. In layman's terms, even though only around 21% of the participants were accurately identified (VG's contribution to VP), the impact of circadian rhythm on RMFG still reached the threshold of nominal significance, and underdiagnosis (contribution of VE and VGE to VP) might have resulted in the study's findings not passing the Bonferroni correction. Taking all the above concerns into account, an indirect and comprehensive assessment for VE and VGE could be viewed as the influence of underdiagnosis. This notion emphasizes the importance of considering VE and VGE in investigating the impact of phenotypes and diseases. It can be assumed that the causal relationship exists in the real world if VE and VGE were taken into account because it is not surprising that the circadian rhythm in our daily life would be easily influenced by many factors, such as children busy with morning classes and adults trapped by working hours. In other words, it is good news for us that making a behavior change would be useful for preventing RMFG-related diseases.

But the present study has several limitations: (1) the participants enrolled were all European, hence, whether the relationship between morningness and the RMFG is causal or not in other populations

remains unknown; and (2) the study only reported the variates of the cortical structure in the morning person, but the underlying mechanisms warrant further investigation.

Our results provide a clue for researchers to explore the relationship between circadian rhythm and other neuropsychiatric disorders, especially focusing on the specific gyrus of the circadian rhythm. Future studies should focus on the mechanism of how circadian rhythm acts on the RMFG or designing RCTs for circadian treatment modalities to prevent or treat RMFG-related neuropsychiatric disorders.

Data availability statement

Publicly available datasets were analyzed in this study. This data can be found here: the exposure data for the top 10,000 morningness-related SNPs of the GWAS summary statistics can be accessed at: https://static-content.springer.com/esm/art%3A10.1038%2Fncomms10448/MediaObjects/41467_2016_BFncomms10448_MOESM584_ESM.txt. The outcome GWAS summary statistics for brain cerebral cortex structure can be accessed at: https://enigma.ini.usc.edu/research/download-enigma-gwas-results/ by applying for the data access.

Ethics statement

This study used publicly available de-identified data from participant studies that were approved by an ethical standards committee concerning human experimentation. No separate ethical approval was required in this study.

Author contributions

FY and RL: writing—original draft preparation, conceptualization, and methodology. SH, SR, and BH: formal analysis. JL: resources. LP: writing—review and editing. The guarantor (LP) confirms that all listed authors meet the authorship criteria and that no others meeting the criteria have been omitted. All authors contributed to the article and approved the submitted version.

Funding

This study was supported by the Health Commission of Hunan Province (Grant no. 202204113461 on FY) and the Natural Science Foundation of Hunan Province (Grant no. 2021JJ70046 on BH).

Acknowledgments

We extend our great appreciation to the 23andMe Consortium and the ENIGMA Consortium for generously providing us with GWAS data.

Conflict of interest

The authors declare that the research was conducted in the absence of any commercial or financial relationships that could be construed as a potential conflict of interest.

Publisher's note

Supplementary material

The Supplementary material for this article can be found online at: https://www.frontiersin.org/articles/10.3389/fnins.2023.1222551/full#supplementary-material

References

Amunts, K., and Zilles, K. (2015). Architectonic mapping of the human brain beyond Brodmann. *Neuron* 88, 1086–1107. doi: 10.1016/j.neuron.2015.12.001

Andrew, R. L., Wallis, I. R., Harwood, C. E., and Foley, W. J. (2010). Genetic and environmental contributions to variation and population divergence in a broad-spectrum foliar defence of Eucalyptus tricarpa. *Ann. Bot.* 105, 707–717. doi: 10.1093/aob/mcq034

Badre, D., and D'esposito, M. (2009). Is the rostro-caudal axis of the frontal lobe hierarchical? *Nat. Rev. Neurosci.* 10, 659–669. doi: 10.1038/nrn2667

Bashir, S., Al-Sultan, F., Jamea, A. A., Almousa, A., Alzahrani, M. S., Alhargan, F. A., et al. (2021). Physical exercise and cortical thickness in healthy controls: a pilot study. *Eur. Rev. Med. Pharmacol. Sci.* 25, 7375–7379. doi: 10.26355/eurrev_202112_27432

Baxter, M., and Ray, D. W. (2020). Circadian rhythms in innate immunity and stress responses. *Immunology* 161, 261–267. doi: 10.1111/imm.13166

Besiroglu, L., Zalesky, A., Kasal, M. I., Dikmeer, N., Bilge, A., Durmaz, E., et al. (2022). Cortical thickness and surface area in patients with obsessive compulsive disorder and their unaffected siblings. *Brain Imaging Behav.* 16, 1946–1953. doi: 10.1007/s11682-022-00660-7

Bowden, J., Davey Smith, G., and Burgess, S. (2015). Mendelian randomization with invalid instruments: effect estimation and bias detection through egger regression. *Int. J. Epidemiol.* 44, 512–525. doi: 10.1093/ije/dyv080

Bowden, J., Davey Smith, G., Haycock, P. C., and BURGESS, S. (2016). Consistent estimation in Mendelian randomization with some invalid instruments using a weighted median estimator. *Genet. Epidemiol.* 40, 304–314. doi: 10.1002/gepi.21965

Bowden, J., and Holmes, M. V. (2019). Meta-analysis and Mendelian randomization: a review. *Res. Synth. Methods* 10, 486–496. doi: 10.1002/jrsm.1346

Burgess, S., Butterworth, A., and Thompson, S. G. (2013). Mendelian randomization analysis with multiple genetic variants using summarized data. *Genet. Epidemiol.* 37, 658–665. doi: 10.1002/gepi.21758

Burgess, S., and Thompson, S. G. (2015). Multivariable Mendelian randomization: the use of pleiotropic genetic variants to estimate causal effects. *Am. J. Epidemiol.* 181, 251–260. doi: 10.1093/aje/kwu283

Carmona, S., Martinez-Garcia, M., Paternina-Die, M., Barba-Muller, E., Wierenga, L. M., Aleman-Gomez, Y., et al. (2019). Pregnancy and adolescence entail similar neuroanatomical adaptations: a comparative analysis of cerebral morphometric changes. *Hum. Brain Mapp.* 40, 2143–2152. doi: 10.1002/hbm.24513

Chen, X., Kong, J., Diao, X., Cai, J., Zheng, J., Xie, W., et al. (2020). Depression and prostate cancer risk: a Mendelian randomization study. *Cancer Med.* 9, 9160–9167. doi: 10.1002/cam4.3493

Desikan, R. S., Segonne, F., Fischl, B., Quinn, B. T., Dickerson, B. C., Blacker, D., et al. (2006). An automated labeling system for subdividing the human cerebral cortex on

MRI scans into gyral based regions of interest. *NeuroImage* 31, 968–980. doi: 10.1016/j.neuroimage.2006.01.021

Dufford, A. J., Bianco, H., and Kim, P. (2019). Socioeconomic disadvantage, brain morphometry, and attentional bias to threat in middle childhood. *Cogn. Affect. Behav. Neurosci.* 19, 309–326. doi: 10.3758/s13415-018-00670-3

Dufford, A. J., Evans, G. W., Liberzon, I., Swain, J. E., and Kim, P. (2021). Childhood socioeconomic status is prospectively associated with surface morphometry in adulthood. *Dev. Psychobiol.* 63, 1589–1596. doi: 10.1002/dev.22096

Eriksson, N., Macpherson, J. M., Tung, J. Y., Hon, L. S., Naughton, B., Saxonov, S., et al. (2010). Web-based, participant-driven studies yield novel genetic associations for common traits. *PLoS Genet.* 6:e1000993. doi: 10.1371/journal.pgen.1000993

Falush, D., Stephens, M., and Pritchard, J. K. (2007). Inference of population structure using multilocus genotype data: dominant markers and null alleles. *Mol. Ecol. Notes* 7, 574–578. doi: 10.1111/j.1471-8286.2007.01758.x

Grasby, K. L., Jahanshad, N., Painter, J. N., Colodro-Conde, L., Bralten, J., Hibar, D. P., et al. (2020). The genetic architecture of the human cerebral cortex. *Science* 367:aay6690. doi: 10.1126/science.aay6690

Gu, Z., Wang, B., Zhang, Y. B., Ding, H., Zhang, Y., Yu, J., et al. (2015). Association of ARNTL and PER1 genes with Parkinson's disease: a case-control study of Han Chinese. *Sci. Rep.* 5:15891. doi: 10.1038/srep15891

Han, Y., Yang, Y., Zhou, Z., Jin, X., Shi, H., Shao, M., et al. (2023). Cortical anatomical variations, gene expression profiles, and clinical phenotypes in patients with schizophrenia. *Neuroimage Clin* 39:103451. doi: 10.1016/j.nicl.2023.103451

Hartescu, I., Morgan, K., and Stevinson, C. D. (2015). Increased physical activity improves sleep and mood outcomes in inactive people with insomnia: a randomized controlled trial. *J. Sleep Res.* 24, 526–534. doi: 10.1111/jsr.12297

Hibar, D. P., Westlye, L. T., Doan, N. T., Jahanshad, N., Cheung, J. W., Ching, C. R. K., et al. (2018). Cortical abnormalities in bipolar disorder: an MRI analysis of 6503 individuals from the ENIGMA bipolar disorder working group. *Mol. Psychiatry* 23, 932–942. doi: 10.1038/mp.2017.73

Hoekzema, E., Barba-Muller, E., Pozzobon, C., Picado, M., Lucco, F., Garcia-Garcia, D., et al. (2017). Pregnancy leads to long-lasting changes in human brain structure. *Nat. Neurosci.* 20, 287–296. doi: 10.1038/nn.4458

Horne, J. A., and Ostberg, O. (1976). A self-assessment questionnaire to determine morningness-eveningness in human circadian rhythms. *Int. J. Chronobiol.* 4, 97–110.

Hu, Y., Shmygelska, A., Tran, D., Eriksson, N., Tung, J. Y., and Hinds, D. A. (2016). GWAS of 89, 283 individuals identifies genetic variants associated with self-reporting of being a morning person. *Nat. Commun.* 7:10448. doi: 10.1038/ncomms10448

Johnson, S. B., Riis, J. L., and Noble, K. G. (2016). State of the art review: poverty and the developing brain. *Pediatrics* 137:3075. doi: 10.1542/peds.2015-3075

Ketchesin, K. D., Zong, W., Hildebrand, M. A., Scott, M. R., Seney, M. L., Cahill, K. M., et al. (2023). Diurnal alterations in gene expression across striatal subregions in psychosis. *Biol. Psychiatry* 93, 137–148. doi: 10.1016/j.biopsych.2022.08.013

Kim, P., Dufford, A. J., and Tribble, R. C. (2018). Cortical thickness variation of the maternal brain in the first 6 months postpartum: associations with parental self-efficacy. *Brain Struct. Funct.* 223, 3267–3277. doi: 10.1007/s00429-018-1688-z

Kleitman, N. (1939). Sleep and wakefulness as alternating phases in the cycle of existence. *J. Am. Med. Assoc.* 113:2086.

Koenigs, M., and Grafman, J. (2009). The functional neuroanatomy of depression: distinct roles for ventromedial and dorsolateral prefrontal cortex. *Behav. Brain Res.* 201, 239–243. doi: 10.1016/j.bbr.2009.03.004

Krudop, W. A., and Pijnenburg, Y. A. (2015). Historical evolution of the frontal lobe syndrome. *Psychopathology* 48, 222–229. doi: 10.1159/000381986

Laansma, M. A., Bright, J. K., Al-Bachari, S., Anderson, T. J., Ard, T., Assogna, F., et al. (2021). International multicenter analysis of brain structure across clinical stages of Parkinson's disease. *Mov. Disord.* 36, 2583–2594. doi: 10.1002/mds.28706

Leon, I., Rodrigo, M. J., Quinones, I., Hernandez-Cabrera, J. A., and Garcia-Penton, L. (2021). Distinctive frontal and Occipitotemporal surface features in neglectful parenting. *Brain Sci.* 11:30387. doi: 10.3390/brainsci11030387

Li, M. J., Huang, S. H., Huang, C. X., and Liu, J. (2022). Morphometric changes in the cortex following acute mild traumatic brain injury. *Neural Regen. Res.* 17, 587–593. doi: 10.4103/1673-5374.320995

Li, Q., Wang, J., Liu, J., Wang, Y., and Li, K. (2021). Magnetic resonance imaging measurement of entorhinal cortex in the diagnosis and differential diagnosis of mild cognitive impairment and Alzheimer's disease. *Brain Sci.* 11:91129. doi: 10.3390/brainsci11091129

Lo, K., Chiang, L. L., Hsu, S. M., Tsai, C. Y., Wu, D., Chou, C. J., et al. (2021). Association of short-term exposure to air pollution with depression in patients with sleep-related breathing disorders. *Sci. Total Environ.* 786:147291. doi: 10.1016/j.scitotenv.2021.147291

Lo, C. C., Liu, W. T., Lu, Y. H., Wu, D., Wu, C. D., Chen, T. C., et al. (2022). Air pollution associated with cognitive decline by the mediating effects of sleep cycle disruption and changes in brain structure in adults. *Environ. Sci. Pollut. Res. Int.* 29, 52355–52366. doi: 10.1007/s11356-022-19482-7

Martinez-Cayuelas, E., Gavela-Perez, T., Rodrigo-Moreno, M., Merino-Andreu, M., Vales-Villamarin, C., Perez-Nadador, I., et al. (2022). Melatonin rhythm and its relation to sleep and circadian parameters in children and adolescents with autism Spectrum disorder. *Front. Neurol.* 13:813692. doi: 10.3389/fneur.2022.813692

Neves, A. R., Albuquerque, T., Quintela, T., and Costa, D. (2022). Circadian rhythm and disease: relationship, new insights, and future perspectives. *J. Cell. Physiol.* 237, 3239–3256. doi: 10.1002/jcp.30815

Pan, N., Lin, L. Z., Wang, X., Shi, L., Xu, X. Y., Jin, Y. Y., et al. (2023). Brain structure underlying the empathizing-systemizing difference in children with autism spectrum disorder. *World J. Pediatr.* doi: 10.1007/s12519-023-00732-8

Panagiotou, M., Michel, S., Meijer, J. H., and Deboer, T. (2021). The aging brain: sleep, the circadian clock and exercise. *Biochem. Pharmacol.* 191:114563. doi: 10.1016/j.bcp.2021.114563

Quan, M., Lee, S. H., Kubicki, M., Kikinis, Z., Rathi, Y., Seidman, L. J., et al. (2013). White matter tract abnormalities between rostral middle frontal gyrus, inferior frontal gyrus and striatum in first-episode schizophrenia. *Schizophr. Res.* 145, 1–10. doi: 10.1016/j.schres.2012.11.028

Quan, M., Zhao, T., Tang, Y., Luo, P., Wang, W., Qin, Q., et al. (2020). Effects of gene mutation and disease progression on representative neural circuits in familial Alzheimer's disease. *Alzheimers Res. Ther.* 12:14. doi: 10.1186/s13195-019-0572-2

Rakic, P. (1988). Specification of cerebral cortical areas. *Science* 241, 170–176. doi: 10.1126/science.3291116

Rakic, P. (1995). A small step for the cell, a giant leap for mankind: a hypothesis of neocortical expansion during evolution. *Trends Neurosci.* 18, 383–388. doi: 10.1016/0166-2236(95)93934-P

Rakic, P. (2009). Evolution of the neocortex: a perspective from developmental biology. *Nat. Rev. Neurosci.* 10, 724–735. doi: 10.1038/nrn2719

Richmond, R. C., and Davey Smith, G. (2022, 2022). Mendelian randomization: Concepts and scope. *Cold Spring Harb Perspect Med* 4:a040501:12. doi: 10.1101/cshperspect.a040501

Shivshankar, P., Fekry, B., Eckel-Mahan, K., and Wetsel, R. A. (2020). Circadian clock and complement immune system-complementary control of physiology and pathology? *Front. Cell. Infect. Microbiol.* 10:418. doi: 10.3389/fcimb.2020.00418

Stomby, A., Boraxbekk, C. J., Lundquist, A., Nordin, A., Nilsson, L. G., Adolfsson, R., et al. (2016). Higher diurnal salivary cortisol levels are related to smaller prefrontal cortex surface area in elderly men and women. *Eur. J. Endocrinol.* 175, 117–126. doi: 10.1530/EJE-16-0352

Strike, L. T., Hansell, N. K., Couvy-Duchesne, B., Thompson, P. M., De Zubicaray, G. I., Mcmahon, K. L., et al. (2019). Genetic complexity of cortical structure: differences in genetic and environmental factors influencing cortical surface area and thickness. *Cereb. Cortex* 29, 952–962. doi: 10.1093/cercor/bhy002

Takaesu, Y., Kanda, Y., Nagahama, Y., Shiroma, A., Ishii, M., and Hashimoto, T. (et al.) (2022). Delayed sleep-wake rhythm is associated with cognitive dysfunction, social dysfunction, and deteriorated quality of life in patients with major depressive disorder. *Front Psychiatry*. 7:1022144. doi: 10.3389/fpsyt.2022.1022144

Tung, N. T., Lee, Y. L., Lin, S. Y., Wu, C. D., Dung, H. B., Thuy, T. P. C., et al. (2021). Associations of ambient air pollution with overnight changes in body composition and sleep-related parameters. *Sci. Total Environ.* 791:148265. doi: 10.1016/j.scitotenv.2021.148265

Voineskos, A. N., Mulsant, B. H., Dickie, E. W., Neufeld, N. H., Rothschild, A. J., Whyte, E. M., et al. (2020). Effects of antipsychotic medication on brain structure in patients with major depressive disorder and psychotic features: neuroimaging findings in the context of a randomized placebo-controlled clinical trial. *JAMA Psychiat.* 77, 674–683. doi: 10.1001/jamapsychiatry.2020.0036

Vuksanovic, V., Staff, R. TAhearn, T., Murray, A. D., and Wischik, C. M. (2019). Cortical thickness and surface area networks in healthy aging, Alzheimer's disease and behavioral variant Fronto-temporal dementia. *Int. J. Neural Syst.* 29:1850055. doi: 10.1142/S0129065718500557

Vuoksimaa, E., Panizzon, M. S., Chen, C. H., Fiecas, M., Eyler, L. T., Fennema-Notestine, C., et al. (2015). The genetic association between neocortical volume and general cognitive ability is driven by global surface area rather than thickness. *Cereb. Cortex* 25, 2127–2137. doi: 10.1093/cercor/bhu018

Walker, W. H., Walton, J. C., and Nelson, R. J. (2021). Disrupted circadian rhythms and mental health. *Handb. Clin. Neurol.* 179, 259–270. doi: 10.1016/B978-0-12-819975-6.00016-9

Weissova, K., Bartos, A., Sladek, M., Novakova, M., and Sumova, A. (2016). Moderate changes in the circadian system of Alzheimer's disease patients detected in their home environment. *PLoS One* 11:e0146200. doi: 10.1371/journal.pone.0146200

Willer, C. J., Li, Y., and Abecasis, G. R. (2010). METAL: fast and efficient meta-analysis of genomewide association scans. *Bioinformatics* 26, 2190–2191. doi: 10.1093/bioinformatics/btq340

Xu, H., Xu, C., Gu, P., Hu, Y., Guo, Y., and Bai, G. (2023). Neuroanatomical restoration of salience network links reduced headache impact to cognitive function improvement in mild traumatic brain injury with posttraumatic headache. *J. Headache Pain* 24:43. doi: 10.1186/s10194-023-01579-0

Yang, J., Lee, S. H., Goddard, M. E., and Visscher, P. M. (2011). GCTA: a tool for genome-wide complex trait analysis. *Am. J. Hum. Genet.* 88, 76–82. doi: 10.1016/j.ajhg.2010.11.011

Yin, W., Li, A., Yang, B., Gao, C., Hu, Y., Luo, Z., et al. (2022). Abnormal cortical atrophy and functional connectivity are associated with depression in Parkinson's disease. *Front. Aging Neurosci.* 14:957997. doi: 10.3389/fnagi.2022.957997

Zhang, K., Wang, M., Zhang, J., Du, X., and Chen, Z. (2019). Brain structural plasticity associated with maternal caregiving in mothers: a voxel– and surface-based morphometry study. *Neurodegener Dis* 19, 192–203. doi: 10.1159/000506258

frontiers | Frontiers in Neuroscience

TYPE Review
PUBLISHED 24 August 2023
DOI 10.3389/fnins.2023.1152959

OPEN ACCESS

EDITED BY
Daisuke Ono,
Nagoya University, Japan

REVIEWED BY
Daniela Polese,
Sant'Andrea University Hospital, Italy
Yasuhiro Umemura,
Kyoto Prefectural University of Medicine, Japan
Prakash Adhikari,
Queensland University of Technology, Australia

*CORRESPONDENCE
Hidenobu Ohta
✉ hideohta@med.akita-u.ac.jp

RECEIVED 28 January 2023
ACCEPTED 26 July 2023
PUBLISHED 24 August 2023

CITATION
Arimitsu T, Fukutomi R, Kumagai M, Shibuma H, Yamanishi Y, Takahashi K-i, Gima H, Seto Y, Adachi H, Arai H, Higuchi M, Ohgi S and Ohta H (2023) Designing artificial circadian environments with multisensory cares for supporting preterm infants' growth in NICUs. *Front. Neurosci.* 17:1152959. doi: 10.3389/fnins.2023.1152959

Designing artificial circadian environments with multisensory cares for supporting preterm infants' growth in NICUs

Takeshi Arimitsu[1,2], Rika Fukutomi[3], Mayuko Kumagai[4], Hayato Shibuma[5], Yoko Yamanishi[6], Kei-ichi Takahashi[7], Hirotaka Gima[2,8], Yoshitaka Seto[9], Hiroyuki Adachi[10], Hirokazu Arai[11], Masakatsu Higuchi[2,12], Shohei Ohgi[2,13] and Hidenobu Ohta[2,7,14,15]*

[1]Department of Pediatrics, Keio University School of Medicine, Tokyo, Japan, [2]The Japan Developmental Care Study Group, School of Rehabilitation Sciences, Seirei Christopher University, Hamamatsu, Japan, [3]Section of Pediatric Nursing, Graduate School of Nursing Science, St. Luke's International University, Tokyo, Japan, [4]Department of Nursing, Akita University Graduate School of Medicine, Akita, Japan, [5]Department of Rehabilitation, Yamagata Saisei Hospital, Yamagata, Japan, [6]Department of Occupational Therapy, Faculty of Health Sciences, Tokyo Metropolitan University, Tokyo, Japan, [7]Department of Occupational Therapy, Akita University Graduate School of Medicine, Akita, Japan, [8]Department of Physical Therapy, Faculty of Health Sciences, Tokyo Metropolitan University, Tokyo, Japan, [9]Maternity and Perinatal Care Center, Hokkaido University Hospital, Sapporo, Japan, [10]Department of Pediatrics, Akita University Graduate School of Medicine, Akita, Japan, [11]Department of Neonatology, Akita Red Cross Hospital, Akita, Japan, [12]Department of Occupational Therapy, Faculty of Health and Medical Science, Teikyo Heisei University, Tokyo, Japan, [13]Department of Physical Therapy, School of Rehabilitation Sciences, Seirei Christopher University, Hamamatsu, Japan, [14]Department of Sleep-Wake Disorders, National Institute of Mental Health, National Center of Neurology and Psychiatry, Tokyo, Japan, [15]Department of Psychiatry, Asai Hospital, Chiba, Japan

Previous studies suggest the importance of stable circadian environments for fetuses to achieve sound physiology and intrauterine development. This idea is also supported by epidemiological and animal studies, in which pregnant females exposed to repeated shifting of light–dark cycles had increased rates of reproductive abnormalities and adverse pregnancy outcomes. In response to such findings, artificial circadian environments with light–dark (LD) cycles have been introduced to NICUs to promote better physical development of preterm infants. Such LD cycles, however, may not be fully effective for preterm infants who are less than 30 weeks gestational age (WGA) since they are too premature to be adequately responsive to light. Instead, circadian rhythmicity of incubated preterm infants less than 30 WGA may be able to be developed through stimulation of the non-visual senses such as touch and sound.

KEYWORDS

designing artificial environments, NICUs, preterm infants, circadian rhythm, multisensory cares

Introduction

British author Aldous Huxley used his genius to predict future Neonatal Intensive Care Units (NICUs) in his 1932 fictional novel 'Brave New World' (Huxley, 1932). In the NICU he describes, human embryos are incubated in transparent bottles under a dim red light similar to the red colored sunshine we see when we close our eyelids outside on a summer afternoon.

The NICU described in his novel also has an artificially-controlled environment high in temperature and humidity, like in some tropical areas.

Huxley's description of temperature and humidity for the fetuses as being "tropical" matches well with the present settings for preterm infants in modern incubators. In Japan, preterm infants with a weight of <1,000 g are usually accommodated in incubators at a temperature of approximately 34–35°C and a humidity of 60–70% for their first week of life after birth. However, the lighting conditions he states – a constant dim red light – differs from the light–dark cycle which several circadian studies and the American Academy of Pediatrics (AAP) and American Colleges of Obstetrician and Gynecologists (ACOG) recommend for preterm infants in NICUs to encourage circadian entrainment (White, 2013; AAP Committee on Fetus and Newborn and ACOG Committee on Obstetric Practice, 2017). More recent studies have suggested that appropriate multisensory exposures to preterm infants in the NICU may also improve their postnatal development (Pineda et al., 2021; Schmidt Mellado et al., 2022). However, further research on achieving sound physiology and extrauterine development of preterm infants though NICU environment is still required. This review focuses on constructing possibly better NICU environments, particularly paying attention to circadian effects on the body growth of preterm infants.

Does biological clock influence fetal growth?

Among past literature, only two types of studies seem to report the possibility that biological clocks affect fetal body growth. One is an animal study in which rat fetal growth was measured in pregnant mother rats exposed to different lighting conditions. According to the study, the fetal weights in pregnant mother rats exposed to constant light were decreased compared to the fetal weights in pregnant rats exposed to light–dark (LD) cycles (Mendez et al., 2012). In LD conditions, the mother rats had circadian peaks of melatonin at night while the mothers in constant light lost their melatonin circadian rhythms. Moreover, restoration of maternal melatonin rhythmicity via night-time melatonin injection in mother rats exposed to constant light rescued their fetal growth restriction. The authors suggest that maternal circadian rhythm of melatonin leads to fetal circadian rhythm of corticosterone in the adrenal gland and that fetal corticosterone rhythm then contributes to fetal growth. The physiological mechanism linking fetal corticosterone rhythm and body growth, however, remains unclear.

The other type of study is clinical studies in which weight gains of human preterm infants were found to be better in LD conditions than in constant light or dark conditions (Watanabe et al., 2013; Morag and Ohlsson, 2016). Preterm infants are born before term and raised in incubators with a 24-h monitoring system, and an artificial ventilator or an ECMO (extra-corporeal membrane oxygenator), depending on their medical situation. The 24-h monitoring systems tell us that no circadian rhythms exist in the heart rate, respiratory rate, oxygen saturation or EEG of preterm infants (Glotzbach et al., 1995) in non-LD conditions. This is in contrast to human fetuses, who have been reported to have circadian rhythms in heart rates and fetal movements at around 20–22 weeks gestational age (WGA) (de Vries et al., 1987; Lunshof et al., 1998). Previous studies suggest that the circadian systems of fetuses are still premature and dependent on maternal circadian signals such as hormonal or nutritional signals, or on signals through maternal physical activity (Seron-Ferre et al., 2007; Watanabe et al., 2013). The researchers suggest a possibility that LD conditions support the immature biological clocks of preterm infants and premature animals by directly affecting their suprachiasmatic nuclei (SCN) through their photoreceptors, the intrinsically-photosensetive RGCs (ipRGCs) and/or rods, in their eyes, leading to stable circadian rhythms within the SCN (Sekaran et al., 2005; Sernagor, 2005; Schmidt et al., 2008; Van Gelder, 2008; Watanabe et al., 2013; Hazelhoff et al., 2021; Caval-Holme et al., 2022; Polese et al., 2022). Mouse studies have also revealed that the circadian systems of the SCN are disrupted by constant light at the cellular level (Ohta et al., 2005, 2006). The physiological mechanism linking LD conditions and body growth in preterm infants, however, remains unclear and further research in this area is still required.

If these animal and clinical studies present correct results, at least the following three hypotheses can be derived. First, the clinical studies suggest that the circadian mechanism for the growth of preterm infants does not need to depend on maternal signals. Since human preterm infants in incubators, who are completely separated from their mother, are able to achieve appropriate growth in an LD cycle, it can be assumed that maternal signals are not absolutely necessary for the appropriate growth of preterm infants.

Second, clinical studies also suggest that melatonin does not directly contribute to the circadian mechanism for the growth of preterm infants. In humans, melatonin does not have circadian rhythms at birth - at around 40 WGA - and do not exist until approximately 3 months of age (Kennaway, 2000; Rivkees, 2003). Although nighttime increase in melatonin concentration of breast milk in a circadian manner has been reported to occur 9 days after delivery and may support development of the circadian rhythms of infants (Illnerová et al., 1993), their circadian rhythms in sleep–wake only start to be observed after approximately 2 months of age (Rivkees, 2003). Since preterm infants do not have circadian rhythms of melatonin, circadian signals from external or internal factors, such as lighting, nutrition or other hormones must affect the biological clocks of preterm infants. Detection of these, however, is difficult to achieve, as it would require blood samples to be taken from infants every three to 4 h for examination, which is ethically unacceptable (Dupont-Thibodeau and Janvier, 2016).

Third, the animal study with melatonin injections into pregnant rats (Mendez et al., 2012) suggests that the SCN or the organ biological clocks, which modulate circadian phases through melatonin receptors, contribute to the circadian mechanism for the body growth of preterm infants, although melatonin itself does not seem to directly affect the body growth of preterm infants (Gombert and Codoñer-Franch, 2021). To date, two membrane-bound melatonin receptors have been identified and characterized - MT1 and MT2. MT1 receptors are expressed in the brain, cardiovascular system (including peripheral blood vessels, aorta and heart), immune system, testes, ovary, skin, liver, kidney, adrenal cortex, placenta, breast, retina, pancreas and spleen (Dubocovich and Markowska, 2005; Slominski et al., 2005; Fischer et al., 2008; Pandi-Perumal et al., 2008; Slominski et al., 2008). In the brain, the MT1 receptor is predominantly found in the SCN, hypothalamus, cerebellum, hippocampus, substantia nigra and ventral tegmental area (Pandi-Perumal et al., 2008). MT2 has been found in the brain (SCN, hypothalamus and pituitary), retina, immune system,

blood vessels, testes, kidney, gastrointestinal tract, mammary glands, adipose tissue, and the skin (Reppert et al., 1995; Roca et al., 1996; Dubocovich and Markowska, 2005; Slominski et al., 2005).

These three hypotheses lead us to a possible conclusion that the retina, the SCN, and the adrenal gland, each of which can be affected by both light and melatonin, may each possibly be part of the pathway for the circadian mechanism for the growth of preterm infants.

Regarding the retina and SCN, the retina has a wide range of efferent visual and non-visual pathways to the brain. The visual pathways, which contribute to both image formation and light–dark detection, are based on the nerve innervations from the rods and cones in the retina. The visual pathways have direct projections to the dorsal lateral geniculate nucleus (dLGN) and superior colliculus (SC). Non-visual pathways, which contribute to only light–dark detection, are composed of intrinsically-photosensetive RGCs (ipRGCs). The non-visual pathways have direct projections to the suprachiasmatic nucleus (SCN), supraoptic nucleus (SON), subparaventricular zone (SPZ), ventral lateral preoptic area (VLPO), lateral hypothalamic area (LH), anterior hypothalamus (AH), medial amygdaloid nucleus (MA), habenula (Hb), bed nucleus of the stria terminalis (BST), dorsal lateral geniculate nucleus (dLGN), ventral lateral geniculate nucleus (vLGN), intergeniculate leaflet (IGL), periaqueductal gray (PAG), olivary pretectal nucleus core (OPN), and superior colliculus (SC). Via the SCN, the non-visual pathways also have indirect projections to the paraventricular nucleus (PVN), dorsomedial hypothalamus (DMH), locus coeruleus (LC), ventral tegmental area (VTA), and septal area (Sept) (Dacey et al., 2005; Hattar et al., 2006; Brown et al., 2010; Noseda et al., 2010; Milosavljevic, 2019; Aranda and Schmidt, 2021).

No direct efferent pathway from the retina to the visual or frontal cortex has been anatomically detected (Gaillard et al., 2013). A human EEG study, however, using light stimulus on blind people, in whom no visual pathway but only the non-visual pathway is supposed to function, suggests that the non-visual pathway may have possible projections to the visual cortex (Vandewalle et al., 2018). A mouse study also indicates that the non-visual pathway can affect cortical synaptogenesis at early developmental stages via the SON and PVN by light-dependent oxytocin secretion (Hu et al., 2022). The ipRGCs-dependent non-visual pathway contributes to various physiological functions such as entrainment of circadian rhythms (Panda et al., 2002; Ruby et al., 2002), sleep–wake regulations (Lupi et al., 2008), pupil constriction (Hattar et al., 2003; Watanabe et al., 2013; Adhikari et al., 2015; Ikeda et al., 2015), alertness (Milosavljevic, 2019), mood (LeGates et al., 2012; Fernandez et al., 2018), learning (Fernandez et al., 2018), and visual perception (Aranda and Schmidt, 2021). In particular, in terms of circadian rhythms and sleep–wake regulation, the SCN directly controls circadian rhythms and the IGL also indirectly entrains circadian rhythms (Hatori and Panda, 2010; Aranda and Schmidt, 2021). In addition, the lateral and posterior hypothalamus, the VLPO, the Hb, and the SPZ are believed to mediate the effects of light on the hypothalamic regulation of sleep, behavior, and other physiological functions (Hatori and Panda, 2010; Aranda and Schmidt, 2021). These facts imply that the retina and/or SCN may contribute to the circadian mechanisms for the body growth of preterm infants.

The adrenal cortex is another candidate partial pathway since light information is conveyed from the SCN to the adrenal gland via the SCN-sympathetic nervous system (Ishida et al., 2005) and MT1 receptors are also detected in the adrenal cortex in adult animals (Torres-Farfan et al., 2003; Richter et al., 2008). Like the development of melatonin circadian rhythms, however, no clear cortisol circadian rhythms are detected in humans until approximately 1 month of age (Ivars et al., 2015, 2017), suggesting that cortisol may not contribute to the circadian mechanism for the body growth of preterm infants until that time.

Overall, the above suggests that we might be able to improve the body growth of preterm infants by providing the SCN and retina with artificial circadian signals, such as a light–dark (LD) cycle, or nighttime-injected melatonin.

Discussion

Is a light–dark cycle beneficial for the body growth of preterm infants? – from an implication of intrauterine circadian effects on fetal growth

The concept of a stable circadian uterine environment having positive effects on fetal development is also supported by clinical studies in which pregnant females exposed to repeated shifting of their LD cycle had increased rates of reproductive abnormalities and adverse pregnancy outcomes such as preterm delivery and particularly low birth weight of offspring. Several epidemiological studies on humans have identified associations between shift work or repeated travel across time zones and reduced fertility (Bisanti et al., 1996) as well as negative pregnancy outcomes, including increased incidence of low birth weight, preterm birth and miscarriage (Cone et al., 1998; Aspholm et al., 1999; Knutsson, 2003). However, whether these adverse outcomes are due to circadian dysregulation or some other lifestyle factor associated with shift work has not been clearly determined.

Also, the study mentioned earlier in which pregnant mother rats were exposed to different lighting conditions reported that exposure of pregnant rats to constant light, which disrupts the circadian environment for fetuses, induced intrauterine growth restriction and also lowered corticosterone production in fetal adrenal glands (Mendez et al., 2012). Other studies using rodent models indicated that repeated shifting of the light–dark cycle of pregnant rats and mice increased rates of miscarriage and induced hyperleptinemia and hyperinsulinemia in offspring lasting into adulthood (Varcoe et al., 2011; Summa et al., 2012). Shifts in rats' LD cycle are known to transiently disrupt normal phase relationships between the SCN and peripheral biological clocks (Yamazaki et al., 2000), thus desynchronized circadian rhythms, either between central and peripheral maternal tissues or between maternal and fetal tissues (or both), may in part contribute to the adverse effects of chronic environmentally-mediated circadian disruption on pregnancy outcomes.

When should a light–dark cycle be started for preterm infants?

In theory, an LD cycle might best be introduced to preterm infants at around 26–30 WGA, when the eyes of preterm infants can start to perceive light. Robinson and Fielder (1990) reported that preterm

infants can respond to light from 30 weeks postmenstrual age (WPA), equivalent to 30 WGA, based on measurements they had made of the pupillary light reflex (PLR). Another study by Hao and Rivkees (1999) using a baboon model indicated that the SCN in the baboon fetus of an age corresponding to human 24 weeks conceptional age (WCA), approximately equivalent to 26 WGA in the human fetus, was already responsive to light stimuli. The data suggest that preterm infants might start to respond to light from around 26–30 WGA.

In practice, however, an LD cycle would best be introduced to preterm infants just after birth without considering when preterm infants start to perceive light. The reason for this is the large individual difference in when preterm infants start to respond to light. In a study of the development of PLR, Robinson and Fielder reported that the earliest that some preterm infants start to respond to light is at 30 WGA, while others start to respond to light as late as 34 WGA (Robinson and Fielder, 1990), indicating that the onset of the PLR could vary up to 5 weeks between individual preterm infants. It is quite time-consuming and stress inducing to examine preterm infants' PLR every week to confirm whether the infants have started to respond to light. Instead, if the NICU is always set to an LD cycle, each preterm infant will automatically entrain their biological clock to the LD cycle as their biological clocks start to respond to light without any need for regular PLR checks.

Strict light control of LD cycles in NICUs, however, might not provide the best benefit for preterm infants of <30 WGA being intensively treated for serious medical conditions just after birth. Since they are in a critical physiological state and have minimal sensitivity to light because of the immaturity of their photoreceptors, a constantly lit environment would allow easier performance of intensive medical treatments and cares, operation of medical equipment and observation of the infants' physiological condition and behavior without any major adverse effect on the rhythm of their biological clock.

What type of light- dark cycle should be provided for preterm infants?

To design appropriate lighting conditions for preterm infants in NICUs, we have to take into account at least the following three factors: duration, light intensity, and light wavelengths of light/dark periods.

What durations of light/dark periods are appropriate for NICUs?

Previous studies suggest that a 12 L:12D LD cycle would be safe as a NICU lighting cycle. However, no clinical study in human neonatal physiology has investigated an optimum ratio of light/dark period duration for NICUs. Adult studies, however, have demonstrated that humans maintain stable circadian rhythms of behavior and hormonal secretions by adapting to different day lengths (photoperiods) between short day (8 h light period: 16 h dark period (8 L:16D)) and long day (14 L,10D). Compared to the long-day photoperiod, the short-day photoperiod provides us with longer sleep durations, longer nocturnal periods of low rectal temperature, longer nocturnal periods of active melatonin secretion, and higher levels of prolactin and cortisol secretion (Thomas et al., 2002).

Animal studies have also examined the effects of photoperiod during early infancy on development of circadian clocks and other physiological parameters. Ciarleglio et al. (2011) found that mice reared in long days (16 L:8D) exhibited a shorter free-running period of locomotor activity rhythms compared to mice reared in short days (8 L:16D). This is consistent with their results from Per1, a clock gene expression in the SCN, in which perinatal exposure to long days (16 L:8D) induced a narrower Per1 expression waveform and shorter rhythm period compared to short-day (8 L:16D) exposure. Using the same animal model, Ohta and coworkers demonstrated that perinatal exposure to constant light (24 L:0D) leads mice to have disrupted Per1 expression waveform in the developing SCN with desynchronization of the circadian rhythms of individual clock neurons within the SCN, but without reduction in the ability of single neurons to generate circadian rhythms (Ohta et al., 2005, 2006). Another group found that mice reared in constant light (24 L:0D) showed a higher locomotor activity rhythm amplitude and lower levels of vasoactive intestinal peptide (VIP) and arginine vasopressin (AVP) in the SCN compared to mice reared in constant darkness (0 L:24D) or 12 L:12D LD cycles (Smith and Canal, 2009). These results suggest that postnatal light experiences affect the SCN neuronal network that regulates seasonal adaptation by affecting the clock functions and output of SCN neurons. Recently, the same group found that mice raised in constant light showed stronger and shorter-period circadian rhythms of body temperature compared to mice raised in constant darkness and also displayed a greater tendency for depression-like behavior compared to 12 L:12D LD cycle-raised mice (Coleman et al., 2016). Moreover, compared to 12 L:12D LD cycle-raised mice, both constant-light and constant-dark-raised mice showed a decreased glucocorticoid receptor expression in the hippocampus and increased plasma corticosterone concentration at the onset of night. This demonstrates a possibility that the postnatal light environment induces long-term effects on the hypothalamic–pituitary–adrenal axis and circadian system leading to a depressive phenotype in adulthood.

These clinical and animal studies suggest that a 12 L:12D LD cycle would be safe as a NICU lighting cycle for the promotion of sleep and psychological development of preterm infants.

What light intensities are appropriate for light/dark cycles in NICUs?

Lighting recommendations by the American Academy of Pediatrics (AAP) and American College of Obstetricians and Gynecologists (ACOG) suggest that the light intensity of NICU illumination should range between 10 and 600 lux to allow continuous assessment of infants, as well as examination of skin color and perfusion (White, 2013; AAP Committee on Fetus and Newborn and ACOG Committee on Obstetric Practice, 2017). The Australian Health Infrastructure Alliance (AHIA) recommends an ambient light range of 100–600 lux [The Australian Health Infrastructure Alliance (AHIA), 2014]. Villalba et al. (2018) also stated that when using individual procedure lights, which are capable of reaching 2000 lux, care should be taken to avoid exposing the neonate's eyes to high levels of light.

However, none of these guidelines specify optimal intensity ranges for varying gestational ages (Best et al., 2018). For light intensity during night, studies demonstrated that adult humans are responsive to a light intensity of approximately 30 lux and above when assessed by melatonin phase delay response to light and also responsive to a light intensity of approximately 50 lux and above when assessed by the acute melatonin suppressive effects of light (the phase change of melatonin circadian rhythm and suppression of plasma melatonin level have been used as the gold standard to evaluate the effects of light

on biological clock) (St. Hilaire et al., 2012). The data indicate that human adults biologically recognize brightness at night when light intensity is 30–50 lux or above. The adult data suggest that the light intensity in NICUs at night should be lower than 30 lux, which preterm infants would not biologically perceive as brightness. The light sensitivity of preterm infants at each gestational age, however, has not been investigated. The light sensitivity of preterm infants can vary depending on their developmental stage. According to our own preterm study (Watanabe et al., 2013), 5 lux does not induce pupillary light reflex in preterm infants between 30 and 38 WGA, suggesting a light intensity of <5 lux, which was recommended for night NICUs by the American Academy of Pediatrics (AAP) and American College of Obstetricians and Gynecologists (ACOG), would be safe for preterm infants of all gestational ages in a NICU lighting environment (White, 2013; AAP Committee on Fetus and Newborn and ACOG Committee on Obstetric Practice, 2017).

For light intensity during daytime, an intensity between 30 and 440 lux would be safe for a NICU lighting environment. As earlier mentioned, adult data on phase change of daily melatonin rhythm suggest that preterm infants are likely to perceive daytime brightness at a light intensity of ≥30 lux. A safe brightness level during daytime would be 440 lux since a US multicenter study demonstrated that no clinical damage was detected in the eyes of preterm infants who were raised in constant light at an average light intensity of 447 lux (Reynolds et al., 1998).

What light wave lengths are appropriate for the light/dark periods in NICUs?

Previous clinical studies indicate that the optimum light wavelengths for light/dark periods depend on the developmental stages of the preterm infants since the three types of visual photoreceptors in the retina (ipRGCs, rods, and cones) each start to function at a different time somewhere between approximately 26 WGA and 1 month after birth (where birth occurs at 40 WGA). Studies of the pupillary light reflex (PLR) of preterm infants revealed that only ipRGCs provide visual perception at the early stages of human development – at approximately 30 WGA – and contributes to the detection of changes in environmental light radiance (Robinson and Fielder, 1990; Hanita et al., 2009; Watanabe et al., 2013). Rods start to function at around 34 WGA and provides image detection (Figure 1; Watanabe et al., 2013; Ikeda et al., 2015). Cones begin to function 1 month after birth (where birth occurs at 40 WGA) (Field et al., 1982; Teller, 1997) and perform image and color detection.

Adult studies have clarified the properties of the three types of photoreceptors and indicate that ipRGCs detect light of wave lengths up to 580 nm (maximum light sensitivity: 480 nm), rods detect wave lengths up to 610 nm (maximum light sensitivity: 500 nm), and cones detect wave lengths up to 690 nm (maximum light sensitivities of S, M, and L cones: 420, 530, and 560 nm, respectively) (Figure 2; Zaidi et al., 2007). A PLR study of preterm infants of 38 WGA, the age at which most preterm infants are discharged from hospital, demonstrated that they did not respond to 635 nm light but responded to 470 nm (Ikeda et al., 2015). This indicates that cones do not function at that age since 635 nm falls within the wave-length range normally detected by cones. However, since the preterm infants could respond to 470 nm light, this also indicates they are very likely to perceive light through ipRGCs and/or rods, which detect wave lengths up to 580 nm and 610 nm, respectively. Since ipRGCs starts to function earlier than rods and cones and convey light information well enough to control the SCN, the light wave length of <580 nm might be best for use in the design of NICU light–dark cycles.

How can we entrain the biological clocks of young preterm infants who are not able to perceive light? - touch and sound may be effective ways of entraining preterms' biological clocks

Since preterm infants are still in the process of developing the visual system and biological clock, further research should be carefully explored to understand their light sensitivity and entrainment (Hazelhoff et al., 2021; Polese et al., 2022). Light is the most powerful stimuli for the SCN, the biological clock, to synchronize to the environment. However, in the absence of light (i.e., constant darkness), the SCN of human adults can be synchronized by tactile and auditory cues. The physiological conditions of human adults in constant darkness are quite similar to the conditions of preterm infants less than 30 WGA, who do not yet fully respond to light. Human fetuses start to develop their tactile and auditory perceptions at around 16 and 28 WGA, respectively. Their tactile perception starts to function earlier than light perception and their auditory perception starts at approximately the same developmental age as light perception (Humphrey, 1964; Birnholz and Benacerraf, 1983; Lary et al., 1985; Schaal et al., 2004; Table 1).

Despite few dedicated human neonate trials on the influence of tactile contact on the circadian clock, tactile stimulation has been medically performed on preterm infants in NICUs through massage therapy since the 1980s (Figure 3; Field et al., 2006; Badr et al., 2015). Randomized controlled trials (RCTs) on the effects of massage therapy in preterm infants confirm improved weight gain and shortened length of hospital stay (Badr et al., 2015; Niemi, 2017). Previous studies have reported that tactile stimulation leads to higher salivary concentration of both norepinephrine and epinephrine and an increase in the alert state (Kuhn et al., 1991; White-traut et al., 1997), suggesting that tactile stimuli may indeed contribute to the formation of circadian sleep/wake rhythms with more arousal during wake-time period of preterm infants of around 33–34 WGA. In a study of term infants equivalent to 40–42 WGA, massage therapy was reported to enhance their circadian rest-activity rhythms and elevated their nighttime excretion of urinary 6-sulphatoxymelatonin, the melatonin metabolite (Ferber et al., 2002). Massage therapy has also been reported to decrease infant crying and salivary cortisol, suggesting that tactile stimuli may also contribute to reducing psychophysiological stress in preterm infants. This is consistent with an animal study in which elevated cortisol levels caused by maternal deprivation were reduced in response to tactile stimulation (Pauk et al., 1986).

One means of improving the efficacy of massage therapy is to perform it with the infant in intermittent kangaroo position. It has been reported that massage therapy in intermittent kangaroo position leads to greater daily weight gain compared to massage therapy in incubators (Aldana Acosta et al., 2019). Kangaroo care is well known for decreasing mortality among preterm infants and improving rates of exclusive breast feeding in both developed and developing countries (Boundy et al., 2016). Tactile stimulation provided by kangaroo care, as well as continuous interaction with the parent, may also contribute

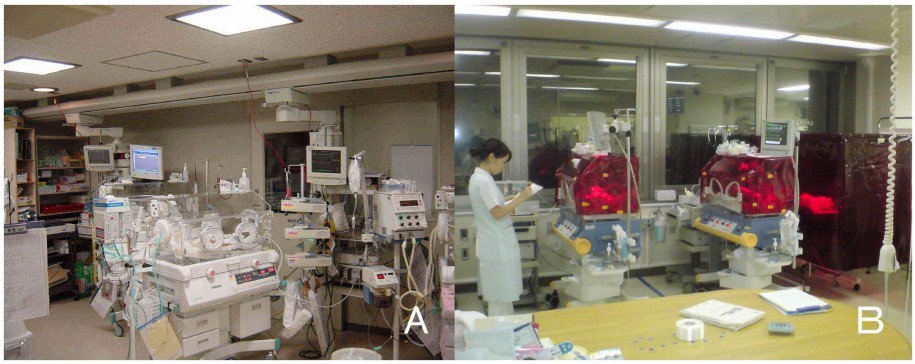

FIGURE 1
Bed-site illumination before and after introduction of a monochromatic light red filter. **(A)** In a former NICU, continuous lighting was selected to allow instant reaction to emergency situations such as respiratory and cardiovascular dysfunctions, brain hemorriage, and infections. The background lighting was generally between 50 and 600 lux. **(B)** Artificial night was achieved by covering the isolette or crib every night with a light filter, which specifically cuts the wavelength of light that the ipRGCs and rods of preterm infants detect. During daytime, the light filter was removed from the isolette (Watanabe et al., 2013).

to the organization of sleep–wake cyclicity and better modulation of the arousal system (Feldman et al., 2002). There is also a possibility that parental circadian body temperature supports the formation of the infant's own circadian rhythms.

Auditory stimuli can also have a circadian synchronization effect on preterm infants. Auditory stimuli are known to influence the circadian rhythms of a variety of animals. For instance, the behavioral rhythms of the house sparrow (*Passer domesticus*) can be entrained by conspecific bird songs (Menaker and Eskin, 1966) and even by white noise (Reebs, 1989). Mice also show circadian responses to auditory cues, while other rodents like rats and hamsters do not (Davidson and Menaker, 2003). The efficacy of auditory stimuli entrainment thus varies among species. In human adults, presentation of an auditory stimulus at nighttime can phase shift circadian rhythms of melatonin and core body temperature (Goel, 2005), as well as synchronize activity rhythms in constant darkness but not in LD conditions (Davidson and Menaker, 2003). Preterm infants whose eyes are still immature (< 30 WGA) do not yet have matured ability to perceive light and therefore experience near-constant darkness. In the absence of visual cues, it is possible that such infants' circadian systems can instead influenced by auditory stimuli.

Regarding sense of smell, no olfactory stimuli have been reported to phase-shift human behavioral or hormonal circadian rhythms. In animals, however, olfactory stimuli are known to affect the circadian clocks of a number of both invertebrate and vertebrate species. A study of social interaction effects on circadian rhythms suggests that olfactory signals can function as synchronizers in fruit flies (*Drosophila melanogaster*). Olfactory cues (possibly pheromonal) have also been implicated as synchronizers in a mammalian species, the degu (Octogon degus), a diurnal rodent. In addition, a mammary pheromone, aldehyde 2-methylbut-2-enal (2 MB2), was reported to act as a maternal olfactory cue to synchronize the circadian clock of artificially raised European newborn rabbits (Montúfar-Chaveznava et al., 2013).

Among the above mentioned three social cues of touch, sound, and smell, both tactile and auditory stimuli can phase-shift circadian clocks of preterm infants in normal lighting conditions: a light–dark cycle. Since tactile sensitivity is the first of the human senses to appear (at 16 WGA), appropriate tactile

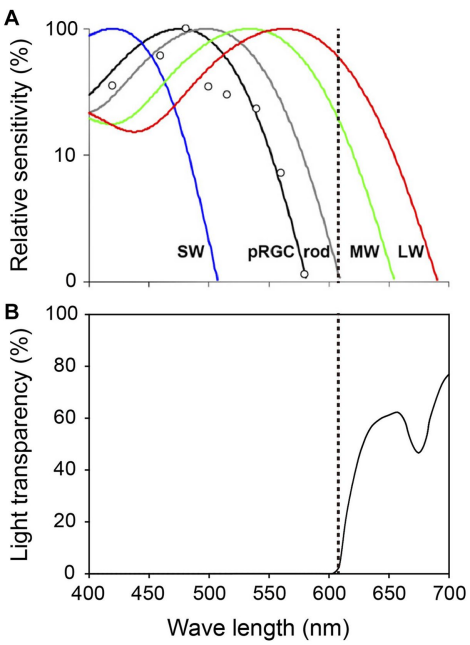

FIGURE 2
Spectral properties of human photoreceptors and spectral transmission characteristics of the red filter. **(A)** Spectral sensitivity of rods, cones and ipRGCs measured by pupil responses to light. Maximum light sensitivity wavelengths of human rods (R), S cones (SW), M cones (MW) and L cones (LW) are approximately 500 nm, 420 nm, 530 nm and 560 nm, respectively. The ipRGCs (depicted as pRGCs in the figure) exhibit their peak sensitivity at around 480 nm. The dashed line on the figure indicates 610 nanometers. Figure cited from Zaidi et al. (2007). White circles indicate the pupil responses to light in a blind woman. **(B)** Spectral transmission characteristics of the red filter in Figure 1B. Note that the red filter cut light of wave lengths <610 nm perceived by ipRGCs and rods, which function in preterm infants, while allowing wave lengths >610 nm perceived by adult MW and LW to pass through (Watanabe et al., 2013).

TABLE 1 Developmental time line of human sensory systems and circadian entrainment.

Weeks gestational age (WGA)	Sensory systems	Circadian entrainment
16	Tactile perception[a]	
26	Possible SCN light responsiveness[b]	
28	Auditory perception[c]	
29	Olfactory perception[d]	
30	Pupil light reflex[e]	
33–42		Possible tactile entrainment[f]
38–43		Possible light entrainment[g]

a. Humphrey, 1964; b. Hao and Rivkees, 1999; c. Birnholz and Benacerraf, 1983, Lary et al., 1985; d. Schaal et al., 2004; e. Robinson and Fielder, 1990, f. Kuhn et al., 1991, White-traut et al., 1997, Ferber et al., 2002; g. Rivkees et al., 2004, Watanabe et al., 2013.

stimuli may be able to act as signals to synchronize the circadian clocks of preterm infants before they begin to perceive light at around 26–30 WGA. Auditory stimuli may also potentially support the stability of circadian rhythmicity once infants become sensitive to sound at approximately 28 WGA.

Conclusion and near future goals

Preterm infants of approximately 22 WGA, the earliest age at which artificial ventilators are able to be applied, can be saved with medical treatments in Japan. Past literature suggests that the circadian rhythms of preterm infants of >26–30 WGA can be safely and effectively supported by LD cycles of 12 L:12D at a light intensity of >50 lux during daytime and < 5 lux during nighttime with wavelengths of up to 580 nm, which the ipRGCs of preterm infants, the first functioning photoreceptors in life, can detect.

The circadian rhythms of preterm infants of <30 WGA, however, are not likely to be fully assisted by LD cycles since their visual photoreceptors are still premature and do not yet function effectively. At such an age, tactile stimuli such as massage therapy in a circadian manner might be an effective way to entrain the circadian rhythms of preterm infants, leading to better body growth, since human tactile perception starts to function at 16 WGA, far before 26 WGA when ipRGCs start to function. In addition, auditory stimuli, such as parents' voices may also entrain preterm infants' circadian rhythms since auditory stimuli has been found to affect human circadian clocks in constant darkness, which preterm infants of <30 WGA experience due to immature visual function.

Moreover, a multisensory approach such as the combination of touch, sound and smell might be an important strategy for generating circadian rhythmicity in preterm infants more effectively in the future (Ferber et al., 2002; Neel et al., 2019). Animal neonate studies using rodents such as hamsters, mice and rats, clearly demonstrated that maternal multisensory stimuli such as touch, sound, smell and feeding phase-shifts neonatal circadian rhythms of behavior, hormones, and clock gene expressions. In one such study, newborn rats of mothers kept in an LD cycle were blinded immediately after birth and reared by foster mothers under either LD (LD blind pups) or a reversed light–dark (DL) cycle (DL blind pups). At postnatal day 6, significant phase differences were observed in the circadian gene expression rhythms of the SCN between the LD and DL blind pups, indicating that the two different maternal circadian behavioral patterns with multisensory stimuli in antiphase affected the circadian rhythms of the two different groups of blind pups, respectively, (Ohta et al., 2002). Recent studies on preterm and term infants have also suggested that not only circadian synchronization (entrainment) but also general brain functional connectivity can be affected by multisensory systems when they are exposed to various stimuli in extrauterine environments (Gatti et al., 2012; De Asis-Cruz et al., 2020; Polese et al., 2021; Pineda et al., 2021; Schmidt Mellado et al., 2022).

FIGURE 3
Preterm infant being massaged. Figure cited from Imura et al. (2014).

If, using circadian science, clinicians and researchers are able to redesign the presently employed protocol of kangaroo care, which is composed of parental touch, voice, and smell, the resulting modified form of kangaroo care may be a strong synchronizer for the circadian clock of preterm infants.

Author contributions

TA, RF, MK, K-iT, HG, MH, SO, and HO conceived of the review. TA, RF, MK, HS, YY, K-iT, HG, YS, HAd, HAr, MH, SO, and HO wrote the paper. All authors contributed to the article and approved the submitted version.

Funding

This work was supported by Grants-in-Aid for Scientific Research from the Ministry of Education, Culture, Sports,

Science and Technology (to TA, RF, MK, YY, K-iT, HG, HAd, HAr, SO, and HO), from the Japan Science and Technology Agency (to HO), and also from the Uehara Memorial Foundation (to HO).

Acknowledgments

We thank members of the Japan Developmental Care study group for helpful discussions and comments on the manuscript. We would also like to acknowledge the excellent mentoring by Professor Hiroshi Nishida, who has supported the clinical and research activities of the Japan Developmental Care study group.

Conflict of interest

The authors declare that the research was conducted in the absence of any commercial or financial relationships that could be construed as a potential conflict of interest.

Publisher's note

References

AAP Committee on Fetus and Newborn and ACOG Committee on Obstetric Practice (2017). *Guidelines for perinatal care, 8th*. Itasca: AAP Books.

Adhikari, P., Pearson, C. A., Anderson, A. M., Zele, A. J., and Feigl, B. (2015). Effect of age and refractive error on the melanopsin mediated post-illumination pupil response (PIPR). *Sci. Rep.* 5:17610. doi: 10.1038/srep17610

The Australian Health Infrastructure Alliance (AHIA) (2014). *Australasian health facility guidelines, part B-health facility briefing and planning, 390 – Intensive care-neonatal care/special care nursery*. Adelaide, Australia.

Aldana Acosta, A. C., Tessier, R., Charpak, N., and Tarabulsy, G. (2019). Randomised controlled trial on the impact of kinesthetic stimulation on early somatic growth of preterm infants in kangaroo position. *Acta Paediatr.* 108, 1230–1236. doi: 10.1111/apa.14675

Aranda, M. L., and Schmidt, T. M. (2021). Diversity of intrinsically photosensitive retinal ganglion cells: circuits and functions. *Cell. Mol. Life Sci.* 78, 889–907. doi: 10.1007/s00018-020-03641-5

Aspholm, R., Lindbohm, M. L., Paakkulainen, H., Taskinen, H., Nurminen, T., and Tiitinen, A. (1999). Spontaneous abortions among Finnish flight attendants. *J. Occup. Environ. Med.* 41, 486–491. doi: 10.1097/00043764-199906000-00015

Badr, L. K., Abdallah, B., and Kahale, L. (2015). A meta-analysis of preterm infant massage: an ancient practice with contemporary applications. *MCN Am. J. Matern. Child Nurs.* 40, 344–358. doi: 10.1097/NMC.0000000000000177

Best, K., Bogossian, F., and New, K. (2018). Sensory exposure of neonates in single-room environments (SENSE): an observational study of light. *Arch. Dis. Child. Fetal Neonatal Ed.* 103, F436–F440. doi: 10.1136/archdischild-2017-312977

Birnholz, J. C., and Benacerraf, B. R. (1983). The development of human fetal hearing. *Science* 222, 516–518. doi: 10.1126/science.6623091

Bisanti, L., Olsen, J., Basso, O., Thonneau, P., and Karmaus, W. (1996). Shift work and subfecundity: a European multicenter study. European study group on infertility and subfecundity. *J. Occup. Environ. Med.* 38, 352–358. doi: 10.1097/00043764-199604000-00012

Boundy, E. O., Dastjerdi, R., Spiegelman, D., Fawzi, W. W., Missmer, S. A., Lieberman, E., et al. (2016). Kangaroo mother care and neonatal outcomes: a meta-analysis. *Pediatrics* 137:e20152238. doi: 10.1542/peds.2015-2238

Brown, T. M., Gias, C., Hatori, M., Keding, S. R., Semo, M., Coffey, P. J., et al. (2010). Melanopsin contributions to irradiance coding in the thalamo-cortical visual system. *PLoS Biol.* 8:e1000558. doi: 10.1371/journal.pbio.1000558

Caval-Holme, F. S., Aranda, M. L., Chen, A. Q., Tiriac, A., Zhang, Y., Smith, B., et al. (2022). The retinal basis of light aversion in neonatal mice. *J. Neurosci.* 42, 4101–4115. doi: 10.1523/JNEUROSCI.0151-22.2022

Ciarleglio, C. M., Axley, J. C., Strauss, B. R., Gamble, K. L., and McMahon, D. G. (2011). Perinatal photoperiod imprints the circadian clock. *Nat. Neurosci.* 14, 25–27. doi: 10.1038/nn.2699

Coleman, G., Gigg, J., and Canal, M. M. (2016). Postnatal light alters hypothalamic-pituitary-adrenal axis function and induces a depressive-like phenotype in adult mice. *Eur. J. Neurosci.* 44, 2807–2817. doi: 10.1111/ejn.13388

Cone, J. E., Vaughan, L. M., Huete, A., and Samuels, S. J. (1998). Reproductive health outcomes among female flight attendants: an exploratory study. *J. Occup. Environ. Med.* 40, 210–216. doi: 10.1097/00043764-199803000-00002

Dacey, D. M., Liao, H. W., Peterson, B. B., Robinson, F. R., Smith, V. C., Pokorny, J., et al. (2005). Melanopsin-expressing ganglion cells in primate retina signal colour and irradiance and project to the LGN. *Nature* 433, 749–754. doi: 10.1038/nature03387

Davidson, A. J., and Menaker, M. (2003). Birds of a feather clock together--sometimes: social synchronization of circadian rhythms. *Curr. Opin. Neurobiol.* 13, 765–769. doi: 10.1016/j.conb.2003.10.011

De Asis-Cruz, J., Kapse, K., Basu, S. K., Said, M., Scheinost, D., Murnick, J., et al. (2020). Functional brain connectivity in ex utero premature infants compared to in utero fetuses. *NeuroImage* 219:117043. doi: 10.1016/j.neuroimage.2020.117043

de Vries, J. I., Visser, G. H., Mulder, E. J., and Prechtl, H. F. (1987). Diurnal and other variations in fetal movement and heart rate patterns at 20-22 weeks. *Early Hum. Dev.* 15, 333–348. doi: 10.1016/0378-3782(87)90029-6

Dubocovich, M. L., and Markowska, M. (2005). Functional MT1 and MT2 melatonin receptors in mammals. *Endocrine* 27, 101–110. doi: 10.1385/ENDO:27:2:101

Dupont-Thibodeau, A., and Janvier, A. (2016). "When do we become a person and why should it matter to pediatricians?" in *Ethical dilemmas for critically III babies*. eds. E. Verhagen and A. Janvier (Dordrecht: Springer), 13–24.

Feldman, R., Weller, A., Sirota, L., and Eidelman, A. I. (2002). Skin-to-skin contact (Kangaroo care) promotes self-regulation in premature infants: sleep-wake cyclicity, arousal modulation, and sustained exploration. *Dev. Psychol.* 38, 194–207. doi: 10.1037/0012-1649.38.2.194

Ferber, S. G., Laudon, M., Kuint, J., Weller, A., and Zisapel, N. (2002). Massage therapy by mothers enhances the adjustment of circadian rhythms to the nocturnal period in full-term infants. *J. Dev. Behav. Pediatr.* 23, 410–415. doi: 10.1097/00004703-200212000-00003

Fernandez, D. C., Fogerson, P. M., Lazzerini Ospri, L., Thomsen, M. B., Layne, R. M., Severin, D., et al. (2018). Light affects mood and learning through distinct retina-brain pathways. *Cells* 175, 71–84.e18. doi: 10.1016/j.cell.2018.08.004

Field, T., Diego, M. A., Hernandez-Reif, M., Deeds, O., and Figuereido, B. (2006). Moderate versus light pressure massage therapy leads to greater weight gain in preterm infants. *Infant Behav. Dev.* 29, 574–578. doi: 10.1016/j.infbeh.2006.07.011

Field, T. M., Woodson, R., Greenberg, R., and Cohen, D. (1982). Discrimination and imitation of facial expression by neonates. *Science* 218, 179–181. doi: 10.1126/science.7123230

Fischer, T. W., Slominski, A., Tobin, D. J., and Paus, R. (2008). Melatonin and the hair follicle. *J. Pineal Res.* 14, 1–15. doi: 10.1111/j.1600-079X.2007.00512.x

Gaillard, F., Karten, H. J., and Sauvé, Y. (2013). Retinorecipient areas in the diurnal murine rodent *Arvicanthis niloticus*: a disproportionally large superior colliculus. *J. Comp. Neurol.* 521:Spc1. doi: 10.1002/cne.23330

Gatti, M. G., Becucci, E., Fargnoli, F., Fagioli, M., Ådén, U., and Buonocore, G. (2012). Functional maturation of neocortex: a base of viability. *J. Matern. Fetal Neonatal Med.* 25, 101–103. doi: 10.3109/14767058.2012.664351

Glotzbach, S. F., Edgar, D. M., and Ariagno, R. L. (1995). Biological rhythmicity in preterm infants prior to discharge from neonatal intensive care. *Pediatrics* 95, 231–237. doi: 10.1542/peds.95.2.231

Goel, N. (2005). Late-night presentation of an auditory stimulus phase delays human circadian rhythms. *Am. J. Physiol. Regul. Integr. Comp. Physiol.* 289, R209–16. doi: 10.1152/ajpregu.00754.2004

Gombert, M., and Codoñer-Franch, P. (2021). Melatonin in early nutrition: long-term effects on cardiovascular system. *Int. J. Mol. Sci.* 22:6809. doi: 10.3390/ijms22136809

Hanita, T., Ohta, H., Matsuda, T., and Miyazawa, H. (2009). Monitoring preterm infants' vision development with light-only melanopsin is functional. *J. Pediatr.* 155, 596–596.e1. doi: 10.1016/j.jpeds.2009.03.005

Hao, H., and Rivkees, S. A. (1999). The biological clock of very premature primate infants is responsive to light. *Proc. Natl. Acad. Sci. U. S. A.* 96, 2426–2429. doi: 10.1073/pnas.96.5.2426

Hatori, M., and Panda, S. (2010). The emerging roles of melanopsin in behavioral adaptation to light. *Trends Mol. Med.* 16, 435–446. doi: 10.1016/j.molmed.2010.07.005

Hattar, S., Kumar, M., Park, A., Tong, P., Tung, J., Yau, K. W., et al. (2006). Central projections of melanopsin-expressing retinal ganglion cells in the mouse. *J. Comp. Neurol.* 497, 326–349. doi: 10.1002/cne.20970

Hattar, S., Lucas, R. J., Mrosovsky, N., Thompson, S., Douglas, R. H., Hankins, M. W., et al. (2003). Melanopsin and rod-cone photoreceptive systems account for all major accessory visual functions in mice. *Nature* 424, 76–81. doi: 10.1038/nature01761

Hazelhoff, E. M., Dudink, J., Meijer, J. H., and Kervezee, L. (2021). Beginning to see the light: lessons learned from the development of the circadian system for optimizing light conditions in the neonatal intensive care unit. *Front. Neurosci.* 15:634034. doi: 10.3389/fnins.2021.634034

Hu, J., Shi, Y., Zhang, J., Huang, X., Wang, Q., Zhao, H., et al. (2022). Melanopsin retinal ganglion cells mediate light-promoted brain development. *Cells* 185, 3124–3137.e15. doi: 10.1016/j.cell.2022.07.009

Humphrey, T. (1964). Embryology of the central nervous system: with some correlations with functional development. *Ala. J. Med. Sci.* 1, 60–64.

Huxley, A.Herman Finkelstein Collection (Library of Congress). (1932). *Brave new world, a novel*. Garden City, NY. Doubleday, Doran & company, Inc.

Ikeda, T., Ishikawa, H., Shimizu, K., Asakawa, K., and Goseki, T. (2015). Pupillary size and light reflex in premature infants. *Neuroophthalmology* 39, 175–178. doi: 10.3109/01658107.2015.1055363

Illnerová, H., Buresová, M., and Presl, J. (1993). Melatonin rhythm in human milk. *J. Clin. Endocrinol. Metab.* 77, 838–841. doi: 10.1210/jcem.77.3.8370707

Imura, M., Suzuki, C., and Fuse, K. (2014). "Massage thrapy" in *Standard developmental care*. eds. H. Nishida, S. Ohgi, T. Watanabe and H. Kihara (Osaka: Medicus Shuppan), 231–248.

Ishida, A., Mutoh, T., Ueyama, T., Bando, H., Masubuchi, S., Nakahara, D., et al. (2005). Light activates the adrenal gland: timing of gene expression and glucocorticoid release. *Cell Metab.* 2, 297–307. doi: 10.1016/j.cmet.2005.09.009

Ivars, K., Nelson, N., Theodorsson, A., Theodorsson, E., Ström, J. O., and Mörelius, E. (2015). Development of salivary cortisol circadian rhythm and reference intervals in full-term infants. *PLoS One* 10:e0129502. doi: 10.1371/journal.pone.0129502

Ivars, K., Nelson, N., Theodorsson, A., Theodorsson, E., Ström, J. O., and Mörelius, E. (2017). Development of salivary cortisol circadian rhythm in preterm infants. *PLoS One* 12:e0182685. doi: 10.1371/journal.pone.0182685

Kennaway, D. J. (2000). Melatonin and development: physiology and pharmacology. *Semin. Perinatol.* 24, 258–266. doi: 10.1053/sper.2000.8594

Knutsson, A. (2003). Health disorders of shift workers. *Occup. Med. (Lond.)* 53, 103–108. doi: 10.1093/occmed/kqg048

Kuhn, C. M., Schanberg, S. M., Field, T., Symanski, R., Zimmerman, E., Scafidi, F., et al. (1991). Tactile-kinesthetic stimulation effects on sympathetic and adrenocortical function in preterm infants. *J. Pediatr.* 119, 434–440. doi: 10.1016/s0022-3476(05)82059-1

Lary, S., Briassoulis, G., de Vries, L., Dubowitz, L. M., and Dubowitz, V. (1985). Hearing threshold in preterm and term infants by auditory brainstem response. *J. Pediatr.* 107, 593–599. doi: 10.1016/s0022-3476(85)80030-5

LeGates, T. A., Altimus, C. M., Wang, H., Lee, H. K., Yang, S., Zhao, H., et al. (2012). Aberrant light directly impairs mood and learning through melanopsin-expressing neurons. *Nature* 491, 594–598. doi: 10.1038/nature11673

Lunshof, S., Boer, K., Wolf, H., van Hoffen, G., Bayram, N., and Mirmiran, M. (1998). Fetal and maternal diurnal rhythms during the third trimester of normal pregnancy: outcomes of computerized analysis of continuous twenty-four-hour fetal heart rate recordings. *Am. J. Obstet. Gynecol.* 178, 247–254. doi: 10.1016/s0002-9378(98)80008-2

Lupi, D., Oster, H., Thompson, S., and Foster, R. G. (2008). The acute light-induction of sleep is mediated by OPN4-based photoreception. *Nat. Neurosci.* 11, 1068–1073. doi: 10.1038/nn.2179

Menaker, M., and Eskin, A. (1966). Entrainment of circadian rhythms by sound in *Passer domesticus*. *Science* 154, 1579–1581. doi: 10.1126/science.154.3756.1579

Mendez, N., Abarzua-Catalan, L., Vilches, N., Galdames, H. A., Spichiger, C., Richter, H. G., et al. (2012). Timed maternal melatonin treatment reverses circadian disruption of the fetal adrenal clock imposed by exposure to constant light. *PLoS One* 7:e42713. doi: 10.1371/journal.pone.0042713

Milosavljevic, N. (2019). How does light regulate mood and behavioral state? *Clocks Sleep* 1, 319–331. doi: 10.3390/clockssleep1030027

Montúfar-Chaveznava, R., Trejo-Muñoz, L., Hernández-Campos, O., Navarrete, E., and Caldelas, I. (2013). Maternal olfactory cues synchronize the circadian system of artificially raised newborn rabbits. *PLoS One* 8:e74048. doi: 10.1371/journal.pone.0074048

Morag, I., and Ohlsson, A. (2016). Cycled light in the intensive care unit for preterm and low birth weight infants. *Cochrane Database Syst. Rev.* 2020:CD006982. doi: 10.1002/14651858.CD006982.pub4

Neel, M. L., Yoder, P., Matusz, P. J., Murray, M. M., Miller, A., Burkhardt, S., et al. (2019). Randomized controlled trial protocol to improve multisensory neural processing, language and motor outcomes in preterm infants. *BMC Pediatr.* 19:81. doi: 10.1186/s12887-019-1455-1

Niemi, A. K. (2017). Review of randomized controlled trials of massage in preterm infants. *Children (Basel).* 4:21. doi: 10.3390/children4040021

Noseda, R., Kainz, V., Jakubowski, M., Gooley, J. J., Saper, C. B., Digre, K., et al. (2010). A neural mechanism for exacerbation of headache by light. *Nat. Neurosci.* 13, 239–245. doi: 10.1038/nn.2475

Ohta, H., Honma, S., Abe, H., and Honma, K. (2002). Effects of nursing mothers on rPer1 and rPer2 circadian expressions in the neonatal rat suprachiasmatic nuclei vary with developmental stage. *Eur. J. Neurosci.* 15, 1953–1960. doi: 10.1046/j.1460-9568.2002.02016.x

Ohta, H., Mitchell, A. C., and McMahon, D. G. (2006). Constant light disrupts the developing mouse biological clock. *Pediatr. Res.* 60, 304–308. doi: 10.1203/01.pdr.0000233114.18403.66

Ohta, H., Yamazaki, S., and McMahon, D. G. (2005). Constant light desynchronizes mammalian clock neurons. *Nat. Neurosci.* 8, 267–269. doi: 10.1038/nn1395

Panda, S., Sato, T. K., Castrucci, A. M., Rollag, M. D., DeGrip, W. J., Hogenesch, J. B., et al. (2002). Melanopsin (Opn4) requirement for normal light-induced circadian phase shifting. *Science* 298, 2213–2216. doi: 10.1126/science.1076848

Pandi-Perumal, S. R., Trakht, I., Srinivasan, V., Spence, D. W., Maestroni, G. J., Zisapel, N., et al. (2008). Physiological effects of melatonin: role of melatonin receptors and signal transduction pathways. *Prog. Neurobiol.* 85, 335–353. doi: 10.1016/j.pneurobio.2008.04.001

Pauk, J., Kuhn, C. M., Field, T. M., and Schanberg, S. M. (1986). Positive effects of tactile versus kinesthetic or vestibular stimulation on neuroendocrine and ODC activity in maternally-deprived rat pups. *Life Sci.* 39, 2081–2087. doi: 10.1016/0024-3205(86)90359-0

Pineda, R., Roussin, J., Kwon, J., Heiny, E., Colditz, G., and Smith, J. (2021). Applying the RE-AIM framework to evaluate the implementation of the supporting and enhancing NICU sensory experiences (SENSE) program. *BMC Pediatr.* 21:137. doi: 10.1186/s12887-021-02594-3

Polese, D., Fagioli, M., Virgili, F., and Nastro, P. F. (2021). Something must happen before first breath. *BMC Med. Ethics.* 22:57. doi: 10.1186/s12910-021-00624-4

Polese, D., Riccio, M. L., Fagioli, M., Mazzetta, A., Fagioli, F., and Parisi, P. (2022). The Newborn's reaction to light as the determinant of the Brain's activation at human birth. *Front. Integr. Neurosci.* 16:933426. doi: 10.3389/fnint.2022.933426

Reebs, S. G. (1989). Acoustical entrainment of circadian activity rhythms in house sparrows: constant light is not necessary. *Ethology* 80, 172–181.

Reppert, S. M., Godson, C., Mahle, C. D., Weaver, D. R., Slaugenhaupt, S. A., and Gusella, J. F. (1995). Molecular characterization of a second melatonin receptor expressed in human retina and brain: the Mel 1b melatonin receptor. *Proc. Natl. Acad. Sci. U. S. A.* 92, 8734–8738. doi: 10.1073/pnas.92.19.8734

Reynolds, J. D., Hardy, R. J., Kennedy, K. A., Spencer, R., van Heuven, W. A., and Fielder, A. R. (1998). Lack of efficacy of light reduction in preventing retinopathy of prematurity. Light reduction in retinopathy of prematurity (LIGHT-ROP) cooperative group. *N. Engl. J. Med.* 338, 1572–1576. doi: 10.1056/NEJM199805283382202

Richter, H. G., Torres-Farfan, C., Garcia-Sesnich, J., Abarzua-Catalan, L., Henriquez, M. G., Alvarez-Felmer, M., et al. (2008). Rhythmic expression of functional MT1 melatonin receptors in the rat adrenal gland. *Endocrinology* 149, 995–1003. doi: 10.1210/en.2007-1009

Rivkees, S. A. (2003). Developing circadian rhythmicity in infants. *Pediatrics* 112, 373–381. doi: 10.1542/peds.112.2.373

Rivkees, S. A., Mayes, L., Jacobs, H., and Gross, I. (2004). Rest-activity patterns of premature infants are regulated by cycled lighting. *Pediatrics* 113, 833–839. doi: 10.1542/peds.113.4.833

Robinson, J., and Fielder, A. R. (1990). Pupillary diameter and reaction to light in preterm neonates. *Arch. Dis. Child.* 65, 35–38. doi: 10.1136/adc.65.1_Spec_No.35

Roca, A. L., Godson, C., Weaver, D. R., and Reppert, S. M. (1996). Structure, characterization, and expression of the gene encoding the mouse Mel1a melatonin receptor. *Endocrinology* 137, 3469–3477. doi: 10.1210/endo.137.8.8754776

Ruby, N. F., Brennan, T. J., Xie, X., Cao, V., Franken, P., Heller, H. C., et al. (2002). Role of melanopsin in circadian responses to light. *Science* 298, 2211–2213. doi: 10.1126/science.1076701

Schaal, B., Hummel, T., and Soussignan, R. (2004). Olfaction in the fetal and premature infant: functional status and clinical implications. *Clin. Perinatol.* 31, 261–285. doi: 10.1016/j.clp.2004.04.003

Schmidt Mellado, G., Pillay, K., Adams, E., Alarcon, A., Andritsou, F., Cobo, M. M., et al. (2022). The impact of premature extrauterine exposure on infants' stimulus-evoked brain activity across multiple sensory systems. *Neuroimage Clin.* 33:102914. doi: 10.1016/j.nicl.2021.102914

Schmidt, T. M., Taniguchi, K., and Kofuji, P. (2008). Intrinsic and extrinsic light responses in melanopsin-expressing ganglion cells during mouse development. *J. Neurophysiol.* 100, 371–384. doi: 10.1152/jn.00062.2008

Sekaran, S., Lupi, D., Jones, S. L., Sheely, C. J., Hattar, S., Yau, K. W., et al. (2005). Melanopsin-dependent photoreception provides earliest light detection in the mammalian retina. *Curr. Biol.* 15, 1099–1107. doi: 10.1016/j.cub.2005.05.053

Sernagor, E. (2005). Retinal development: second sight comes first. *Curr. Biol.* 15, R556–R559. doi: 10.1016/j.cub.2005.07.004

Seron-Ferre, M., Valenzuela, G. J., and Torres-Farfan, C. (2007). Circadian clocks during embryonic and fetal development. *Birth Defects Res. C. Embryo. Today* 81, 204–214. doi: 10.1002/bdrc.20101

Slominski, A., Fischer, T. W., Zmijewski, M. A., Wortsman, J., Semak, I., Zbytek, B., et al. (2005). On the role of melatonin in skin physiology and pathology. *Endocrine* 27, 137–148. doi: 10.1385/ENDO:27:2:137

Slominski, A., Tobin, D. J., Zmijewski, M. A., Wortsman, J., and Paus, R. (2008). Melatonin in the skin: synthesis, metabolism and functions. *Trends Endocrinol. Metab.* 19, 17–24. doi: 10.1016/j.tem.2007.10.007

Smith, L., and Canal, M. M. (2009). Expression of circadian neuropeptides in the hypothalamus of adult mice is affected by postnatal light experience. *J. Neuroendocrinol.* 21, 946–953. doi: 10.1111/j.1365-2826.2009.01914.x

St. Hilaire, M. A., Gooley, J. J., Khalsa, S. B., Kronauer, R. E., Czeisler, C. A., and Lockley, S. W. (2012). Human phase response curve to a 1 h pulse of bright white light. *J. Physiol.* 590, 3035–3045. doi: 10.1113/jphysiol.2012.227892

Summa, K. C., Vitaterna, M. H., and Turek, F. W. (2012). Environmental perturbation of the circadian clock disrupts pregnancy in the mouse. *PLoS One* 7:e37668. doi: 10.1371/journal.pone.0037668

Teller, D. Y. (1997). First glances: the vision of infants. The Friedenwald lecture. *Invest. Ophthalmol. Vis. Sci.* 38, 2183–2203.

Thomas, L., Purvis, C. C., Drew, J. E., Abramovich, D. R., and Williams, L. M. (2002). Melatonin receptors in human fetal brain: 2-[(125)I]iodomelatonin binding and MT1 gene expression. *J. Pineal Res.* 33, 218–224. doi: 10.1034/j.1600-079X.2002.02921.x

Torres-Farfan, C., Richter, H. G., Rojas-García, P., Vergara, M., Forcelledo, M. L., Valladares, L. E., et al. (2003). mt1 melatonin receptor in the primate adrenal gland: inhibition of adrenocorticotropin-stimulated cortisol production by melatonin. *J. Clin. Endocrinol. Metab.* 88, 450–458. doi: 10.1210/jc.2002-021048

Vandewalle, G., van Ackeren, M. J., Daneault, V., Hull, J. T., Albouy, G., Lepore, F., et al. (2018). Light modulates oscillatory alpha activity in the occipital cortex of totally visually blind individuals with intact non-image-forming photoreception. *Sci. Rep.* 8:16968. doi: 10.1038/s41598-018-35400-9

Van Gelder, R. N. (2008). Non-visual photoreception: sensing light without sight. *Curr. Biol.* 18, R38–9. doi: 10.1016/j.cub.2007.11.027

Varcoe, T. J., Wight, N., Voultsios, A., Salkeld, M. D., and Kennaway, D. J. (2011). Chronic phase shifts of the photoperiod throughout pregnancy programs glucose intolerance and insulin resistance in the rat. *PLoS One* 6:e18504. doi: 10.1371/journal.pone.0018504

Villalba, A., Monteoliva, J. R. R., and Pattini, A. (2018). A dynamic performance analysis of passive sunlight control strategies in a neonatal intensive care unit. *Light. Res. Technol.* 50, 191–204. doi: 10.1177/1477153516656225

Watanabe, S., Akiyama, S., Hanita, T., Li, H., Nakagawa, M., Kaneshi, Y., et al. (2013). Designing artificial environments for preterm infants based on circadian studies on pregnant uterus. *Front. Endocrinol.* 4:113. doi: 10.3389/fendo.2013.00113

White, R. D. (2013). Recommended NICU design standards and the physical environment of the NICU. *J. Perinatol.* 33:S1. doi: 10.1038/jp.2013.9

White-Traut, R. C., Nelson, M. N., Silvestri, J. M., Cunningham, N., and Patel, M. (1997). Responses of preterm infants to unimodal and multimodal sensory intervention. *Pediatr. Nurs.* 23:193.

Yamazaki, S., Numano, R., Abe, M., Hida, A., Takahashi, R., Ueda, M., et al. (2000). Resetting central and peripheral circadian oscillators in transgenic rats. *Science* 288, 682–685. doi: 10.1126/science.288.5466.682

Zaidi, F. H., Hull, J. T., Peirson, S. N., Wulff, K., Aeschbach, D., Gooley, J. J., et al. (2007). Short-wavelength light sensitivity of circadian, pupillary, and visual awareness in humans lacking an outer retina. *Curr. Biol.* 17, 2122–2128. doi: 10.1016/j.cub.2007.11.034

frontiers | Frontiers in Neuroscience

TYPE Review
PUBLISHED 05 September 2023
DOI 10.3389/fnins.2023.1196606

OPEN ACCESS

EDITED BY
Rae Silver,
Columbia University, United States

REVIEWED BY
Eric L. Bittman,
University of Massachusetts Amherst, United States
Jihwan Myung,
Taipei Medical University, Taiwan
Javier Stern,
Georgia State University, United States

*CORRESPONDENCE
Martha U. Gillette
✉ mgillett@illinois.edu

RECEIVED 30 March 2023
ACCEPTED 14 August 2023
PUBLISHED 05 September 2023

CITATION
Mitchell JW and Gillette MU (2023) Development of circadian neurovascular function and its implications. *Front. Neurosci.* 17:1196606. doi: 10.3389/fnins.2023.1196606

Development of circadian neurovascular function and its implications

Jennifer W. Mitchell[1,2,3] and Martha U. Gillette[1,2,3,4,5]*

[1]Department of Cell and Developmental Biology, University of Illinois Urbana-Champaign, Urbana, IL, United States, [2]Neuroscience Program, University of Illinois Urbana-Champaign, Urbana, IL, United States, [3]Beckman Institute for Advanced Science and Technology, University of Illinois Urbana-Champaign, Urbana, IL, United States, [4]Department of Molecular and Integrative Physiology, University of Illinois Urbana-Champaign, Urbana, IL, United States, [5]Carle-Illinois College of Medicine, University of Illinois Urbana-Champaign, Urbana, IL, United States

The neurovascular system forms the interface between the tissue of the central nervous system (CNS) and circulating blood. It plays a critical role in regulating movement of ions, small molecules, and cellular regulators into and out of brain tissue and in sustaining brain health. The neurovascular unit (NVU), the cells that form the structural and functional link between cells of the brain and the vasculature, maintains the blood–brain interface (BBI), controls cerebral blood flow, and surveils for injury. The neurovascular system is dynamic; it undergoes tight regulation of biochemical and cellular interactions to balance and support brain function. Development of an intrinsic circadian clock enables the NVU to anticipate rhythmic changes in brain activity and body physiology that occur over the day-night cycle. The development of circadian neurovascular function involves multiple cell types. We address the functional aspects of the circadian clock in the components of the NVU and their effects in regulating neurovascular physiology, including BBI permeability, cerebral blood flow, and inflammation. Disrupting the circadian clock impairs a number of physiological processes associated with the NVU, many of which are correlated with an increased risk of dysfunction and disease. Consequently, understanding the cell biology and physiology of the NVU is critical to diminishing consequences of impaired neurovascular function, including cerebral bleeding and neurodegeneration.

KEYWORDS

clock, blood–brain interface, neuroendothelial, tight junctions, circadian rhythm disruption

1. Introduction

The neurovasculature regulates the flow of blood through the arteries, veins, and capillaries within the brain. It is composed of cells of the neurovascular unit (NVU), which include neuroendothelial cells, mural cells (smooth muscle and pericytes), astrocytes, and microglia as well as extracellular matrix components within the basement membrane. Arteries arising from the subarachnoid space vascularize the brain. They form NVUs comprised of smooth muscle cells, endothelial cells, pia mater, the perivascular space, and astrocytic end feet. As these arterial vessels penetrate deeper into the brain, they lose smooth muscle cells and pia mater. Pericytes, which are contractile, assume positions between the endothelial cells and astrocytic endfeet (Figure 1).

The cells of the NVU to undergo dynamic daily and environmental changes, making regulatory adjustments to maintain homeostasis. Interactions of the NVU with neuronal networks are responsible for the regulating cerebral blood flow (CBF), maintaining the integrity of the

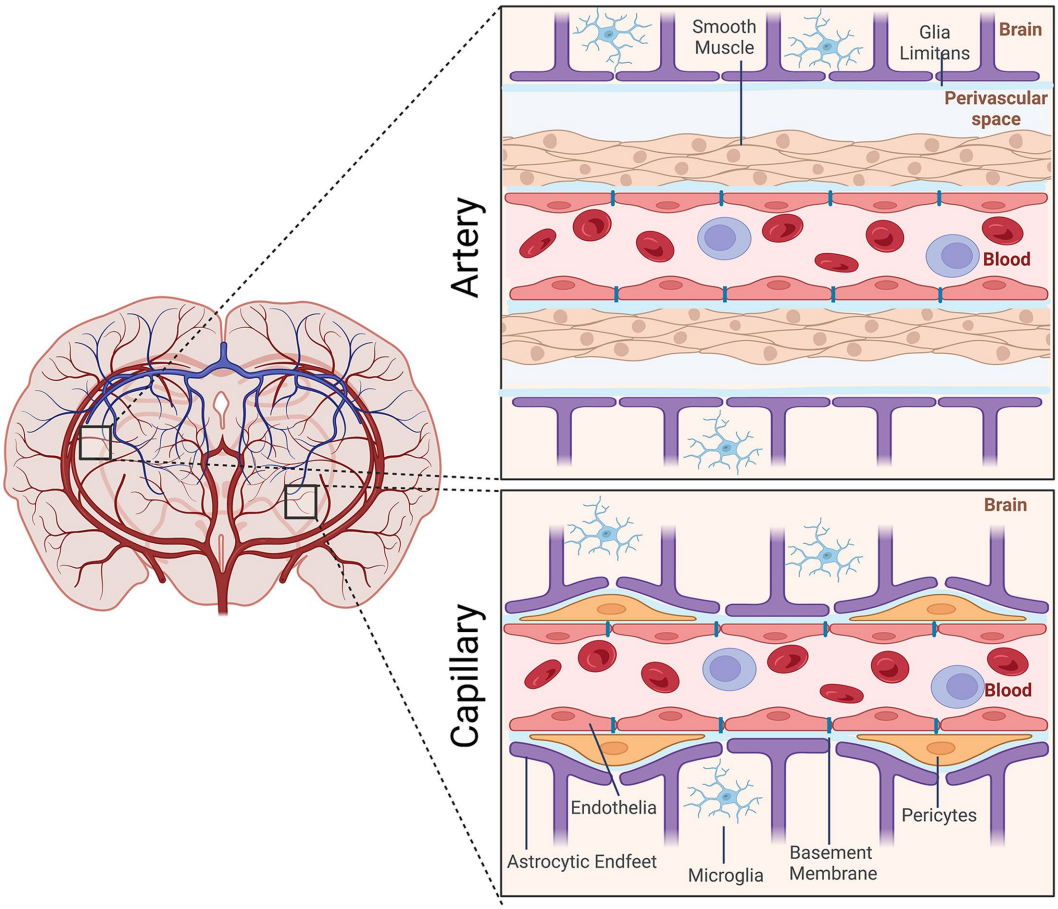

FIGURE 1
Schematic representation of the cellular elements of the neurovascular unit (NVU). Elements of the NVU include neuroendothelial cells, mural cells (vascular smooth muscle cells, pericytes), microglia, astrocytic endfeet. The cellular composition differs along the vascular tree. At the level of the artery/arteriole (top), the NVU is composed of neuroendothelial cells making up the inner layer of the vessel wall covered by a thin extracellular basement membrane, ringed by vascular smooth muscle cells, and ensheathed by a glial limitans. The perivascular space containing the cerebrospinal fluid is between pia and the glia limitans formed by astrocytic endfeet. At the capillary level (bottom), the NVU is composed of neuroendothelial cells that share a common basement membrane with pericytes. Pericytes stretch their processes along and around capillaries. Pericytes and endothelial cells are covered by astrocyte endfeet. Created by Biorender.com.

blood–brain interface (BBI), and immune surveilling-, which recognizes harmful pathogens, responds to injury, recruits resident microglia to clear cellular debris, and releases neuroprotective factors (Kaplan et al., 2020).

1.1. Blood–brain interface (BBI)

The cerebrovasculature continuously provides resources supporting the brain's high metabolic rate, the necessary rapid, on-demand delivery of oxygen and energy supporting neuronal activity, as well as efficient clearance of waste products. The brain's high metabolic rate requires the continuous supply of nutrients and oxygen by the blood. The blood–brain interface (BBI), a multicellular structure separating the CNS from systemic circulation, regulates this interaction. Tight junctions between endothelial cells of the NVU form a physical barrier, restricting permeability. The surrounding pericytes and astrocytic endfeet are encased in the extracellular matrix-containing basement membrane, enhancing this structural barrier (Abbott et al., 2010; Keaney and Campbell, 2015; Liebner et al., 2018). Vesicular transport across these endothelial cells is very low compared to vascular endothelial cells of other organs, distinguishing them as *neuroendothelium* (Brightman and Reese, 1969). The BBI restricts the exchange of material between the brain and the blood, except for small molecules and gases such as oxygen and carbon dioxide. Larger molecules can cross the BBI only through transporters and endocytic vesicles (pinocytosis). Loss of BBI integrity results not only in reduced oxygen and nutrient flux into the brain, but also diminished clearance of neurotoxic substances. Other components, such as astrocytic endfeet and pericytes, also express some transporters and receptors that contribute to the BBI transport system.

Neuroendothelial cells are the central regulatory components of the BBI. Characterized by few transporters, low level of paracellular diffusion and pinocytotic activity, neuroendothelial cells are joined laterally by tight junctions. Pericytes wrap around the vessels and are embedded in extra cellular matrix, the basement membrane (Abbott et al., 2010). The restrictive properties of the BBI are determined primarily by tight-junction proteins, which form a physical barrier between adjacent neuroendothelial cells (Kniesel and Wolburg, 2000). The BBI restricts entry of cytokines and antibodies, which can impair neurotransmission, into the brain (Abbott et al., 2006), as well as participates in the clearance of

cellular metabolites from the brain to the blood (Winkler et al., 2011).

1.2. Cerebral blood flow

Cerebral blood flow (CBF) in the human brain is accomplished through a network of interconnected blood vessels over 400-miles long (Zlokovic, 2011; Kisler et al., 2017). Irreversible brain damage can occur within minutes if proper CBF is compromised (Moskowitz et al., 2010). Mural cells, vascular smooth muscle cells (vSMC), and pericytes are involved in regulating cerebral blood flow (Peterson et al., 2011; Hall et al., 2014; Hill et al., 2015; Attwell et al., 2016). Active contraction and relaxation of vSMCs around the larger arterioles controls flow by altering the vascular diameter (Hill et al., 2015). Pericytes are spatially isolated contractile cells in the microvasculature that are responsible for regulating the cerebral blood flow within capillaries (Attwell et al., 2016; Cai et al., 2017; Mughal et al., 2023; Figure 2). The capillary dilation created by pericyte relaxation is regulated by the blood pressure from upstream arterioles. Pericytes alter capillary diameter by actively responding to neuronal activity (Wu et al., 2003; Peppiatt et al., 2006). The dilation response in capillaries is rapid, completing prior to arteriole dilation (Hall et al., 2014).

Regulation of CBF can be grouped into three broad mechanisms: (1) Autoregulation, which maintains stable blood flow despite fluctuations in systemic blood pressure; (2) Vasomotor reactivity, which is in response to modification of the arterial pCO_2/pH of the brain tissue reporting the need for oxygen; and (3) Neurovascular coupling, which is in response to local changes in neuronal and metabolic activity (Peterson et al., 2011; Silverman and Petersen, 2022). *Autoregulation* is largely controlled by changes in vasoconstriction and vasodilation in the smooth muscle of arterioles (Attwell et al., 2016; Hosford and Gourine, 2019; Hoiland et al., 2020; Duffin et al., 2021). This may be mediated by the release of vasoactive substances, myogenic regulation adapting vascular tone, and

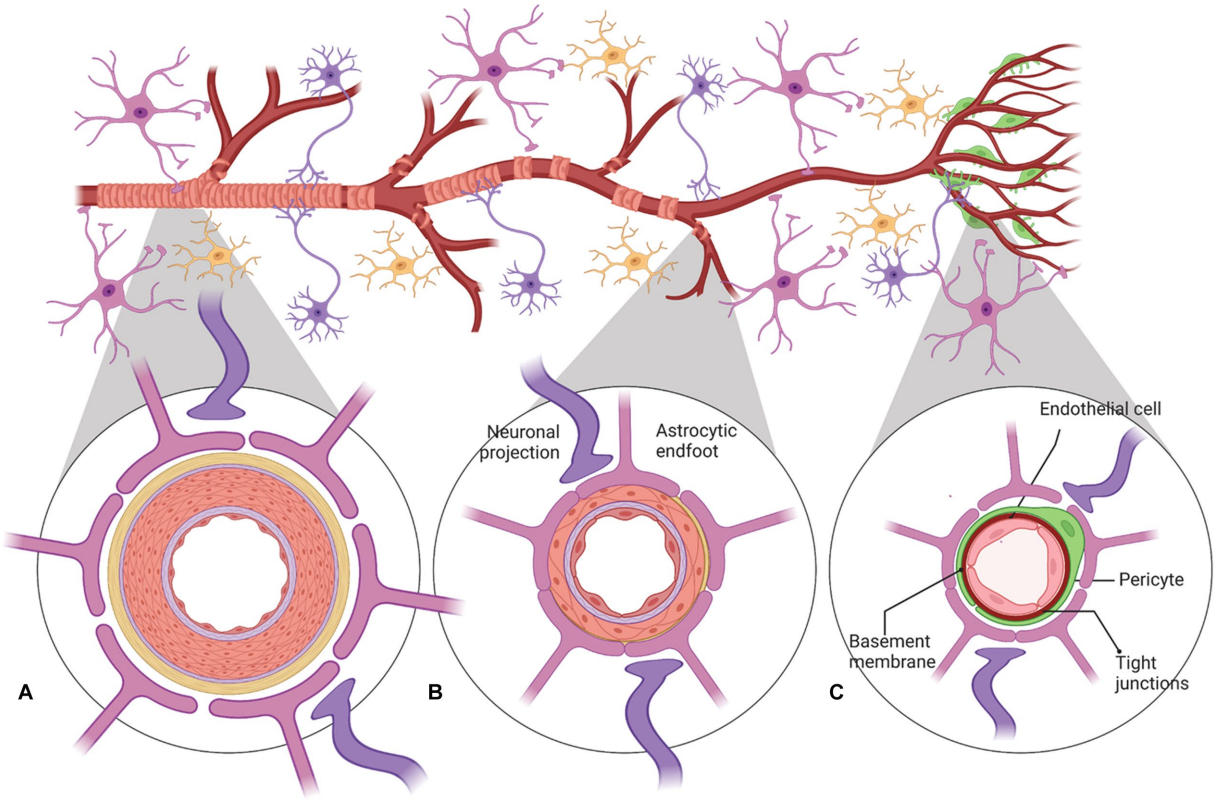

FIGURE 2
A schematic representation of neurovascular units with cellular elements that regulate cerebral blood flow along the vascular tree. The various types of cells that form the neurovascular unit (NVU) (neurons, astrocytes, mural cells – vascular smooth muscle cells (VSMCs) and pericytes, and neuroendothelium) regulate cerebral blood flow throughout the vascular tree. The cellular composition of the NVU differs along the vascular tree, but the principal cellular components all remain represented, as illustrated here. **(A)** At the level of penetrating arteries, the NVU is composed of neuroendothelial cells, making up the inner layer of the vessel wall, covered by a thin extracellular basement membrane, ringed by one to three layers of VSMCs, and ensheathed by pia. The Virchow-Robin space containing the cerebrospinal fluid is between the pia and glia limitans formed by astrocytic endfeet. Both VSMCs and astrocytes are innervated by local neurons. **(B)** Arterioles differ in that (i) there is only one layer of VSMCs, (ii) astrocyte coverage and innervation of the vessel wall and endothelial inner layer are continuous with penetrating arteries and brain capillaries, above and below the arteriole level, respectively. Precapillary arterioles may also contain transitional pericytes, a cell type between pericyte and VSMCs. **(C)** At the capillary level, the NVU is composed of endothelial cells that share a common basement membrane with pericytes. Pericytes stretch their processes along and around capillaries and make direct, interdigitated or "peg-socket"-like contacts with neuroendothelial cells. Pericytes and neuroendothelial cells are covered by astrocyte endfeet. Both astrocytes and pericytes are innervated by local neurons similar to astrocytes and VSMCs in the upper segments of the vascular tree. Created by Biorender.com.

neurogenic regulation due to sympathetic innervation of vascular smooth muscle cells (Silverman and Petersen, 2022). *Vasomotor reactivity* reflects changes due to arterial CO_2 pressure and coupled pH shifts of the brain microenvironment. Small arterioles are extremely sensitive, vasodilating with elevated arterial CO_2 concentrations (Yoshihara et al., 1995). It has been suggested that this vasomotor response is regulated by the proton concentration in smooth muscle cells of cerebral vessels through the pH sensitivity of carbonic anhydrase activity (Budohoski et al., 2013). *Neurovascular Coupling* responses to elevated neuronal activity and metabolism lead to an increase in local blood flow providing the brain with enhanced blood flow for a given demand (functional hyperemia). Chemical signals secreted from cells of the NVU, which can cause vasodilation or vasoconstriction. The neuroendothelial cells produce several vasoactive factors, including nitric oxide (NO), endothelium-dependent hyperpolarization factor, eicosanoids, and endothelins; their release is regulated by cerebral blood flow (Peterson et al., 2011). Additionally, astrocytic end-feet that directly border the vessels also play key roles in regulating CBF (Peterson et al., 2011). Increased neuronal activity is can initiate the release of synaptic glutamate and thereby activate two different signaling pathways: (1) a signaling pathway that includes the activation of Ca^{2+}-dependent enzymes, such as neuronal nitric oxide synthase (nNOS) and cyclooxygenase-2 (COX-2), can produce the vasodilators NO and prostanoids, respectively, and (2) an astrocytic-dependent signaling pathway that includes Ca^{2+}-dependent activation of phospholipase A2 and ultimately the production of vasodilatory metabolites including epoxyeicosatrienoic acids (EETs) (Attwell et al., 2010; Stackhouse and Mishra, 2021) (Shi et al., 2008). Additionally, K^+ and H^+ are produced during synaptic transmission; elevation of these ions stimulates vasodilation (Paulson and Newman, 1987; Nielsen and Lauritzen, 2001). However, neural activation can also stimulate vasoconstriction as is the case via BK channels from altered astrocytic endfeet calcium signal in brain slices mimicking subarachnoid hemorrhage (Koide et al., 2012; Pappas et al., 2015).

1.3. Immune surveillance and repair

Despite barriers that prevent immune cells from traversing into the brain, the CNS is continuously monitoring for damage and agents that would disrupt normal brain function. Resident microglia and immune cells within the bordering meninges are primarily responsible for this surveillance (Ousman and Kubes, 2012). Although the border immune cells are outside the scope of this review, they have been thoroughly discussed (Kwon, 2022; Rustenhoven and Kipnis, 2022). The role of microglia in immune surveillance is facilitated by their close proximity to one another with minimal overlap between processes of neighboring microglia (Raivich, 2005; Ousman and Kubes, 2012). Under physiological conditions, microglia are quiescent (M0), yet they are constantly surveying the local environment and communicating with other cell types via their motile processes. This allows the full extracellular space to be sampled by at least one microglial process every a few hours (Nimmerjahn et al., 2005).

Within the NVU, the microglia are activated by minor alterations to the BBI, responding to various stimuli such as vascular injury, stroke, trauma, bacterial infection as well as diseases states such as Alzheimer's disease and multiple sclerosis (Dudvarski Stankovic et al., 2016; Orihuela et al., 2016; Zhao et al., 2018). The microglial processes are recruited rapidly and form a dense, continuous, stable aggregate at the site of BBI leakage (Davalos et al., 2012; Jolivel et al., 2015; Lou et al., 2016). Microglia can be activated within minutes of tissue damage. They undergo a spectrum of responses when activated, including polarization and differentiation toward pro-inflammatory and neurotoxicity (M1) or anti-inflammatory, healing (M2) forms (Guo et al., 2022). Microglia driven toward the M1 state can produce inflammatory cytokines and chemokines as well as expressing NADPH oxidase, which produces superoxide and reactive oxygen species (ROS). The M2 state of microglia generate anti-inflammatory cytokines, growth factors, as in insulin-like growth factor 1 (IGF-1) and fibroblastic growth factor (FGF), and neurotropic growth factors, including neurotrophic growth factor (NGF) and brain-derived neurotrophic factor (BDNF). Signals shifting between M1 and M2 polarizations can have profound effects on being either neuroprotective or pathogenetic on brain physiology (Ma et al., 2017; Zhao et al., 2018; Guo et al., 2022).

2. Development of the neurovasculature

The developing CNS does not produce vascular progenitor cells; thus, blood vessels must enter into the developing CNS to form the neurovasculature (Bautch and James, 2009). Early studies demonstrate that vascularization of the brain is initiated by vessels outside of the CNS through angiogenic sprouting, namely the peri-neural vascular plexus (Feeney and Watterson, 1946; Strong, 1964). The blood vessels invade and form distinct patterns once they enter the brain (Bautch and James, 2009; Tata et al., 2015). Ultimately, the neurovasculature expands into a vast network and remodels into a vascular tree organized into a hierarchical network of arteries, arterioles, capillary beds, venules, and veins.

Early in embryogenesis, a blood–brain interface is formed to protect neural tissue from variations in blood composition, maintain ionic homeostasis, and exclude toxins. This complex developing structure involves nascent vessels emerging by ingression from endothelial cells. Tight junctions are present between these neuroendothelial cells restricting the passage of low molecular weight molecules very early in development (Ek et al., 2012) The nascent vessels recruit pericytes which are required for barrier formation (Daneman et al., 2010). Notably, this occurs before astrocyte generation (Daneman et al., 2010). Astrocytes extend processes that contact blood vessels after birth, and thus are not required to initially induce the BBI, but likely are involved in maintenance. A number of known signaling molecules between the neural and vascular cells are involved in crosstalk to regulate development of the neurovasculature, all of which allow formation of the intricate architecture through the brain (Tata et al., 2015).

3. Specialized neurovascular structures: circumventricular organs and the cerebral portal system

3.1. Circumventricular organs

The brain has a number of circumventricular organs (CVOs). CVOs possess characteristically highly permeable, fenestrated

capillaries, in contrast to the barrier nature of capillaries of the BBI. As the name implies, these specializations form around (*Lat.*, *circum*) ventricles, including the area postrema (AP), median eminence (ME), neurhypophyis (NP), organum vaculosum of the lamina terminalis (OVLT), pineal gland, and subfornical organ (SFO) (Miyata, 2015). The subcommissural organ (SCO) is often included among the seven CVOs, although it lacks fenestrated capillaries. On the other hand, the choroid plexus, which does have fenestrated capillaries but lacks neurons, may also be grouped with the CVO (Oldfield and McKinley, 2015). Because of the lack of the endothelial barrier, the CVOs permit the direct exchange of chemical information between the brain and circulating blood. Broadly, the CVOs can be separated into two categories, sensory and secretory. The *secretory CVOs* include the NH, ME, and pineal (as well as the SCO&/or choroid plexus). These neurosecretory nuclei release neurohormones and hormone-releasing factors into the blood via the fenestrated capillaries. The *sensory CVOs*, which are often described as "windows of the brain," detect circulating hormones and ions and initiate responses that maintain homeostasis (Gross et al., 1987) and include the SFO, OVLT and AP.

The presence of these leaky, fenestrated capillaries may allow diffusible timing signals to entrain brain regions outside of the suprachiasmatic nucleus (SCN), the site of the central circadian clock (see section 5). To our knowledge, no prior publication reports movement of signals that traverse from the brain directly into the neurovasculature. However, the dense capillaries within the SCN, specifically, within the shell region, suggest a pathway that transports diffusible signals from the SCN into the blood (Yao et al., 2023). There is evidence that diffusible signals from the SCN can interact locally with the CSF. Taub et al. demonstrated that arginine vasopressin (AVP), an established SCN output timing signal that synchronizes 24-h rhythms of physiology and behavior, was found to contribute to AVP levels in the CSF (Taub et al., 2021). AVP levels exhibit 24-h rhythms in CSF, but not in blood (Schwartz et al., 1983). Previous reports have demonstrated a disparate regulation in neuropeptides between plasma and the CSF (Kagerbauer et al., 2013). However, direct access through CVOs to potential timing signals raises an interesting possibility for regulation of circadian oscillations in the neurovasculature.

3.2. Cerebral portal systems

Portal systems carry blood from one capillary bed to another rather than from a capillary bed to a vein. This facilitates the rapid transport of chemical signals from one region to another while maintaining high concentrations of solutes, as the fluid is not transported via the vascular system back through to the heart. The hypophyseal-pituitary portal system is a well-known portal system. Neuropeptides packaged in vesicles within the neuronal cell bodies travel along the axons of the supraoptic and paraventricular neurons that synthesize them to the capillary bed of the median eminence (ME). They are released on demand into the capillary beds of the anterior pituitary (Harris, 1948; Clarke, 2015). Notably, the capillaries and veins of this portal system are leaky due to fenestrations in their vessel walls; thus, the neurohormones pass directly from axon terminals into the blood without encountering a BBI. This portal system allows hypothalamic hormones, such as gonadotropin releasing hormone (GnRH), to stimulate the secretory cells they control.

A new brain portal system has been described that links the SCN and the OVLT (Yao et al., 2021). These portal vessels arise from the rostral SCN and join the capillaries at the base of the OVLT (Yao et al., 2021, 2023). The OVLT participates in osmotic regulation and is involved in the release of AVP (McKinley et al., 2004; Samson and Ferguson, 2015). Many OVLT functions are under circadian control, including anticipatory thirst and osmoregulation (Trudel and Bourque, 2010; Gizowski et al., 2018; Gizowski and Bourque, 2020). The SCN secretes a number of paracrine output signals (Cheng et al., 2002; Kraves and Weitz, 2006; Maywood et al., 2011). This portal system may provide a pathway by which these diffusible circadian-timing signals are maintained at levels that directly influence other brain regions.

4. The neurovascular system is dynamic and diurnally rhythmic

Modulation of blood flow, metabolism, and neural activity within the brain is dynamically regulated. The complex multicellular NVU responds accordingly. Beside the changes that occur with aging (Fabiani et al., 2021; Zimmerman et al., 2021), many of these alterations display rhythmic, anticipatory variations that are correlated with specific phases of the 24-h day-night cycle. These circadian rhythms, derived from the Latin *circa* (approximately) and *dies* (day), are driven by endogenous clocks that enable organisms to anticipate and prepare for changes over the day-night cycle. Although not restricted to the neurovasculature, one of the most notable vascular functions that displays circadian rhythmicity is blood pressure (Conroy et al., 2005; Paschos and FitzGerald, 2010). In humans, blood pressure rises before awaking, reaches a peak in midmorning and then decrease as the day progresses (Millar-Craig et al., 1978). Circadian rhythms of regulators of blood pressure, plasma epinephrine, norepinephrine, cortisol, cardiac vagal tone, and heart rate all have been noted (Kalsbeek et al., 2006). Ablation of the hypothalamic SCN disrupts the circadian variation in blood pressure, demonstrating that the central circadian clock is necessary to orchestrate these diverse vascular changes (Janssen et al., 1994; Sano et al., 1995; Witte et al., 1998).

Platelet activation, which mediates blot clot formation, and fibrinolysis, the dissolution of these clots, also displays circadian rhythmicity (Paschos and FitzGerald, 2010; Thosar et al., 2018; Budkowska et al., 2019). With regard to clot formation, platelet aggregation and platelet activation markers show strong time-of-day variation, peaking mid-morning in humans. These include factors promoting blood coagulation, such as platelet factor 4 (PF4), glycoprotein Ib (GPIb), β-thromboglobulin (βTG), P-selectin, and activated integrin αIIbβ3 (also known as GP11b/IIIa) (Tofler et al., 1987; Jafri et al., 1992; Scheer et al., 2011; Thosar et al., 2018; Crnko et al., 2019). Additionally, fibrinogen, the circulating precursor of fibrin, a protein that propagates clotting, demonstrates a 24-h variation in humans (Bremner et al., 2000). In tandem, fibrinolytic activity is significantly reduced in the morning (Andreotti and Kluft, 1991). The concentration of plasminogen activator inhibitor-1 (PAI-1), which inhibits fibrinolysis, peaks in the morning (Andreotti et al., 1988; Kluft et al., 1988; Angleton et al., 1989). This is endogenously driven,

independent of the sleep cycle (Scheer and Shea, 2014). Together these findings suggest that mornings, with the increase in platelet activation and decrease in fibrinolysis, constitute an adverse stressor toward negative cardio-and neurovascular events.

Indeed, adverse neurovascular events, including ischemic stroke and hemorrhagic stroke, demonstrate daily fluctuations (Elliott, 1998; Chaturvedi et al., 1999; Manfredini et al., 2005; Butt et al., 2009; Turin et al., 2010; Ripamonti et al., 2017). In intracerebral hemorrhage and subarachnoid hemorrhage detection, a bimodality in the rhythm is present, with the peak in morning and second smaller peak in afternoon/early evening (Butt et al., 2009; Turin et al., 2010). Additionally, differential damage outcome is associated with the time of day of the stroke. In the morning, the increases in paracellular permeability and immune-cell trafficking are associated with more severe stroke phenotype and more adverse outcomes compared to strokes at that occur in the afternoon (Liu et al., 2021). Thus, circadian rhythms may influence stroke vulnerability of the NVU. A more in depth understanding could allow targeted prevention in the development and progression of neurovascular dysfunction and disease.

5. The circadian system and the molecular clock

Circadian rhythms are orchestrated by a central pacemaker within the hypothalamus, the SCN. Lesions of the SCN abolish or attenuate daily rhythms in locomotor activity, body temperature, blood pressure, and heart rate in rodents (Stephan and Zucker, 1972; Ralph et al., 1990; Witte et al., 1998), indicating that these are endogenous rhythms rather than driven by 24-h changes in the environment or daily behaviors. SCN rhythms are synchronized to the external environment primarily by light signals via the retinohypothalamic tract (Ding et al., 1994; Gooley et al., 2001). Other salient entrainers, or *zeitgebers*, are food and behavioral activity. The SCN is an autonomous oscillator, maintaining rhythms *in vitro* (Gillette and Reppert, 1987; Yamazaki and Takahashi, 2005). Notably, dissociated SCN cells also remain rhythmic in culture, demonstrating the cell-intrinsic property of rhythmicity (Welsh et al., 2004).

At its core, the endogenous circadian clock is a transcriptional-translational negative feedback loop (TTFL). Several interlocking TTFLs act in collaboration with a key negative feedback loop (Figure 3). In this key loop are the positive transcriptional regulators, the proteins BMAL1 and CLOCK. These two positive regulators heterodimerize and bind to *cis*-acting E-box promoter elements to activate the expression of negative regulators, which include the repressors CRYPTOCHROME 1 and 2 (CRY1, CRY2) and PERIOD 1, 2, and 3 (PER1-3). As the cycle progresses, the negative regulators accumulate, form complexes and are transported to the nucleus where they inhibit BMAL/CLOCK-activated transcription, thereby inhibiting their own transcription (Takahashi, 2017; Cox and Takahashi, 2019; Rosensweig and Green, 2020). An auxiliary loop involving REV-ERB and ROR modulates the main TTFL to further controls the expression of CLOCK and BMAL1 (Takahashi, 2017). The regulation and machinery of the molecular clock mechanism has been extensively reviewed (Takahashi, 2017; Cox and Takahashi, 2019; Rosensweig and Green, 2020).

This TTFL generates endogenous circadian rhythms even under constant conditions (absent environmental or behavioral rhythms). These endogenous rhythms are present in nearly all cells and physiological systems, including those of involved with neuronal, metabolic, immune, inflammatory, and vascular function (Thosar et al., 2018, 2019). Collapse of this TTLF leads to internal cellular desynchrony and systemic circadian rhythm disruption. Circadian rhythm disruption results in a higher risk, as well as being an early indicator, for disease (Foster, 2020).

6. Circadian influences on cells of the NVU

Although much of the circadian variation in the neurovascular system is coordinated by the pacemaker function of the SCN, there are also likely local rhythms present within the molecular clocks of the cellular components of the NVU. Each component of the NVU is closely linked. The circadian influences on cells of the NVU are numerous resulting in discrete alterations in these cells across the day night cycle (Figure 4). There is a need to investigate the free-running rhythms in cells of the NVU under constant conditions. Nevertheless, to understand these influences as they currently stand, the various cell types of the NVU will be evaluated individually.

6.1. Neuroendothelial cells

The endothelial cells of the BBI are distinct from other endothelial cells. Rather than forming a semi-permeable conduit for the blood, as in the periphery, neuroendothelial cells form a barrier between the brain and the blood, permitting only a few types of molecules to cross. They form a cellular layer with high electrical resistance, tight intercellular junctions, specific transporters, and decreased levels of vesicular transcellular transport compared to peripheral endothelial cells (Betz and Goldstein, 1978; Betz et al., 1980; Daneman, 2012). The activity of efflux transporters is an important regulator of permeability across the BBI. Except in areas of the CVO, there is a general absence of fenestrae in the brain neuroendothelium (Abbott et al., 2010).

Neuroendothelial cells of the luminal membrane of the BBI highly express the ATPase-binding cassette (ABC) efflux transporter, ABCB1, alternatively named permeability glycoprotein (Pgp) and multi-drug resistant protein 1 (MDR1) (Cordon-Cardo et al., 1989; Schinkel et al., 1994). ABCB1 substrate-specific efflux oscillates across the circadian cycle in mouse and human neuroendothelia (Zhang et al., 2021). Although dependent on a functional molecular clock, the ABCB1 transcript family does not exhibit a circadian oscillation nor does the ABC transporter family demonstrate regulation at the transcript level by the circadian clock (Zhang et al., 2021). However, the necessary cofactor in the regulation of ABC transports, intracellular Mg^{2+}, demonstrate circadian oscillations that persist in constant conditions in such diverse examples as a human cell line with epithelial morphology, U2OS cells, as well as a unicellular algae, Osteocossus tauri (Feeney et al., 2016). Further, the transient receptor potential cation channel, subfamily M, member 7 (Trpm7), a Mg^{2+} transporter expressed in neuroendothelial cells, exhibits circadian oscillations in

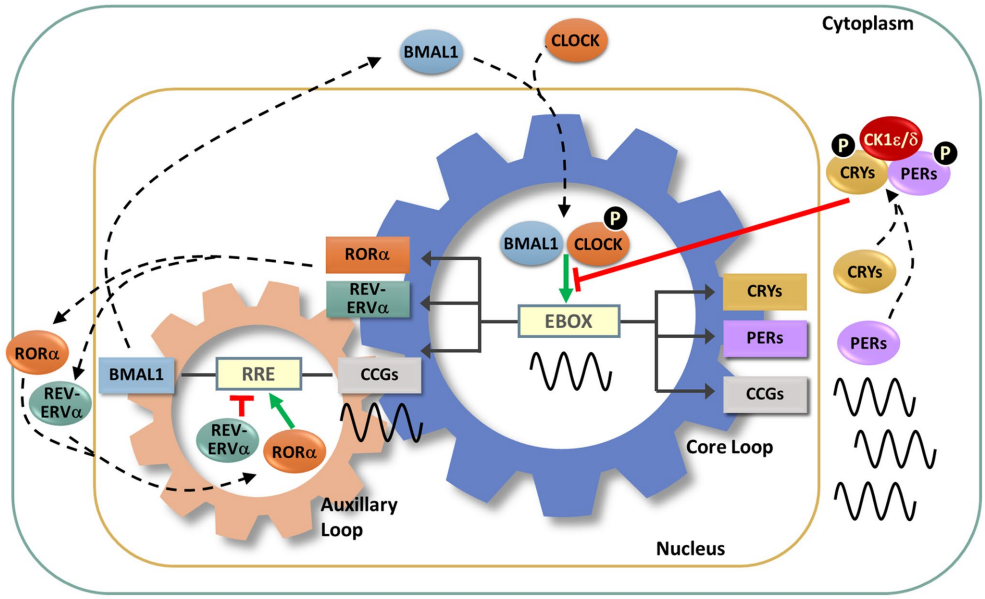

FIGURE 3
Molecular circadian clockwork is composed of two interlocking transcription/translation feedback loops (TTFLs). The clock proteins, CLOCK and BMAL1, are integral components of the core circadian timekeeping loop. They form a heterodimer, then induce E-box-mediated transcription of negative regulators, *Period* (*Per1,2,3*) and *Cryptochrome* (*Cry1,2*) genes. Accumulated PER and CRY proteins repress E-box-mediated transcription until their levels decrease, allowing the cycle to repeat. CLOCK and BMAL1 also control the transcription of the nuclear receptors RORα and REV-ERBα, which modulate BMAL1 mRNA levels by competitive actions on the RRE element residing in the *Bmal1* promoter. The cycling of clock components collectively determines the temporal patterning and levels of clock-controlled genes (CCGs), thus generating diverse circadian rhythmic outputs. In addition, a number of signaling molecules, including kinases and ubiquitinases, fine-tune these molecular clock loops. Casein kinase Iε (CKIε) and CKIδ form a complex with PERs and CRYs, phosphorylate (P) PERs and then promote proteasome-dependent degradation of these negative regulators. Phosphorylation of CLOCK facilitates its dimerization with BMAL1 and nuclear entry.

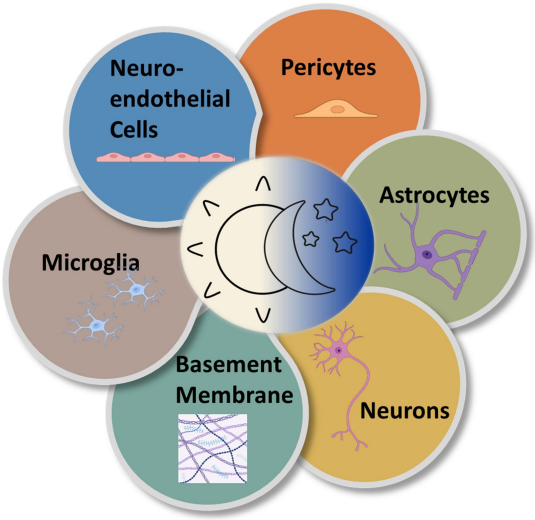

FIGURE 4
Circadian rhythms are expressed in the various cell types of the NVU. Multiple types of cells comprise the NVU and contribute to neurovascular function. All express near-24-h oscillations in functionality.

its transcript (Zhang et al., 2021). Thus, efflux by transporters, such as ABCB1, may be regulated through its co-factor, via daily fluctuations in intracellular Mg^{2+}.

The barrier function of the BBI is regulated by neuroendothelial tight-junction proteins. Tight junctions contain multiple protein complexes, which may include occludins, claudins, zonula occludens (ZO), and junctional adhesion molecules (JAM). Multiple studies have demonstrated circadian regulation of tight proteins at both the RNA and protein levels, although not specifically in the BBI. In retinal pigment epithelium, claudin 2 (cldn2) was found to display circadian rhythms in both protein and RNA expression (Louer et al., 2020). In the inner retinal blood vessels, claudin-5 was found to be highly dynamic and regulated in a circadian manner by the clock protein BMAL1 (Hudson et al., 2019). In intestinal epithelial cells, occludin and claudin-1 mRNA display oscillations across the day-night cycle and their expression is inversely associated with colonic permeability (Oh-oka et al., 2014). This suggests the potential for diurnal or circadian oscillations in the BBI, but this has yet to be determined.

Additionally, neuroendothelial cells can secrete molecules that affect microglia. One such molecule is the proinflammatory cytokine, tumor necrosis factor alpha (TNFα). Although the primary source of TNFα is macrophages and monocytes, TNFα production in neuroendothelial cells has been noted (Imaizumi et al., 2000). TNFα undergoes circadian oscillations in its uptake and can activate interleukin-15 (IL-15). Notably, IL-15 affects the growth of microglia as well as nitric oxide production. Further, IL-15 and its receptor can feedback, exerting anti-inflammatory roles (Pan et al., 2011).

Neuroendothelial cells contribute to the aforementioned circadian fluctuation in the coagulation/fibrinolytic factors. Thrombomodulin, an endothelial membrane protein that exerts anti-coagulation effects through protein C (de Wouwer et al., 2004), displays circadian

oscillations at both the level of the RNA and protein in lung and heart (Takeda et al., 2007). Plasminogen activator inhibitor-1 (PAI-1), the principal inhibitor of fibrinolysis *in vivo*, exhibits significant circadian variation with peak circulating levels observed in the morning (Angleton et al., 1989), as well as activation by the core clock proteins, CLOCK and BMAL1 (Schoenhard et al., 2003). Whereas tissue plasminogen antigen (t-PA) which catalyzes the conversion of plasminogen into plasmin and thereby promoter of fibrinolysis, also demonstrated daily variations in levels with increasing concentrations found in the afternoon in humans (Liu et al., 2021).

6.2. Astrocytes

The function of astrocytes in the BBI is not fully understood; however, evidence suggests that they induce barrier-like properties in neuroendothelial cells by releasing factors that include TGFβ, glial-derived neurotrophic factor (GDNF), bFGF, and angiopoietin 1 (Abbott et al., 2006), as well as exerting an effect on BBI polarity (Beck et al., 1984). They control neurotransmitter and ion concentrations to maintain homeostatic balance. Astrocytes interface with neuroendothelial cells through the endfeet of specialized processes that line the outer side of cerebral capillaries. They contribute importantly in regulating metabolite levels and brain water content, and they modulate vasodilation. Astrocytes release several molecules that enhance and maintain barrier properties: members of the Hedgehog family, proteins of the renin-angiotensin system, and apolipoprotein (a cholesterol and phospholipid transporter).

Circadian fluctuations in astrocyte structure and function throughout the brain are well documented (McKee et al., 2020; Naseri Kouzehgarani et al., 2022; Rojo et al., 2022; Hastings et al., 2023). Astrocytes contribute to cell–cell coupling in the SCN, undergo daily changes in GFAP distribution and structural complexity, and physical coverage of neurons. Glia respond to daily oscillations in neuronal activity (McKee et al., 2020, Naseri Kouzehgarani et al., 2022, Rojo et al., 2022, Hastings et al., 2023). They may also be involved in thermoregulation, hormonal secretion, and sleep (McKee et al., 2020).

The role of circadian rhythms in astrocyte structure and function in neurovascular function is less understood. However, it is notable that the water channel, aquaporin 4 (AQP4) displays day-night differences in expression levels. AQP4 can control fluid exchange bidirectionally. It is abundant in astrocytes associated with the neurovasculature and is present in high density in astrocytic endfeet bordering blood vessels. Although no difference in the total level of AQP4 has been reported, its polarization to vascular structures is highest during the day in the cortex of rodents suggesting diurnal variation in water exchange across the BBI (Hablitz et al., 2020). Mice deficient in AQP4 display profound reduction in glymphatic clearance (Iliff et al., 2012; Lundgaard et al., 2017), however with regard to BBI integrity, studies lack consensus (Zhou et al., 2008; Saadoun et al., 2009; Haj-Yasein et al., 2011). This topic merits further careful analysis.

6.3. Neurons

There is significant heterogeneity in the innervation of the NVU. Broadly, larger, surface extracranial cerebral vessels (such as carotid arteries, vertebral arteries and jugular veins) and intracranial vessels (pial arteries, perforant arteries and pial veins) receive peripheral or extrinsic innervation by cranial autonomic ganglia. Input is derived from sympathetic nerves originating from the superior cervical ganglia, parasympathetic nerves from the sphenopalatine ganglion or otic ganglion, and sensory nerves from the trigeminal ganglion releasing a number of neuropeptides (including substance P, calcitonin gene-related peptide, vasoactive intestinal peptide, pituitary adenylate cyclase-activating peptide, neuropeptide Y, and somatostatin) (Hamel, 2006; Schaeffer and Iadecola, 2021). On the other hand, smaller penetrating arterioles and capillaries receive central or intrinsic innervation via nerve terminals from local interneurons or subcortical pathways, such as the thalamus, locus coeruleus, raphe nucleus and basal forebrain. Communication is mediated via a number of different factors, including neuropeptides, neurotransmitters, prostaglandins, ions, and NO (Giorgi et al., 2020; Schaeffer and Iadecola, 2021).

At the local level, neurons of the NVU directly and indirectly control local cerebral blood flow via neurovascular coupling or function hyperemia in response to neuronal activity, as well as impact vascular networks and BBI formation through release of vasoactive agents (Attwell et al., 2010; Whiteus et al., 2014; McConnell et al., 2017; Kugler et al., 2021). Much of the local neurovascular coupling involved the increased release of glutamate with neuronal activity. Glutamate release can activate neuronal and glial signaling pathways that release vasoactive effectors. Mediators of local neurovascular coupling through inhibitory interneurons have demonstrated the ability to either induce vasodilation or vasoconstriction (Cauli et al., 2004; Rancillac et al., 2006).

Much less is known about the role of circadian neuronal activity in regulating neurovascular function. The numerous neuronal releasates involved in NVU regulation are beyond the scope of this review. We focus on examples with regards to circadian function rather than those involved in acute, inducible alterations to the NVU. Regarding intrinsic innervations that project to cortical microvessels, a number of subcortical pathways are associated with wakefulness and undergo alterations with sleep deprivation. The locus coeruleus expresses 24-h rhythms in the noradrenaline rate-limiting enzyme tyrosine hydroxylase in animals housed under both light:dark (LD) and continuous dark (DD) conditions (Caputo et al., 2023). Additionally, functional MRI in humans has linked cerebral blood flow to diurnal modulation in regions of the default-mode network displaying a decrease in from morning into the afternoon. The default mode network is primarily composed of the medial temporal lobe, the medial prefrontal cortex, and the posterior cingulate cortex and associated with internal thought, active while not engaged in specific tasks (Hodkinson et al., 2014). One of these mediators is nitric active during oxide (NO). NO is generated by a family of three nitric oxide synthase (NOS) isoforms: neuronal NOS (nNOS); endothelial NOS (eNOS), and inducible NOS (iNOS). Although nNOS is abundantly expressed in neurons, it is also expressed in non-neuronal cells (Boulanger et al., 1998; Loesch et al., 1998; Schwarz et al., 1999). It has been argued that the nNOS form participates significantly in regulating microvascular tone (Costa et al., 2016). However, both eNOS and nNOS have been linked to control of vascular tone (Kurihara et al., 1998; Fleming, 2003; Hagioka et al., 2005; Förstermann and Münzel, 2006; Lemmer and Arraj, 2008; Seddon et al., 2008) Multiple genes

(*eNOS*, *caveolin1* and *3*) and proteins (tetrahydrobiopterin, phospho-Akt, phospho-eNOS) linked to NO-induced vasodilation display circadian expression, however, their rhythmic regulation in the neurons of the NVU has not been determined (Panda et al., 2002; Rudic et al., 2005; Kunieda et al., 2008; Anea et al., 2009).

Although much research has focused on the effect of neuronal activities on CBF, recent work also has demonstrated an influence of neurons of the NVU on BBI permeability. Elevated expression and function of a major neuroendothelial ABC efflux transporter, P-glycoprotein (pgp), was found to be correlated to decreases in neuronal activity. A diurnal rhythm in pgp substrates efflux was negated in a knockout of the clock gene, Bmal1 (Pulido et al., 2020).

6.4. Pericytes

Pericytes are imbedded in the basement membrane in direct contact with neuroendothelial cells, wrapping around the tightly-connected neuroendothelial cells. They are found in the capillary bed but display a marked preference for junctional locations within branching capillaries (Mughal et al., 2023). They have been found to play a regulatory role in brain angiogenesis (the formation of new capillaries from existing ones), neuroendothelial cell-tight junction formation, and differentiation of the blood–brain interface, as well as contribute to structural stability. The CNS vasculature has a significantly higher pericyte coverage compared with peripheral vessels (Winkler et al., 2011; Hall et al., 2014).

Pericytes rhythmically express a number of circadian genes (Mastrullo et al., 2022). A mouse line lacking BMAL1 exhibited a decrease in pericyte coverage within the NVU. This decrease in pericyte coverage increased permeability within the BBI, led to a decrease in platelet-derived growth factor receptor β (PDGFRβ) transcription. The PDGFR is important for BBI integrity (Nakazato et al., 2017b). Exposure to synchronized pericytes in a contact co-culture also synchronizes neuroendothelial circadian rhythms of Bmal1:luciferase, a clock gene reporter (Mastrullo et al., 2022).

6.5. Vascular smooth muscle cells

Vascular smooth muscle cells (VSMC) of the NVU are responsible for constriction and dilation of larger arterial and arteriole blood vessels, regulating vascular resistance and blood pressure and stabilizing smaller downstream vessels from the pulsative effect of heartbeat. At this level neurovascular tone is regulated by the relaxation and contraction of VSMC. Hyperpolarization results in the relaxation of the VSMC whereas depolarization results in contraction of the VSMC and constriction of the blood vessels. A number of factors can influence VSMC, including the sympathetic nervous system (discussed in section 6.3) circulating mediators, and endothelial cells (Sandoo et al., 2010; Kisler et al., 2017).

Most work on the influence of the circadian clock in smooth muscle has focused on the peripheral vascular system and not specifically on smooth muscle within neurovascular system. Mesenteric smooth muscle and the aorta exhibit time-of-day variation in contractility in response to vasoconstricting and vasodilating stimuli (Keskil et al., 1996; Witte et al., 2001; Denniff et al., 2014). Molecular clocks have been described in smooth muscle cells (Nonaka et al., 2001) and mesenteric arteries (Denniff et al., 2014). They rhythmically display a number of genes involve in structural integrity in an immortalized vascular smooth muscle cell line, including metalloproteinase 1 and 3 (*timp1*/3), collagen 3a1 (*col3a1*), transgelin 1 (*sm22alpha*), and calponin 1 (*cnn1*) (Chalmers et al., 2008). Deletion of the clock gene, Bmal1, specifically in vascular smooth muscle cells abolishes the circadian variation in pulse pressure and attenuates the amplitude of the daily rhythm in systolic and diastolic blood pressure (Xie et al., 2015). Insights on the molecular circadian clock as well as the effect of a dysfunctional clock specifically on the VSMC within the NVU would be useful, but this has yet to be studied.

6.6. Microglia

Microglia are associated with numerous functions within the brain including trophic support, angiogenesis, the regulation of synaptic pruning and neuronal activity (Geloso and D'Ambrosi, 2021; Umpierre and Wu, 2021); however, within the context of the NVU, they are more closely linked to immune surveillance, repairing damage to the BBI as well as regulating vascular tone (Lou et al., 2016; Bisht et al., 2021). Microglia are the resident immune cells in the CNS. In this role, they actively monitor the brain parenchyma via highly motile protrusions and increase phagocytic activity and cytokine production in response to pathogens, neuroinflammation and tissue damage (Madore et al., 2020). Their role in regulating vascular tone involves capillary-associated microglia (CAMS), found in close contact with the capillary wall in the brain in areas not covered by astrocytic endfeet. Loss of CAMS increases blood flow by increasing capillary diameter and results in impaired responses to vasodilation (Bisht et al., 2021).

Microglia have been shown to contain a functional molecular clock and exhibit circadian expression of a number of clock genes, which remain rhythmic in constant conditions, as well as rhythmic expression of a number of microglial markers (Nakazato et al., 2011; Hayashi et al., 2013; Guzman-Ruiz et al., 2023). In addition, Wang et al. demonstrated daily oscillations in the expression of pro-inflammatory cytokines (IL-1β and IL-6) and oxidation-related genes (NADPH oxidase 2, Nox2), as well as molecules involved in nutrient utilization (glucose transporter member 5, Glut5) (Wang et al., 2020). Elevated levels of pro-inflammatory cytokine transcripts during the light (inactive) phase in rodents may indicate a higher innate immune activity when they are sleeping during the day.

Functionally, microglia also exhibit diurnal oscillation in phagocytic activity linked to synaptic pruning during sleep (Choudhury et al., 2020). Furthermore, just as peripheral immune cells display circadian alterations in their response to an immune challenge (Marpegan et al., 2009; Spengler et al., 2012), time-of-day effects within the CNS also have been reported. Microglial process extension are more pronounced at a rodent's inactive state (day) compared to night (Takayama et al., 2016). Expression of microglial proinflammatory cytokines (IL-1β, TNFα and IL-6) and the inflammatory pathway are elevated with a immune challenge during a rodent's day (inactive) as compared to night (active) (Fonken et al., 2015; Takayama et al., 2016). It will be important to determine if these day-night differences persist under constant conditions.

Intriguingly, although Cathepsin S (CatS) has not been investigated for a role in altered BBI permeability across the day-night

cycle, its demonstrated circadian expression suggests a possible mechanism by which this could occur. CatS, a microglial-specific cysteine protease within the CNS, displays clock-driven expression (Hayashi et al., 2013). CatS-deficient mice exhibited impaired migration across peripheral endothelial basement membranes (Sukhova et al., 2003). It has the ability to degrade ECM molecules at neutral pH (Liuzzo et al., 1999; Vizovišek et al., 2019) and can mediate BBI permeability through proteolytic processing of the junctional adhesion molecule B (JAM-B) (Sevenich et al., 2014).

6.7. Basement membrane

The vascular basement membrane, an extracellular matrix (ECM) of structural proteins secreted by cells of the NVU, supports vessel development and maintenance of the BBI. It consists predominately of (1) glycoproteins, such as the integrins laminin, collagen, fibronectin, and vitronectin, (2) enzymes associated with ECM remodeling and processing, and (3) soluble growth factors and cytokines. It is sandwiched between neuroendothelial cells and pericytes on one side and astrocytic endfeet on the other. The ECM proteins are key regulators of cell signaling. The ECM exert its effect through adhesion signaling receptors that sense and report the environment and the surrounding cells (Streuli, 2016).

Although less is known about the role of the ECM in circadian neurovascular function, there is a link of the ECM to clock-gene expression. Changes in the stiffness of the microenvironment of the mammary epithelia can modulate BMAL1-CLOCK activity (Yang et al., 2017). The extracellular environment via integrins transmits signals to the cytoskeleton (Akhtar and Streuli, 2013) and daily oscillations in actin polymerization state have been observed in liver (Gerber et al., 2013) and brain (Gillette, unpublished). The depletion of globular (G) actin toward filamentous (F) actin assemblies release myocardin-related transcription factor (MRTF) from the cytoplasm allowing a rhythmic translocation into the nucleus. MRTF is a serum response factor (SRF) cofactor, and as such leads to 24-h cycles of transcriptional activation by genes targeted though the MRTF-SRF signaling pathway. Thus, a link between the ECM and the circadian molecular clock within the NVU may be through actin dynamics (Streuli and Meng, 2019).

7. Impaired neurovascular function with circadian dysregulation

Circadian neurovascular function is essential in balancing the influx and efflux between blood and the brain parenchyma; and thereby, modulating the exchange of nutrients and ions as well as protecting neural tissue from access by toxins and pathogens. Circadian rhythm disruption, interference with a stable circadian cycle, can have profound effects on the regulation CNS homeostasis. There has been a rise in human circadian rhythm disruption due to sleep disruption, travel to different time zones, shift work, and social jetlag that has let in an increase in neurological disorders, cancer, metabolic disorders, and mood disorders (Hatori et al., 2017; Lunn et al., 2017; Schurhoff and Toborek, 2023). Alterations of normal circadian rhythms can have profound effects on the neurovasculature, affecting the BBI, cerebral blood flow (CBF), and immune surveillance (Figure 5). These disruptions can contribute to the severity of pathology and response to treatment, most notably with stroke (Thosar et al., 2018; Ramsey et al., 2020; Liu et al., 2021) and traumatic brain injury (Li et al., 2016).

7.1. Blood–brain interface (BBI)

The BBI plays an integral role in maintaining tight control of brain chemical composition. Understanding the consequences of alterations to the BBI becomes paramount, considering loss of BBI integrity is present in many neurodegenerative disorders, such as Alzheimer's disease and Parkinson's disease (Sweeney et al., 2018). As these diseases involve the accumulation of protein that form fibrils and aggregates, it is important that BBI maintain proper regulation across the interface for removal of waste. Additionally, proteasomal activity follows a circadian rhythm and disruption of these rhythms leads to diminished neuroprotection against protein-plaque formation (Musiek and Holtzman, 2016). Loss of BBI integrity can increase vascular permeability and is associated with cell damage from impaired blood flow and the entrance of toxins into the brain, which can stimulate inflammatory and immune responses. Increases in BBI permeability have been noted with disruption of the molecular clock (Bmal1 knockout) and sleep deprivation (Gómez-González et al., 2013; He et al., 2014; Nakazato et al., 2017b).

With stroke, the blood supply is disrupted, causing essential nutrients not to reach the irreversibly damaged ischemic core, as well as the reversibly injured brain tissue around the ischemic core, the penumbra. Due to an imbalance in ion transport, secondary neuronal damage can occur. Circadian disruptions initiated by weekly phase advances prior to ischemic events exacerbate inflammation and increase in infarct volume (Earnest et al., 2016; Ramsey et al., 2020). It has been suggested that circadian rhythm disruption leads to a propensity for clotting, a prothrombotic state (Liu et al., 2021). A dysfunctional molecular clock in mice, due to either a disruption of *Bmal1* expression or a *Clock* gene mutation, causes a more hypercoagulable state, with alterations in platelet counts and clotting components (Westgate et al., 2008; Hemmeryckx et al., 2011). Considered together, these findings suggest that circadian rhythm dysfunction elevates the risk for greater stroke damage and negative outcome.

7.2. Cerebral blood flow

Circadian regulation of blood flow is well documented in the periphery (Wang et al., 1992; Sano et al., 1995; Hermida et al., 2007; Xie et al., 2015; Douma and Gumz, 2018). Blood pressure rises sharply early in the active period and declines to its lowest levels during sleep. However, in a cohort termed "normal dippers," the mean blood pressure during sleep is 10–20% compared to the daytime-active mean (Hermida et al., 2007). Subjects with a diminished decline in blood pressure ("non-dippers"), have a significantly higher risk for cerebrovascular disease and vascular dementia. Less is known about diurnal alterations in CBF and the consequences of circadian rhythm dysfunction on CBF. Non-invasive measurements of cerebral blood

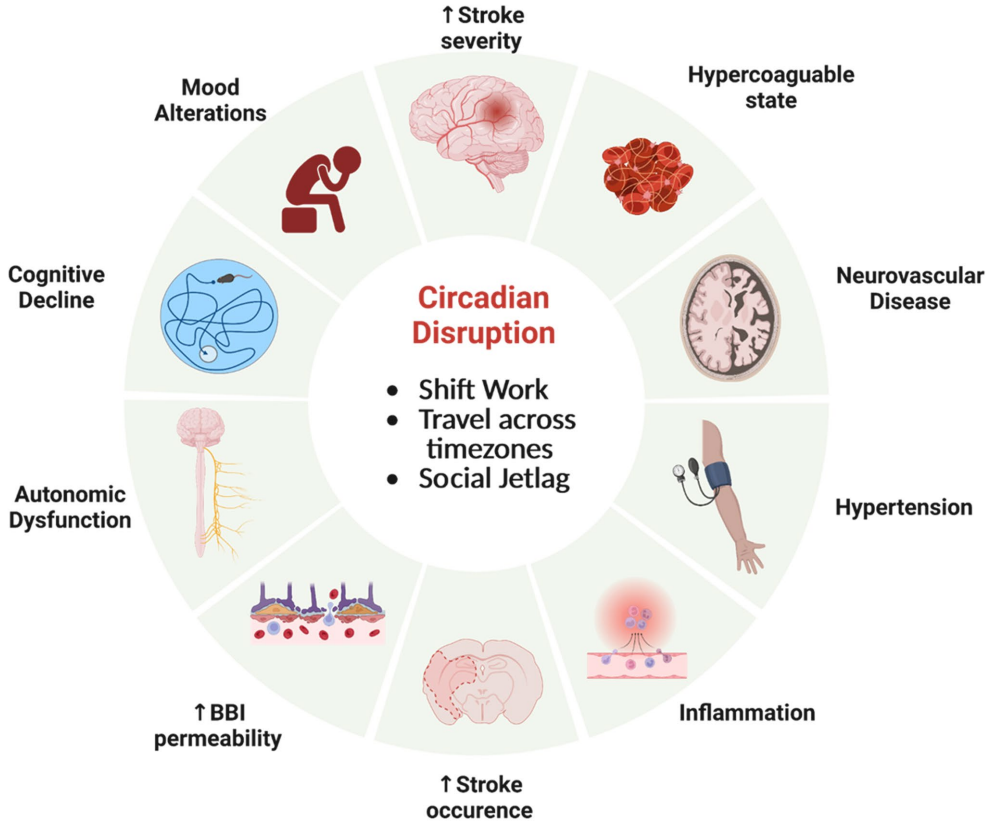

FIGURE 5
Circadian rhythm disfunction adversely effects physiology. Misalignment of circadian clocks between cells, brain regions, tissue, across the organism and the natural world can increase the risk of significant health consequences involving the neurovasculature and brain. Created by Biorender.com.

flow velocity (CBFV) in the middle cerebral artery have been used as a surrogate for CBF. Using these methods, daily rhythms in CBFV in human subjects are lower in morning than in afternoon and evening (Sawaya and Ingvar, 1989; Madsen et al., 1991; Droste et al., 1993; Conroy et al., 2005; Kotajima et al., 2005). This phenomenon is often linked with sleep–wake behaviors. CBFV in healthy humans is reduced in non-REM sleep compared to wakefulness (Madsen et al., 1991; Droste et al., 1993; Kotajima et al., 2005). However, Conroy et al. noted time-of-day variations in human CBFV is not altered following 30-h of sustained wakefulness, and therefore not dependent on sleep (Conroy et al., 2005). Similarly in rats, CBF measured a by laser-Doppler flow probe (over 3–4 days) demonstrated diurnal changes independent of peripheral arterial blood pressure or locomotion (Wauschkuhn et al., 2005). These studies were performed under 12:12-h environmental light:dark conditions. This area would benefit from further studies under constant dark conditions to establish the endogenous nature of these oscillations across the circadian cycle.

Regional CBF has been measured by perfusion MRI. CBF in specific regions was altered in workers performing shift work for >2 years. When compared to daytime workers, the cuneus, fusiform/parahippocampal gyri, and cerebellum of shift workers were significantly decreased, while the inferior occipital gyrus was increased (Park et al., 2019). Alterations in circadian rhythms of blood pressure may have significant consequences for cerebral microbleeds. Patients with cerebral microbleeds have higher nocturnal mean systolic blood pressure and lower nocturnal dipping rates (Chen et al., 2022). Patients with cerebral small vessel disease (CSVD) show disturbance of the circadian rhythms in blood pressure (non-dippers and reverse-dippers) as well as cognitive dysfunction (Xu et al., 2023).

7.3. Immune surveillance and repair

Disruption of circadian rhythms can have deleterious outcomes for immune surveillance and repair within the brain. Mice exposed to experimental jetlag exhibit increases in inflammatory markers in the blood (Castanon-Cervantes et al., 2010). Circadian rhythm disruption by irregular rest-activity cycles that involve light at night enhances pro-inflammatory cytokine expression following an immune challenge (Fonken et al., 2013). Loss of a functional molecular clock alters microglial immune responses. Pro-inflammatory cytokines were reduced in microglia isolated from Bmal1-deficient mice (Wang et al., 2020). The induction of pro-inflammatory cytokines was attenuated under lipopolysaccharide (LPS) immune challenge of a microglial cell line model with Bmal1 knockdown and in Bmal1-deficient mice (Nakazato et al., 2017a; Wang et al., 2020). Disruption of Rev-erbα caused unprompted microglial activation in the hippocampus increased expression of inflammatory transcripts (*IL-1β*/*Trem2*) and elevated the inflammatory response to LPS. Together these data suggest that disruption of the circadian clock alters shifts the pro−/anti-inflammatory balance necessary to maintain normal microglial responses to inflammatory challenges.

Circadian rhythm disruptions also can have profound effects on increasing risk and exacerbating disease states. This is likely mediate

via changes in immune and inflammatory responses to damage or disease, including to ischemia, traumatic brain injury, and neurodegenerative diseases (i.e., Alzheimer's disease, Huntington's disease, and Parkinson's disease) (Li et al., 2016; Ramsey et al., 2020). Alterations to immune surveillance and repair functions within the NVU have significant effects. For example, in mice subjected to cerebral artery occlusion and reperfusion, then chronic circadian rhythm-disruption group displayed increased infarcts. The interpretation is that this is due to alterations in the ratio of pro-to anti-inflammatory cytokine expression (Ramsey et al., 2020). Although circadian rhythm disruption is known to disrupt peripheral immune responses and to alter circulating proinflammatory cytokines and the complement immune system (Comas et al., 2017; Shivshankar et al., 2020), a defective central immune response also is likely to exacerbate diseases states requiring removal of pathogens and damaged cells in brain.

8. Conclusion

The development of the circadian clock in the neurovascular enables anticipation of rhythmic variations that adjust internal states to the 24-h day. In the brain, these changes include oscillations in metabolism, neurohormone secretion, and neurophysiological regulation along with neurovascular components, including cells that form the neurovascular unit and regulate blood flow and platelet aggregation/fibrinolysis. Disruption of the circadian clock has profound effects on mental and physical health. Many disease states are at elevated risk or exacerbated by misalignment of the internal circadian clock (Evans and Davidson, 2013; Foster, 2020; Schurhoff and Toborek, 2023).

Despite significant progress in understanding circadian clocks within the cells of the NVU, knowledge of how the neurovascular units and systems participate in acute responses to cerebrovascular challenges, neurodegenerative diseases, and the aging of the brain is still in its infancy. The roles and risk factors caused by alterations in the circadian system via shift work, travel, and social jet lag are now beginning to be understood. Integrated study of circadian clocks and neurovascular systems has the potential to contribute importantly to understanding cerebral vascular disease, neurodegenerative diseases, and aging, as well as identify isolated key nodes for translational interventions for chronotherapies and other therapeutic benefits.

Author contributions

JM and MG: drafting and refining the manuscript and critical reading of the manuscript. All authors contributed to the article and approved the submitted version.

Funding

The authors gratefully acknowledge support in preparation of this manuscript by the National Heart, Lung, and Blood Institute (1R61/R33HL159948) and the Beckman Institute for Advanced Science and Technology.

Conflict of interest

The authors declare that the research was conducted in the absence of any commercial or financial relationships that could be construed as a potential conflict of interest.

Publisher's note

References

Abbott, N. J., Patabendige, A. A., Dolman, D. E., Yusof, S. R., and Begley, D. J. (2010). Structure and function of the blood-brain barrier. *Neurobiol. Dis.* 37, 13–25. doi: 10.1016/j.nbd.2009.07.030

Abbott, N. J., Ronnback, L., and Hansson, E. (2006). Astrocyte-endothelial interactions at the blood-brain barrier. *Nat. Rev. Neurosci.* 7, 41–53. doi: 10.1038/nrn1824

Andreotti, F., Davies, G. J., Hackett, D. R., Khan, M. I., De Bart, A. C., Aber, V. R., et al. (1988). Major circadian fluctuations in fibrinolytic factors and possible relevance to time of onset of myocardial infarction, sudden cardiac death and stroke. *Am. J. Cardiol.* 62, 635–637. doi: 10.1016/0002-9149(88)90669-8

Andreotti, F., and Kluft, C. (1991). Circadian variation of fibrinolytic activity in blood. *Chronobiol. Int.* 8, 336–351.

Anea, C. B., Zhang, M., Stepp, D. W., Simkins, G. B., Reed, G., Fulton, D. J., et al. (2009). Vascular disease in mice with a dysfunctional circadian clock. *Circulation* 119, 1510–1517. doi: 10.1161/CIRCULATIONAHA.108.827477

Angleton, P., Chandler, W. L., and Schmer, G. (1989). Diurnal variation of tissue-type plasminogen activator and its rapid inhibitor (PAI-1). *Circulation* 79, 101–106. doi: 10.1161/01.CIR.79.1.101

Akhtar, N., and Streuli, C. H. (2013). An integrin–ILK–microtubule network orients cell polarity and lumen formation in glandular epithelium. *Nat. cell bio.* 15, 17–27.

Attwell, D., Buchan, A. M., Charpak, S., Lauritzen, M., Macvicar, B. A., and Newman, E. A. (2010). Glial and neuronal control of brain blood flow. *Nature* 468, 232–243. doi: 10.1038/nature09613

Attwell, D., Mishra, A., Hall, C. N., O'farrell, F. M., and Dalkara, T. (2016). What is a pericyte? *J. Cereb. Blood Flow Metab.* 36, 451–455. doi: 10.1177/0271678X15610340

Bautch, V. L., and James, J. M. (2009). Neurovascular development: the beginning of a beautiful friendship. *Cell Adhes. Migr.* 3, 199–204. doi: 10.4161/cam.3.2.8397

Beck, D. W., Vinters, H. V., Hart, M. N., and Cancilla, P. A. (1984). Glial cells influence polarity of the blood-brain barrier. *J. Neuropathol. Exp. Neurol.* 43, 219–224. doi: 10.1097/00005072-198405000-00001

Betz, A. L., Firth, J. A., and Goldstein, G. W. (1980). Polarity of the blood-brain barrier: distribution of enzymes between the luminal and antiluminal membranes of brain capillary endothelial cells. *Brain Res.* 192, 17–28. doi: 10.1016/0006-8993(80)91004-5

Betz, A. L., and Goldstein, G. W. (1978). Polarity of the blood-brain barrier: neutral amino acid transport into isolated brain capillaries. *Science* 202, 225–227. doi: 10.1126/science.211586

Bisht, K., Okojie, K. A., Sharma, K., Lentferink, D. H., Sun, Y. Y., Chen, H. R., et al. (2021). Capillary-associated microglia regulate vascular structure and function through PANX1-P2RY12 coupling in mice. *Nat. Commun.* 12:5289. doi: 10.1038/s41467-021-25590-8

Boulanger, C. M., Heymes, C., Benessiano, J., Geske, R. S., Lévy, B. I., and Vanhoutte, P. M. (1998). Neuronal nitric oxide synthase is expressed in rat vascular smooth muscle cells: activation by angiotensin II in hypertension. *Circ. Res.* 83, 1271–1278. doi: 10.1161/01.RES.83.12.1271

Bremner, W. F., Sothern, R. B., Kanabrocki, E. L., Ryan, M., Mccormick, J. B., Dawson, S., et al. (2000). Relation between circadian patterns in levels of circulating lipoprotein(a), fibrinogen, platelets, and related lipid variables in men. *Am. Heart J.* 139, 164–173. doi: 10.1016/S0002-8703(00)90324-7

Brightman, M. W., and Reese, T. S. (1969). Junctions between intimately apposed cell membranes in the vertebrate brain. *J. Cell Biol.* 40, 648–677. doi: 10.1083/jcb.40.3.648

Budkowska, M., Lebiecka, A., Marcinowska, Z., Woźniak, J., Jastrzębska, M., and Dołęgowska, B. (2019). The circadian rhythm of selected parameters of the hemostasis system in healthy people. *Thromb. Res.* 182, 79–88. doi: 10.1016/j.thromres.2019.08.015

Budohoski, K. P., Czosnyka, M., Kirkpatrick, P. J., Smielewski, P., Steiner, L. A., and Pickard, J. D. (2013). Clinical relevance of cerebral autoregulation following subarachnoid haemorrhage. *Nat. Rev. Neurol.* 9, 152–163. doi: 10.1038/nrneurol.2013.11

Butt, M. U., Zakaria, M., and Hussain, H. M. (2009). Circadian pattern of onset of ischaemic and haemorrhagic strokes, and their relation to sleep/wake cycle. *J. Pak. Med. Assoc.* 59, 129–132.

Cai, W., Liu, H., Zhao, J., Chen, L. Y., Chen, J., Lu, Z., et al. (2017). Pericytes in brain injury and repair after ischemic stroke. *Transl. Stroke Res.* 8, 107–121. doi: 10.1007/s12975-016-0504-4

Caputo, R., Poirel, V. J., Paiva, I., Boutillier, A. L., Challet, E., Meijer, J. H., et al. (2023). Circadian functioning of locus Cœruleus of the nocturnal rat and diurnal rodent Arvicanthis. *Neurosci. Lett.* 799:137091. doi: 10.1016/j.neulet.2023.137091

Castanon-Cervantes, O., Wu, M., Ehlen, J. C., Paul, K., Gamble, K. L., Johnson, R. L., et al. (2010). Dysregulation of inflammatory responses by chronic circadian disruption. *J. Immunol.* 185, 5796–5805. doi: 10.4049/jimmunol.1001026

Cauli, B., Tong, X. K., Rancillac, A., Serluca, N., Lambolez, B., Rossier, J., et al. (2004). Cortical GABA interneurons in neurovascular coupling: relays for subcortical vasoactive pathways. *J. Neurosci.* 24, 8940–8949. doi: 10.1523/JNEUROSCI.3065-04.2004

Chalmers, J. A., Martino, T. A., Tata, N., Ralph, M. R., Sole, M. J., and Belsham, D. D. (2008). Vascular circadian rhythms in a mouse vascular smooth muscle cell line (Movas-1). *Am. J. Phys. Regul. Integr. Comp. Phys.* 295, R1529–R1538. doi: 10.1152/ajpregu.90572.2008

Chaturvedi, S., Adams, H. P. Jr., and Woolson, R. F. (1999). Circadian variation in ischemic stroke subtypes. *Stroke* 30, 1792–1795. doi: 10.1161/01.STR.30.9.1792

Chen, Y. K., Liang, W. C., Yuan, S. L., Ni, Z. X., Li, W., Liu, Y. L., et al. (2022). Circadian rhythms of blood pressure in hypertensive patients with cerebral microbleeds. *Brain Behav.* 12:e2530. doi: 10.1002/brb3.2530

Cheng, M. Y., Bullock, C. M., Li, C., Lee, A. G., Bermak, J. C., Belluzzi, J., et al. (2002). Prokineticin 2 transmits the behavioural circadian rhythm of the suprachiasmatic nucleus. *Nature* 417, 405–410. doi: 10.1038/417405a

Choudhury, M. E., Miyanishi, K., Takeda, H., Islam, A., Matsuoka, N., Kubo, M., et al. (2020). Phagocytic elimination of synapses by microglia during sleep. *Glia* 68, 44–59. doi: 10.1002/glia.23698

Clarke, I. J. (2015). Hypothalamus as an endocrine organ. *Compr. Physiol.* 5, 217–253. doi: 10.1002/cphy.c140019

Comas, M., Gordon, C. J., Oliver, B. G., Stow, N. W., King, G., Sharma, P., et al. (2017). A circadian based inflammatory response–implications for respiratory disease and treatment. *Sleep Sci. Pract.* 1, 1–19. doi: 10.1186/s41606-017-0019-2

Conroy, D. A., Spielman, A. J., and Scott, R. Q. (2005). Daily rhythm of cerebral blood flow velocity. *J. Circadian Rhythms* 3, 1–11. doi: 10.1186/1740-3391-3-3

Cordon-Cardo, C., O'brien, J. P., Casals, D., Rittman-Grauer, L., Biedler, J. L., Melamed, M. R., et al. (1989). Multidrug-resistance gene (P-glycoprotein) is expressed by endothelial cells at blood-brain barrier sites. *Proc. Natl. Acad. Sci.* 86, 695–698. doi: 10.1073/pnas.86.2.695

Costa, E. D., Rezende, B. A., Cortes, S. F., and Lemos, V. S. (2016). Neuronal nitric oxide synthase in vascular physiology and diseases. *Front. Physiol.* 7:206. doi: 10.3389/fphys.2016.00206

Cox, K. H., and Takahashi, J. S. (2019). Circadian clock genes and the transcriptional architecture of the clock mechanism. *J. Mol. Endocrinol.* 63, R93–R102. doi: 10.1530/JME-19-0153

Crnko, S., Du Pré, B. C., Sluijter, J. P., and Van Laake, L. W. (2019). Circadian rhythms and the molecular clock in cardiovascular biology and disease. *Nat. Rev. Cardiol.* 16, 437–447. doi: 10.1038/s41569-019-0167-4

Daneman, R. (2012). The blood–brain barrier in health and disease. *Ann. Neurol.* 72, 648–672. doi: 10.1002/ana.23648

Daneman, R., Zhou, L., Kebede, A. A., and Barres, B. A. (2010). Pericytes are required for blood-brain barrier integrity during embryogenesis. *Nature* 468, 562–566. doi: 10.1038/nature09513

Davalos, D., Kyu Ryu, J., Merlini, M., Baeten, K. M., Le Moan, N., Petersen, M. A., et al. (2012). Fibrinogen-induced perivascular microglial clustering is required for the development of axonal damage in neuroinflammation. *Nat. Commun.* 3:1227. doi: 10.1038/ncomms2230

De Wouwer, M. V., Collen, D., and Conway, E. M. (2004). Thrombomodulin-protein C-EPCR system: integrated to regulate coagulation and inflammation. *Arterioscler. Thromb. Vasc. Biol.* 24, 1374–1383. doi: 10.1161/01.ATV.0000134298.25489.92

Denniff, M., Turrell, H. E., Vanezis, A., and Rodrigo, G. C. (2014). The time-of-day variation in vascular smooth muscle contractility depends on a nitric oxide signalling pathway. *J. Mol. Cell. Cardiol.* 66, 133–140. doi: 10.1016/j.yjmcc.2013.11.009

Ding, J. M., Chen, D., Weber, E. T., Faiman, L. E., Rea, M. A., and Gillette, M. U. (1994). Resetting the biological clock: mediation of nocturnal circadian shifts by glutamate and NO. *Science* 266, 1713–1717. doi: 10.1126/science.7527589

Douma, L. G., and Gumz, M. L. (2018). Circadian clock-mediated regulation of blood pressure. *Free Radic. Biol. Med.* 119, 108–114. doi: 10.1016/j.freeradbiomed.2017.11.024

Droste, D., Berger, W., Schuler, E., and Krauss, J. (1993). Middle cerebral artery blood flow velocity in healthy persons during wakefulness and sleep: a transcranial Doppler study. *Sleep* 16, 603–609.

Dudvarski Stankovic, N., Teodorczyk, M., Ploen, R., Zipp, F., and Schmidt, M. H. (2016). Microglia–blood vessel interactions: a double-edged sword in brain pathologies. *Acta Neuropathol.* 131, 347–363. doi: 10.1007/s00401-015-1524-y

Duffin, J., Mikulis, D. J., and Fisher, J. A. (2021). Control of cerebral blood flow by blood gases. *Front. Physiol.* 12:640075. doi: 10.3389/fphys.2021.640075

Earnest, D. J., Neuendorff, N., Coffman, J., Selvamani, A., and Sohrabji, F. (2016). Sex differences in the impact of shift work schedules on pathological outcomes in an animal model of ischemic stroke. *Endocrinology* 157, 2836–2843. doi: 10.1210/en.2016-1130

Ek, C. J., Dziegielewska, K. M., Habgood, M. D., and Saunders, N. R. (2012). Barriers in the developing brain and Neurotoxicology. *Neurotoxicology* 33, 586–604. doi: 10.1016/j.neuro.2011.12.009

Elliott, W. J. (1998). Circadian variation in the timing of stroke onset: a meta-analysis. *Stroke* 29, 992–996. doi: 10.1161/01.STR.29.5.992

Evans, J. A., and Davidson, A. J. (2013). "Chapter ten-health consequences of circadian disruption in humans and animal models" in *Progress in molecular biology and translational science*. ed. M. U. Gillette (Cambridge, MA: Academic Press)

Fabiani, M., Rypma, B., and Gratton, G. (2021). Aging and cerebrovascular health: structural, functional, cognitive, and methodological implications. *Psychophysiology* 58:e13842. doi: 10.1111/psyp.13842

Feeney, K. A., Hansen, L. L., Putker, M., Olivares-Yañez, C., Day, J., Eades, L. J., et al. (2016). Daily magnesium fluxes regulate cellular timekeeping and energy balance. *Nature* 532, 375–379. doi: 10.1038/nature17407

Feeney, J. F. Jr., and Watterson, R. L. (1946). The development of the vascular pattern within the walls of the central nervous system of the chick embryo. *J. Morphol.* 78, 231–303. doi: 10.1002/jmor.1050780205

Fleming, I. (2003). Brain in the brawn: The neuronal nitric oxide synthase as a regulator of myogenic tone. *Circ Res* 93, 586–588. doi: 10.1161/01.RES.0000095380.06622.D8

Fonken, L. K., Frank, M. G., Kitt, M. M., Barrientos, R. M., Watkins, L. R., and Maier, S. F. (2015). Microglia inflammatory responses are controlled by an intrinsic circadian clock. *Brain Behav. Immun.* 45, 171–179. doi: 10.1016/j.bbi.2014.11.009

Fonken, L. K., Weil, Z. M., and Nelson, R. J. (2013). Mice exposed to dim light at night exaggerate inflammatory responses to lipopolysaccharide. *Brain Behav. Immun.* 34, 159–163. doi: 10.1016/j.bbi.2013.08.011

Förstermann, U., and Münzel, T. (2006). Endothelial nitric oxide synthase in vascular disease. *Circulation* 113, 1708–1714. doi: 10.1161/CIRCULATIONAHA.105.602532

Foster, R. G. (2020). Sleep, circadian rhythms and health. *Interface Focus* 10:20190098. doi: 10.1098/rsfs.2019.0098

Geloso, M. C., and D'ambrosi, N. (2021). Microglial pruning: relevance for synaptic dysfunction in multiple sclerosis and related experimental models. *Cells* 10:686. doi: 10.3390/cells10030686

Gerber, A., Esnault, C., Aubert, G., Treisman, R., Pralong, F., and Schibler, U. (2013). Blood-borne circadian signal stimulates daily oscillations in actin dynamics and SRF activity. *Cells* 152, 492–503. doi: 10.1016/j.cell.2012.12.027

Gillette, M. U., and Reppert, S. M. (1987). The hypothalamic suprachiasmatic nuclei: circadian patterns of vasopressin secretion and neuronal activity in vitro. *Brain Res. Bull.* 19, 135–139. doi: 10.1016/0361-9230(87)90176-6

Giorgi, F. S., Galgani, A., Puglisi-Allegra, S., Limanaqi, F., Busceti, C. L., and Fornai, F. (2020). Locus Coeruleus and neurovascular unit: from its role in physiology to its potential role in Alzheimer's disease pathogenesis. *J. Neurosci. Res.* 98, 2406–2434. doi: 10.1002/jnr.24718

Gizowski, C., and Bourque, C. W. (2020). Sodium regulates clock time and output via an excitatory GABAergic pathway. *Nature* 583, 421–424. doi: 10.1038/s41586-020-2471-x

Gizowski, C., Zaelzer, C., and Bourque, C. W. (2018). Activation of organum vasculosum neurones and water intake in mice by vasopressin neurones in the suprachiasmatic nucleus. *J. Neuroendocrinol.* 30:e12577. doi: 10.1111/jne.12577

Gómez-González, B., Hurtado-Alvarado, G., Esqueda-León, E., Santana-Miranda, R., Rojas-Zamorano, J., and Velázquez-Moctezuma, J. (2013). REM sleep loss and recovery regulates blood-brain barrier function. *Curr. Neurovasc. Res.* 10, 197–207. doi: 10.2174/15672026113109990002

Gooley, J. J., Lu, J., Chou, T. C., Scammell, T. E., and Saper, C. B. (2001). Melanopsin in cells of origin of the retinohypothalamic tract. *Nat. Neurosci.* 4:1165. doi: 10.1038/nn768

Gross, P. M., Weindl, A., and Knigge, K. M. (1987). Peering through the windows of the brain. *J. Cereb. Blood Flow Metab.* 7, 663–672. doi: 10.1038/jcbfm.1987.120

Guo, S., Wang, H., and Yin, Y. (2022). Microglia polarization from M1 to M2 in neurodegenerative diseases. *Front. Aging Neurosci.* 14:815347. doi: 10.3389/fnagi.2022.815347

Guzman-Ruiz, M. A., Guerrero-Vargas, N. N., Lagunes-Cruz, A., Gonzalez-Gonzalez, S., Garcia-Aviles, J. E., Hurtado-Alvarado, G., et al. (2023). Circadian modulation of microglial physiological processes and immune responses. *Glia* 71, 155–167. doi: 10.1002/glia.24261

Hablitz, L. M., Plá, V., Giannetto, M., Vinitsky, H. S., Stæger, F. F., Metcalfe, T., et al. (2020). Circadian control of brain glymphatic and lymphatic fluid flow. *Nat. Commun.* 11:4411. doi: 10.1038/s41467-020-18115-2

Hagioka, S., Takeda, Y., Zhang, S., Sato, T., and Morita, K. (2005). Effects of 7-nitroindazole and N-nitro-l-arginine methyl ester on changes in cerebral blood flow and nitric oxide production preceding development of hyperbaric oxygen-induced seizures in rats. *Neurosci. Lett.* 382, 206–210. doi: 10.1016/j.neulet.2005.01.006

Haj-Yasein, N. N., Vindedal, G. F., Eilert-Olsen, M., Gundersen, G. A., Skare, Ø., Laake, P., et al. (2011). Glial-conditional deletion of aquaporin-4 (Aqp4) reduces blood–brain water uptake and confers barrier function on perivascular astrocyte endfeet. *Proc. Natl. Acad. Sci.* 108, 17815–17820. doi: 10.1073/pnas.1110655108

Hall, C. N., Reynell, C., Gesslein, B., Hamilton, N. B., Mishra, A., Sutherland, B. A., et al. (2014). Capillary pericytes regulate cerebral blood flow in health and disease. *Nature* 508, 55–60. doi: 10.1038/nature13165

Hamel, E. (2006). Perivascular nerves and the regulation of cerebrovascular tone. *J. Appl. Physiol.* 1985, 1059–1064. doi: 10.1152/japplphysiol.00954.2005

Harris, G. (1948). Neural control of the pituitary gland. *Physiol. Rev.* 28, 139–179. doi: 10.1152/physrev.1948.28.2.139

Hastings, M. H., Brancaccio, M., Gonzalez-Aponte, M. F., and Herzog, E. D. (2023). Circadian rhythms and astrocytes: the good, the bad, and the ugly. *Annu. Rev. Neurosci.* 46, 123–143. doi: 10.1146/annurev-neuro-100322-112249

Hatori, M., Gronfier, C., Van Gelder, R. N., Bernstein, P. S., Carreras, J., Panda, S., et al. (2017). Global rise of potential health hazards caused by blue light-induced circadian disruption in modern aging societies. *NPJ Aging Mech. Dis.* 3:9. doi: 10.1038/s41514-017-0010-2

Hayashi, Y., Koyanagi, S., Kusunose, N., Okada, R., Wu, Z., Tozaki-Saitoh, H., et al. (2013). The intrinsic microglial molecular clock controls synaptic strength via the circadian expression of cathepsin S. *Sci. Rep.* 3:2744. doi: 10.1038/srep02744

He, J., Hsuchou, H., He, Y., Kastin, A. J., Wang, Y., and Pan, W. (2014). Sleep restriction impairs blood-brain barrier function. *J. Neurosci.* 34, 14697–14706. doi: 10.1523/JNEUROSCI.2111-14.2014

Hemmeryckx, B., Van Hove, C. E., Fransen, P., Emmerechts, J., Kauskot, A., Bult, H., et al. (2011). Progression of the prothrombotic state in aging Bmal1-deficient mice. *Arterioscler. Thromb. Vasc. Biol.* 31, 2552–2559. doi: 10.1161/ATVBAHA.111.229062

Hermida, R. C., Ayala, D. E., and Portaluppi, F. (2007). Circadian variation of blood pressure: the basis for the chronotherapy of hypertension. *Adv. Drug Deliv. Rev.* 59, 904–922. doi: 10.1016/j.addr.2006.08.003

Hill, R. A., Tong, L., Yuan, P., Murikinati, S., Gupta, S., and Grutzendler, J. (2015). Regional blood flow in the normal and ischemic brain is controlled by arteriolar smooth muscle cell contractility and not by capillary pericytes. *Neuron* 87, 95–110. doi: 10.1016/j.neuron.2015.06.001

Hodkinson, D. J., O'daly, O., Zunszain, P. A., Pariante, C. M., Lazurenko, V., Zelaya, F. O., et al. (2014). Circadian and homeostatic modulation of functional connectivity and regional cerebral blood flow in humans under normal entrained conditions. *J. Cereb. Blood Flow Metab.* 34, 1493–1499. doi: 10.1038/jcbfm.2014.109

Hoiland, R. L., Caldwell, H. G., Howe, C. A., Nowak-Flück, D., Stacey, B. S., Bailey, D. M., et al. (2020). Nitric oxide is fundamental to neurovascular coupling in humans. *J. Physiol.* 598, 4927–4939. doi: 10.1113/JP280162

Hosford, P. S., and Gourine, A. V. (2019). What is the key mediator of the neurovascular coupling response? *Neurosci. Biobehav. Rev.* 96, 174–181. doi: 10.1016/j.neubiorev.2018.11.011

Hudson, N., Celkova, L., Hopkins, A., Greene, C., Storti, F., Ozaki, E., et al. (2019). Dysregulated claudin-5 cycling in the inner retina causes retinal pigment epithelial cell atrophy. *JCI insight* 4:e130273. doi: 10.1172/jci.insight.130273

Iliff, J., Wang, M., Liao, Y., Plogg, B., Peng, W., Gundersen, G., et al. (2012, 2012). A paravascular pathway facilitates CSF flow through the brain parenchyma and the clearance of interstitial solutes, including amyloid β. *Sci. Transl. Med.* 4:147ra111. doi: 10.1126/scitranslmed.3003748

Imaizumi, T., Itaya, H., Fujita, K., Kudoh, D., Kudoh, S., Mori, K., et al. (2000). Expression of tumor necrosis factor-α in cultured human endothelial cells stimulated with lipopolysaccharide or interleukin-1α. *Arterioscler. Thromb. Vasc. Biol.* 20, 410–415. doi: 10.1161/01.ATV.20.2.410

Jafri, S. M., Vanrollins, M., Ozawa, T., Mammen, E. F., Goldberg, A. D., and Goldstein, S. (1992). Circadian variation in platelet function in healthy volunteers. *Am. J. Cardiol.* 69, 951–954. doi: 10.1016/0002-9149(92)90799-5

Janssen, B. J., Tyssen, C. M., Duindam, H., and Rietveld, W. J. (1994). Suprachiasmatic lesions eliminate 24-h blood pressure variability in rats. *Physiol. Behav.* 55, 307–311. doi: 10.1016/0031-9384(94)90138-4

Jolivel, V., Bicker, F., Binamé, F., Ploen, R., Keller, S., Gollan, R., et al. (2015). Perivascular microglia promote blood vessel disintegration in the ischemic penumbra. *Acta Neuropathol.* 129, 279–295. doi: 10.1007/s00401-014-1372-1

Kagerbauer, S. M., Martin, J., Schuster, T., Blobner, M., Kochs, E. F., and Landgraf, R. (2013). Plasma oxytocin and vasopressin do not predict neuropeptide concentrations in human cerebrospinal fluid. *J. Neuroendocrinol.* 25, 668–673. doi: 10.1111/jne.12038

Kalsbeek, A., Perreau-Lenz, S., and Buijs, R. M. (2006). A network of (autonomic) clock outputs. *Chronobiol. Int.* 23, 521–535. doi: 10.1080/07420520600651073

Kaplan, L., Chow, B. W., and Gu, C. (2020). Neuronal regulation of the blood–brain barrier and neurovascular coupling. *Nat. Rev. Neurosci.* 21, 416–432. doi: 10.1038/s41583-020-0322-2

Keaney, J., and Campbell, M. (2015). The dynamic blood-brain barrier. *FEBS J.* 282, 4067–4079. doi: 10.1111/febs.13412

Keskil, Z., Gorgun, C. Z., Hodoglugil, U., and Zengil, H. (1996). Twenty-four-hour variations in the sensitivity of rat aorta to vasoactive agents. *Chronobiol. Int.* 13, 465–475.

Kisler, K., Nelson, A. R., Montagne, A., and Zlokovic, B. V. (2017). Cerebral blood flow regulation and neurovascular dysfunction in Alzheimer disease. *Nat. Rev. Neurosci.* 18, 419–434. doi: 10.1038/nrn.2017.48

Kluft, C., Jie, A., Rijken, D., and Verheijen, J. (1988). Daytime fluctuations in blood of tissue-type plasminogen activator (t-PA) and its fast-acting inhibitor (PAI-1). *Thromb. Haemost.* 59, 329–332.

Kniesel, U., and Wolburg, H. (2000). Tight junctions of the blood–brain barrier. *Cell. Mol. Neurobiol.* 20, 57–76. doi: 10.1023/A:1006995910836

Koide, M., Bonev, A. D., Nelson, M. T., and Wellman, G. C. (2012). Inversion of neurovascular coupling by subarachnoid blood depends on large-conductance Ca2+−activated K+ (BK) channels. *Proc. Natl. Acad. Sci. U. S. A.* 109, E1387–E1395. doi: 10.1073/pnas.1121359109

Kotajima, F., Meadows, G. E., Morrell, M. J., and Corfield, D. R. (2005). Cerebral blood flow changes associated with fluctuations in alpha and theta rhythm during sleep onset in humans. *J. Physiol.* 568, 305–313. doi: 10.1113/jphysiol.2005.092577

Kraves, S., and Weitz, C. J. (2006). A role for cardiotrophin-like cytokine in the circadian control of mammalian locomotor activity. *Nat. Neurosci.* 9, 212–219. doi: 10.1038/nn1633

Kugler, E. C., Greenwood, J., and Macdonald, R. B. (2021). The "neuro-glial-vascular" unit: the role of glia in neurovascular unit formation and dysfunction. *Front. Cell Develop. Biol.* 9:732820. doi: 10.3389/fcell.2021.732820

Kunieda, T., Minamino, T., Miura, K., Katsuno, T., Tateno, K., Miyauchi, H., et al. (2008). Reduced nitric oxide causes age-associated impairment of circadian rhythmicity. *Circ. Res.* 102, 607–614. doi: 10.1161/CIRCRESAHA.107.162230

Kurihara, N., Alfie, M. E., Sigmon, D. H., Rhaleb, N.-E., Shesely, E. G., and Carretero, O. A. (1998). Role of nNOS in blood pressure regulation in eNOS null mutant mice. *Hypertension* 32, 856–861. doi: 10.1161/01.HYP.32.5.856

Kwon, D. (2022). Guardians of the brain: how a special immune system protects our grey matter. *Nature* 606, 22–24. doi: 10.1038/d41586-022-01502-8

Lemmer, B., and Arraj, M. (2008). Effect of NO synthase inhibition on cardiovascular circadian rhythms in wild-type and eNOS-knock-out mice. *Chronobiol. Int.* 25, 501–510. doi: 10.1080/07420520802257695

Li, D., Ma, S., Guo, D., Cheng, T., Li, H., Tian, Y., et al. (2016). Environmental circadian disruption worsens neurologic impairment and inhibits hippocampal neurogenesis in adult rats after traumatic brain injury. *Cell. Mol. Neurobiol.* 36, 1045–1055. doi: 10.1007/s10571-015-0295-2

Liebner, S., Dijkhuizen, R. M., Reiss, Y., Plate, K. H., Agalliu, D., and Constantin, G. (2018). Functional morphology of the blood-brain barrier in health and disease. *Acta Neuropathol.* 135, 311–336. doi: 10.1007/s00401-018-1815-1

Liu, J. A., Walton, J. C., Devries, A. C., and Nelson, R. J. (2021). Disruptions of circadian rhythms and thrombolytic therapy during ischemic stroke intervention. *Front. Neurosci.* 15:675732. doi: 10.3389/fnins.2021.766648

Liuzzo, J. P., Petanceska, S. S., Moscatelli, D., and Devi, L. A. (1999). Inflammatory mediators regulate cathepsin S in macrophages and microglia: a role in attenuating heparan sulfate interactions. *Mol. Med.* 5, 320–333. doi: 10.1007/BF03402068

Loesch, A., Milner, P., and Burnstock, G. (1998). Endothelin in perivascular nerves. An electronimmunocytochemical study of rat basilar artery. *Neuroreport* 9, 3903–3904. doi: 10.1097/00001756-199812010-00025

Lou, N., Takano, T., Pei, Y., Xavier, A. L., Goldman, S. A., and Nedergaard, M. (2016). Purinergic receptor P2RY12-dependent microglial closure of the injured blood–brain barrier. *Proc. Natl. Acad. Sci.* 113, 1074–1079. doi: 10.1073/pnas.1520398113

Louer, E. M. M., Günzel, D., Rosenthal, R., Carmone, C., Yi, G., Stunnenberg, H. G., et al. (2020). Differential day-night expression of tight junction components in murine retinal pigment epithelium. *Exp. Eye Res.* 193:107985. doi: 10.1016/j.exer.2020.107985

Lundgaard, I., Lu, M. L., Yang, E., Peng, W., Mestre, H., Hitomi, E., et al. (2017). Glymphatic clearance controls state-dependent changes in brain lactate concentration. *J. Cereb. Blood Flow Metab.* 37, 2112–2124. doi: 10.1177/0271678X16661202

Lunn, R. M., Blask, D. E., Coogan, A. N., Figueiro, M. G., Gorman, M. R., Hall, J. E., et al. (2017). Health consequences of electric lighting practices in the modern world: a report on the National Toxicology Program's workshop on shift work at night, artificial light at night, and circadian disruption. *Sci. Total Environ.* 607–608, 1073–1084. doi: 10.1016/j.scitotenv.2017.07.056

Ma, Y., Wang, J., Wang, Y., and Yang, G. Y. (2017). The biphasic function of microglia in ischemic stroke. *Prog. Neurobiol.* 157, 247–272. doi: 10.1016/j.pneurobio.2016.01.005

Madore, C., Yin, Z., Leibowitz, J., and Butovsky, O. (2020). Microglia, lifestyle stress, and neurodegeneration. *Immunity* 52, 222–240. doi: 10.1016/j.immuni.2019.12.003

Madsen, P. L., Holm, S., Vorstrup, S., Friberg, L., Lassen, N. A., and Wildschiødtz, G. (1991). Human regional cerebral blood flow during rapid-eye-movement sleep. *J. Cereb. Blood Flow Metab.* 11, 502–507. doi: 10.1038/jcbfm.1991.94

Manfredini, R., Boari, B., Smolensky, M. H., Salmi, R., La Cecilia, O., Maria Malagoni, A., et al. (2005). Circadian variation in stroke onset: identical temporal pattern in ischemic and hemorrhagic events. *Chronobiol. Int.* 22, 417–453. doi: 10.1081/CBI-200062927

Marpegan, L., Leone, M. J., Katz, M. E., Sobrero, P. M., Bekinstein, T. A., and Golombek, D. A. (2009). Diurnal variation in endotoxin-induced mortality in mice: correlation with proinflammatory factors. *Chronobiol. Int.* 26, 1430–1442. doi: 10.3109/07420520903408358

Mastrullo, V., Van Der Veen, D. R., Gupta, P., Matos, R. S., Johnston, J. D., Mcvey, J. H., et al. (2022). Pericytes' circadian clock affects endothelial Cells' synchronization and angiogenesis in a 3D tissue engineered scaffold. *Front. Pharmacol.* 13:867070. doi: 10.3389/fphar.2022.867070

Maywood, E. S., Chesham, J. E., O'Brien, J. A., and Hastings, M. H. (2011). A diversity of paracrine signals sustains molecular circadian cycling in suprachiasmatic nucleus circuits. *Proc. Natl. Acad. Sci.* 108, 14306–14311. doi: 10.1073/pnas.1101767108

Mcconnell, H. L., Kersch, C. N., Woltjer, R. L., and Neuwelt, E. A. (2017). The translational significance of the neurovascular unit. *J. Biol. Chem.* 292, 762–770. doi: 10.1074/jbc.R116.760215

Mckee, C. A., Lananna, B. V., and Musiek, E. S. (2020). Circadian regulation of astrocyte function: implications for Alzheimer's disease. *Cell. Mol. Life Sci.* 77, 1049–1058. doi: 10.1007/s00018-019-03314-y

Mckinley, M. J., Mathai, M. L., Mcallen, R. M., Mcclear, R. C., Miselis, R. R., Pennington, G. L., et al. (2004). Vasopressin secretion: osmotic and hormonal regulation by the lamina terminalis. *J. Neuroendocrinol.* 16, 340–347. doi: 10.1111/j.0953-8194.2004.01184.x

Millar-Craig, M., Bishop, C., and Raftery, E. (1978). Circadian variation of blood-pressure. *Lancet* 311, 795–797. doi: 10.1016/S0140-6736(78)92998-7

Miyata, S. (2015). New aspects in fenestrated capillary and tissue dynamics in the sensory circumventricular organs of adult brains. *Front. Neurosci.* 9:390. doi: 10.3389/fnins.2015.00390

Moskowitz, M. A., Lo, E. H., and Iadecola, C. (2010). The science of stroke: mechanisms in search of treatments. *Neuron* 67, 181–198. doi: 10.1016/j.neuron.2010.07.002

Mughal, A., Nelson, M. T., and Hill-Eubanks, D. (2023). The post-arteriole transitional zone: a specialized capillary region that regulates blood flow within the CNS microvasculature. *J. Physiol.* 601, 889–901. doi: 10.1113/JP282246

Musiek, E. S., and Holtzman, D. M. (2016). Mechanisms linking circadian clocks, sleep, and neurodegeneration. *Science* 354, 1004–1008. doi: 10.1126/science.aah4968

Nakazato, R., Hotta, S., Yamada, D., Kou, M., Nakamura, S., Takahata, Y., et al. (2017a). The intrinsic microglial clock system regulates interleukin-6 expression. *Glia* 65, 198–208. doi: 10.1002/glia.23087

Nakazato, R., Kawabe, K., Yamada, D., Ikeno, S., Mieda, M., Shimba, S., et al. (2017b). Disruption of Bmal1 impairs blood-brain barrier integrity via pericyte dysfunction. *J. Neurosci.* 37, 10052–10062. doi: 10.1523/JNEUROSCI.3639-16.2017

Nakazato, R., Takarada, T., Yamamoto, T., Hotta, S., Hinoi, E., and Yoneda, Y. (2011). Selective upregulation of Per1 mRNA expression by ATP through activation of P2X7 purinergic receptors expressed in microglial cells. *J. Pharmacol. Sci.* 116, 350–361. doi: 10.1254/jphs.11069FP

Naseri Kouzehgarani, G., Kandel, M. E., Sakakura, M., Dupaty, J. S., Popescu, G., and Gillette, M. U. (2022). Circadian volume changes in hippocampal glia studied by label-free interferometric imaging. *Cells* 11:2073. doi: 10.3390/cells11132073

Nielsen, A. N., and Lauritzen, M. (2001). Coupling and uncoupling of activity-dependent increases of neuronal activity and blood flow in rat somatosensory cortex. *J. Physiol.* 533, 773–785. doi: 10.1111/j.1469-7793.2001.00773.x

Nimmerjahn, A., Kirchhoff, F., and Helmchen, F. (2005). Resting microglial cells are highly dynamic surveillants of brain parenchyma in vivo. *Science* 308, 1314–1318. doi: 10.1126/science.1110647

Nonaka, H., Emoto, N., Ikeda, K., Fukuya, H., Rohman, M. S., Raharjo, S. B., et al. (2001). Angiotensin II induces circadian gene expression of clock genes in cultured vascular smooth muscle cells. *Circulation* 104, 1746–1748. doi: 10.1161/hc4001.098048

Oh-Oka, K., Kono, H., Ishimaru, K., Miyake, K., Kubota, T., Ogawa, H., et al. (2014). Expressions of tight junction proteins Occludin and Claudin-1 are under 634 the circadian control in the mouse large intestine: implications in intestinal permeability 635 and susceptibility to colitis. *PLoS One* 9:636. doi: 10.1371/journal.pone.0098016

Oldfield, B. J., and Mckinley, M. J. (2015). "Chapter 15- Circumventricular Organs" in *The rat nervous system*. ed. G. Paxinos. *4th* ed (San Diego: Academic Press)

Orihuela, R., Mcpherson, C. A., and Harry, G. J. (2016). Microglial M1/M2 polarization and metabolic states. *Br. J. Pharmacol.* 173, 649–665. doi: 10.1111/bph.13139

Ousman, S. S., and Kubes, P. (2012). Immune surveillance in the central nervous system. *Nat. Neurosci.* 15, 1096–1101. doi: 10.1038/nn.3161

Pan, W., Wu, X., Kastin, A. J., Zhang, Y., Hsuchou, H., Halberg, F., et al. (2011). Potential protective role of IL15Rα during inflammation. *J. Mol. Neurosci.* 43, 412–423. doi: 10.1007/s12031-010-9459-1

Panda, S., Antoch, M. P., Miller, B. H., Su, A. I., Schook, A. B., Straume, M., et al. (2002). Coordinated transcription of key pathways in the mouse by the circadian clock. *Cells* 109, 307–320. doi: 10.1016/S0092-8674(02)00722-5

Pappas, A. C., Koide, M., and Wellman, G. C. (2015). Astrocyte Ca2+ signaling drives inversion of neurovascular coupling after subarachnoid hemorrhage. *J. Neurosci.* 35, 13375–13384. doi: 10.1523/JNEUROSCI.1551-15.2015

Park, Y. K., Kim, J. H., Choi, S. J., Kim, S. T., and Joo, E. Y. (2019). Altered regional cerebral blood flow associated with mood and sleep in shift workers: cerebral perfusion magnetic resonance imaging study. *J. Clin. Neurol.* 15, 438–447. doi: 10.3988/jcn.2019.15.4.438

Paschos, G. K., and Fitzgerald, G. A. (2010). Circadian clocks and vascular function. *Circ. Res.* 106, 833–841. doi: 10.1161/CIRCRESAHA.109.211706

Paulson, O. B., and Newman, E. A. (1987). Does the release of potassium from astrocyte endfeet regulate cerebral blood flow? *Science* 237, 896–898. doi: 10.1126/science.3616619

Peppiatt, C. M., Howarth, C., Mobbs, P., and Attwell, D. (2006). Bidirectional control of CNS capillary diameter by pericytes. *Nature* 443, 700–704. doi: 10.1038/nature05193

Peterson, E. C., Wang, Z., and Britz, G. (2011). Regulation of cerebral blood flow. *J. Vasc. Med.* 2011:823525. doi: 10.1155/2011/823525

Pulido, R. S., Munji, R. N., Chan, T. C., Quirk, C. R., Weiner, G. A., Weger, B. D., et al. (2020). Neuronal activity regulates blood-brain barrier efflux transport through endothelial circadian genes. *Neuron* 108:e7. doi: 10.1016/j.neuron.2020.09.002

Raivich, G. (2005). Like cops on the beat: the active role of resting microglia. *Trends Neurosci.* 28, 571–573. doi: 10.1016/j.tins.2005.09.001

Ralph, M. R., Foster, R. G., Davis, F. C., and Menaker, M. (1990). Transplanted suprachiasmatic nucleus determines circadian period. *Science* 247, 975–978. doi: 10.1126/science.2305266

Ramsey, A. M., Stowie, A., Castanon-Cervantes, O., and Davidson, A. J. (2020). Environmental circadian disruption increases stroke severity and dysregulates immune response. *J. Biol. Rhythm.* 35, 368–376. doi: 10.1177/0748730420929450

Rancillac, A., Rossier, J., Guille, M., Tong, X. K., Geoffroy, H., Amatore, C., et al. (2006). Glutamatergic control of microvascular tone by distinct GABA neurons in the cerebellum. *J. Neurosci.* 26, 6997–7006. doi: 10.1523/JNEUROSCI.5515-05.2006

Ripamonti, L., Riva, R., Maioli, F., Zenesini, C., and Procaccianti, G. (2017). Daily variation in the occurrence of different subtypes of stroke. *Stroke Res. Treat* 2017:9091250. doi: 10.1155/2017/9091250

Rojo, D., Badner, A., and Gibson, E. M. (2022). Circadian control of glial cell homeodynamics. *J. Biol. Rhythm.* 37, 593–608. doi: 10.1177/07487304221120966

Rosensweig, C., and Green, C. B. (2020). Periodicity, repression, and the molecular architecture of the mammalian circadian clock. *Eur. J. Neurosci.* 51, 139–165. doi: 10.1111/ejn.14254

Rudic, R. D., Mcnamara, P., Reilly, D., Grosser, T., Curtis, A.-M., Price, T. S., et al. (2005). Bioinformatic analysis of circadian gene oscillation in mouse aorta. *Circulation* 112, 2716–2724. doi: 10.1161/CIRCULATIONAHA.105.568626

Rustenhoven, J., and Kipnis, J. (2022). Brain borders at the central stage of neuroimmunology. *Nature* 612, 417–429. doi: 10.1038/s41586-022-05474-7

Saadoun, S., Tait, M., Reza, A., Davies, D. C., Bell, B., Verkman, A., et al. (2009). AQP4 gene deletion in mice does not alter blood–brain barrier integrity or brain morphology. *Neuroscience* 161, 764–772. doi: 10.1016/j.neuroscience.2009.03.069

Samson, W. K., and Ferguson, A. V. (2015). Exploring the OVLT: insight into a critically important window into the brain. *Am. J. Physiol. Regul. Integr. Comp. Physiol.* 309, R322–R323. doi: 10.1152/ajpregu.00305.2015

Sandoo, A., Veldhuijzen Van Zanten, J. J., Metsios, G. S., Carroll, D., and Kitas, G. D. (2010). The endothelium and its role in regulating vascular tone. *Open Cardiovasc. Med. J.* 4, 302–312. doi: 10.2174/1874192401004010302

Sano, H., Hayashi, H., Makino, M., Takezawa, H., Hirai, M., Saito, H., et al. (1995). Effects of suprachiasmatic lesions on circadian rhythms of blood pressure, heart rate and locomotor activity in the rat. *Jpn. Circ. J.* 59, 565–573. doi: 10.1253/jcj.59.565

Sawaya, R., and Ingvar, D. (1989). Cerebral blood flow and metabolism in sleep. *Acta Neurol. Scand.* 80, 481–491. doi: 10.1111/j.1600-0404.1989.tb03915.x

Schaeffer, S., and Iadecola, C. (2021). Revisiting the neurovascular unit. *Nat. Neurosci.* 24, 1198–1209. doi: 10.1038/s41593-021-00904-7

Scheer, F. A., Michelson, A. D., Frelinger Iii, A. L., Evoniuk, H., Kelly, E. E., Mccarthy, M., et al. (2011). The human endogenous circadian system causes greatest platelet activation during the biological morning independent of behaviors. *PLoS One* 6:e24549. doi: 10.1371/journal.pone.0024549

Scheer, F. A. J. L., and Shea, S. A. (2014). Human circadian system causes a morning peak in prothrombotic plasminogen activator inhibitor-1 (PAI-1) independent of the sleep/wake cycle. *Blood* 123, 590–593. doi: 10.1182/blood-2013-07-517060

Schinkel, A., Smit, J., Van Tellingen, M., Beijnen, J., Wagenaar, E., Van Deemter, L., et al. (1994). Disruption of the mouse mdr1a P-glycoprotein gene leads to a deficiency in the blood-brain barrier and to increased sensitivity to drugs. *Cells* 77, 491–502. doi: 10.1016/0092-8674(94)90212-7

Schoenhard, J. A., Smith, L. H., Painter, C. A., Eren, M., Johnson, C. H., and Vaughan, D. E. (2003). Regulation of the PAI-1 promoter by circadian clock components: differential activation by BMAL1 and BMAL2. *J. Mol. Cell. Cardiol.* 35, 473–481. doi: 10.1016/S0022-2828(03)00051-8

Schurhoff, N., and Toborek, M. (2023). Circadian rhythms in the blood-brain barrier: impact on neurological disorders and stress responses. *Mol. Brain* 16:5. doi: 10.1186/s13041-023-00997-0

Schwartz, W. J., Coleman, R. J., and Reppert, S. M. (1983). A daily vasopressin rhythm in rat cerebrospinal fluid. *Brain Res.* 263, 105–112. doi: 10.1016/0006-8993(83)91205-2

Schwarz, P. M., Kleinert, H., and FöRstermann, U. (1999). Potential functional significance of brain-type and muscle-type nitric oxide synthase I expressed in adventitia and media of rat aorta. *Arterioscler. Thromb. Vasc. Biol.* 19, 2584–2590. doi: 10.1161/01.ATV.19.11.2584

Seddon, M. D., Chowienczyk, P. J., Brett, S. E., Casadei, B., and Shah, A. M. (2008). Neuronal nitric oxide synthase regulates basal microvascular tone in humans in vivo. *Circulation* 117, 1991–1996. doi: 10.1161/CIRCULATIONAHA.107.744540

Sevenich, L., Bowman, R. L., Mason, S. D., Quail, D. F., Rapaport, F., Elie, B. T., et al. (2014). Analysis of tumour-and stroma-supplied proteolytic networks reveals a brain-metastasis-promoting role for cathepsin S. *Nat. Cell Biol.* 16, 876–888. doi: 10.1038/ncb3011

Shi, Y., Liu, X., Gebremedhin, D., Falck, J. R., Harder, D. R., and Koehler, R. C. (2008). Interaction of mechanisms involving epoxyeicosatrienoic acids, adenosine receptors, and metabotropic glutamate receptors in neurovascular coupling in rat whisker barrel cortex. *J. Cereb. Blood Flow Metab.* 28, 111–125. doi: 10.1038/sj.jcbfm.9600511

Shivshankar, P., Fekry, B., Eckel-Mahan, K., and Wetsel, R. A. (2020). Circadian clock and complement immune system—complementary control of physiology and pathology? *Front. Cell. Infect. Microbiol.* 10:418.

Silverman, A., and Petersen, N. H. (2022). *Physiology, cerebral autoregulation*, StatPearls Treasure Island, FL.

Spengler, M. L., Kuropatwinski, K. K., Comas, M., Gasparian, A. V., Fedtsova, N., Gleiberman, A. S., et al. (2012). Core circadian protein CLOCK is a positive regulator of NF-κB–mediated transcription. *Proc. Natl. Acad. Sci.* 109, E2457–E2465. doi: 10.1073/pnas.1206274109

Stackhouse, T. L., and Mishra, A. (2021). Neurovascular coupling in development and disease: focus on astrocytes. *Front. Cell Devel. Biol.* 9:702832. doi: 10.3389/fcell.2021.702832

Stephan, F. K., and Zucker, I. (1972). Circadian rhythms in drinking behavior and locomotor activity of rats are eliminated by hypothalamic lesions. *Proc. Natl. Acad. Sci.* 69, 1583–1586. doi: 10.1073/pnas.69.6.1583

Streuli, C. H. (2016). Integrins as architects of cell behavior. *Mol. Biol. Cell* 27, 2885–2888. doi: 10.1091/mbc.E15-06-0369

Streuli, C. H., and Meng, Q. J. (2019). Influence of the extracellular matrix on cell-intrinsic circadian clocks. *J. Cell Sci.* 132:jcs207498. doi: 10.1242/jcs.207498

Strong, L. H. (1964). The early embryonic pattern of internal vascularization of the mammalian cerebral cortex. *J. Comp. Neurol.* 123, 121–138. doi: 10.1002/cne.901230111

Sukhova, G. K., Zhang, Y., Pan, J. H., Wada, Y., Yamamoto, T., Naito, M., et al. (2003). Deficiency of cathepsin S reduces atherosclerosis in LDL receptor-deficient mice. *J. Clin. Invest.* 111, 897–906. doi: 10.1172/JCI200314915

Sweeney, M. D., Sagare, A. P., and Zlokovic, B. V. (2018). Blood–brain barrier breakdown in Alzheimer disease and other neurodegenerative disorders. *Nat. Rev. Neurol.* 14, 133–150. doi: 10.1038/nrneurol.2017.188

Takahashi, J. S. (2017). Transcriptional architecture of the mammalian circadian clock. *Nat. Rev. Genet.* 18, 164–179. doi: 10.1038/nrg.2016.150

Takayama, F., Hayashi, Y., Wu, Z., Liu, Y., and Nakanishi, H. (2016). Diurnal dynamic behavior of microglia in response to infected bacteria through the UDP-P2Y6 receptor system. *Sci. Rep.* 6, 1–10. doi: 10.1038/srep30006

Takeda, N., Maemura, K., Horie, S., Oishi, K., Imai, Y., Harada, T., et al. (2007). Thrombomodulin is a clock-controlled gene in vascular endothelial cells. *J. Biol. Chem.* 282, 32561–32567. doi: 10.1074/jbc.M705692200

Tata, M., Ruhrberg, C., and Fantin, A. (2015). Vascularisation of the central nervous system. *Mech. Dev.* 138, 26–36. doi: 10.1016/j.mod.2015.07.001

Taub, A., Carbajal, Y., Rimu, K., Holt, R., Yao, Y., Hernandez, A. L., et al. (2021). Arginine vasopressin-containing neurons of the suprachiasmatic nucleus project to CSF. *eNeuro* 8:ENEURO.0363-20.2021. doi: 10.1523/ENEURO.0363-20.2021

Thosar, S. S., Berman, A. M., Herzig, M. X., Mchill, A. W., Bowles, N. P., Swanson, C. M., et al. (2019). Circadian rhythm of vascular function in midlife adults. *Arterioscler. Thromb. Vasc. Biol.* 39, 1203–1211. doi: 10.1161/ATVBAHA.119.312682

Thosar, S. S., Butler, M. P., and Shea, S. A. (2018). Role of the circadian system in cardiovascular disease. *J. Clin. Invest.* 128, 2157–2167. doi: 10.1172/JCI80590

Tofler, G. H., Brezinski, D., Schafer, A. I., Czeisler, C. A., Rutherford, J. D., Willich, S. N., et al. (1987). Concurrent morning increase in platelet aggregability and the risk of myocardial infarction and sudden cardiac death. *N. Engl. J. Med.* 316, 1514–1518. doi: 10.1056/NEJM198706113162405

Trudel, E., and Bourque, C. W. (2010). Central clock excites vasopressin neurons by waking osmosensory afferents during late sleep. *Nat. Neurosci.* 13, 467–474. doi: 10.1038/nn.2503

Turin, T. C., Kita, Y., Rumana, N., Takashima, N., Ichikawa, M., Sugihara, H., et al. (2010). Diurnal variation in onset of hemorrhagic stroke is independent of risk factor status: Takashima stroke registry. *Neuroepidemiology* 34, 25–33. doi: 10.1159/000255463

Umpierre, A. D., and Wu, L. J. (2021). How microglia sense and regulate neuronal activity. *Glia* 69, 1637–1653. doi: 10.1002/glia.23961

Vizovišek, M., Fonović, M., and Turk, B. (2019). Cysteine cathepsins in extracellular matrix remodeling: extracellular matrix degradation and beyond. *Matrix Biol.* 75, 141–159. doi: 10.1016/j.matbio.2018.01.024

Wang, Z., Wang, L., Zhang, L., Liu, Q., Xue, Z., Cornélissen, G., et al. (1992). Circadian relations among cardiovascular variables of young adults. *Chronobiologia* 19, 111–120.

Wang, X. L., Wolff, S. E. C., Korpel, N., Milanova, I., Sandu, C., Rensen, P. C. N., et al. (2020). Deficiency of the circadian clock gene Bmal1 reduces microglial Immunometabolism. *Front. Immunol.* 11:586399. doi: 10.3389/fimmu.2020.586399

Wauschkuhn, C. A., Witte, K., Gorbey, S., Lemmer, B., and Schilling, L. (2005). Circadian periodicity of cerebral blood flow revealed by laser-Doppler flowmetry in awake rats: relation to blood pressure and activity. *Am. J. Phys. Heart Circ. Phys.* 289, H1662–H1668. doi: 10.1152/ajpheart.01242.2004

Welsh, D. K., Yoo, S. H., Liu, A. C., Takahashi, J. S., and Kay, S. A. (2004). Bioluminescence imaging of individual fibroblasts reveals persistent, independently phased circadian rhythms of clock gene expression. *Curr. Biol.* 14, 2289–2295. doi: 10.1016/j.cub.2004.11.057

Westgate, E. J., Cheng, Y., Reilly, D. F., Price, T. S., Walisser, J. A., Bradfield, C. A., et al. (2008). Genetic components of the circadian clock regulate thrombogenesis in vivo. *Circulation* 117, 2087–2095. doi: 10.1161/CIRCULATIONAHA.107.739227

Whiteus, C., Freitas, C., and Grutzendler, J. (2014). Perturbed neural activity disrupts cerebral angiogenesis during a postnatal critical period. *Nature* 505, 407–411. doi: 10.1038/nature12821

Winkler, E. A., Bell, R. D., and Zlokovic, B. V. (2011). Central nervous system pericytes in health and disease. *Nat. Neurosci.* 14, 1398–1405. doi: 10.1038/nn.2946

Witte, K., Hasenberg, T., Rueff, T., Hauptfleisch, S., Schilling, L., and Lemmer, B. (2001). Day-night variation in the in vitro contractility of aorta and mesenteric and renal arteries in transgenic hypertensive rats. *Chronobiol. Int.* 18, 665–681.

Witte, K., Schnecko, A., Buijs, R. M., Van Der Vliet, J., Scalbert, E., Delagrange, P., et al. (1998). Effects of Scn lesions on orcadian blood pressure rhythm in normotensive and transgenic hypertensive rats. *Chronobiol. Int.* 15, 135–145. doi: 10.1081/cbi-100106080

Wu, D. M., Kawamura, H., Sakagami, K., Kobayashi, M., and Puro, D. G. (2003). Cholinergic regulation of pericyte-containing retinal microvessels. *Am. J. Phys. Heart Circ. Phys.* 284, H2083–H2090. doi: 10.1152/ajpheart.01007.2002

Xie, Z., Su, W., Liu, S., Zhao, G., Esser, K., Schroder, E. A., et al. (2015). Smooth-muscle BMAL1 participates in blood pressure circadian rhythm regulation. *J. Clin. Invest.* 125, 324–336. doi: 10.1172/JCI76881

Xu, Y., Gong, C., Liao, J., Ge, Z., Tan, Y., Jiang, Y., et al. (2023). Absence of fluctuation and inverted circadian rhythm of blood pressure increase the risk of cognitive dysfunction in cerebral small vessel disease patients. *BMC Neurol.* 23:73. doi: 10.1186/s12883-023-03107-8

Yamazaki, S., and Takahashi, J. S. (2005). Real-time luminescence reporting of circadian gene expression in mammals. *Methods Enzymol.* 393, 288–301. doi: 10.1016/S0076-6879(05)93012-7

Yang, N., Williams, J., Pekovic-Vaughan, V., Wang, P., Olabi, S., Mcconnell, J., et al. (2017). Cellular mechano-environment regulates the mammary circadian clock. *Nat. Commun.* 8:14287. doi: 10.1038/ncomms14287

Yao, Y., Green, I. K., Taub, A. B., Tazebay, R., Lesauter, J., and Silver, R. (2023). Vasculature of the suprachiasmatic nucleus: pathways for diffusible output signals. *J. Biol. Rhythms*. 8:7487304231189537. doi: 10.1177/07487304231189537

Yao, Y., Taub, A. B. N., Lesauter, J., and Silver, R. (2021). Identification of the suprachiasmatic nucleus venous portal system in the mammalian brain. *Nat. Commun.* 12:5643. doi: 10.1038/s41467-021-25793-z

Yoshihara, M., Bandoh, K., and Marmarou, A. (1995). Cerebrovascular carbon dioxide reactivity assessed by intracranial pressure dynamics in severely head injured patients. *J. Neurosurg.* 82, 386–393. doi: 10.3171/jns.1995.82.3.0386

Zhang, S. L., Lahens, N. F., Yue, Z., Arnold, D. M., Pakstis, P. P., Schwarz, J. E., et al. (2021). A circadian clock regulates efflux by the blood-brain barrier in mice and human cells. *Nat. Commun.* 12:617. doi: 10.1038/s41467-020-20795-9

Zhao, X., Eyo, U. B., Murugan, M., and Wu, L. J. (2018). Microglial interactions with the neurovascular system in physiology and pathology. *Dev. Neurobiol.* 78, 604–617. doi: 10.1002/dneu.22576

Zhou, J., Kong, H., Hua, X., Xiao, M., Ding, J., and Hu, G. (2008). Altered blood–brain barrier integrity in adult aquaporin-4 knockout mice. *Neuroreport* 19, 1–5. doi: 10.1097/WNR.0b013e3282f2b4eb

Zimmerman, B., Rypma, B., Gratton, G., and Fabiani, M. (2021). Age-related changes in cerebrovascular health and their effects on neural function and cognition: a comprehensive review. *Psychophysiology* 58:e13796. doi: 10.1111/psyp.13796

Zlokovic, B. V. (2011). Neurovascular pathways to neurodegeneration in Alzheimer's disease and other disorders. *Nat. Rev. Neurosci.* 12, 723–738. doi: 10.1038/nrn3114

frontiers | Frontiers in Neuroscience

TYPE Brief Research Report
PUBLISHED 27 September 2023
DOI 10.3389/fnins.2023.1242800

OPEN ACCESS

EDITED BY
Elzbieta M. Pyza,
Jagiellonian University, Poland

REVIEWED BY
Mino Belle,
The University of Manchester, United Kingdom
Barbara Pavan,
University of Ferrara, Italy

*CORRESPONDENCE
Jihwan Myung
✉ jihwan@tmu.edu.tw
Mei-Yi Wu
✉ e220121@gmail.com

RECEIVED 19 June 2023
ACCEPTED 29 August 2023
PUBLISHED 27 September 2023

CITATION
Myung J, Hong S, Schmal C, Vitet H and Wu M-Y (2023) Weak synchronization can alter circadian period length: implications for aging and disease conditions.
Front. Neurosci. 17:1242800.
doi: 10.3389/fnins.2023.1242800

Weak synchronization can alter circadian period length: implications for aging and disease conditions

Jihwan Myung[1,2,3]*, Sungho Hong[3], Christoph Schmal[4], Hélène Vitet[1,2,5] and Mei-Yi Wu[6,7,8,9]*

[1]Graduate Institute of Mind, Brain and Consciousness (GIMBC), Taipei Medical University, Taipei City, Taiwan, [2]Brain and Consciousness Research Centre (BCRC), TMU-Shuang Ho Hospital, New Taipei City, Taiwan, [3]Computational Neuroscience Unit, Okinawa Institute of Science and Technology, Okinawa, Japan, [4]Institute for Theoretical Biology, Humboldt-Universität zu Berlin, Berlin, Germany, [5]Department of Pediatrics, College of Medicine, National Cheng Kung University, Tainan City, Taiwan, [6]Division of Nephrology, Department of Internal Medicine, Taipei Medical University-Shuang Ho Hospital, New Taipei City, Taiwan, [7]Division of Nephrology, Department of Internal Medicine, School of Medicine, College of Medicine, Taipei Medical University, Taipei, Taiwan, [8]Institute of Epidemiology and Preventive Medicine, College of Public Health, National Taiwan University, Taipei, Taiwan, [9]TMU Research Center of Urology and Kidney, Taipei Medical University, Taipei, Taiwan

The synchronization of multiple oscillators serves as the central mechanism for maintaining stable circadian rhythms in physiology and behavior. Aging and disease can disrupt synchronization, leading to changes in the periodicity of circadian activities. While our understanding of the circadian clock under synchronization has advanced significantly, less is known about its behavior outside synchronization, which can also fall within a predictable domain. These states not only impact the stability of the rhythms but also modulate the period length. In C57BL/6 mice, aging, diseases, and removal of peripheral circadian oscillators often result in lengthened behavioral circadian periods. Here, we show that these changes can be explained by a surprisingly simple mathematical relationship: the frequency is the reciprocal of the period, and its distribution becomes skewed when the period distribution is symmetric. The synchronized frequency of a population in the skewed distribution and the macroscopic frequency of combined oscillators differ, accounting for some of the atypical circadian period outputs observed in networks without synchronization. Building on this finding, we investigate the dynamics of circadian outputs in the context of aging and disease, where synchronization is weakened.

KEYWORDS

unsynchronized states, period-frequency relation, circadian rhythms, frequency synchronization, Kuramoto model, period distribution, macroscopic period, mean internal period

Introduction

Animals innately follow a near-24-h cycle of rest and activity, known as the circadian rhythm, which prepares them for daily environmental changes. The endogenous rhythm in behavioral activities is maintained with remarkable precision under constant darkness, exhibiting robust periodicity over months and minimal cycle-to-cycle variation in activity phase (Pittendrigh and Daan, 1976a; Schwartz and Zimmerman, 1990). In mammals, the suprachiasmatic nucleus (SCN) serves as the central clock, orchestrating both behavioral circadian rhythms and physiological rhythms throughout the body. The SCN is a network of circadian oscillators, with single neurons and glial cells as the cellular identities, that

maintain rhythmic expressions of circadian clock molecules through the transcription-translation feedback loop (TTFL).

The oscillation within a single cell is both autonomous and persistent, yet displays a variation in period across the population (Leise et al., 2012). These oscillators couple within the network to generate a synchronized oscillation, reducing period heterogeneity and facilitating high temporal precision for the circadian clock output at the organismal level (Herzog et al., 2004). The synchronization is the essential mechanism of the SCN network that transforms diverse period, phase, and amplitude of individual oscillators into predictable and coherent outputs. However, biological systems often operate in the metastable state between complete synchronization and desynchronization (Kelso, 1995). This is sometimes due to the functional needs, such as the internal representation of seasonal time within the SCN (Pittendrigh and Daan, 1976b; Myung et al., 2015; Schmal, 2023), but it can also be due to degradation of the network through aging and disruptive timing cues such as constant light (Ohta et al., 2005; Farajnia et al., 2012).

Aging is known to cause changes in the period of circadian locomotor activity (Pittendrigh and Daan, 1974). In the widely studied laboratory mouse strain C57BL, circadian activities persist through aging, with periods typically lengthening with increasing age (Davis and Menaker, 1981; Welsh et al., 1986; Possidente et al., 1995; Valentinuzzi et al., 1997). Depending on the strain and entrainment history, periods can also shorten (Pittendrigh and Daan, 1976a). Chronic illnesses often lead to changes in circadian periodicity, which can result in sleep disturbances, as seen in diseases like Alzheimer's or Huntington's (Witting et al., 1990; Aziz et al., 2010). Disruptions in circadian gene expression have been observed in animal models of chronic kidney disease (CKD) (Hsu et al., 2012). This disruption causes instability in circadian activity when in constant darkness (Myung et al., 2019). Furthermore, disturbances in circadian rhythm have been identified in conditions such as acute respiratory failure (ARF) (Yang et al., 2020) and chronic pulmonary disease (COPD) (Giri et al., 2022). In critically ill patients, there have been reports of misalignment in internal circadian rhythms (Felten et al., 2023).

Yet, within the widely recognized Kuramoto model for synchronization, explaining these changes in period remains a challenge (Acebrón et al., 2005). Emerging evidence suggests a correlation between the period and amplitude (Myung et al., 2018; del Olmo et al., 2023). As synchronization increases, so does the circadian amplitude of a clock ensemble (Schmal et al., 2018). Oscillators achieving synchronization is fundamentally about aligning their frequencies. In systems with a finite number of oscillators, it has been numerically shown that skewness in the frequency distribution can eventually alter the mean frequency of macroscopic ensemble oscillations (Peter and Pikovsky, 2018). Given the reciprocal relationship between period and frequency, we note that a symmetric period distribution, such as Gaussian, results in a skewed frequency distribution. This skewness can influence the mean period of an oscillator ensemble, particularly when the standard deviation of the period distribution is large. This may provide additional insight into the changes of circadian period under weak synchronization observed in aging and disease conditions.

Results

Skewed frequency distribution: mean, median, and the mode

A circadian oscillator within a single cell emerges from nonlinear molecular feedback networks that contain ultrasensitive response motifs (Zhang et al., 2013). The oscillatory trajectory is believed to follow a stable limit cycle, allowing the oscillation in the phase space to be mapped onto a unit circle. This property enables the reduction of the nonlinear oscillator to a phase oscillator which, in turn, facilitates the investigation of collective behavior of multiple oscillators (Winfree, 1980). The temporal evolution of a circadian oscillator at phase θ with constant frequency f (where f is the reciprocal of the intrinsic period, τ) can be described by a differential equation $\mathrm{d}\theta/\mathrm{d}t = 2\pi f = 2\pi/\tau$. The Kuramoto model extends this framework by introducing a coupling term with a sine of the phase difference (Acebrón et al., 2005). At least for a certain class of oscillators with a particular type of phase response curve (PRC), this provides a concise formalism for describing the synchronization behavior among multiple oscillators under various coupling scenarios (Myung and Pauls, 2018). Under the assumption of a symmetric distribution of the individual oscillator frequencies, the model predicts that the frequency of the synchronized ensemble is determined by the average frequency of the population, which appears true for the SCN (Liu et al., 1997).

The periods of circadian firing rates in dissociated single SCN neurons show Gaussian distribution in both rats and C57BL/6J mice (Honma et al., 2004, 2012). For the mean period τ_0 and standard deviation σ, the Gaussian probability density function p is

$$p(\tau) = \frac{1}{\sqrt{2\pi\sigma^2}} e^{-(\tau-\tau_0)^2/2\sigma^2} \tag{1}$$

which satisfies $\int d\tau p(\tau)=1$.

By change of variables, the probability density function for the frequency f can be written as

$$q(f) = \frac{1}{\sqrt{2\pi\sigma^2 f^2}} e^{-(1/f-\tau_0)^2/2\sigma^2} \tag{2}$$

which has a singularity at $f = 0$.

The reciprocal transformation maps shorter periods to a wider range on the higher frequency side, resulting in a skewed distribution with a peak (mode) shifted to the lower frequency side (Figures 1A, B). The $1/f^2$ term in the equation (2) implies this shift, which gives higher weight to the lower frequency side. Due to the singularity, there is no simple closed-form solution for the mean $\langle f \rangle$ but via the Dawson function F,

$$\langle f \rangle = \frac{\sqrt{2}}{\sigma} F\left(\frac{\tau_0}{\sqrt{2}\sigma}\right) \approx \frac{1}{\tau_0} + \frac{\sigma^2}{\tau_0^3} + \frac{3\sigma^4}{\tau_0^5} + \cdots. \tag{3}$$

Since we are interested in the regime $\sigma \ll \tau_0$, the reciprocal of the mean frequency approximates to

$$1/\langle f \rangle \approx \tau_0 - \frac{\sigma^2}{\tau_0}. \tag{4}$$

This provides a good approximation compared to the mean values of the randomly generated populations (Figure 1C) when

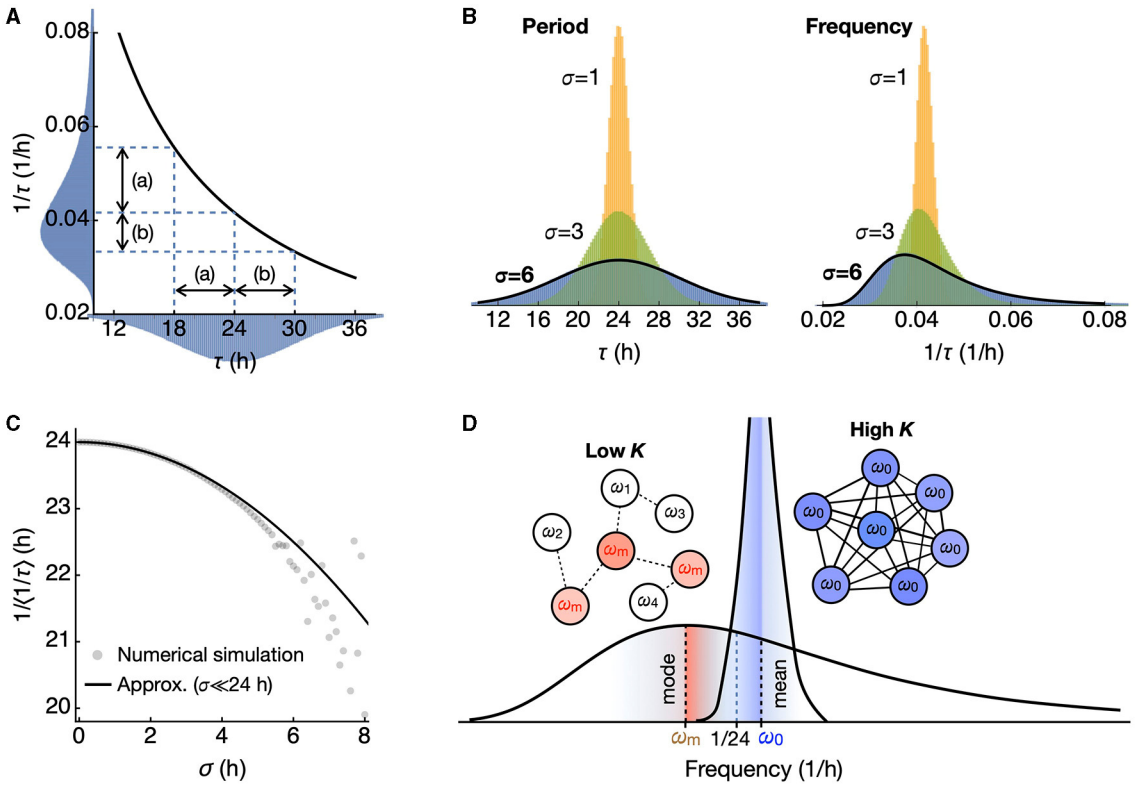

FIGURE 1
A symmetric period distribution corresponds to a right-skewed frequency distribution. **(A)** The reciprocal function connects period (τ) and frequency ($1/\tau$). In a symmetric period distribution with a 24-h mean, shorter periods correspond to a broader frequency range (a), while longer periods correspond to a narrower range (b). This results in a right-skewed frequency distribution. **(B)** The skewness of the frequency distribution increases as the standard deviation σ of the symmetric period distribution increases. **(C)** The inverse of the mean frequency $<1/\tau>$ shows a quadratic decrease as the standard deviation σ increases. **(D)** In the skewed frequency distribution, the mode (ω_m; red) leans toward lower frequencies (longer periods), while the mean (ω_0; blue) leans toward higher frequencies (shorter periods), compared to 1/24 h, the inverse of the mean period. Upon oscillator coupling, synchronization occurs at the mean frequency, distinct from the inverse of the mean period.

standard deviations are small. It ensures that, for nonzero σ, the reciprocal of the mean frequency is shorter than the mean period τ_0. This effect becomes more pronounced as σ increases. The reciprocal of the median frequency is approximately τ_0 and can be found at the half-maximal point of the cumulative probability distribution. The reciprocal of the mode frequency, found where $q'(\tau)=0$, is longer than τ_0. In the regime where $\sigma \ll \tau_0$ it approximates to

$$1/f_{\text{mode}} \approx \tau_0 + \frac{2\sigma^2}{\tau_0}. \tag{5}$$

Therefore, the reciprocal of the mean frequency is the shortest, followed by the reciprocal of the median frequency, and then by the reciprocal of the mode frequency when the frequency distribution is skewed (Figure 1D). As we show later, the macroscopic period resulting from the summation of uncoupled oscillators is longer than the average of the intrinsic periods. In contrast, the reciprocal of the synchronization frequency of coupled oscillators corresponds to that of the mean frequency, as predicted by the Kuramoto model (Saha and Amritkar, 2014; Peter and Pikovsky, 2018).

Macroscopic period of uncoupled oscillators

We begin with an extreme case of a collection of oscillators with a given frequency distribution that are uncoupled but start oscillation at the synchronized state. Then, their macroscopic oscillation is the result of integrating each oscillator multiplied by its probability density as

$$I = \int d\tau e^{-(\tau-\tau_0)^2/2\sigma^2} \cdot e^{2\pi i t/\tau}. \tag{6}$$

However, this integration is not straightforward for the period distribution because the period τ appears in the denominator, leading to a singularity. We can find an approximate expression for small $\sigma \ll \tau_0$ using the steepest descent method (see Materials and Methods).

$$I \approx \frac{1}{\sqrt{2\pi\sigma^2}} \exp\left[\frac{2\pi i}{\tau_0}t - \frac{2\pi^2\sigma^2}{\tau_0^4}t^2 - \frac{8\pi^3\sigma^4 i}{\tau_0^7}t^3\right] \tag{7}$$

Therefore, with higher σ, the macroscopic oscillation I damps while its period increases. If their frequencies, not periods, were from a Gaussian distribution, we would still see dampening, but

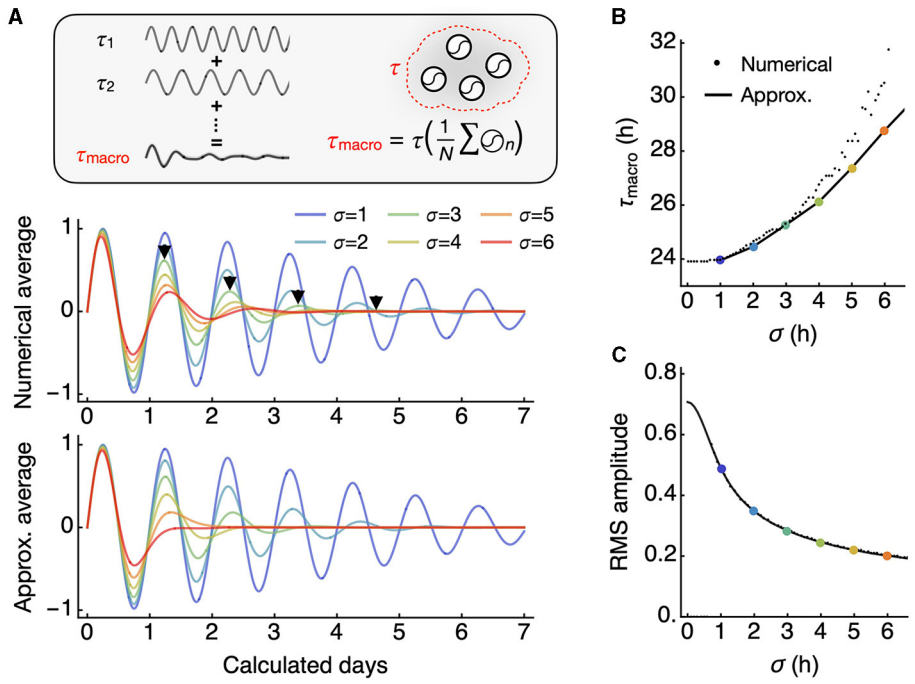

FIGURE 2
The macroscopic oscillation period is longer than the mean of individual oscillator periods. **(A)** The macroscopic oscillation represents the whole-field average of all individual oscillators (inset). The numerical integration of all oscillators over a continuous distribution results in a damped macroscopic oscillation with an increasing period, as indicated by each arrowhead marking peak positions (middle). The integral has an approximation in closed form that also shows an increasing period (bottom). **(B)** As the standard deviation of the period distribution increases, there is a corresponding increase in the macroscopic period. For smaller standard deviations, the analytic approximation (line) aligns closely with the numerical averages (small dots). **(C)** The root mean square (RMS) amplitude decreases with an increasing standard deviation, in an inverse relationship. The approximation (line) closely predicts the numerical averages (small dots).

the period would remain the same. This result is confirmed by numerical integration compared to the approximation (Eq. 7) (Figure 2A). Both the period of I (the macroscopic period) and the root mean square (RMS; square root of mean of squared values) as collective amplitude of I align well with the approximation (Figures 2B, C).

Synchronization period through increased coupling

In the other case, increasing coupling drives oscillators toward synchronized oscillation with the mean frequency. On its course, the discrepancy between the macroscopic period and the mean period in the distribution of individual oscillators narrows. With the coupling strength K, the evolution of phase θ_i in each oscillator is described by the following equation:

$$\frac{d\theta_i}{dt} = \frac{2\pi}{\tau_i} + \frac{K}{N}\sum_{j}^{N}\sin(\theta_j - \theta_i) \quad (8)$$

We generated 30 simulated networks, each consisting of 300 oscillators with a Gaussian period distribution ($\sigma = 4$ h). When the coupling strength (K) is below the critical level, the macroscopic period tends to be longer than the mean period on average, and this can be accurately predicted by the reciprocal of the mode frequency (Figure 3A, red). However, as K exceeds the critical level (approximately 0.1 in this case), synchronization occurs at a period shorter than the median (24 h). The reciprocal of the mean frequency provides a good estimate of the synchronized frequency for the given period distribution (Figure 3A, blue).

We present the simulation results for all 30 networks in Figure 3B. The Kuramoto order parameter R indicates the degree of synchronization of the oscillators at each level of K. Notably, R evolves into a stable orbit, even when R is below 1 (Figure 3B, inset). We note that the RMS amplitude serves as a good indicator of R, reflecting the switch-like characteristic of R with respect to K. In the absence of coupling, the macroscopic period of I can vary, but both the macroscopic period and the mean period converge toward a shorter period, as we have described. This results in an inverse correlation between the average period and the RMS amplitude (Figure 3C), a relationship reminiscent of the twist relationship observed in the choroid plexus (Myung et al., 2018). This relationship effectively captures the broader impacts of synchronization, given that R is proportional to the RMS amplitude.

Discussion

It is plausible that, within the mammalian circadian system, coupling and the resulting synchronization are integral components of its design. Most discussions on synchronization

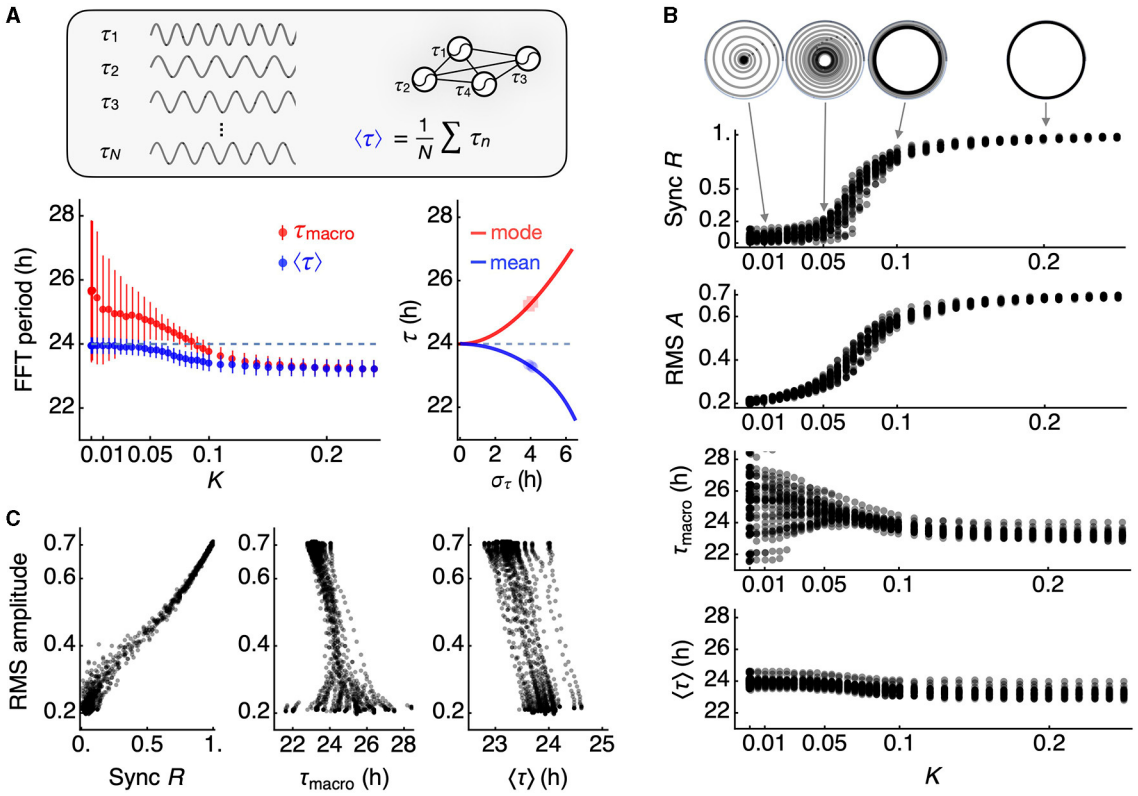

FIGURE 3
Changes in macroscopic circadian parameters under network coupling. **(A)** The mean of individual oscillator periods (inset), estimated by FFT (blue datapoints), differs from the macroscopic oscillation period (red datapoints). At a low coupling constant *K*, the mean of individual oscillator periods (24 h, dashed line) follows the inverse of the mean frequency, in contrast with the macroscopic period of the mean oscillation. As network coupling strengthens, these two estimates of periods converge (left panel). The error bars represent the standard deviation across 30 simulated networks. When coupling falls below a critical level for synchronization, the mode of the frequency distribution predicts the macroscopic period, while the mean of the frequency distribution predicts the mean of individual periods (right panel). The periods of 300 individual oscillators are randomly selected from 30 normal distributions with a standard deviation of 4 h. **(B)** Synchronization emerges in a switch-like fashion with increasing coupling strength. The collective phase evolves over time under each coupling condition but settles into a collective amplitude *R*, known as the Kuramoto order parameter (top), and the RMS amplitude of the macroscopic oscillation closely follows *R* (second from top). The macroscopic period is variable when the coupling is below a critical level (third from top), while the mean of individual oscillator periods is less variable (bottom). Both estimates of periods converge to a period shorter than the mean period in the original period distribution. **(C)** The order parameter *R* shows a strong correlation with the RMS amplitude (correlation coefficient = 0.996 ± 0.002 for 30 network simulations) (left panel). A generally negative relationship is observed between the macroscopic period and the RMS amplitude (correlation coefficient = −0.770 ± 0.313 for 30 network simulations) (mid panel), while the mean of oscillator periods exhibits a perfect negative correlation (-0.997 ± 0.002 for 30 network simulations) (right panel).

assume a Gaussian distribution of periods, where synchronization occurs at the mean period. However, the formalism of the Kuramoto model predicts that synchronization is achieved at the mean frequency. This distinction might seem subtle but could carry significant implications.

The effects of the skewed frequency distribution due to period variance that we explored are for $\sigma = 4$ h. Data on the electrical firing rate and the bioluminescent clock gene reporter activity from dissociated single SCN neurons show a standard deviation of <2 h (Herzog et al., 2004; Honma et al., 2004, 2012). This amounts to <10% difference between the mean and median frequencies. This difference diminishes as the synchronization tightens the distribution (Figure 1D). When the system is coupled below the critical level, the effects of a skewed frequency distribution become apparent in externally observable states of period and amplitude. Specifically, the period systematically deviates from the mean period. Our analytical and numerical approach provides insights into these deviations.

The effect described above is closely related to another issue in chronobiology, namely the skewed Arnold tongue when presented in terms of period instead of frequency (Schmal et al., 2015, 2020). The simplest form of synchronization, commonly referred to as entrainment, is the unidirectional synchronization of an internal clock to an external Zeitgeber signal, such as rhythmic light or temperature cues. Entrainment typically occurs within a wedge-shaped entrainment region within the Zeitgeber period (T) and Zeitgeber strength (K) parameter plane that broadens for large Zeitgeber strength and tapers toward the intrinsic period (τ) for decreasing strength K. Since the information of the Zeitgeber signal typically enters the underlying system's equations via the frequency, the reciprocal relationship between frequency and period leads to an asymmetric entrainment region in the period domain. This has implications for circadian physiology

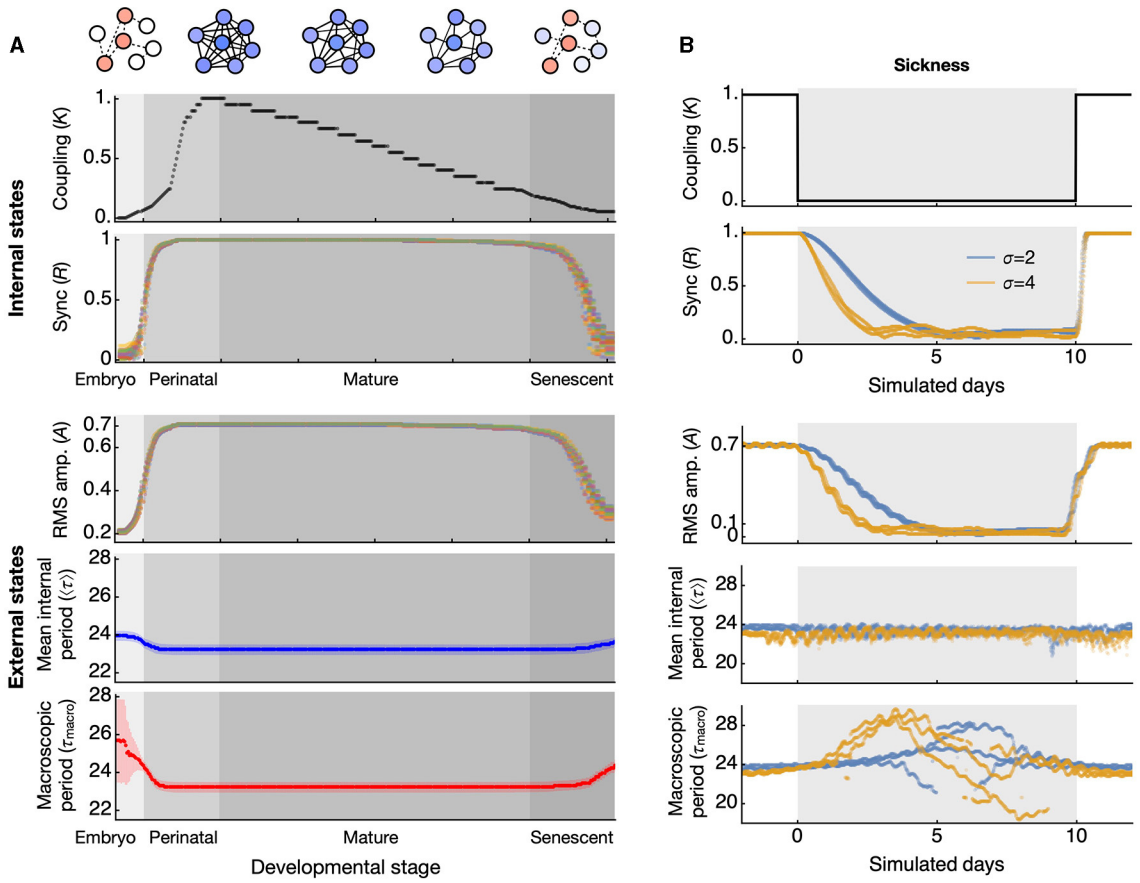

FIGURE 4
Simulated test of synchronization-induced amplitude and period alterations at the whole-animal level in aging and disease conditions. **(A)** Throughout development and aging, the coupling of the circadian clock network is hypothesized to increase and mature at the end of the perinatal stage, then gradually decrease until senescence (top panel). The synchronization of circadian clocks, quantified by the order parameter *R*, shows a discrete transition of states (second from top). These two are internal states that cannot be directly observed. The externally observable circadian rhythms alter according to the state of synchronization. The amplitude of circadian activity correlates positively with the synchronization state (third from top). The datapoints in different colors represent simulated data from 30 different networks, each composed of 300 oscillators randomly selected from period distributions with a standard deviation of 4 h. The period generally correlates negatively with the synchronization state, with less variation in the mean period (blue, fourth from top) than in the macroscopic period (red, bottom panel). The error bars indicate the standard deviation across 30 networks. **(B)** Under abrupt changes in coupling strength, which can occur during acute disease conditions (top panel), the degree of synchronization gradually decreases during the transition (second from top). This transitional change is reflected in the RMS amplitude of circadian activity (third from top). The mean of all oscillator periods slightly increases during the abrupt drop in coupling (fourth from top), while the macroscopic period changes drastically during the same drop in coupling (bottom). The periods indicated are evaluated from a 5-day sliding window FFT. The datapoints in pale blue and light orange colors represent results from simulations of three networks each, derived from two distributions with standard deviations of 2 and 4 h, respectively.

as it could directly translate into asymmetric distributions of chronotypes.

In a broader biological context, our findings have potential implications for both development and disease. It is believed that the coupling within the circadian clock network changes throughout development (Olejniczak et al., 2023). Around the time of birth, the circadian period displays wide variations across species (Rivkees, 2003; Yamazaki et al., 2005; Bellavia et al., 2006), a phenomenon potentially explained by the lack of coupling (Weinert and Weiß, 1997). As aging progresses, the clock network is thought to deteriorate (Farajnia et al., 2014). Thus, the network coupling, established during embryonic and perinatal stages, might peak and then gradually decline throughout mature and senescent stages (Figure 4A, upper, "Internal states"). Although this deterioration is gradual, the switch-like relationship between coupling strength (K) and synchronization (R) implies that R will remain stable as long as K stays above a critical level. As senescence begins and coupling weakens, there may be stage-specific alterations in circadian amplitude and periods (Figure 4A, lower, "External states"). In humans, these senescence-related changes are evident among Alzheimer's disease (AD) patients, with low circadian activity amplitude and delayed acrophase (Satlin et al., 1995).

Similarly, a sudden illness will not have immediate effects on the circadian rhythm since the underlying oscillators have already been well synchronized, and they require time to gradually fall into desynchronization (Myung et al., 2012). Even if an illness were to completely disrupt the coupling, the RMS amplitude

would decay gradually and the mean period would remain initially unaffected (Figure 4B). However, over time the macroscopic period will experience significant fluctuations, a phenomenon consistent with the unstable circadian period observed in chronic illnesses, such as CKD (Myung et al., 2019). A significant alteration in circadian period is also observed in AD (Volicer et al., 2012).

There is a question concerning the interpretation of the macroscopic period (τ_{macro}) compared to the mean internal period (τ_0). This question ties into a longstanding debate within SCN physiology regarding the preferred extracellular signal pathway: diffusive signaling (also known as volume transmission) vs. synaptic signaling (also known as wiring transmission) (Moore, 2013). The macroscopic period is estimated from the average oscillation of the entire ensemble. In the bioluminescent reporter system, this value corresponds to the whole-field luminometry data from a culture dish. The signal through volume transmission would carry information of the macroscopic period as it is the average of the entire ensemble output. In contrast, the mean internal period is calculated as the average period of each individual cellular oscillator, as determined from imaging data. From a distant tissue receiving the circadian signal through volume transmission, the detailed individual activities are unknown. Synaptic signaling originates from individual neurons, and therefore, individual periods can be accessed. In this context, the macroscopic period corresponds to the period observed in volume transmission, while the mean internal period can be evaluated through synaptic signaling. The circadian amplitude of volume transmission reflects the RMS amplitude of the clock assembly I, whereas the amplitude of wiring transmission reflects the order parameter R. These two are comparable, as seen in Figure 3. However, the variation of period at low coupling strength is much larger in the volume transmission (as reflected by the macroscopic period) than in the synaptic transmission (reflected by the mean internal period). At least for the circadian locomotor outputs, the macroscopic period from our simulation seems to better represent realistic observations, where the diffusible clock signals originate in the SCN (LeSauter and Silver, 1998) and propagate through cerebrospinal fluid irrigation (Leak and Moore, 2012).

In this study, we demonstrated that synchronization can influence the observed period of an ensemble. One potential application is assessing the synchronization state of the cell population by examining the macroscopic period of total reporter activities from cultured cells or tissues. The degree of synchronization can vary due to factors such as development, the level of integration within a tissue, or pathological conditions. Therefore, synchronization can serve as a qualitative indicator of these states, which can be gauged by the macroscopic period and/or period distribution. In principle, it is possible to evaluate the phenotype of an *in vitro* culture reflecting these states (Kumpošt et al., 2021). Although obtaining an exact measure of synchronization might be challenging, as indicated in Figure 4A, the macroscopic period can provide insights into developmental maturation, cellular interactions, or even the pathological phenotype of cellular ensembles modeling a disease. This becomes particularly relevant when individual periods are not directly accessible. Since synchronization can influence the macroscopic period, such determinations can be made solely by observing this period. This approach can be especially valuable in studies, for example, of spheroids.

Although the coupling strength may not be directly measurable in a given individual, our study suggests that other observable features could indicate decreased coupling. For instance, a decrease in amplitude of activities and core temperature can signal a loss of synchrony and/or coupling. It is also conceivable that the changes in the circadian period caused by decreased coupling could lead to a desynchronization of behavioral organization within the same individual, such as timings of eating and motor behaviors. These potential indicators could be used to evaluate the loss of internal synchrony or coupling, which could in turn inform the development of personalized chronotherapies, an approach that has yet to demonstrate significant benefits (Lee et al., 2021).

It is interesting to note that in our schematic simulation over the course of life, the critical coupling level to enter or exit the stable period would be crossed twice. However, the components of the network can change through aging (Farajnia et al., 2014), and it is unclear whether the critical coupling strength at these two points corresponds to the same value. It would also be important to note that the environmental factors can affect differently toward synchronization at these two points of development. These factors can be systemic, given that other peripheral clocks can influence the pacing of the master clock (Myung et al., 2018, 2019; Chrobok et al., 2022). Therefore, it would be valuable to investigate what other factors, in conjunction with the local network coupling, determine the fate of synchrony.

Materials and methods

Approximate mean period of the skewed frequency distribution

If the period follows a Gaussian distribution with mean τ_0, and variance σ^2, a generating function can be defined as follows.

$$Z[\omega] = \int \frac{d\tau}{\sqrt{2\pi\sigma^2}} e^{-(\tau-\tau_0)^2/2\sigma^2+\omega\tau}.$$

Then Z[ω] satisfies

$$\int d\tau\ p(\tau) = Z[\omega = 0] = 1$$
$$\langle\tau\rangle = \partial_\omega Z[\omega = 0] = \tau_0$$
$$\langle\tau^2\rangle = \partial_\omega^2 Z[\omega = 0] = \tau_0^2 + \sigma^2.$$

Here we define another function

$$Y[\omega] = \int \frac{d\tau}{\sqrt{2\pi\sigma^2}} \cdot \frac{1}{\tau} \cdot e^{-(\tau-\tau_0)^2/2\sigma^2+\omega\tau},$$

such that $\partial_\omega Y[\omega]$=$Z[\omega]$.

By direct integration, we get

$$Z[\omega] = \exp\left[-\frac{\tau_0}{2\sigma^2} + \frac{\sigma^2}{2}(\omega + \tau_0/\sigma^2)^2\right].$$

Using this,

$$Y[\omega] = \int d\omega\ Z[\omega] = \frac{\sqrt{2}}{\sigma} e^{\tau_0\omega+\frac{\sigma^2\omega^2}{2}} F\left(\frac{\tau_0 + \sigma^2\omega}{\sqrt{2}\sigma}\right) + C,$$

where F is the Dawson function. $C = 0$ will become evident later. Then,

$$\left\langle \frac{1}{\tau} \right\rangle = Y[0] = \frac{\sqrt{2}}{\sigma} F\left(\frac{\tau_0}{\sqrt{2}\sigma} \right).$$

which gives equation (3).

Approximate expression for the macroscopic oscillator *I*

We use the steepest descent method for approximation (Strogatz, 2014). Equation (6) can be re-written for simplification such that

$$I = \int d\tau \; e^{-L(\tau)/2\sigma^2}$$

where

$$L(\tau) = (\tau - \tau_0)^2 - 2i\alpha\sigma^2\tau^{-1}, \quad \alpha = 2\pi t$$

We find the stationary point by $L'(\tau) = 0$ and therefore,

$$L'(\tau)/2 = (\tau - \tau_0)^2 + i\alpha\sigma^2\tau^{-2} = 0$$

If we assume that the solution is $\tau = \tau_0 + \delta\tau$ where $\delta\tau/\tau_0 \ll 1$,

$$L'(\tau_0 + \delta\tau)/2 = \delta\tau + i\alpha\sigma^2\tau_0^{-2}\left(1 + \frac{\delta\tau}{\tau_0}\right)^{-2}.$$

This leads to the approximation

$$(1 - 2i\beta)\left(\frac{\delta\tau}{\tau_0}\right) \approx -i\beta \quad ,$$

where $\beta = \alpha\sigma^2\tau_0^{-3} = 2\pi\sigma^2\tau_0^{-3}\, t$ is dimensionless. Since we can regard $0 \le t \le \tau_0$, we have $0 \le \beta \le 2\pi\sigma^2\tau_0^{-2}$. Therefore, $\beta \ll 1$ if $\sigma^2 \ll \tau_0^2/2\pi$. Then,

$$\frac{\delta\tau}{\tau_0} \approx -\frac{i\beta}{1 - 2i\beta} \quad .$$

With a little algebra, we obtain

$$\begin{aligned} L(\tau_0 + \delta\tau)/\tau_0^2 &\approx (\delta\tau/\tau_0)^2 - 2i\beta(1 + \delta\tau/\tau_0)^{-1} \\ &\approx -2i\beta + \beta^2 + 2i\beta^3 - \cdots . \end{aligned}$$

Therefore,

$$I = \int d\tau \; e^{-L(\tau)/2\sigma^2} = \int du \; e^{-L(\tau_0+\delta\tau+u)/2\sigma^2}$$

which approximates to

$$I \approx \int du \; e^{-u^2/2\sigma^2 - (-2i\beta+\beta^2+2i\beta^3)\tau_0^2/2\sigma^2}$$

and gives the expression in equation (7).

Numerical simulations

All numerical simulations were performed using Mathematica 13 (Wolfram Research, Champaign, IL). 30 sets of periods of 300 oscillators were generated from a Gaussian distribution at mean 24 h and various standard deviations (mostly 4 h for Figures 3, 4) at different random seeds. Simulation was performed for the 30 circadian cycles (corresponding to 30 days). Estimation of period from these simulated oscillators were performed using fast Fourier transform after discretization into 15-min sampling interval as introduced earlier (Myung et al., 2012). The order parameter was estimated at the end of the simulation duration.

Data availability statement

The original contributions presented in the study are included in the article/supplementary material, further inquiries can be directed to the corresponding authors.

Author contributions

JM conceptualized the study and wrote the first draft of the manuscript. JM, SH, and CS performed mathematical analysis. JM, HV, and M-YW interpreted the results. All authors discussed the results, contributed to the article and final manuscript, and approved the submitted version.

Funding

This work was financially supported by the Higher Education Sprout Project of the Ministry of Education (MOE) in Taiwan. JM was supported through the National Science and Technology Council (NSTC), Taiwan (112-2314-B-038-063 and 111-2314-B-038-008). SH was supported by the Okinawa Institute of Science and Technology Graduate University. CS acknowledges support by the German Research Foundation (Deutsche Forschungsgemeinschaft, DFG) through grant SCHM 3362/4-1, project number 511886499. HV acknowledges support from the NSTC, Taiwan, (110-2811-B006-540, 111-2811-B006-028, and 112-2811-B006-033). M-YW acknowledges support by the NSTC, Taiwan (109-2314-B-038-106-MY3).

Conflict of interest

The authors declare that the research was conducted in the absence of any commercial or financial relationships that could be construed as a potential conflict of interest.

Publisher's note

All claims expressed in this article are solely those of the authors and do not necessarily represent those of their affiliated

organizations, or those of the publisher, the editors and the reviewers. Any product that may be evaluated in this article, or claim that may be made by its manufacturer, is not guaranteed or endorsed by the publisher.

References

Acebrón, J. A., Bonilla, L. L., Vicente, C. J. P., Ritort, F., and Spigler, R. (2005). The Kuramoto model: a simple paradigm for synchronization phenomena. *Rev. Mod. Phys.* 77:137. doi: 10.1103/RevModPhys.77.137

Aziz, N. A., Anguelova, G. V., Marinus, J., Lammers, G. J., and Roos, R. A. (2010). Sleep and circadian rhythm alterations correlate with depression and cognitive impairment in Huntington's disease. *Parkinsonism Relat. Disord.* 16, 345–350. doi: 10.1016/j.parkreldis.2010.02.009

Bellavia, S. L., Carpentieri, A. R., Vaqué, A. M., Macchione, A. F., and Vermouth, N. T. (2006). Pup circadian rhythm entrainment—effect of maternal ganglionectomy or pinealectomy. *Physiol. Behav.* 89, 342–349. doi: 10.1016/j.physbeh.2006.06.018

Chrobok, L., Ahern, J., and Piggins, H. D. (2022). Ticking and talking in the brainstem satiety centre: circadian timekeeping and interactions in the diet-sensitive clock of the dorsal vagal complex. *Front. Physiol.* 13:931167. doi: 10.3389/fphys.2022.931167

Davis, F. C., and Menaker, M. (1981). Development of the mouse circadian pacemaker: independence from environmental cycles. *J. Comp. Physiol.* 143, 527. doi: 10.1007/BF00609919

del Olmo, M., Schmal, C., Mizaikoff, C., Grabe, S., Gabriel, C., Kramer, A., et al. (2023). Are circadian amplitudes and periods correlated? a new twist in the story. *bioRxiv* 2023–05. doi: 10.12688/f1000research.135533.1

Farajnia, S., Deboer, T., Rohling, J. H., Meijer, J. H., and Michel, S. (2014). Aging of the suprachiasmatic clock. *Neuroscientist* 20, 44–55. doi: 10.1177/1073858413498936

Farajnia, S., Michel, S., Deboer, T., Tjebbe vanderLeest, H., Houben, T., Rohling, J. H., et al. (2012). Evidence for neuronal desynchrony in the aged suprachiasmatic nucleus clock. *J. Neurosci.* 32, 5891–5899. doi: 10.1523/JNEUROSCI.0469-12.2012

Felten, M., Dame, C., Lachmann, G., Spies, C., Rubarth, K., Balzer, F., et al. (2023). Circadian rhythm disruption in critically ill patients. *Acta Physiol.* 238:e13962. doi: 10.1111/apha.13962

Giri, A., Wang, Q., Rahman, I., and Sundar, I. K. (2022). Circadian molecular clock disruption in chronic pulmonary diseases. *Trends Mol. Med.* 28, 513–527. doi: 10.1016/j.molmed.2022.04.002

Herzog, E. D., Aton, S. J., Numano, R., Sakaki, Y., and Tei, H. (2004). Temporal precision in the mammalian circadian system: a reliable clock from less reliable neurons. *J. Biol. Rhythms* 19, 35–46. doi: 10.1177/0748730403260776

Honma, S., Nakamura, W., Shirakawa, T., and Honma, K. I. (2004). Diversity in the circadian periods of single neurons of the rat suprachiasmatic nucleus depends on nuclear structure and intrinsic period. *Neurosci. Lett.* 358, 173–176. doi: 10.1016/j.neulet.2004.01.022

Honma, S., Ono, D., Suzuki, Y., Inagaki, N., Yoshikawa, T., Nakamura, W., et al. (2012). Suprachiasmatic nucleus: cellular clocks and networks. *Prog. Brain Res.* 199, 129–141. doi: 10.1016/B978-0-444-59427-3.00029-0

Hsu, C. Y., Chang, F. C., Ng, H. Y., Kuo, C. C., Lee, Y. T., Lu, C. Y., et al. (2012). Disrupted circadian rhythm in rats with nephrectomy-induced chronic kidney disease. *Life Sci.* 91, 127–131. doi: 10.1016/j.lfs.2012.06.024

Kelso, J. S. (1995). *Dynamic Patterns: The Self-Organization of Brain and Behavior*. Cambridge, MA: MIT Press.

Kumpošt, V., Vallone, D., Gondi, S. B., Foulkes, N. S., Mikut, R., and Hilbert, L. (2021). A stochastic oscillator model simulates the entrainment of vertebrate cellular clocks by light. *Sci. Rep.* 11, 14497. doi: 10.1038/s41598-021-93913-2

Leak, R. K., and Moore, R. Y. (2012). Innervation of ventricular and periventricular brain compartments. *Brain Res.* 1463, 51–62. doi: 10.1016/j.brainres.2012.04.055

Lee, Y., Field, J. M., and Sehgal, A. (2021). Circadian rhythms, disease and chronotherapy. *J. Biol. Rhythms* 36, 503–531. doi: 10.1177/07487304211044301

Leise, T. L., Wang, C. W., Gitis, P. J., and Welsh, D. K. (2012). Persistent cell-autonomous circadian oscillations in fibroblasts revealed by six-week single-cell imaging of PER2: LUC bioluminescence. *PLoS ONE* 7:e33334. doi: 10.1371/journal.pone.0033334

LeSauter, J., and Silver, R. (1998). Output signals of the SCN. *Chronobiol. Int.* 15, 535–550. doi: 10.3109/07420529808998706

Liu, C., Weaver, D. R., Strogatz, S. H., and Reppert, S. M. (1997). Cellular construction of a circadian clock: period determination in the suprachiasmatic nuclei. *Cell* 91, 855–860. doi: 10.1016/S0092-8674(00)80473-0

Moore, R. Y. (2013). The suprachiasmatic nucleus and the circadian timing system. *Prog. Mol. Biol. Transl. Sci.* 119, 1–28. doi: 10.1016/B978-0-12-396971-2.00001-4

Myung, J., Hong, S., DeWoskin, D., De Schutter, E., Forger, D. B., and Takumi, T. (2015). GABA-mediated repulsive coupling between circadian clock neurons in the SCN encodes seasonal time. *Proc. Nat. Acad. Sci.* 112, E3920–E3929. doi: 10.1073/pnas.1421200112

Myung, J., Hong, S., Hatanaka, F., Nakajima, Y., De Schutter, E., and Takumi, T. (2012). Period coding of *Bmal1* oscillators in the suprachiasmatic nucleus. *J. Neurosci.* 32, 8900–8918. doi: 10.1523/JNEUROSCI.5586-11.2012

Myung, J., and Pauls, S. D. (2018). Encoding seasonal information in a two-oscillator model of the multi-oscillator circadian clock. *Eur. J. Neurosci.* 48, 2718–2727. doi: 10.1111/ejn.13697

Myung, J., Schmal, C., Hong, S., Tsukizawa, Y., Rose, P., Zhang, Y., et al. (2018). The choroid plexus is an important circadian clock component. *Nat. Commun.* 9, 1062. doi: 10.1038/s41467-018-03507-2

Myung, J., Wu, M. Y., Lee, C. Y., Rahim, A. R., Truong, V. H., Wu, D., et al. (2019). The kidney clock contributes to timekeeping by the master circadian clock. *Int. J. Mol. Sci.* 20:2765. doi: 10.3390/ijms20112765

Ohta, H., Yamazaki, S., and McMahon, D. G. (2005). Constant light desynchronizes mammalian clock neurons. *Nat. Neurosci.* 8, 267–269. doi: 10.1038/nn1395

Olejniczak, I., Pilorz, V., and Oster, H. (2023). Circle (s) of life: the circadian clock from birth to death. *Biology.* 12:383. doi: 10.3390/biology12030383

Peter, F., and Pikovsky, A. (2018). Transition to collective oscillations in finite Kuramoto ensembles. *Phys. Rev. E.* 97:032310. doi: 10.1103/PhysRevE.97.032310

Pittendrigh, C. S., and Daan, S. (1974). Circadian oscillations in rodents: a systematic increase of their frequency with age. *Science.* 186, 548–550. doi: 10.1126/science.186.4163.548

Pittendrigh, C. S., and Daan, S. (1976a). A functional analysis of circadian pacemakers in nocturnal rodents: I. the stability and lability of spontaneous frequency. *J. Comp. Physiol.* 106, 223–252. doi: 10.1007/BF01417856

Pittendrigh, C. S., and Daan, S. (1976b). A functional analysis of circadian pacemakers in nocturnal rodents: V. pacemaker structure: a clock for all seasons. *J. Comp. Physiol.* 106, 333–355. doi: 10.1007/BF01417860

Possidente, B., McEldowney, S., and Pabon, A. (1995). Aging lengthens circadian period for wheel-running activity in C57BL mice. *Physiol. Behav.* 57, 575–579. doi: 10.1016/0031-9384(94)00298-J

Rivkees, S. A. (2003). Developing circadian rhythmicity in infants. *Pediatrics* 112, 373–381. doi: 10.1542/peds.112.2.373

Saha, A., and Amritkar, R. E. (2014). Dependence of synchronization frequency of Kuramoto oscillators on symmetry of intrinsic frequency in ring network. *Pramana* 83, 945–953. doi: 10.1007/s12043-014-0831-5

Satlin, A., Volicer, L., Stopa, E. G., and Harper, D. (1995). Circadian locomotor activity and core-body temperature rhythms in Alzheimer's disease. *Neurobiol. Aging* 16, 765–771. doi: 10.1016/0197-4580(95)00059-N

Schmal, C. (2023). The seasons within: a theoretical perspective on photoperiodic entrainment and encoding. *J. Comp. Physiol. A.* doi: 10.1007/s00359-023-01669-z

Schmal, C., Herzel, H., and Myung, J. (2020). Clocks in the wild: entrainment to natural light. *Front. Physiol.* 11:272. doi: 10.3389/fphys.2020.00272

Schmal, C., Herzog, E. D., and Herzel, H. (2018). Measuring relative coupling strength in circadian systems. *J. Biol. Rhythms* 33, 84–98. doi: 10.1177/0748730417740467

Schmal, C., Myung, J., Herzel, H., and Bordyugov, G. (2015). A theoretical study on seasonality. *Front. Neurol.* 6:94. doi: 10.3389/fneur.2015.00094

Schwartz, W. J., and Zimmerman, P. (1990). Circadian timekeeping in BALB/c and C57BL/6 inbred mouse strains. *J. Neurosci.* 10, 3685–3694. doi: 10.1523/JNEUROSCI.10-11-03685.1990

Strogatz, S. H. (2014). *Nonlinear Dynamics and Chaos: With Applications to Physics, Biology, Chemistry, and Engineering. 2nd edn.* Boulder: Westview Press.

Valentinuzzi, V. S., Scarbrough, K., Takahashi, J. S., and Turek, F. W. (1997). Effects of aging on the circadian rhythm of wheel-running activity in C57BL/6 mice. *Am. J. Physiol.* 273, R1957–R1964. doi: 10.1152/ajpregu.1997.273.6.R1957

Volicer, L., Harper, D. G., and Stopa, E. G. (2012). Severe impairment of circadian rhythm in Alzheimer's disease. *J. Nutr. Health Aging* 16, 888–890. doi: 10.1007/s12603-012-0413-5

Weinert, D., and Weiß, T. (1997). A nonlinear interrelationship between period length and the amount of activity-age-dependent changes. *Biol. Rhythm Res.* 28, 105–120. doi: 10.1076/brhm.28.1.105.12983

Welsh, D. K., Richardson, G. S., and Dement, W. C. (1986). Effect of age on the circadian pattern of sleep and wakefulness in the mouse. *J. Gerontol.* 41, 579–586. doi: 10.1093/geronj/41.5.579

Winfree, A. T. (1980). *The Geometry of Biological Time (Vol. 2)*. New York, NY: Springer.

Witting, W., Kwa, I. H., Eikelenboom, P., Mirmiran, M., and Swaab, D. F. (1990). Alterations in the circadian rest-activity rhythm in aging and Alzheimer's disease. *Biol. Psychiatry* 27, 563–572. doi: 10.1016/0006-3223(90)90523-5

Yamazaki, A., Ohtsuki, Y., Yoshihara, T., Honma, S., and Honma, K. I. (2005). Maternal deprivation in neonatal rats of different conditions affects growth rate, circadian clock, and stress responsiveness differentially. *Physiol. Behav.* 86, 136–144. doi: 10.1016/j.physbeh.2005.07.013

Yang, P. L., Ward, T. M., Burr, R. L., Kapur, V. K., McCurry, S. M., Vitiello, M. V., et al. (2020). Sleep and circadian rhythms in survivors of acute respiratory failure. *Front. Neurol.* 11:94. doi: 10.3389/fneur.2020.00094

Zhang, Q., Bhattacharya, S., and Andersen, M. E. (2013). Ultrasensitive response motifs: basic amplifiers in molecular signalling networks. *Open Biol.* 3:130031. doi: 10.1098/rsob.130031

frontiers | Frontiers in Neuroscience

TYPE Original Research
PUBLISHED 17 April 2024
DOI 10.3389/fnins.2024.1186677

OPEN ACCESS

EDITED BY
Takahiro J. Nakamura,
Meiji University, Japan

REVIEWED BY
Atomu Sawatari,
The University of Sydney, Australia
Shigenori Nonaka,
Graduate University for Advanced Studies (Sokendai), Japan

*CORRESPONDENCE
Rika Numano
✉ numano@eiiris.tut.ac.jp

RECEIVED 15 March 2023
ACCEPTED 18 March 2024
PUBLISHED 17 April 2024

CITATION
Nakazawa K, Matsuo M, Kikuchi Y, Nakajima Y and Numano R (2024) Melanopsin DNA aptamers can regulate input signals of mammalian circadian rhythms by altering the phase of the molecular clock. *Front. Neurosci.* 18:1186677. doi: 10.3389/fnins.2024.1186677

Melanopsin DNA aptamers can regulate input signals of mammalian circadian rhythms by altering the phase of the molecular clock

Kazuo Nakazawa[1,2], Minako Matsuo[3], Yo Kikuchi[1,3], Yoshihiro Nakajima[4] and Rika Numano[1,3]*

[1]Department of Applied Chemistry and Life Science, Toyohashi University of Technology, Toyohashi, Aichi, Japan, [2]TechnoPro, Inc., Tokyo, Japan, [3]Institute for Research on Next-Generation Semiconductor and Sensing Science, Toyohashi University of Technology, Toyohashi, Aichi, Japan, [4]Health and Medical Research, National Institute of Advanced Industrial Science and Technology (AIST), Takamatsu, Kagawa, Japan

DNA aptamers can bind specifically to biomolecules to modify their function, potentially making them ideal oligonucleotide therapeutics. Herein, we screened for DNA aptamer of melanopsin (OPN4), a blue-light photopigment in the retina, which plays a key role using light signals to reset the phase of circadian rhythms in the central clock. Firstly, 15 DNA aptamers of melanopsin (Melapts) were identified following eight rounds of Cell-SELEX using cells expressing melanopsin on the cell membrane. Subsequent functional analysis of each Melapt was performed in a fibroblast cell line stably expressing both *Period2:ELuc* and melanopsin by determining the degree to which they reset the phase of mammalian circadian rhythms in response to blue-light stimulation. *Period2* rhythmic expression over a 24-h period was monitored in *Period2:ELuc* stable cell line fibroblasts expressing melanopsin. At subjective dawn, four Melapts were observed to advance phase by >1.5 h, while seven Melapts delayed phase by >2 h. Some Melapts caused a phase shift of approximately 2 h, even in the absence of photostimulation, presumably because Melapts can only partially affect input signaling for phase shift. Additionally, some Melaps were able to induce phase shifts in *Per1::luc* transgenic (Tg) mice, suggesting that these DNA aptamers may have the capacity to affect melanopsin *in vivo*. In summary, Melapts can successfully regulate the input signal and shifting phase (both phase advance and phase delay) of mammalian circadian rhythms *in vitro* and *in vivo*.

KEYWORDS

melanopsin (OPN4), DNA aptamer, Melapt, circadian rhythm, molecular clock, phase shift, period gene

Introduction

Most living organisms exposed to sunlight have evolved a ~ 24-h internal clock, known as a circadian rhythm, and synchronize the phases of this autonomous clock according to environmental clues (Ralph et al., 1990; Pittendrigh, 1993; Davidson et al., 2003; Yoo et al., 2004). Therefore, each organism resets the phase of its circadian rhythm to match the environmental light and dark cycle each morning. In mammals, circadian rhythms are influenced primarily by light, an input signal perceived through the eyes, which is capable of resetting the phase of transcriptional oscillations of clock genes (Takahashi, 1995; Menaker, 2003).

The central pacemaker of mammalian circadian rhythms is located in the suprachiasmatic nucleus (SCN). The retinohypothalamic tract (RHT) immediately transmits information about blue light in the early morning to the SCN via the photoreceptor melanopsin (OPN4) in the retina and resets the phase of the circadian clock along the environmental cycle. Melanopsin mainly transfers environmental blue-light signals to the central clock early in the morning to reset the phase of the clock in the SCN (Hattar et al., 2003; Lucas et al., 2003; Foster, 2005; Pulivarthy et al., 2007; Ukai et al., 2007; Guler et al., 2008; LeGates et al., 2012).

Melanopsin is a photoreceptor protein expressed in retinal ganglion cells that absorbs blue light with a maximum absorbance of 477 nm. Although the exact function of melanopsin was unclear until melanopsin-knockout (KO) mice were generated in 2003, melanopsin was known to play an important role in resetting the phase of the mammalian circadian clock by blue light. In the first step, the melanopsin receptor is activated by binding *trans*-isomerized retinal ligands under blue light through the Gq family. The photosignal affects SCN neurons through Gq family-mediated transient receptor potential polycystin (TRPP) control of cell firing, glutamate transmitters, and pituitary adenylate cyclase-activating polypeptide (PACAP). The transmitted stimuli eventually increase calcium ion flux in the cytoplasm of cells in the SCN to activate protein kinase A (PKA) and PKC. These kinases phosphorylate cAMP response element-binding protein (CREB) and activate the connected to the cAMP response element (CRE) consensus sequence in the *Period 1* (*Per1*) promoter to transiently induce *Per1* transcription and reset the phase of circadian rhythms (King et al., 1997; Sun et al., 1997; Tei et al., 1997; Hida et al., 2000; Yamazaki et al., 2000).

The phase of the molecular circadian clock is reset by, and depends on, the timing of light stimulation and transient induction of *Per1* by the melanopsin photoreceptor. Autonomous circadian clocks in individual cells of both the SCN and peripheral clocks are constituted by transcription and translation feedback loops involving clock genes, such as *Clock, Bmal1, Per1-3,* and *Cryptochromes*, as well as their protein products (Albrecht et al., 1997; Antoch et al., 1997; King et al., 1997; Shearman et al., 1997; Takumi et al., 1998; Zylka et al., 1998; Kume et al., 1999; Bunger et al., 2000; Numano et al., 2006). The photosignal by melanopsin transiently induces transcription of photoreactive clock genes such as *Per1* and *Per2* in the SCN from 30 min to 2 h following delivery of a light pulse to the retina. Induction of transient expression of these input genes influences the transcriptional and translational feedback loop within a 24-h period as well as the phase of the autonomous clock (Ellington and Szostak, 1990; Albrecht et al., 1997; Shearman et al., 1997; Shigeyoshi et al., 1997; Giebultowicz, 2004; Yan and Silver, 2004).

DNA aptamers are short, single-stranded RNA/DNA molecules that can bind selectively to specific targets, proteins, peptides, and other molecules and can be used clinically to switch the function of target molecules. The main advantages of these aptamers are high target specificity, lack of immunogenicity, and ease of synthesis.

The function of the melanopsin protein is easily modified by the DNA aptamer because it is located on the cell membrane. DNA aptamers are powerful pharmaceutical agents because, unlike antibodies, they can be stored stably and duplicated easily in large quantities using PCR.

People with sleep–wake phase disorder and shift workers who only sleep for 1–4 h may have difficulty falling asleep and waking up immediately in the morning (Takahashi et al., 2008; Gentry et al., 2021). Thus, it would be socially and economically advantageous to improve the sleep–wake cycle indirectly by manipulating the ability of melanopsin to input signals into a central clock. Antagonists of melanopsin acquired via chemical screening of chemical libraries primarily contribute to delaying the rhythm phase (Jones et al., 2013).

In this study, we used the cell systematic evolution of ligands by exponential enrichment (Cell-SELEX) method to identify DNA aptamers (single-stranded DNA; ssDNA) that caused melanopsin (expressed on the cell membrane) to shift the phase of circadian rhythms (Tuerk and Gold, 1990; Hida et al., 2000; Yamazaki et al., 2000; Umekage and Kikuchi, 2006; Dua et al., 2011). In total, 15 types of melanopsin aptamers were analyzed to assess their ability to shift the phase of *Per2::ELuc* bioluminescent oscillations in *Per2:ELuc*:TK:Mel stable cells, in which a bioluminescent reporter follows the *Per2* promoter region controlling an enhanced green-emitting luciferase from *Pyrearinus termitilluminans*, with melanopsin overexpressed under the control of the thymidine kinase (TK) promotor (Nakajima et al., 2010). In these stable fibroblast cell lines, the signal pathway is incorporated into a fibroblast cell mimicking the signal pathway from the retina to the SCN by melanopsin.

Among these 15 DNA aptamers of melanopsin (Melapts), four Melapts induced phase advance and seven Melapts induced delay of circadian rhythms (by >1.5 h and > 2 h, respectively) in the *Per2::ELuc* cell line. Some Melapts induced phase shifts of ~2 h even in the absence of photostimulation *in vitro*. As the results from *Per1::luc* transgenic (Tg) mice were similar to the *in vitro* results from the *Per2::ELuc* cell line, melanopsin was used to induce phase Shifts *in vivo*. In summary, Melapts were able to regulate input signals and phase shifts to achieve both phase advance and phase delay of mammalian circadian rhythms *in vitro* and *in vivo*.

Materials and methods

Screening of DNA aptamers by the cell-SELEX method

A random ssDNA library for screening of DNA aptamers by the Cell-SELEX method was designed based on a random DNA aptamer (5‘-AAAGGGGAATTCGGATCC-N-40-CTGCAGAAGCTTCCGAAAA-3′) with regions of 40 bases, and 10^{17} types of DNA aptamers with a fixed leading and trailing region were prepared by Hokkaido System Science (Hokkaido, Japan). A floating PC12 cell (obtained from the Cell Bank, RIKEN BRC, Ibaraki, Japan) was used to perform the Cell-SELEX method, and cells were cultured in low-glucose DMEM (FUJIFILM Wako, Tokyo, Japan) containing 10% fetal bovine serum (FBS; Wako, Tokyo, Japan), 5% donor horse serum (DHS; Wako, Tokyo, Japan), and 1% penicillin–streptomycin (Wako, Tokyo, Japan). The melanopsin expression plasmid (provided by Professor Ueda of the University of Tokyo) was transfected into PC12 cells using Lipofectamine 3000 (Invitrogen, Massachusetts, United States) to prepare (+) melanopsin-transfected PC12 cells ([+] melanopsin cells) in which melanopsin was overexpressed on the cell membrane, whereas in (−) melanopsin-free PC12-negative control cells (other [−] melanopsin cells without transfecting melanopsin: negative selection), melanopsin was not expressed. First, DNA aptamers

were mixed and incubated with (−) melanopsin cells, and only unbound DNA aptamers were recovered. Second, the recovered DNA aptamers in solution were mixed and incubated with (+) melanopsin cells, and only DNA aptamer bound to cells was recovered. Then, the recovered DNA aptamers specifically bound to (+) melanopsin cells but not bound to (−) melanopsin cells were amplified by asymmetric PCR amplofication (Figure 1A).

The obtained Melapts were amplified with forward and reverse primers in a 10:1 ratio by asymmetric PCR with reactions containing 10 pmol Melapt, 20 pmol forward primer

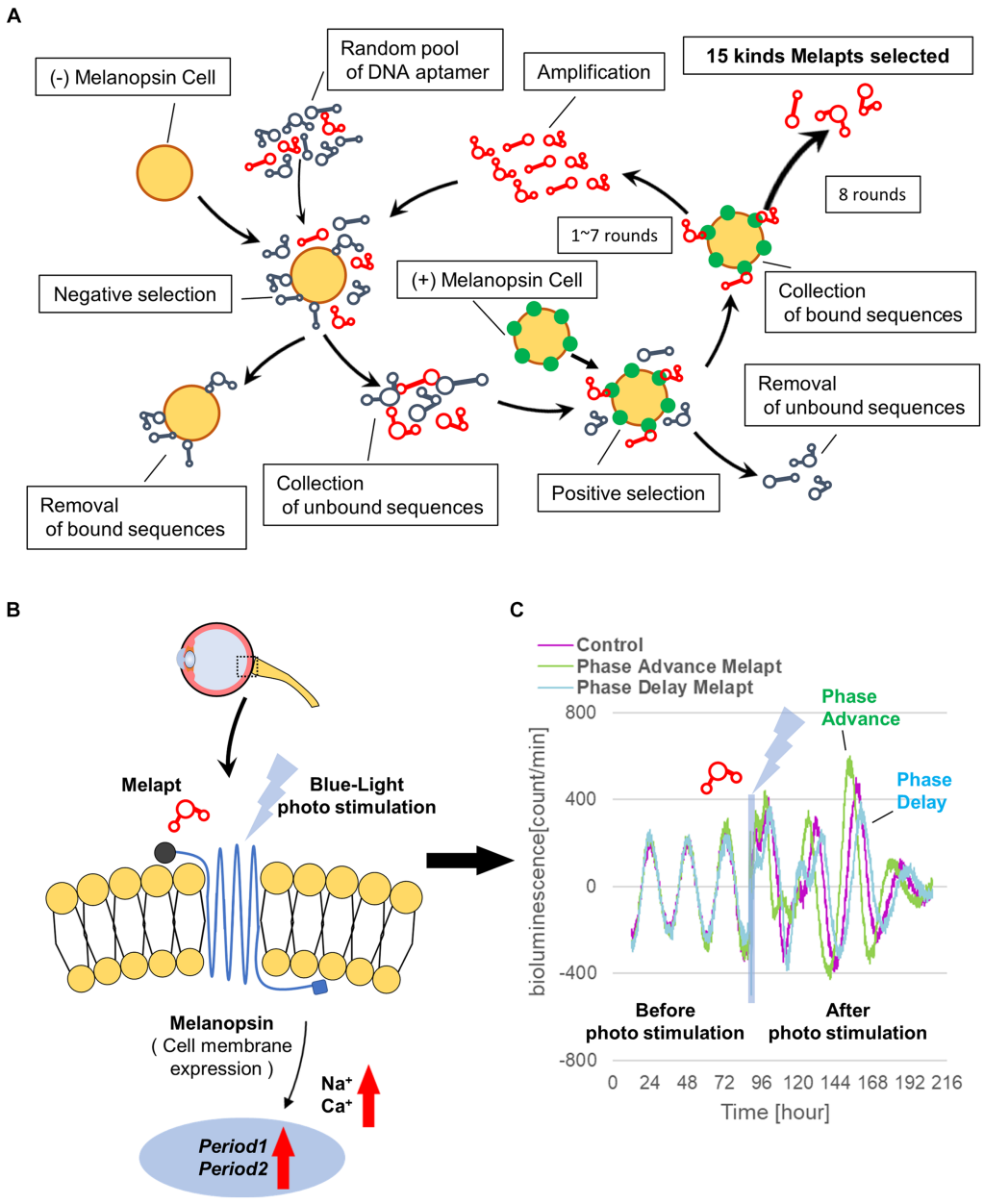

FIGURE 1
Cell-SELEX method for screening Melapts. Melapts that specifically bind melanopsin were selected by Cell-SELEX because melanopsin is a membrane protein bound and accessible from outside cells. **(A)** 10^{17} DNA aptamer were selected from a random ssDNA library. DNA aptamers were mixed and bound to (−) melanopsin cells (negative selection). When unbound DNA aptamers were retrieved, they were combined with (+) melanopsin cells to promote binding to melanopsin protein (positive selection). The Cell-SELEX process was performed over 8 rounds, and 15 types of Melapt were screened. Fluorescence intensity in the wells was measured (at λex 495 nm and λem 517 nm) using a microplate reader (Infinite 1,000; TECAN). **(B)** Conceptual diagram of Melapt binding to melanopsin followed by induction of the expression of the clock gene *Per2*. When melanopsin expressed on the surface of the cell membrane is photostimulated by a Melapt, the concentration of Na^+ and Ca^+ in the cytoplasm increases transiently, inducing the activation of transcriptional factors and the upregulation of *Per2* in the cell nucleus. **(C)** Phase shift of luciferase emission rhythms in *Per2:ELuc:*TK:Mel cells stably expressing melanopsin. When *Per2:ELuc* cells expressing melanopsin were photostimulated post-addition of Melapts, *Per2:ELuc* emission rhythms showed phase advance (green curve) or phase delay (blue curve) relative to controls (purple curve); these shifts were Melapt-dependent. PBS buffer alone was added to control cells.

10.3389/fnins.2024.1186677

(5′-AAAGGGGAATTCGGATCC-3′, FASMAC), 2 pmol reverse primer (5′-AAACGGAAGCTTCTGCAG-3′, FASMAC), 5 units Go Taq DNA polymerase (Promega; Wisconsin, USA), 30 nmol Mg^{2+} (Promega), 2.5 nmol dNTPs (Promega), and PCR buffer (Promega) in a final volume of 20 µL. The PCR amplification profile for Melapts involved preliminary denaturation at 95°C for 5 min, followed by 35 cycles of denaturation at 95°C for 30 s, annealing at 52°C for 1 min, extension at 72°C for 1 min, and a final extension at 72°C for 4 min.

Only those amplified as a significant sense band in gel electrophoresis were used in the next round of Cell-SELEX. These steps were repeated for eight rounds to concentrate DNA aptamers by asymmetric PCR amplification. Then, DNA aptamers were cloned into a T vector (Invitrogen), and aptamer sequences were confirmed by Fasmac Corporation (Kanagawa, Japan; Table 1). Finally, 15 DNA aptamers for melanopsin were selected and named Melapt1-Melapt15 (Supplementary Figure S1). Melapts obtained by the Cell-SELEX method appeared to bind specifically to melanopsin alone. Melanopsin-KO cells and melanopsin-KO mice were not used in this study.

TABLE 1 Sequences of melanopsin aptamers (Melapts).

Melapt01	CGACCCGAAGGAGCGGTGGATAACCCCACCAAGATACGTC
Melapt02	CCCGATTGGACAACTCAAACCATCATCCGAACCAGTACGT
Melapt03	GGCCGTCACGCCCCGGCTGCGAAGCCATCAAGCCTCCATA
Melapt04	CCGCACACGTGGAGCCAAGTCGAGTTTAATTCCCTATCGC
Melapt05	GAACTACCCTACAAACCAAACAAGGCGCACGATCGATATA
Melapt06	CCGATGTAGAAATCCAACACCGCAGTAGAGCATTGCCGAC
Melapt07	GAATCACTGGGCCCATGACCCCATGCAATACAAGAAGACT
Melapt08	TTCACCGATACGGCTCCCTTGGCCAGACAGGAAAAAATAA
Melapt09	AGCGTACGCCCAGGCCGGANTGGGACCGCAAACCCATTCG
Melapt10	GCCCCGGAGTGCGGCCTGAAAACCACCATCTATAAGCCAA
Melapt11	AGGATAATGAACCTTCGCCAGACCTACCCTAACAAGTCCCA
Melapt12	GAATTCCAGCACAGACCACCCTTGTCGAACCCAGCAACTCG
Melapt13	GAAGAGGGTGATCGTAATAACGCGTAAAACGAGACTATCT
Melapt14	GCACGGCGCGGTAGGCATGTCACTACCAGAAACTAGGCCC
Melapt15	CCCAAATCCATGAAAGGGGGAAACACAATCTTACGCCGCG

Sequences span regions of 40 bases. Melapts were generated by the Cell-SELEX method.

Binding assay of Melapts to (+) melanopsin cells

Melapts were amplified and labeled with a 6-FAM-forward primer. Briefly, 10 pmol Melapt, 20 pmol 6-FAM-forward primer (5′-AAAGGGGAATTCGGATCC-′3, Hokkaido System Science), 2 pmol reverse primer (5′-AAACGGAAGCTTCTGCAG-3′, Fasmac Corporation), 1 unit Go Taq DNA polymerase (Promega), 125 pmol dNTPs (Promega), 5× Go Taq Reaction Buffer (Promega), and nuclease-free water were combined in a 20 µL reaction volume using the Cell-SELEX amplification profile (Figure 2A).

Mouse fibroblast cells were cultured in 96-well plates (1.5×10^5 cells/well) using 200 µL DMEM, transfected with melanopsin, and incubated at 37°C and 5% CO_2 for 24 h. Then, 6-FAM-Melapt was added to the culture medium at six different concentrations (1.405 µg/mL, 5.625 µg/mL, 11.25 µg/mL, 22.5 µg/mL, 45.0 µg/mL, and 90.0 µg/mL) and incubated for 15 min. After washing, the binding capacity of 6-FAM-Melapts was estimated by measuring the fluorescence signal in (+) melanopsin cells (λex 495 nm, λem 517 nm) using an Infinite 1,000 microplate reader (Tecan, Zürich, Switzerland; Figure 1). The most suitable concentration of Melapts was 22.5 µg/mL. Before performing each measurement, 6-FAM-Melapt was added to three different wells ($n = 3$). A stable mouse fibroblast cell line (*Per2:ELuc*:TK:Mel) with Melapts was established to monitor the phase shift of *Per2:ELuc* bioluminescent emission rhythms using photo-responsive *ELuc*.

The 5′ flanking region of *Per2* (from −2,858 to +144, where +1 indicates the putative transcription start site) was PCR-amplified from the C57BL/6J mouse genome and cloned into the *Xho*I and *Bgl*II sites of pELuc (PEST)-test (Toyobo, Osaka, Japan). Expression cassettes containing early poly-A (pA) signal, *Per2* promoter, ELuc-PEST, and late pA signal were amplified by PCR and cloned into pENTR-D-TOPO (Thermo Fisher Scientific Inc., Waltham, MA, United States), with the attL1 and attL2 sites flanked by the upstream and downstream regions of early and late pA signals, respectively, resulting in pm*Per2*-ELuc-PEST-pENTR. The expression cassette was recombined into the pBsd-R4 attB vector (a gift from Dr. T. Ohbayashi) by the LR reaction using LR Clonase II Plus Enzyme Mix (Thermo Fisher Scientific, Inc.), yielding pR4-Bsd-m*Per2*-ELuc-PEST.

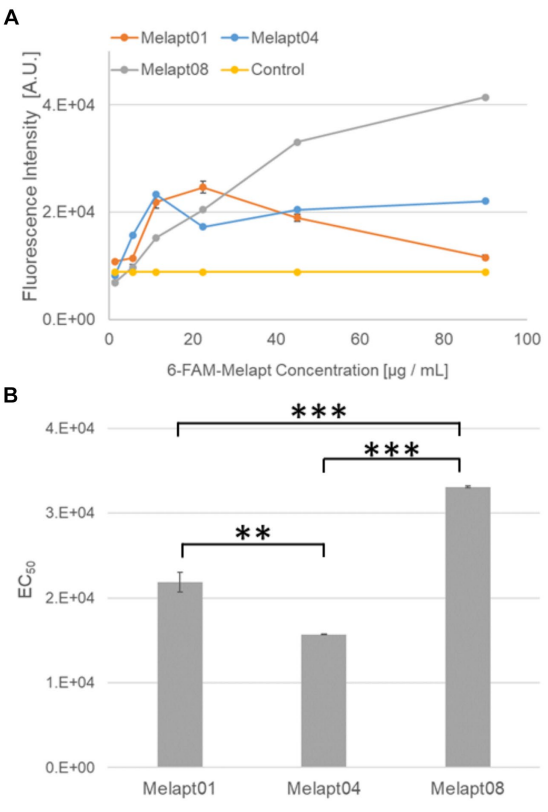

FIGURE 2
Binding of 6-FAM-Melapts to *Per2:ELuc*:TK:Mel stable cells expressing melanopsin. **(A)** 6-FAM-Melapts 01, 04, and 08 were added to cells at 1.405µg/mL, 5.625µg/mL, 11.25µg/mL, 22.5µg/mL, 45.0µg/mL, and 90.0µg/mL, whereas only PBS was added to control cells ($n = 3$). The 6-FAM fluorescence values of cells were plotted against the concentration of 6-FAM-Melapt. **(B)** The concentration resulting in EC_{50} was calculated from Figure 2A and plotted. Melapt01, 11.25µg/mL; Melapt04, 5.625µg/mL; Melapt08, 45.0µg/mL. $n = 3$, $^{**}p < 0.01$, $^{***}p < 0.001$, Tukey–Kramer test.

Furthermore, mOpn4-Flag, wherein the Flag-tag was fused in-frame to the C-terminus of mouse melanopsin cDNA, was synthesized as double-stranded DNA (GenScript, Tokyo, Japan) and cloned into pUC57. The mOpn4-Flag was excised using *Nco*I and *Xba*I and ligated into the *Nco*I and *Xba*I site of pTK-SLG-pENTR-D-Topo (Tabei et al., 2017), from which the SLG cDNA was removed, yielding pTK-mOpn4-Flag-pENTR. The expression cassette containing TK promoter, mOpn4-Flag, and late pA signal was recombined into the pNeo-ϕC31 attB vector (Yamaguchi et al., 2011; a gift from Dr. T. Ohbayashi) by the LR reaction, resulting in pϕC31-Neo-mOpn4-Flag.

Mouse fibroblast A9 cells harboring the multi-integrase mouse artificial chromosome (MI-MAC) vector (Takiguchi et al., 2014; kindly provided by Dr. M. Oshimura and Dr. Y. Kazuki) seeded into six-well plates were co-transfected a day later with pR4-Bsd-m*Per2*-ELuc-PEST and the R4 integrase expression plasmid pCMV-R4 (Yamaguchi et al., 2011; kindly provided by Dr. T. Ohbayashi) and subcultured for selection with 6 μg/mL Blasticidin S (Thermo Fisher Scientific, Inc.). Selected cells were further co-transfected with pϕC31-Neo-mOpn4-Flag and ϕC31 integrase expression plasmid pCMV-ϕC31 (Yamaguchi et al., 2011; kindly provided by Dr. T. Ohbayashi) and subcultured for selection with 800 μg/mL G418 (Nacalai Tesque, Kyoto, Japan). Genomic PCR confirmed the integration of the transgenes into the corresponding sites in the MI-MAC vector. The established cell line was named *Per2:ELuc:*TK:Mel.

The photo-responsive fibroblast stable cell line for functional analysis of DNA aptamers (ELuc:*Per2:ELuc:*TK:Mel) was stably transfected into *Per2*-enhanced green-emitting luciferase cells (*Per2:ELuc*) with melanopsin (mOPN4) expression under the control of the TK promoter to generate photo-responsive A9 fibroblast cells (Nakajima et al., 2010). Screening of DNA aptamers was performed using blue light-responsive and bioluminescence real-time imaging of circadian rhythms (Supplementary Figure S2). *Per2:ELuc* stably expresses ELuc under the control of the *Per2* promoter because the phase due to the transcriptional activity rhythm of *Per2* can be monitored from the emission rhythms of ELuc (Nakajima et al., 2010). *Per2:ELuc:*TK:Mel stable cells constitutively and stably express melanopsin on the cell surface under the control of the TK promoter. Melanopsin expressed on the surface of the cell membrane transmits external photo-stimuli into the cell and transiently induces *Per2* transcription in the cell nucleus. Thus, *Per2:ELuc:*TK:Mel stable cells are suitable for the phase shift of circadian rhythms in response to blue-light photo-stimuli.

Binding assay for Melapts

A total of 1.5×10^5 cells/well were cultured in 96-well plates for 24 h using 200 μL of DMEM and incubated at 37°C and 5% CO_2. 6-FAM-Melapt was added to (+) melanopsin cells at six different concentrations (1.405 μg/mL, 5.625 μg/mL, 11.25 μg/mL, 22.5 μg/mL, 45.0 μg/mL, and 90.0 μg/mL) and incubated for 15 min. After washing, the binding capacity of 6-FAM-Melapt in (+) melanopsin cells was estimated by measuring the 6-FAM signal using a microplate reader (λex 495 nm, λem 517 nm). Before performing each measurement, 6-FAM-Melapt was added to three different wells ($n = 3$).

Estimation of phase shifts by *Per2: Eluc*:TK:Mel stable cells

Screening of DNA aptamers was performed using blue light-responsive and real-time bioluminescence recording of circadian rhythms (Supplementary Figure S2). *Per2:ELuc* cells were expressed in a stable cell line transfected to express ELuc under the control of the *Per2* promoter (Nakajima et al., 2010) because the phase due to the transcriptional activity rhythm of *Per2* can be monitored from the emission rhythms of ELuc. *Per2:ELuc:*TK:Mel stable cells expressed melanopsin stably under the control of the melanopsin under the control of the TK promoter. Melanopsin transmits external photo-stimuli into the cell via signal transduction and transiently induces *Per2* transcription in the cell nucleus. Thus, *Per2:ELuc:*TK:Mel stable cells were deemed suitable for the phase shift of circadian rhythms in response to blue-light photostimulation because of recombinant gene *Per2:ELuc* and TK:Mel.

Per2: ELuc: TK: Mel stable cells (1.5×10^5) were passaged in a 35-mm dish, forskolin (Invitrogen) was added at a final concentration of 10 μM at 24 h after passaging, and cells were incubated for 30 min at 37°C before replacing the medium. This process synchronizes the circadian phase of *Per2* rhythmic expression in all cells to amplify the amplitude of the emission rhythm, monitored by Phot multiple tubes (PMTs). Following forskolin shock, the cells were washed with phosphate-buffered saline (PBS) and exposed to luciferin (Beetle Luciferin, Potassium Salt; Promega) at a final concentration of 0.1 mM in a new medium in a Kronos illuminometer (ATTO, Tokyo, Japan). This was equipped with a PMT to detect luminescence and measure the cell emission signal in dishes in real time for 10 s every 3 min, while the cells were incubated at 37°C with 5% CO_2. The phase of *Per2:Eluc:*TK:Mel stable cells was determined as the middle point between the peak and trough of bioluminescent rhythms as CT12. Then, Melapts were added to the culture medium at 22.5 μg/mL (final concentration) at subjective dawn (CT22) and subjective afternoon (CT8). Photostimulation was then performed in culture dishes in the Kronos for 15 min using a Blue LED (Amon Industry Co., Ltd., Tokyo, Japan). Subsequently, rhythmic bioluminescence in *Per2:ELuc:*TK:Mel stable cells was observed for 3 days.

The obtained rhythmic emission data were analyzed by cosine fitting over a 12-36-h period after forskolin shock, and after photostimulation, using NINJA software (CHURITSU Electric, Aichi, Japan).

Animals

Per1::luc Tg C57BL/N strain mice with a firefly luciferase gene linked to the downstream region of the 6.7-kb *Per1* promoter (provided by Professor Tei, Kanazawa University; Yamazaki et al., 2000) were used to monitor mammalian the circadian rhythm of the central clock in the SCN. Experiments were performed using *Per1::luc* Tg heterozygous mice. Mice (all male and aged 6 to 12 months) were maintained under SPF conditions at 22°C with a 12:12 h light:dark cycle (from 08:00 to 20:00). Mice were fed standard pellets (CLEA Rodent Diet CE-2, CLEA, Tokyo, Japan, Inc.), and water and food were freely available. All animals were handled according to the guidelines for the use of laboratory animals, Toyohashi University of Technology (DO2021-1).

Injection of Melapts into bulbus oculi of *Per1::luc* Tg mice

Mice were injected with abatin anesthetic (1.9% w/v, 0.45 mL/20 g body weight). Response reflexes were assessed by pinching the tail and legs 5 min after anesthesia. For the mydriasis tests, one to two drops of Midorin-P ophthalmic solution (tropicamide phenylephrine hydrochloride ophthalmic solution; Santen Pharmaceutical, Osaka, Japan) were injected into the eyes of three Tg mice (CT22) following Melapt injection. Then, 1 µL of Melapt solution (100 ng-300 ng/µL) was injected into both bulbus oculi using a microsyringe (Hamilton, Nevada, United States) from the border between the cornea and sclera into both eyes. After injection, the mice were illuminated with an LED (Yazawa Corporation, Tokyo, Japan) at 1000 LUX for 30 min. Bulbus oculi were removed to prevent them from responding to light. All animal experiments were conducted under dim red LED lights.

Observing circadian bioluminescence rhythms of SCN cultured slices

We prepared 300-µm coronal section slices of SCN using a microslicer (Dosaka E.M., Kyoto, Japan) in cooled PBS on ice from whole brains of three *Per1::luc* Tg mice following Melapt injection. Under a stereomicroscope, only the SCN on the Chiasma was removed as a 1.5-mm triangular tissue section from coronal section slices in 1.2 mL of media. The SCN tissue slices were grown on Millicell membranes (PICM03050; Millipore, Massachusetts, USA) in serum-free DMEM (Invitrogen) containing 10 mM HEPES (pH 7.2; Invitrogen), 2% B27 (Life Technologies, Carlsbad, CA, United States), 25 unit/mL penicillin, and 25 µg/mL streptomycin (Invitrogen) in a 35-mm dish. Beatle luciferin potassium salt (Promega) was added at 0.2 mM where required. Circadian bioluminescence rhythms were continuously monitored using a PMT (Hamamatsu Photonics) in an incubator at 36°C. Emission values of SCN slices were integrated for 1 min over ~5 days and plotted onto graphs. Circadian bioluminescence cycle data were examined using NINJA software.

Statistical analysis

The Tukey–Kramer method in R software v.4.1.0. (R Foundation for Statistical Computing, Vienna, Austria) was used to analyze data. Statistical significance was set at $p \leq 0.05$. Error bars on graphs show mean ± standard deviation (SD). All analyses were performed at least three times.

Results

Selecting DNA aptamers for melanopsin: Melapts

From the 10^{17} different DNA fragments, we used the Cell-SELEX approach to identify DNA aptamers that bind specifically to melanopsin in PC12 cells; eight rounds of Cell-SELEX were performed using 10^{17} DNA fragments, with (−) melanopsin cells as negative selection and (+) melanopsin cells as positive selection, respectively, by PCR to select 15 Melapts that bind specifically to melanopsin (Figure 1A). Functional screening of the 15 Melapts was performed to identify those able to induce a phase shift in circadian rhythms (Figure 1B). Photostimulation at subjective dawn (CT22) caused phase advance of *Per2* expression rhythms in *Per2:ELuc:*TK:Mel stable fibroblasts expressing melanopsin (Figure 1C, Tables 2, 3). In addition, some Melapts caused a more significant phase advance of circadian rhythms following photostimulation (Figure 1B). These findings suggest that Melapts influence the phase of circadian rhythms by binding to melanopsin, thereby triggering signal transmission into cells and affecting transcription of the clock gene *Per2*.

Estimating the binding capacity of Melapts

We selected three Melapts labeled with 6-FAM (Melapt01, Melapt04, and Melapt08), Melapt01 (group1) induced both phase advance of *Per2::luc* bioluminescence rhythms and rhythm phase delay at CT22 (Figure 2).

That was because15 screened Melapts were divided into three groups, group 1: phase advance or delay in *Per2:ELuc* bioluminescence rhythms at both CT22 and CT8 like Melapt04, group 2: phase advance or delay at CT22 and delay or advance at CT8, respectively, like Melapt01, and group 3: non-phase shifts in *Per2:ELuc* bioluminescence rhythms like Melapt08. Melapt01, Melapt04, and Melapt08 were selected as representatives of each group and were FAM-labeled to determine a final concentration of Melapt for adding on cells. At 22.5 µg/mL, all three Melapts could bind to melanopsin on the cell membrane sufficiently.

Three Melapts labeled with 6-FAM fluorescence using 6-FAM primers were compared in terms of binding capacity to *Per2:ELuc:*TK:Mel stable cells. The higher binding capacity of Melapt04 and Melapt01 to cells was saturated at a concentration of 11.25 µg/mL, whereas that of Melapt08 could not be saturated at a concentration of 90 µg/mL (Figure 2A). Thus, in subsequent experiments, the applied concentration of Melapts was 22.5 µg/mL, sufficient to bind to melanopsin on the cell membrane because the half-maximal effective concentration (EC_{50}) of Melapt08 with even lower binding capacity was 22.5 µg/mL (Figure 2B). These results not only confirmed the successful screening of selective aptamers capable of binding to melanopsin cell membranes but also determined the appropriate concentrations of Melapts in the culture medium for phase-shift experiments.

Screening of Melapts using *Per2: Eluc*:TK:Mel stable cells

Melapt with blue-light photostimulation at CT22

The 15 Melapts were categorized according to their ability to trigger a phase shift in circadian rhythms (Table 2). In addition, Table 3 shows Melapts rearranged from phase advance (positive number) to phase delay (negative number). The phase shift in bioluminescence rhythm depends on the timing of Melapt addition and the presence of photostimulation.

*Per2:ELuc:*TK:Mel cells stably expressing melanopsin were exposed to each Melapt under blue-light photostimulation at CT22 as

TABLE 2 Summary of phase shifts induced by Melapts *in vitro* and *in vivo*.

	In vitro				*In vivo*
Melapt_No.	CT22_BL	CT8_BL	CT22_nonBL	CT8_nonBL	CT22_BL
Control	1.3	−1.0	−0.6	−0.1	0.0
Melapts 1	8.6	9.8	−6.0	−0.1	0.5
Melapt02	7.0	1.3	0.9	−3.5	−0.7
Melapts 3	6.4	1.1	−3.4	−3.1	1.6
Melapts 4	6.0	0.3	7.4	4.4	3.1
Melapt05	1.0	−2.4	−4.8	9.4	ND
Melapt06	−0.4	2.5	6.6	7.7	ND
Melapt07	−1.0	1.3	−10.4	3.1	−1.1
Melapt08	−1.2	6.7	−7.8	1.1	ND
Melapt09	−4.4	7.3	3.0	8.1	−0.7
Melapts 10	−4.6	−1.1	−5.7	−6.3	−2.0
Melapt11	−5.5	0.4	1.0	4.0	0.3
Melapt12	−5.5	5.4	−9.1	4.7	ND
Melapts 13	−5.8	−6.4	5.2	8.3	ND
Melapt14	−8.4	0.5	1.9	1.1	ND
Melapt15	−4.8	4.4	5.2	−3.9	ND
					/h

Summary of phase shifts in circadian rhythms induced by each Melapt in *Per2: Eluc*:TK:Mel stable cells and in SCN of *Per1::luc* Tg mice. Positive and negative numbers indicate phase delay and advance (h), respectively. Melapts 1,3,13 described in red induced phase advance or delay in the absence of blue light, while Melapts described in black induced reverse phase delay or advance in the presence of blue light. Melapts 4,10 described in blue induced phase shifts in both the presence and absence of blue light. In total, six of nine Melapts displayed similar phase shifts at CT22 *in vitro* and *in vivo* in the absence of blue light.

a model for exposure of the retina to intense blue light at dawn (Figure 3; Tables 2, 3).

Phase advance of *Per2:ELuc* rhythmic emission rhythms by ~1.3 h was observed (using a Kronos bio luminometer) in controls following simple blue-light photostimulation in the absence of Melapts at CT22 (Figure 4; Tables 2, 3). Cells treated with Melapt01 showed a phase advance of *Per2:ELuc* emission rhythms by ~8.6 h (Figure 4A). The group treated with Melapt02 showed a phase advance of *Per2:ELuc* emission rhythms by ~6.9 h (Figures 4B–E). Melapt05 induced a phase advance of *Per2:ELuc* emission rhythms by ~1.0 h (Figure 4E). Conversely, Melapt06 induced a phase delay of *Per2:ELuc* emission rhythms of ~0.4 h (Figure 4F). Groups treated with Melapt07, Melapt08, Melapt09, Melapt10, Melapt11, Melapt12, Melapt13, Melapt14, and Melapt15 showed phase delays of *Per2:ELuc* emission rhythms by approximately 1.0, 1.2, 4.3, 4.6, 5.4, 5.5, 5.8, 8.4, and 4.7 h, respectively (Figures 4G–O).

Melapt with blue-light photostimulation at CT8

Then, we examined the effects on *Per2:ELuc* emission rhythms of applying Melapts and blue-light photostimulation in the subjective afternoon (CT8) to mimic exposure to intense afternoon light. Kronos bio luminometer results revealed that controls receiving only blue-light photostimulation without any Melapts at CT8 showed a phase delay of *Per2:ELuc* emission rhythms by ~0.6 h (Figure 5; Tables 2, 3).

Cells treated with Melapt01 showed a phase delay of *Per2:ELuc* emission rhythms by ~5.9 h (Figure 6A). The Melapt03, Melapt05, Melapt07, Melapt08, Melapt10, and Melapt12 groups showed a phase delay of *Per2:ELuc* emission rhythms by approximately 3.4, 4.8, 10.4, 7.8, 5.6, and 9.1 h, respectively (Figures 6C,E,G,H,J,L). Melapt09 triggered a phase advance of *Per2:ELuc* emission rhythms by approximately 3.0 h (Figure 6I). By contrast, Melapt06 induced a phase delay of *Per2:ELuc* emission rhythms by ~6.6 h (Figure 6F). Groups treated with Melapt02, Melapt04, Melapt11, Melapt13, and Melapt14 displayed a phase advance of *Per2:ELuc* emission rhythms by approximately 0.9, 7.3, 1.0, 8.3, and 1.9 h, respectively (Figures 6B,D,K,M,N). Melapt15 induced a phase advance of *Per2:ELuc* emission rhythms by ~5.1 h (Figure 6O).

Melapt with and without blue-light photostimulation at CT22 and CT8

At CT22, Melapt01, Melapt03, and Melapt04 plus photostimulation induced a phase advance, while Melapt10 and Melapt13 at CT22 induced a phase delay (Figures 7A, 8A). We picked up Melapt4 and Melapt10 as representatives of Melapts in group1, which induced a phase advance and phase delay of *Per2:ELuc* bioluminescence rhythms in the same direction at both CT22 and CT8 (Figure 7). Melapt1, Melapt3, and Melapt13 were selected as representatives of Melapts in group2, which induced those of *Per2:ELuc* rhythms in opposite direction at CT22 and CT8 (Figure 8), for example, phase advance at both CT22 and CT8 by Melapt4, while phase advance at CT22 and phase delay at CT8 by Melapt1.

Although these phase shifts could be observed even without photostimulation when adding Melapts, Melapt04 and Melapt10 enhanced the phase shift compared with controls without photostimulation at CT22 (Figures 7B, 8B).

The phase-shift abilities of Melapts without photostimulation were evaluated (Figures 7B, 8B).

TABLE 3 Summary of phase shifts induced *in vitro* and *in vivo*.

In vitro							
Melapt_No.	CT22_BL	Melapt_No.	CT8_BL	Melapt_No.	CT22_ nonBL	Melapt_No.	CT8_ nonBL
Melapt01	8.6	Melapt01	9.8	Melapt04	7.4	Melapt05	9.4
Melapt02	7.0	Melapt09	7.3	Melapt06	6.6	Melapt13	8.3
Melapt03	6.4	Melapt08	6.7	Melapt13	5.2	Melapt09	8.1
Melapt04	6.0	Melapt12	5.4	Melapt15	5.2	Melapt06	7.7
Control	1.3	Melapt15	4.4	Melapt09	3.0	Melapt12	4.7
Melapt05	1.0	Melapt06	2.5	Melapt14	1.9	Melapt04	4.4
Melapt06	−0.4	Melapt02	1.3	Melapt11	1.0	Melapt11	4.0
Melapt07	−1.0	Melapt07	1.3	Melapt02	0.9	Melapt07	3.1
Melapt08	−1.2	Melapt03	1.1	Control	−0.6	Melapt14	1.1
Melapt09	−4.4	Melapt14	0.5	Melapt03	−3.4	Melapt08	1.1
Melapt10	−4.6	Melapt11	0.4	Melapt05	−4.8	Control	−0.1
Melapt15	−4.8	Melapt04	0.3	Melapt10	−5.7	Melapt01	−0.1
Melapt11	−5.5	Control	−1.0	Melapt01	−6.0	Melapt03	−3.1
Melapt12	−5.5	Melapt10	−1.1	Melapt08	−7.8	Melapt02	−3.5
Melapt13	−5.8	Melapt05	−2.4	Melapt12	−9.1	Melapt15	−3.9
Melapt14	−8.4	Melapt13	−6.4	Melapt07	−10.4	Melapt10	−6.3
							/h

In vivo	
Melapt_No.	CT22_BL
Melapt04	3.1
Melapt03	1.6
Melapt01	0.5
Melapt11	0.3
Control	0.0
Melapt02	−0.7
Melapt09	−0.7
Melapt07	−1.1
Melapt10	−2.0

Summary of the phase shift in circadian rhythms induced by each Melapt in *Per2: Eluc*:TK:Mel stable cells and in the SCN of *Per1::luc* Tg mice. Positive and negative numbers indicate phase delay or advance (hours), respectively. Melapts highlighted in orange and blue lines induce the same phase shifts described in the footnote to Table 2.

Melapts plus intense photostimulation in the subjective afternoon (CT8) caused phase shifts of *Per2* emission rhythms in the same direction (advance or delay) as at dawn (CT22; Figures 7A,C). In addition, at CT22, the degree of phase shift was changed more than at CT8 in both advanced and delayed directions. For Melapt01 and Melapt13, a more significant phase advance or delay at CT22 was observed in the absence of photostimulation. By contrast, for Melapt03, Melapt04, Melapt10, and Melapt13, a more significant phase advance or delay at CT8 was observed in the absence of photostimulation.

Furthermore, Melapt01 and Melapt03 advanced the phase at CT22, and Melapt13 delayed the Phase, while the opposite phase shifts were observed at CT8 (Figures 8A,C). Like Melapt04, Melapt01 and Melapt03 induced expression of *Per2* by binding to melanopsin at CT22, probably resulting in a phase advance, whereas they caused a phase delay at CT8.

Melapt03 induced a phase advance and delay at CT22 and CT8, while Melapt04 induced a phase advance at both CT22 and CT8. Nevertheless, the phase shifts of Melapt03 and Melapt04 without blue-light photostimulation were less than those with photostimulation at CT22, when *Per2* transcription was slightly upregulated (Figures 7A,B, 8A,B). However, phase shifts of Melapt03 and Melapt04 were the same with and without blue-light photostimulation at CT8, when *Per2* transcription was shown to be high (Figures 7A,B, 8A,B). Melapt04 and Melapt10 displayed little difference in phase-shift ability between CT22 and CT8 upon photostimulation (Figures 7A,C).

Functional analysis of Melapts in *Per1::Luc* Tg mice

We performed *in vivo* experiments similar to the *in vitro* experiments to investigate whether Melapts binding to melanopsin in the retina projecting to the SCN affected the phase shifts of the central

10.3389/fnins.2024.1186677

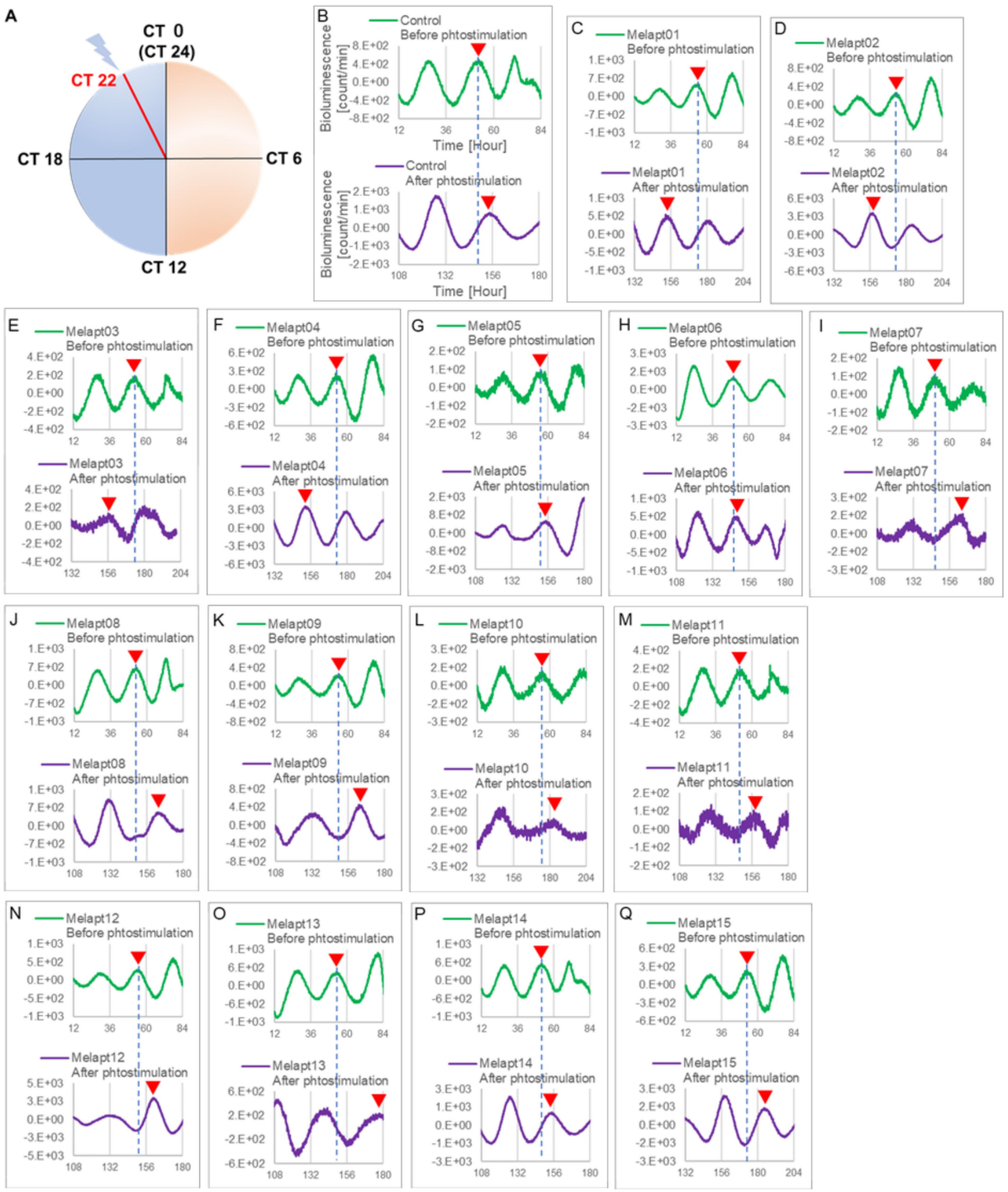

FIGURE 3
Changes in *Per2:ELuc* emission rhythms before and after the addition of each Melapt and blue-light photostimulation at CT22. **(A)** Subjective light period from CT0-12, subjective dark period from CT12-0, and a blue light indicate photostimulation at CT22 of the 24-h clock. **(B)** *Per2:ELuc* emission upon adding PBS and blue-light photostimulation as a control. **(C–Q)**. *Per2:ELuc* emission upon adding Melapt01-Melapt15 and blue-light photostimulation. Upper row (green), *Per2:ELuc* emission before the addition of Melapt observed for 3 days. Lower row (purple), *Per2:ELuc* emission after addition of Melapt and blue-light photostimulation observed for 3 days. A red triangle indicates the peak. Bioluminescence traces in Figure 3 were estimated from an individual sample. The peak bioluminescent emission rhythms monitored over 3 days before the addition of Melapts and photostimulation (green) are denoted by a dotted line to allow comparison with the peak rhythms in the lower graphs (plotted post-stimulation and colored purple).

clock in the SCN. Eight types of Melapt causing phase-shift responses in *Per2* expression rhythms in *in vitro* experiments were injected into the bulbs of eyes of *Per1::luc* Tg mice at CT22 (Figure 9; Tables 2, 3; Supplementary Figure S3). Melapt01, Melapt03, Melapt04, Melapt07, Melapt09, and Melapt10 displayed similar phase-shift abilities in the *in vivo* and *in vitro* experiments. Figures 4, 9 show that Melapt01,

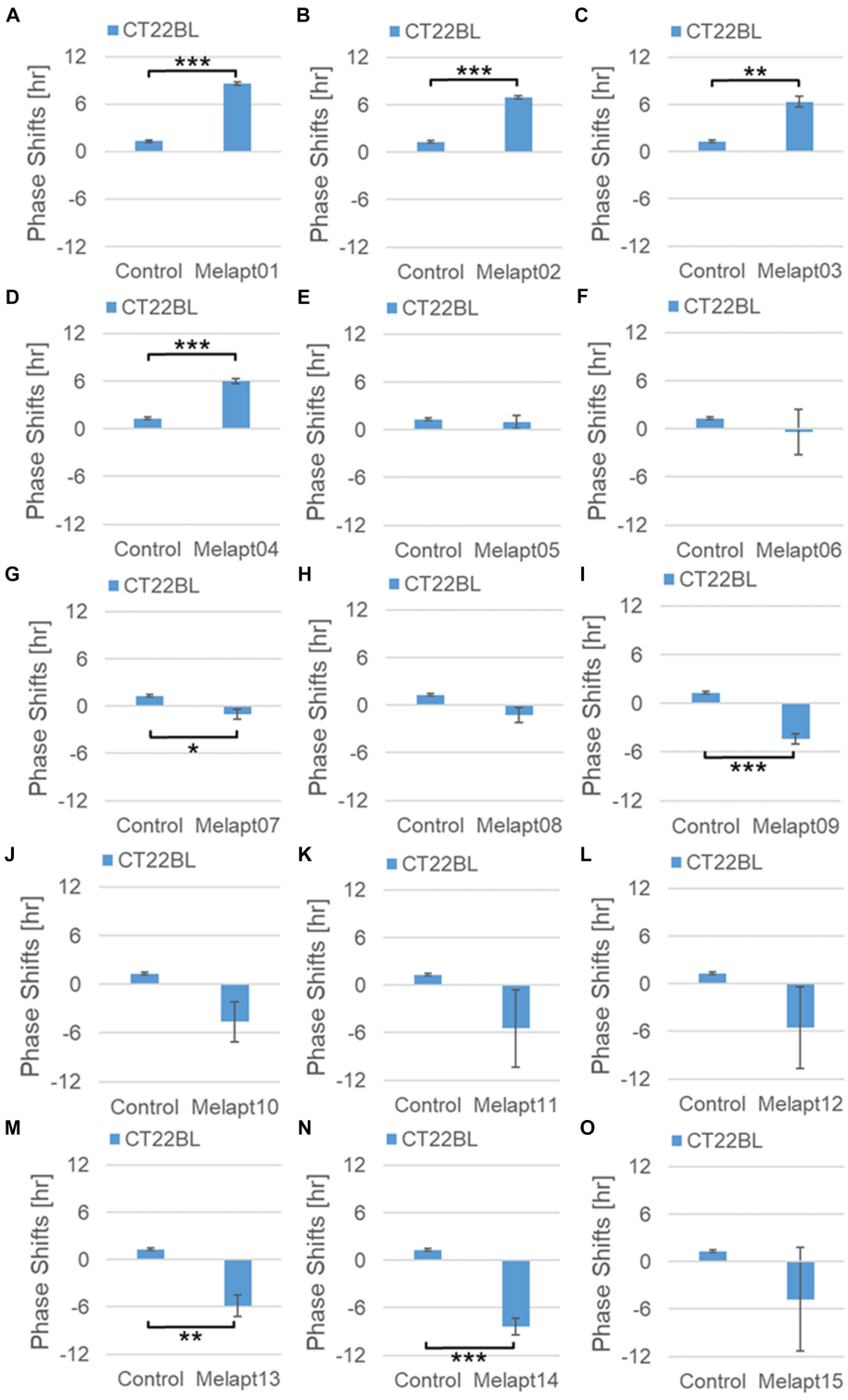

FIGURE 4
Phase shift due to binding of Melapts plus photostimulation at subjective dawn (CT22). **(A–O)** Phase-shifts comparison between Melapts and controls with photo-stimulus at CT22. PBS alone was added to control cells. The phase shift was calculated from the cosine-fitting curve in Figure 3 using the NINJA program and plotted on a graph. $n = 3$ (individual samples); $^{*}p < 0.05$, $^{**}p < 0.01$, $^{***}p < 0.001$, Tukey–Kramer test.

Melapt03, and Melapt04 induce phase advance and that Melapt07, Melapt09, and Melapt10 induce phase delay in CT22 both *in vivo* and *in vitro* as Melapts effect on phase shift by *in vivo* experiments can be predicted from *in vitro* experiments. On the other hand, total phase shifts were limited to 3 h in intact animals, regardless of how much advance or delay by Melapts in *Per2:Eluk:TK:Mel* cells.

For example, Melapt04 caused a maximum phase advance of 3 h, and Melapt10 caused a maximum phase delay at 3 h, in experiments

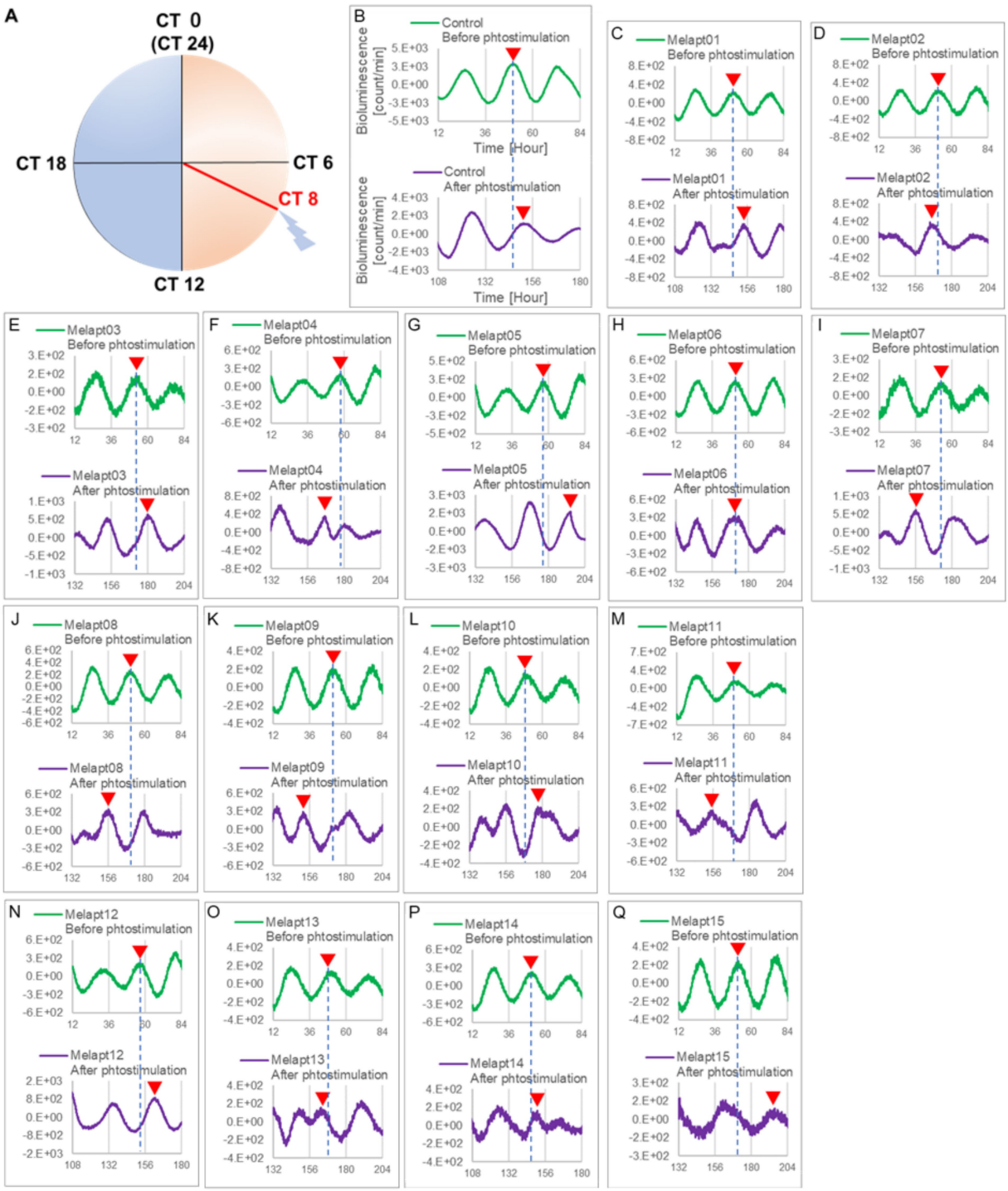

FIGURE 5
Changes in *Per2:ELuc* emission rhythms before and after applying Melapts and blue-light photostimulation at CT8. **(A)** Subjective light period from CT0-12, subjective dark period from CT12-0, and blue light indicate photostimulation at CT8 of the 24-h clock. **(B)** *Per2:ELuc* emission upon applying PBS and blue-light photostimulation to controls. **(C–Q)** *Per2:ELuc* emission upon applying Melapt01- Melapt15 and blue-light photostimulation. Upper row (green), *Per2:ELuc* emission before the addition of Melapt observed for 3 days. Lower row (purple), *Per2:ELuc* emission after addition of Melapt and blue-light photostimulation observed for 3 days. Red triangles indicate the peak. Bioluminescence traces in Figure 5 were estimated from an individual sample. The peak of bioluminescent emission rhythms measured over the 3 days prior to the addition of Melapts and photostimulation (green) is denoted by a dotted line to allow comparison with peak rhythms in the lower graphs (potted post-stimulation).

in *Per2:ELuc:*TK:Mel stable cells and in SCN of *Per1::luc* Tg mice similar to the restriction of phase shifts to a maximum of 3–4 h in mammals (Gillette and Mitchell, 2002; Guler et al., 2008; Iyer et al., 2014; Figure 9; Tables 2, 3).

In total, two/three out of the nine Melapts showed similar phase shifts at CT22 *in vitro* and *in vivo* in the absence of blue light (Tables 2, 3). This suggests that each Melapt induced a similar phase shift in both mice and Per2:*ELuc*:TK:Mel stable cells.

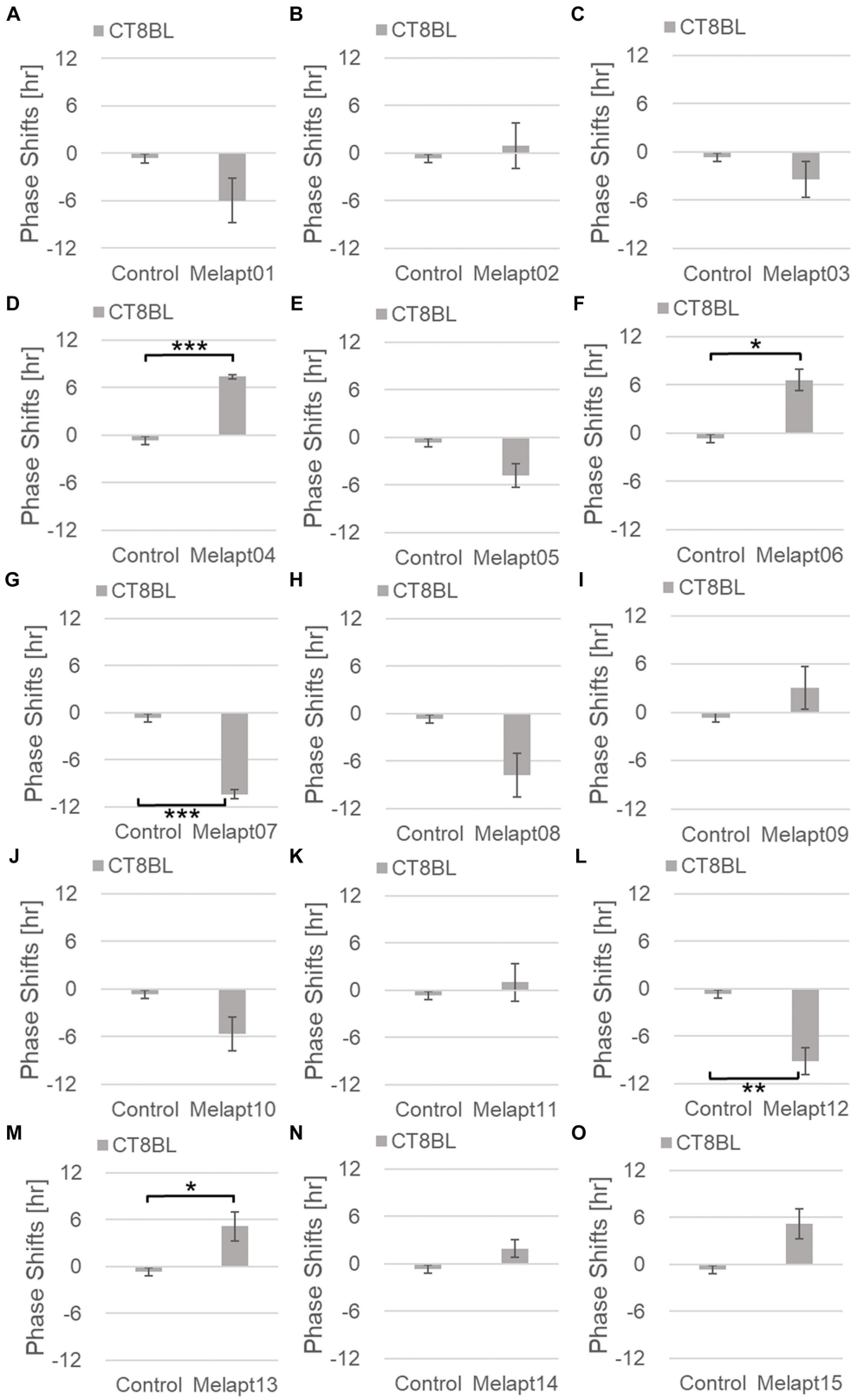

FIGURE 6
Phase shifts upon binding of Melapts plus photostimulation at subjective afternoon (CT8). **(A–O)** Phase-shifts comparison between Melapt-treated groups and controls with photo-stimulus at CT8. PBS alone was added to the controls. $n = 3$, $^{*}p < 0.05$, $^{**}p < 0.01$, $^{***}p < 0.001$, Tukey–Kramer test.

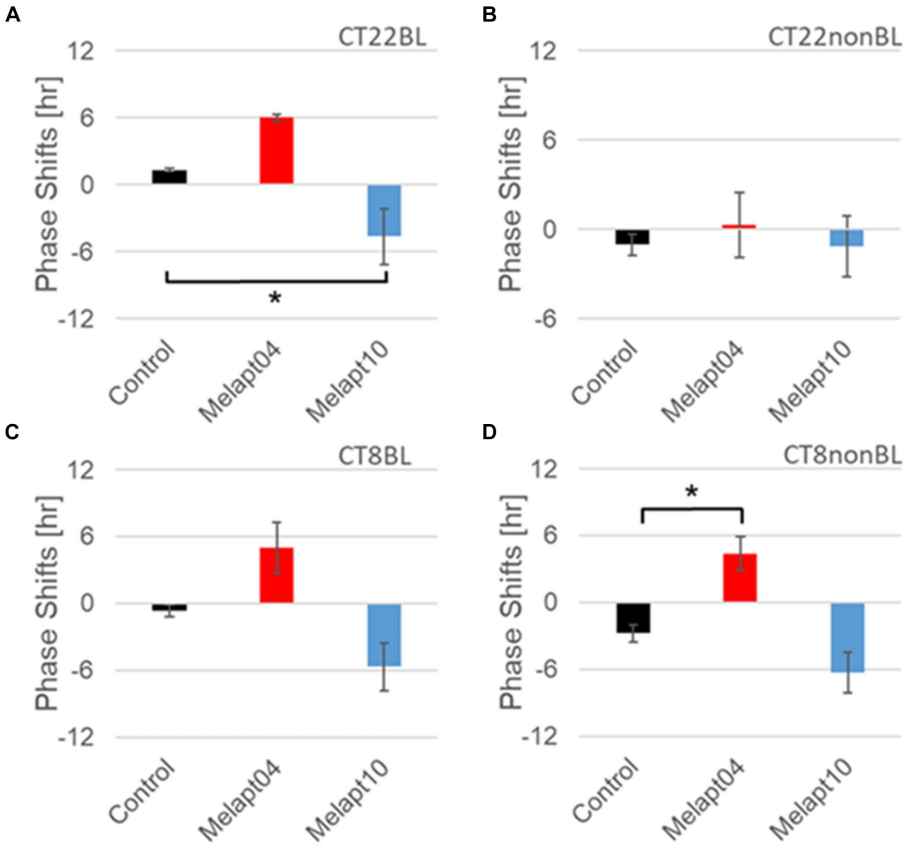

FIGURE 7
Similar phase-shift abilities of representative Melapts at both CT22 and CT8. **(A)** Melapt binding-mediated phase shift induced via photostimulation at subjective dawn (CT22BL). **(B)** Melapt-mediated phase shift at subjective dawn (CT22nonBL). **(C)** Melapt binding-mediated phase shifts induced via photostimulation in the afternoon (CT8BL). **(D)** Melapt-mediated phase shifts in the afternoon (CT8nonBL). Controls showed phase shifts in the absence of Melapts under all conditions. The upper direction shows phase advance, whereas the lower direction shows phase delay. Red: phase advance. Blue: phase delay. *$p < 0.05$, Tukey–Kramer test.

Discussion

Melapts were identified to affect the phase of the circadian rhythms

This study focused on controlling the ability of melanopsin to manipulate the phase resetting of circadian rhythms caused by blue-light input from the eyes using Melapts identified by screening and *Per2*:*ELuc*:TK:Mel stable cells for functional analysis of phase-shift ability in molecular clock rhythms. Because we used cells exhibiting stable expression of melanopsin via the TK promoter, whereas previous studies (Pulivarthy et al., 2007; Ukai et al., 2007) used cells transiently transfected with melanopsin, we were able to perform more quantitative functional analyses of the phase response to aptamer concentration and light intensity.

Among the 15 Melapts obtained by Cell-SELEX, two showed characteristic responses: Melapt04 caused a phase advance and Melapt10 caused a phase delay at both subjective dawn (CT22) and in the afternoon (CT8). At dawn (CT22), when transcript levels of clock gene *Per2* began to increase, Melapt04, Melapt01, and Melapt03 increased signaling into cells to upregulate *Per2* transcription and induce a phase advance, while Melapt10 and Melapt13 repressed intracellular signaling to downregulate *Per2* expression and induce a phase delay. In the afternoon (CT8), *Per2* transcription was almost at its peak. It appeared that Melapt04 and Melapt10 with photostimulation caused the same phase shift as at CT22 and that Melapt1, Melapt3, and Melapt13 with photostimulation caused the opposite phase shift to that at CT22. At CT8, the transition between stopping the upregulation of *Per2* transcription and beginning its downregulation could account for the instability effect of the phase shift upon adding Melapt. Furthermore, we found that in both the presence/absence of blue light, the phase of the molecular clock can be shifted (either advanced or delayed) simply by the addition of a Melapt in contrast with previous reports (Takumi et al., 1998; Pulivarthy et al., 2007; Ukai et al., 2007).

Photostimulation by blue-light exposure of the retina of mice before dawn (CT22) resulted in a phase advance of activity rhythms, similar to previous reports in rats (Honma et al., 1985). However, adding a particular Melapt (01, 03, 04) at CT22 resulted in a more significant phase advance, whereas other Melapts (10 and 13) resulted in a phase delay.

At CT22 (subjective dawn), as *Per2* expression levels were increasing, the melanopsin signal bound to Melapt01, Melapt03, and

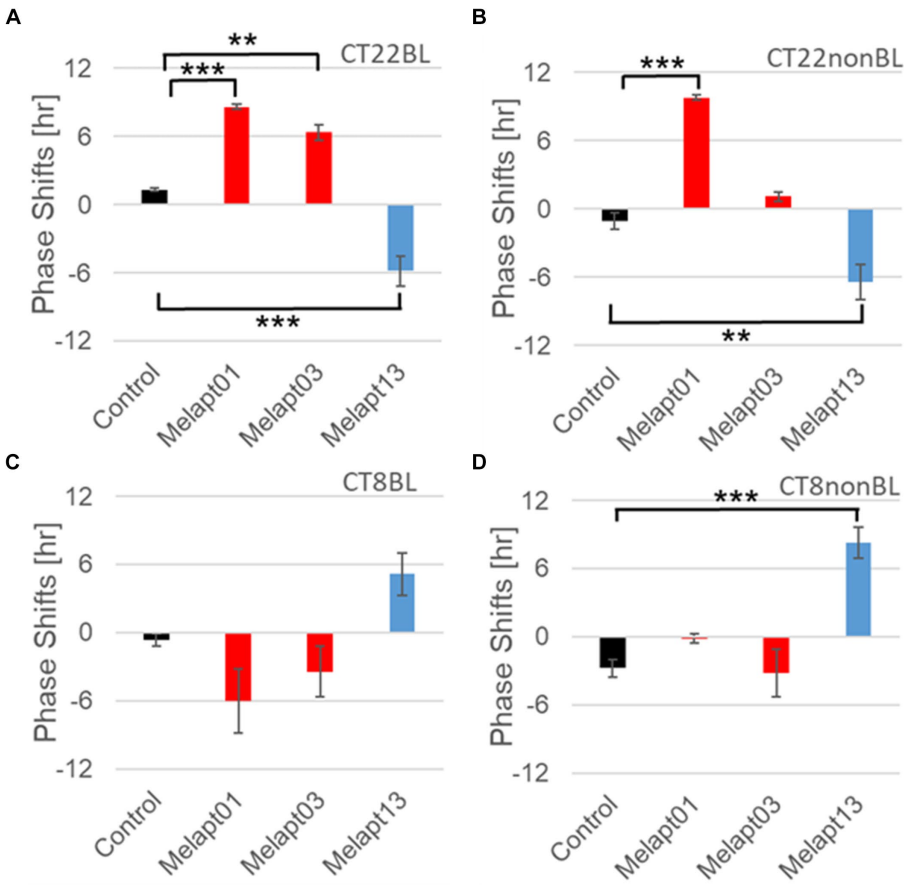

FIGURE 8
Reverse-phase shift abilities of representative Melapts at CT22 and CT8. **(A)** Melapt-mediated phase shift induced by photostimulation at subjective dawn (CT22BL). **(B)** Melapt-mediated phase shift at subjective dawn (CT22nonBL). **(C)** Melapt-mediated phase shift induced by photostimulation in the afternoon (CT8BL). **(D)** Melapt-mediated phase shift in the afternoon (CT8nonBL). Controls were phase shifts without any Melapts under all conditions. The upper direction shows phase advance, whereas the lower direction shows phase delay. Red: phase advance. Blue: phase delay. $^{**}p < 0.01$, $^{***}p < 0.001$, Tukey–Kramer Test.

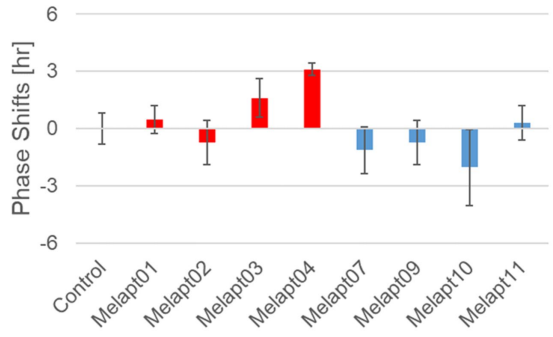

FIGURE 9
Phase shift of *Per1::luc* expressional rhythms in SCN slices following injection of Melapts into both bulbus oculi of *Per1::luc* Tg mice. Phase shifts following injection of Melapts into bulbus oculi with LED light stimulus at subjective dawn (CT22). SCN slices were obtained from mice injected with Melapts, and bioluminescence was observed for approximately 5 days. The NINJA program was used to calculate phase shifts. The upper direction shows phase advance, whereas the lower direction shows phase delay. Red: phase advance. Blue: phase delay. $n = 3$, $^{*}p < 0.05$, Tukey–Kramer test.

Melapt04 with photostimulation had a complementary effect and enhanced *Per2* expression, although the detailed underlying mechanism is not known. The extent of the phase advance was higher than in controls only receiving photostimulation at the same time.

By contrast, among the phase delay group of Melapts, Melapt10 and Melapt13 at CT22 could be binding to melanopsin, leading to upregulation of *Per2* expression and repression of signal transduction in cells, and induction of *Per2* gene expression in cells. Therefore, the delay of PER2 protein accumulation in cells could lead to a phase delay of intracellular circadian rhythms.

Melapts binding to melanopsin could directly or indirectly modify the structure of the domain in melanopsin that binds to the retinal, altering the phase shifts. Melanopsin loses its photosensitivity when its structure, function, and retinoid cycle are altered (Dua et al., 2011; Harrison et al., 2021). For example, *cis*-retinal is present in cells bound to melanopsin without post-stimulation, which mediates photostimulation signal transduction into cells, as Melapts bound to melanopsin may influence intracellular signaling and phase shifts without photostimulation.

The secondary structure of Melapts was assessed (not shown) using GENETYX Ver. 9 (GENETYX CORPORATION). Melapt02 and

Melapt04 in the phase advance group have an outwardly protruding C-A-G-A-G sequence within the secondary structure of the stem and loop. The stem–loop conformation may enhance the binding of Melapts to melanopsin. However, it is unclear whether Melapts directly or indirectly alter their binding domain to affect signal transfer or their ability to phase-shift circadian rhythms.

Both *per1* and *per2* are clock genes involved in an input pathway, and their transcription is induced transiently by photosignals, resulting in a phase shift in rhythmic transcription (Shigeyoshi et al., 1997; Yan et al., 1999; Ikegami et al., 2020). Therefore, the phase shift of *per1::luc* and *per2::luc* rhythm induced by Melapts is synchronized. We confirmed whether the aptamers obtained by Selex screening and functionally analyzed using a *per2::luc* reporter cells *in vitro* could trigger the same phase shift in the SCN of *per1::luc* Tg mice *in vivo*. We identified an agonist DNA aptamer that caused a maximum 8-h shift *in vitro* and a 3-h shift *in vivo*. There was a 3-h phase-shift limit *in vivo* because the photic input signal by melanopsin is transferred to the SCN projected from retinal ganglion cells by synaptic transmission (Hanna et al., 2017).

The 11 *cis*-retinal bound to melanopsin is isomerized to *trans*-retinal using blue light (485 nm), causing its dissociation from melanopsin (Schwartz and Zimmerman, 1990). Compared with photostimulation, Melapts that induced a phase advance (Melapt03 and Melapt04) and a phase delay (Melapt10) displayed lower phase-shift abilities, possibly because most retinal molecules remained in the *cis* isomeric form and therefore did not dissociate from melanopsin and transmit signals into cells, thereby repressing the phase shift. This signal of melanopsin is transmitted inside the cell via G protein-coupled receptors, eventually upregulating transcription of the clock gene *Per2* in cells (Iyer et al., 2014; Krzysztynska-Kuleta et al., 2021), resulting in a phase shift of circadian rhythms. Further studies are needed to understand how the downregulation/upregulation of *Per2* upon Melapt–melanopsin binding induces phase shifts of circadian rhythms via CREB phosphorylation.

Future research on Melapt based regulation of the intracellular clock

Melapt04 and Melapt10 induced phase advance or delay of the circadian clock by ~3 h, respectively, at both CT22 and CT8 during the photo-signal input process. This suggests that Melapt04 regulates the phase of circadian rhythms, and facilitates falling asleep and waking, mainly via Phase Advance. Considering the social desire to advance the phase of the circadian clock to facilitate going to bed earlier at night and waking up earlier in the morning, Melapts could be used to trigger phase advance in humans. We chose to use DNA aptamers because they can be synthesized easily by PCR and are stable in the bloodstream. However, delivering aptamers to the retina is very difficult in humans (Hosoya and Tomi, 2005; Del Amo et al., 2017; Ikegami et al., 2020; Ham et al., 2023); here, we injected aptamers intraocularly into mice. Therefore, we need to develop a method for introducing aptamers efficiently and stably into the retina, possibly using a cell-permeable drug delivery with functions like ribosomes administered via drops into the eye (Wang et al., 2010; An et al., 2019; Yan et al., 2019; Tawfik et al., 2022).

Melapts could be used to regulate the function of membrane proteins by inducing conformational changes, thereby allowing more complex functional switching of the target (i.e., melanopsin) in the presence or absence of external photo-stimuli (Faria and Ulrich, 2002; Ulrich, 2005; Wang et al., 2010; Jones et al., 2013). However, the functional stability of Melapt is uncertain because the 3D structure adopted by the Melapt aptamer when bound to melanopsin is difficult to ascertain. In addition, it can be difficult for DNA aptamers to reach the retina, especially if injected into the eye bulb intravenously (Kwak and D'Amico, 1992; Hosoya and Tomi, 2005; Repetto et al., 2010; Patane et al., 2011); also, the stability of aptamers in blood and other body fluids will need to be assessed (Ma et al., 2021). Despite these limitations, Melapts could contribute to future research focused on resetting the phase of circadian clocks. Melapts could help us to better adapt to modern social life cycles, allow crops and domestic animals to be improved for greater productivity, and help shift workers in overcoming social jet lag by adjusting the phases of the circadian clock (Davidson et al., 2006; Saksvik et al., 2011; Barclay et al., 2012; Vetter et al., 2015; Li et al., 2021). These Melapts could contribute to resetting the phase of circadian clocks in photic input pathways.

Data availability statement

The datasets presented in this study can be found in online repositories. The names of the repository/repositories and accession number(s) can be found at: https://www.ncbi.nlm.nih.gov/genbank/, AF147789.1.

Ethics statement

The animal studies were approved by Animal care and use committee of Toyohashi Tech University. The studies were conducted in accordance with the local legislation and institutional requirements. Written informed consent was obtained from the owners for the participation of their animals in this study.

Author contributions

RN and KN conducted the experiments, analyzed the data, performed the statistical analyses, prepared the figures, and contributed to the manuscript writing. MM assisted the experiments. YN established the photo-responsible cell line, while YK and YN conducted experiments with these cells. We are grateful to YK and YN for their supervision and helpful discussion. All authors contributed to the article and approved the submitted version.

Funding

This study was supported by research funding from TechnoPro, Inc. TechnoPro R&D Company and the Program to Foster Young Researchers in Cutting-Edge Interdisciplinary Research (to RN). Funding for Kiban Scientists (to RN 24590350, 20H00614) was

obtained from the Japan Society for the Promotion of Science (JSPS), the Mitsubishi Science Foundation (to RN), and a Research Grant for Science & Technology Innovation at Toyohashi University of Technology (to RN). This study was also supported by the Ministry of Education, Culture, Sports, Science, and Technology in Japan (to YN 21H02083). KN was supported by a scheme for employees to obtain a Ph.D. from TechnoPro, Inc. TechnoPro R&D Company (0007077240 to KN). TechnoPro, Inc was not involved in the study design, collection, analysis, interpretation of data, the writing of this article, or the decision to submit it for publication.

Acknowledgments

We thank H. Tei, Y. Sakaki, S. Yamazaki, and H. Ueda for providing plasmid DNA and Tg mice. We also thank S. Umekage, S. Yamashita and N. Danno for helpful discussion and technical assistance, and N. Kimura and A. Ohtake (Toyohashi University of Technology) for animal care. We are grateful to T. Ohbayashi, Y. Kazuki, and M. Oshimura (Tottori University) for providing A9 cells harboring the MI-MAC vector and recombinase expression plasmids. We acknowledge the excellent technical assistance from T. Iwaki (Advanced Industrial Science and Technology).

Conflict of interest

KN was employed by company TechnoPro, Inc.

The remaining authors declare that the research was conducted in the absence of any commercial or financial relationships that could be construed as a potential conflict of interest.

Publisher's note

Supplementary material

The Supplementary material for this article can be found online at: https://www.frontiersin.org/articles/10.3389/fnins.2024.1186677/full#supplementary-material

References

Albrecht, U., Sun, Z. S., Eichele, G., and Lee, C. C. (1997). A differential response of two putative mammalian circadian regulators, mper1 and mper2, to light. *Cell* 91, 1055–1064. doi: 10.1016/s0092-8674(00)80495-x

An, Y., Yan, H., Li, X., Li, Z., Duan, J., and Yang, X.-D. (2019). Selection of a novel DNA aptamer against OFA/iLRP for targeted delivery of doxorubicin to AML cells. *Sci. Rep.* 9:7343. doi: 10.1038/s41598-019-43910-3

Antoch, M. P., Song, E. J., Chang, A. M., Vitaterna, M. H., Zhao, Y., Wilsbacher, L. D., et al. (1997). Functional identification of the mouse circadian clock gene by transgenic BAC rescue. *Cell* 89, 655–667. doi: 10.1016/s0092-8674(00)80246-9

Barclay, J. L., Husse, J., Bode, B., Naujokat, N., Meyer-Kovac, J., Schmid, S. M., et al. (2012). Circadian desynchrony promotes metabolic disruption in a mouse model of shiftwork. *PLoS One* 7:e37150. doi: 10.1371/journal.pone.0037150

Bunger, M. K., Wilsbacher, L. D., Moran, S. M., Clendenin, C., Radcliffe, L. A., Hogenesch, J. B., et al. (2000). Mop3 is an essential component of the master circadian pacemaker in mammals. *Cell* 103, 1009–1017. doi: 10.1016/s0092-8674(00)00205-1

Davidson, A. J., Sellix, M. T., Daniel, J., Yamazaki, S., Menaker, M., and Block, G. D. (2006). Chronic jet-lag increases mortality in aged mice. *Curr. Biol.* 16, R914–R916. doi: 10.1016/j.cub.2006.09.058

Davidson, A. J., Yamazaki, S., and Menaker, M. (2003). SCN: ringmaster of the circadian circus or conductor of the circadian orchestra? *Novartis Found. Symp.* 253:110. doi: 10.1002/0470090839.ch9

Del Amo, E. M., Rimpelä, A.-K., Heikkinen, E., Kari, O. K., Ramsay, E., Lajunen, T., et al. (2017). Pharmacokinetic aspects of retinal drug delivery. *Prog. Retin. Eye Res.* 57, 134–185. doi: 10.1016/j.preteyeres.2016.12.001

Dua, P., Kim, S., and Lee, D. K. (2011). Nucleic acid aptamers targeting cell-surface proteins. *Methods* 54, 215–225. doi: 10.1016/j.ymeth.2011.02.002

Ellington, A. D., and Szostak, J. W. (1990). *In vitro* selection of RNA molecules that bind specific ligands. *Nature* 346, 818–822. doi: 10.1038/346818a0

Faria, M., and Ulrich, H. (2002). The use of synthetic oligonucleotides as protein inhibitors and anticode drugs in cancer therapy: accomplishments and limitations. *Curr. Cancer Drug Targets* 2, 355–368. doi: 10.2174/1568009023333827

Foster, R. G. (2005). Neurobiology: bright blue times. *Nature* 433, 698–699. doi: 10.1038/433698a

Gentry, N. W., Ashbrook, L. H., Fu, Y. H., and Ptacek, L. J. (2021). Human circadian variations. *J. Clin. Invest.* 131:16. doi: 10.1172/JCI148282

Giebultowicz, J. (2004). Chronobiology: biological timekeeping. *Integr. Comp. Biol.* 44:266. doi: 10.1093/icb/44.3.266

Gillette, M. U., and Mitchell, J. W. (2002). Signaling in the suprachiasmatic nucleus: selectively responsive and integrative. *Cell Tissue Res.* 309, 99–107. doi: 10.1007/s00441-002-0576-1

Guler, A. D., Ecker, J. L., Lall, G. S., Haq, S., Altimus, C. M., Liao, H. W., et al. (2008). Melanopsin cells are the principal conduits for rod-cone input to non-image-forming vision. *Nature* 453, 102–105. doi: 10.1038/nature06829

Ham, Y., Mehta, H., Kang-Mieler, J., Mieler, W. F., and Chang, A. (2023). Novel drug delivery methods and approaches for the treatment of retinal diseases. *Asia Pac J Ophthalmol (Phila).* 12, 402–413. doi: 10.1097/APO.0000000000000623

Hanna, L., Walmsley, L., Pienaar, A., Howarth, M., and Brown, T. M. (2017). Geniculohypothalamic GABAergic projections gate suprachiasmatic nucleus responses to retinal input. *J. Physiol.* 595, 3621–3649. doi: 10.1113/JP273850

Harrison, K. R., Reifler, A. N., Chervenak, A. P., and Wong, K. Y. (2021). Prolonged Melanopsin-based Photoresponses depend in part on RPE65 and cellular Retinaldehyde-binding protein (CRALBP). *Curr. Eye Res.* 46, 515–523. doi: 10.1080/02713683.2020.1815793

Hattar, S., Lucas, R. J., Mrosovsky, N., Thompson, S., Douglas, R. H., Hankins, M. W., et al. (2003). Melanopsin and rod-cone photoreceptive systems account for all major accessory visual functions in mice. *Nature* 424, 76–81. doi: 10.1038/nature01761

Hida, A., Koike, N., Hirose, M., Hattori, M., Sakaki, Y., and Tei, H. (2000). The human and mouse Period1 genes: five well-conserved E-boxes additively contribute to the enhancement of mPer1 transcription. *Genomics* 65, 224–233. doi: 10.1006/geno.2000.6166

Honma, K., Honma, S., and Hiroshige, T. (1985). Response curve, free-running period, and activity time in circadian locomotor rhythm of rats. *Jpn. J. Physiol.* 35, 643–658. doi: 10.2170/jjphysiol.35.643

Hosoya, K.-i., and Tomi, M. (2005). Advances in the cell biology of transport via the inner blood-retinal barrier: establishment of cell lines and transport functions. *Biol. Pharm. Bull.* 28, 1–8. doi: 10.1248/bpb.28.1

Ikegami, K., Nakajima, M., Minami, Y., Nagano, M., Masubuchi, S., and Shigeyoshi, Y. (2020). cAMP response element induces Per1 in vivo. *Biochem. Biophys. Res. Commun.* 531, 515–521. doi: 10.1016/j.bbrc.2020.07.105

Iyer, R., Wang, T. A., and Gillette, M. U. (2014). Circadian gating of neuronal functionality: a basis for iterative metaplasticity. *Front. Syst. Neurosci.* 8:164. doi: 10.3389/fnsys.2014.00164

Jones, K. A., Hatori, M., Mure, L. S., Bramley, J. R., Artymyshyn, R., Hong, S. P., et al. (2013). Small-molecule antagonists of melanopsin-mediated phototransduction. *Nat. Chem. Biol.* 9, 630–635. doi: 10.1038/nchembio.1333

King, D. P., Zhao, Y., Sangoram, A. M., Wilsbacher, L. D., Tanaka, M., Antoch, M. P., et al. (1997). Positional cloning of the mouse circadian clock gene. *Cell* 89, 641–653. doi: 10.1016/s0092-8674(00)80245-7

Krzysztynska-Kuleta, O. I., Olchawa, M. M., and Sarna, T. J. (2021). Melanopsin signaling pathway in HEK293 cell line with stable expression of human Melanopsin: possible participation of phospholipase C beta 4 and diacylglycerol. *Photochem. Photobiol.* 97, 1136–1144. doi: 10.1111/php.13453

Kume, K., Zylka, M. J., Sriram, S., Shearman, L. P., Weaver, D. R., Jin, X., et al. (1999). mCRY1 and mCRY2 are essential components of the negative limb of the circadian clock feedback loop. *Cell* 98, 193–205. doi: 10.1016/s0092-8674(00)81014-4

Kwak, H. W., and D'Amico, D. J. (1992). Evaluation of the retinal toxicity and pharmacokinetics of dexamethasone after intravitreal injection. *Arch. Ophthalmol.* 110, 259–266. doi: 10.1001/archopht.1992.01080140115038

LeGates, T. A., Altimus, C. M., Wang, H., Lee, H. K., Yang, S., Zhao, H., et al. (2012). Aberrant light directly impairs mood and learning through melanopsin-expressing neurons. *Nature* 491, 594–598. doi: 10.1038/nature11673

Li, H., Li, K., Zhang, K., Li, Y., Haotian, G., Liu, H., et al. (2021). The circadian physiology: implications in livestock health. *Int. J. Mol. Sci.* 22:2111. doi: 10.3390/ijms22042111

Lucas, R. J., Hattar, S., Takao, M., Berson, D. M., Foster, R. G., and Yau, K. W. (2003). Diminished pupillary light reflex at high irradiances in melanopsin-knockout mice. *Science* 299, 245–247. doi: 10.1126/science.1077293

Ma, W., Zhan, Y., Zhang, Y., Mao, C., Xie, X., and Lin, Y. (2021). The biological applications of DNA nanomaterials: current challenges and future directions. *Signal Transduct. Target. Ther.* 6:351. doi: 10.1038/s41392-021-00727-9

Menaker, M. (2003). Circadian rhythms. *Circadian photoreception. Sci.* 299, 213–214. doi: 10.1126/science.1081112

Nakajima, Y., Yamazaki, T., Nishii, S., Noguchi, T., Hoshino, H., Niwa, K., et al. (2010). Enhanced beetle luciferase for high-resolution bioluminescence imaging. *PLoS One* 5:e10011. doi: 10.1371/journal.pone.0010011

Numano, R., Yamazaki, S., Umeda, N., Samura, T., Sujino, M., Takahashi, R., et al. (2006). Constitutive expression of the Period1 gene impairs behavioral and molecular circadian rhythms. *Proc. Natl. Acad. Sci. USA* 103, 3716–3721. doi: 10.1073/pnas.0600060103

Patane, M. A., Cohen, A., From, S., Torkildsen, G., Welch, D., and Ousler 3rd, G. W. (2011). Ocular iontophoresis of EGP-437 (dexamethasone phosphate) in dry eye patients: results of a randomized clinical trial. *Clin. Ophthalmol.* 5, 633–643. doi: 10.2147/OPTH.S19349

Pittendrigh, C. S. (1993). Temporal organization: reflections of a Darwinian clock-watcher. *Annu. Rev. Physiol.* 55, 16–54. doi: 10.1146/annurev.ph.55.030193.000313

Pulivarthy, S. R., Tanaka, N., Welsh, D. K., De Haro, L., Verma, I. M., and Panda, S. (2007). Reciprocity between phase shifts and amplitude changes in the mammalian circadian clock. *Proc. Natl. Acad. Sci. USA* 104, 20356–20361. doi: 10.1073/pnas.0708877104

Ralph, M. R., Foster, R. G., Davis, F. C., and Menaker, M. (1990). Transplanted suprachiasmatic nucleus determines circadian period. *Science* 247, 975–978. doi: 10.1126/science.2305266

Repetto, R., Siggers, J. H., and Stocchino, A. (2010). Mathematical model of flow in the vitreous humor induced by saccadic eye rotations: effect of geometry. *Biomech. Model. Mechanobiol.* 9, 65–76. doi: 10.1007/s10237-009-0159-0

Saksvik, I. B., Bjorvatn, B., Hetland, H., Sandal, G. M., and Pallesen, S. (2011). Individual differences in tolerance to shift work--a systematic review. *Sleep Med. Rev.* 15, 221–235. doi: 10.1016/j.smrv.2010.07.002

Schwartz, W. J., and Zimmerman, P. (1990). Circadian timekeeping in BALB/c and C57BL/6 inbred mouse strains. *J. Neurosci.* 10, 3685–3694. doi: 10.1523/JNEUROSCI.10-11-03685.1990

Shearman, L. P., Zylka, M. J., Weaver, D. R., Kolakowski, L. F. Jr., and Reppert, S. M. (1997). Two period homologs: circadian expression and photic regulation in the suprachiasmatic nuclei. *Neuron* 19, 1261–1269. doi: 10.1016/s0896-6273(00)80417-1

Shigeyoshi, Y., Taguchi, K., Yamamoto, S., Takekida, S., Yan, L., Tei, H., et al. (1997). Light-induced resetting of a mammalian circadian clock is associated with rapid induction of the mPer1 transcript. *Cell* 91, 1043–1053. doi: 10.1016/s0092-8674(00)80494-8

Sun, Z. S., Albrecht, U., Zhuchenko, O., Bailey, J., Eichele, G., and Lee, C. C. (1997). RIGUI, a putative mammalian ortholog of the Drosophila period gene. *Cell* 90, 1003–1011. doi: 10.1016/s0092-8674(00)80366-9

Tabei, Y., Murotomi, K., Umeno, A., Horie, M., Tsujino, Y., Masutani, B., et al. (2017). Antioxidant properties of 5-hydroxy-4-phenyl-butenolide via activation of Nrf2/ARE signaling pathway. *Food Chem. Toxicol.: Int. J. Published British Indus. Biolog. Res. Assoc.* 107, 129–137. doi: 10.1016/j.fct.2017.06.039

Takahashi, J. S. (1995). Molecular neurobiology and genetics of circadian rhythms in mammals. *Annu. Rev. Neurosci.* 18, 531–553. doi: 10.1146/annurev.ne.18.030195.002531

Takahashi, J. S., Hong, H. K., Ko, C. H., and McDearmon, E. L. (2008). The genetics of mammalian circadian order and disorder: implications for physiology and disease. *Nat. Rev. Genet.* 9, 764–775. doi: 10.1038/nrg2430

Takiguchi, M., Kazuki, Y., Hiramatsu, K., Abe, S., Iida, Y., Takehara, S., et al. (2014). A novel and stable mouse artificial chromosome vector. *ACS Synth. Biol.* 3, 903–914. doi: 10.1021/sb3000723

Takumi, T., Taguchi, K., Miyake, S., Sakakida, Y., Takashima, N., Matsubara, C., et al. (1998). A light-independent oscillatory gene mPer3 in mouse SCN and OVLT. *EMBO J.* 17, 4753–4759. doi: 10.1093/emboj/17.16.4753

Tawfik, M., Chen, F., Goldberg, J. L., and Sabel, B. A. (2022). Nanomedicine and drug delivery to the retina: current status and implications for gene therapy. *Naunyn Schmiedeberg's Arch. Pharmacol.* 395, 1477–1507. doi: 10.1007/s00210-022-02287-3

Tei, H., Okamura, H., Shigeyoshi, Y., Fukuhara, C., Ozawa, R., Hirose, M., et al. (1997). Circadian oscillation of a mammalian homologue of the Drosophila period gene. *Nature* 389, 512–516. doi: 10.1038/39086

Tuerk, C., and Gold, L. (1990). Systematic evolution of ligands by exponential enrichment: RNA ligands to bacteriophage T4 DNA polymerase. *Science* 249, 505–510. doi: 10.1126/science.2200121

Ukai, H., Kobayashi, T. J., Nagano, M., Masumoto, K. H., Sujino, M., Kondo, T., et al. (2007). Melanopsin-dependent photo-perturbation reveals desynchronization underlying the singularity of mammalian circadian clocks. *Nat. Cell Biol.* 9, 1327–1334. doi: 10.1038/ncb1653

Ulrich, H. (2005). DNA and RNA aptamers as modulators of protein function. *Med. Chem.* 1, 199–208. doi: 10.2174/1573406053175274

Umekage, S., and Kikuchi, Y. (2006). Production of circular form of streptavidin RNA aptamer *in vitro*. *Nucleic Acids Symp Ser (Oxf).* 50, 323–324. doi: 10.1093/nass/nrl161

Vetter, C., Fischer, D., Matera, J. L., and Roenneberg, T. (2015). Aligning work and circadian time in shift workers improves sleep and reduces circadian disruption. *Curr. Biol.* 25, 907–911. doi: 10.1016/j.cub.2015.01.064

Wang, H., Zhao, P., Wenya, S., Wang, S., Liao, Z., Niu, R., et al. (2010). PLGA/polymeric liposome for targeted drug and gene co-delivery. *Biomaterials* 31, 8741–8748. doi: 10.1016/j.biomaterials.2010.07.082

Yamaguchi, S., Kazuki, Y., Nakayama, Y., Nanba, E., Oshimura, M., and Ohbayashi, T. (2011). A method for producing transgenic cells using a multi-integrase system on a human artificial chromosome vector. *PLoS One* 6:e17267. doi: 10.1371/journal.pone.0017267

Yamazaki, S., Numano, R., Abe, M., Hida, A., Takahashi, R., Ueda, M., et al. (2000). Resetting central and peripheral circadian oscillators in transgenic rats. *Science* 288, 682–685. doi: 10.1126/science.288.5466.682

Yan, G., Chen, X., Wang, Y., Zhou, X., Fang, L., and Cao, F. (2019). Multifunctional nanocomposites based on liposomes and layered double hydroxides conjugated with Glycylsarcosine for efficient topical drug delivery to the posterior segment of the eye. *Mol. Pharm.* 16, 2845–2857. doi: 10.1021/acs.molpharmaceut.8b01136

Yan, L., and Silver, R. (2004). Resetting the brain clock: time course and localization of mPER1 and mPER2 protein expression in suprachiasmatic nuclei during phase shifts. *Eur. J. Neurosci.* 19, 1105–1109. doi: 10.1111/j.1460-9568.2004.03189.x

Yan, L., Takekida, S., Shigeyoshi, Y., and Okamura, H. (1999). Per1 and Per2 gene expression in the rat suprachiasmatic nucleus: circadian profile and the compartment-specific response to light. *Neuroscience* 94, 141–150. doi: 10.1016/s0306-4522(99)00223-7

Yoo, S. H., Yamazaki, S., Lowrey, P. L., Shimomura, K., Ko, C. H., Buhr, E. D., et al. (2004). PERIOD2::LUCIFERASE real-time reporting of circadian dynamics reveals persistent circadian oscillations in mouse peripheral tissues. *Proc. Natl. Acad. Sci. USA* 101, 5339–5346. doi: 10.1073/pnas.0308709101

Zylka, M. J., Shearman, L. P., Weaver, D. R., and Reppert, S. M. (1998). Three period homologs in mammals: differential light responses in the suprachiasmatic circadian clock and oscillating transcripts outside of brain. *Neuron* 20, 1103–1110. doi: 10.1016/s0896-6273(00)80492-4

Frontiers in Neuroscience

Provides a holistic understanding of brain function from genes to behavior

Part of the most cited neuroscience journal series which explores the brain - from the new eras of causation and anatomical neurosciences to neuroeconomics and neuroenergetics.

Discover the latest Research Topics

See more →

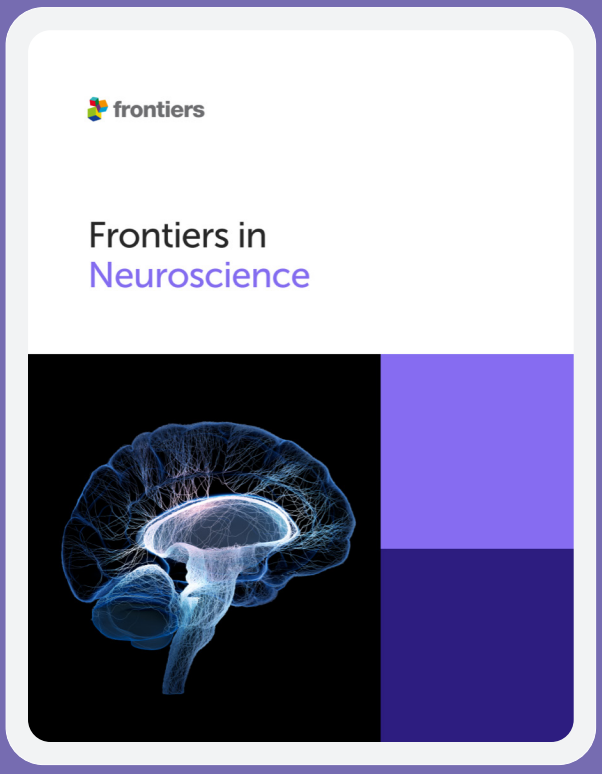

Frontiers

Avenue du Tribunal-Fédéral 34
1005 Lausanne, Switzerland
frontiersin.org

Contact us

+41 (0)21 510 17 00
frontiersin.org/about/contact